LBL-37646
UC-401

Trivalent Metallocene Chemistry of Some Uranium, Titanium, and Zirconium Complexes

Wayne Wendell Lukens, Jr.
Ph.D. Thesis

Department of Chemistry
University of California, Berkeley

and

Chemical Sciences Division
Lawrence Berkeley Laboratory
University of California
Berkeley, CA 94720

May 1995

This work was supported by the Director, Office of Energy Research, Office of Basic Energy Sciences, Chemical Sciences Division, of the U.S. Department of Energy under Contract No. DE-AC03-76SF00098.

DISCLAIMER

DISCLAIMER

Portions of this document may be illegible in electronic image products. Images are produced from the best available original document.

Trivalent Metallocene Chemistry of Some Uranium, Titanium, and Zirconium Complexes

by

Wayne Wendell Lukens, Jr

B.S. (California Institute of Technology) 1988

A dissertation submitted in partial satisfaction of the

requirements for the degree of

Doctor of Philosophy

in

Chemistry

in the

GRADUATE DIVISION

of the

UNIVERSITY of CALIFORNIA at BERKELEY

Committee in charge:

Professor Richard A. Andersen, Chair

Professor Andrew Streitwieser, Jr.

Professor Glenn T. Seaborg

1995

To my family for

your love and support

Acknowledgments

After spending the last seven years of my life here, I certainly have many people to thank. First, I'd like to thank Dick Andersen who was always enthusiastic about chemistry. You pointed me in the right direction and helped me when I got stuck. You were always willing to talk about chemistry and taught me to question why the molecules were doing what they were doing. I'd like to thank my good twin, Marc Weydert, for countless hours arguing about chemistry while hitting the machines. The discussions made me think and kept me on my toes. I'd like to thank Norm Edelstein for many helpful discussion about electronic structure, magnetism, and EPR spectroscopy, and for letting me borrow all of those books. I'd like to thank Jerry Bucher for cheering me up, and for helping me whenever I had computer problems. Thanks to Dave Shuh, Pat Allen, Nick Kaltsoyannis, Tobias Reich, and Eric Hudson for EXAFS help and for keeping me awake during those boring nights at SSRL. Thanks to Alan Zalkin and Fred Hollander for help with crystallography even though it sometimes required yelling at me for hours to get the point home; at least I won't make *that* mistake again. Thanks to Kenn Osborne and George Shalimof for keeping the SQUID happy and for helping me to use it. Thanks to Rob Rosen and Sharon Beshouri for teaching me Schlenk techniques.

I'd also like to thank my coworkers for other chemistry discussions, and for generally being cheerful. Thanks, Chad, Laura, Rob, Mark, Brian, Sharon, Williams, and Piehler for countless machine hits. Thanks, Pielher and Williams, for showing me the peril of phone mail. Thanks, Brian, for saying, "My body is a temple. Marc, your body is a dump." Certainly the funniest thing I've ever heard anyone say on the hill. I'd like to thank the campus idiots, Phil, Dave, Mitch, Mike, and Sable, for generally being good guys, and for all the Stradas runs (Romas this afternoon, perhaps). Thanks to Rick for being a great social director in addition to being a good friend.

Finally, I'd like to thank Kim, Erik, David, Wayne, and Edie. You were always supportive, you always listened, and you made me laugh when I needed it. While I've mentioned you last, I thank you the most.

I would like to thank the National Science Foundation for a graduate fellowship. This work was partially supported by the Director, Office of Energy Research, Office of Basic Energy Sciences, Chemical Sciences Division of the U. S. Department of Energy under Contract No. DE-AC03-76SF00098.

Table of Contents

Abstract

Trivalent Metallocene Chemistry of Some Uranium, Zirconium, and Titanium Complexes

by

Wayne Wendell Lukens, Jr.

Doctor of Philosophy in Chemistry

University of California at Berkeley

Professor Richard A. Andersen, Chair

Dicyclopentadienyluranium halide dimers of the type $[Cp'_2UX]_2$ where X is a halide and Cp' is 1,3-$(Me_3Si)_2C_5H_3$ or 1,3-$(Me_3C)_2C_5H_3$ have been prepared, and their solution behavior has been examined. These molecules exist as dimers in solution, and the halide ligands undergo rapid site exchange on the NMR timescale above 50° C. The analogous dicyclopentadienyluranium hydroxide dimers have also been prepared. These complexes oxidatively eliminate hydrogen to give the corresponding oxide dimers. The mechanism of this reaction has been examined and is consistent with α-migration of one of the hydroxide hydrogen atoms to a uranium center followed by elimination of hydrogen.

The ground state of $[(Me_3Si)_2C_5H_3]_3M$ M = Nd, U and their base adducts has been examined by variable temperature magnetic susceptibility and by EPR spectroscopy. The ground state is found to be $^4I_{9/2}$ with a crystal field state consisting largely of $J_z = 1/2$ lowest. This observation is in agreement with previous studies on tris-cyclopentadienylneodymium complexes.

The zirconium metallocene, Cp_3Zr, has been prepared, characterized crystallographically, and its reactivity has been studied. Its chemical behavior is controlled by the presence of an electron in the non-bonding d_z2 orbital which prevents the formation of base adducts of Cp_3Zr, but allows Cp_3Zr to abstract atoms from other molecules.

The electonic and EPR spectra of a series of Cp^*_2TiX complexes, where Cp* is Me_5C_5 and X is a monodentate, anionic ligand such as halide, have been studied. From these data, a π-bonding spectrochemical series is developed, and the trends in π-bonding ability are found to be similar to those in other inorganic complexes.

The β-agostic interactions in Cp^*_2TiEt and $Cp^*_2TiN(Me)Ph$ have been examined using variable temperature EPR spectroscopy, and the enthalpy and entropy of the interaction have been determined. In Cp^*_2TiEt, the enthalpy of the β-agostic interaction is -1.9 kcal/mol.

The titanocene anion, $Cp^*_2TiLi(TMEDA)$ (TMEDA is N,N,N',N'-tetramethyl-ethylenediamine), has been prepared and its molecular structure and electronic structure have been determined. Some of its reaction chemistry has been explored, and $Cp^*_2TiLi(TMEDA)$ appears to act mainly as a strong reducing agent towards other molecules.

Introduction

Trivalent metallocenes have been known since the advent of organometallic chemistry. The first trivalent metallocene, ferricinium cation, was reported by Wilkinson and Woodward in 1952.[1] The first trivalent bent metallocenes were the tris-cyclopentadienyl complexes of scandium, yttrium, lanthanum, and the lanthanides.[2,3] Along with titanium, niobium, tantalum, and uranium, these complexes make up the bulk of known trivalent bent metallocenes. Examples are also known for zirconium, hafnium, technetium, and rhenium.

Trivalent bent metallocenes fall into two distinct structural types: tris-(η^5-cyclopentadienyl) complexes, exemplified by $(\eta^5\text{-Cp})_3Y$ (Cp is C_5H_5),[4] and di-(η^5-cyclopentadienyl) complexes, of which $(\eta^5\text{-Cp}^*)_2TiCl$ (Cp* is C_5Me_5) is an example.[5] Among the f-elements, the prevalent structural motif is tris-(η^5-cyclopentadienyl). Tris-(η^5-cyclopentadienyl) complexes or base adducts are known for all of the lanthanides and for thorium,[6] uranium,[7] neptunium,[8] plutonium,[9] americium,[10] curium,[11] berkelium,[12] and californium.[12] This structure is ubiquitous in the f-metal series for two reasons. First, the f-metals are large. The ionic radii of the lanthanides vary from 1.01 Å for 6 coordinate Ce(III) falling to 0.86 Å for 6-coordinate Lu(III).[13] The ionic radii of the actinides are, of course, larger; the ionic radius of 6-coordinate U(III) is 1.03 Å.[13] The large size of the f-elements allows three cyclopentadienyl ligands to bond in an η^5-manner without steric effects forcing one of the ligands to adopt a different mode of coordination. The second reason that this bonding mode is common is the presence of f-orbitals. Theoretical[14] and photoelectron spectroscopic studies[15] have suggested that d-orbitals rather than f-orbitals play a predominant role in bonding to ligands. Nonetheless, the f-orbitals play a vital role in the behavior of these complexes because they fill with electrons before the d orbitals.[14] Of the s, p, and d orbitals in a tris-(η^5-cyclopentadienyl) complex, only the d_z2 orbial (taking the 3 fold axis as z) is non-

bonding and available for valence electrons to occupy.[16] In the absence of f-orbitals, any complex having more than two valence electrons will be forced to place the additional electrons in high-lying metal - cyclopentadienyl antibonding orbitals. Rather than doing this, the complex is likely to rearrange so that one of the cyclopentadienyl ligands is no longer coordinated in an η^5-manner. Since, in the lanthanide and actinide series, the occupied f-orbitals are stabilized with respect to the d-orbitals, these complexes are able to retain the tris-(η^5-cyclopentadienyl) structure with up to 13 valence electrons (Cp_3Yb).

A corollary to the ubiquity of tris-(η^5-cyclopentadienyl) complexes among the f-elements is the scarcity of this structural type among the d-metals. Indeed, except for the "psuedolanthanides" yttrium and lanthanum, no trivalent transition metal complex having three η^5-cyclopentadienyl ligands has been described, but tetravalent zirconium and hafnium complexes having three η^5-cyclopentadienyl ligands are known.[17-19] While several tris-cyclopentadienyl complexes have been reported for the transition metals, the third cyclopentadienyl ligand is coordinated in an η^1-manner, as in Cp_3Sc,[20] Cp_3V,[21] Cp_3Tc,[22] and Cp_3Re,[23] or in an η^2-manner as in Cp_3Ti.[24] The small size of the first row metals, Sc, Ti, and V, is presumably responsible for the inability of these metals to form tris-(η^5-cyclopentadienyl) complexes. The d^4 electron count of Cp_3Tc and Cp_3Re would prevent the third ligand from having η^5-coordination for reasons explained earlier.

Among the d-metals, the most common structural motif for trivalent metallocenes is the typical bent sandwich structure $(\eta^5\text{-Cp})_2MX$ (X is a one electron ligand in the Green electron counting scheme). The electronic structure of these complexes has been investigated in several ways including by EPR[25,26] and photoelectron spectroscopy.[27] The model most consistent with these studies is, of course, the Lauher-Hoffmann model.[16] In this model, two non-bonding orbitals are available for filling with valence electrons, allowing complexes with up to four valence electrons to adopt this geometry.

While Cp_3Sc, Cp_3Ti, Cp_3V, Cp_3Re, and Cp_3Tc have three cyclopentadienyl ligands, they actually belong this structural type.

Curiously, the factors that make the tris-(η^5-cyclopentadienyl) complexes so prevalent among the lanthanides and actinides actually make the typical di-(η^5-cyclopentadienyl) bent sandwich structure unstable for the larger f-elements. The equilibrium shown in eq 1 lies to the right for M = Sm, Gd, Ho, Er, and Yb; it lies

$$2\,(\eta^5\text{-Cp})_3M + MCl_3 \rightarrow 3\,(\eta^5\text{-Cp})_2MCl \qquad (1)$$

somewhere in the middle for M = Nd; and lies to the left for M = La, Ce, Pr, and presumably for the actinides since Cp_2UCl and Cp_2UCl_2 are unknown.[28] By increasing the steric demand of the cyclopentadienyl ligands, the normal, bent sandwich structure can be stabilized with respect to ligand redistribution. For uranium, the bent metallocene chlorides $[Cp^*_2UCl]_3$,[29] $[Cp''_2UCl]_2$,[30] and $[Cp^{\ddagger}_2UCl]_2$[31] (Cp" is 1,3-$(Me_3Si)_2C_5H_3$, $Cp^{\ddagger}$ is 1,3-$(Me_3C)_2C_5H_3$) are known. The chemistry of these complexes is quite interesting. In addition to metathesis, they undergo one-electron oxidations as shown in eqs 2a[32] and b[29] or two-electron oxidations as shown in eq 3. [33]

$$[Cp''_2UCl]_2 + Ph_3P{=}S \rightarrow Cp''_2UCl_2 + 1/2\,[Cp''_2US]_2 + PPh_3 \qquad (2a)$$

$$2/3[Cp^*_2UCl]_3 + 2\,PhC{\equiv}CPh \longrightarrow Cp^*_2UCl_2 + Cp^*_2U\langle \text{Ph, Ph, Ph, Ph} \rangle \qquad (2b)$$

$$Cp^*_2UOAr + ONC_5H_5 \longrightarrow Cp^*_2U(OAr)(=O) \qquad (3)$$

Ar is 2,6-$^{i}Pr_2$-C_6H_3

Given the interesting behavior of these complexes, we examined the solution behavior of the $[Cp"_2UX]_2$ and $[Cp^{\ddagger}_2UX]_2$ (X is a halide) dimers especially with regard to ligand exchange. This work is described in chapter 1.

The tris-(η^5-cyclopentadienyl) complexes of uranium are interesting from a theoretical viewpoint. Calculations have suggested that a C_{3h} symmetric Cp'_3U complex (Cp' is a substituted cyclopentadienyl ligand) would have an f^2d^1 ground state.[14] The d^1 ground state of $Cp"_3Th$ would seem to support this assertion.[34] However, later calculations have suggested that the ground state is f^3.[35] In chapter 2, the ground state of $Cp"_3U$, $Cp"_3Nd$, and their base adducts is examined. In addition, we examine the reactivity of $(\eta^5\text{-}C_5H_5)_3Zr$ which is a C_{3h} symmetric d^1 complex, like $Cp"_3Th$.

Finally, in chapter 3, the π-bonding in Cp^*_2TiX complexes is examined. The electronic structure of these complexes allows the straightforward estimation of the π-donor ability of X, a monodentate, one-electron ligand. In addition, EPR spectroscopy is used to examine β-agostic interactions in Cp^*_2TiEt and in $Cp^*_2TiN(Me)Ph$. Finally, some reactivity of the Ti(I) anion $Cp^*_2TiLi(TMEDA)$ is described.

References

(1) Wilkinson, G.; Rosenblum, R.; Whiting, M. C.; Woodward, R. B. *J. Am. Chem. Soc.* **1952**, *74*, 2125-2126.

(2) Wilkinson, G.; Birmingham, J. M. *J. Am. Chem. Soc.* **1954**, *76*, 6210.

(3) Birmingham, J. M.; Wilkinson, G. *J. Am. Chem. Soc.* **1956**, *78*, 42-44.

(4) Adam, M.; Behrens, U.; Fischer, R. D. *Acta Cryst.* **1991**, *C47*, 968-971.

(5) Pattiasina, J. W.; Heeres, H. J.; van Bolhuis, F.; Meetsma, A.; Teuben, J. H. *Organometallics* **1987**, *6*, 1004-1010.

(6) Blake, P. C.; Lappert, M. F.; Atwood, J. L.; Zhang, N. *J. Chem. Soc., Chem. Commun.* **1986**, 1148-1149.

(7) Kanellakopulos, B.; Fischer, E. O.; Dornberger, E.; Baumgärtner, F. *J. Organomet. Chem.* **1970**, *24*, 507.

(8) Karraker, D. G.; Stone, J. A. *Inorg. Chem.* **1972**, *11*, 1742.

(9) Baumgärtner, F.; Fischer, E. O.; Kanellakopulos, B.; Laubereau, P. *Angew. Chem., Int. Ed.* **1965**, *4*, 878.

(10) Grisler, L. R.; Eggerman, W. G. *J. Inorg. Nucl. Chem.* **1974**, *36*, 1424.

(11) Baumgärtner, F.; Fischer, E. O.; Billich, H.; Dornberger, E.; Kanellakopulos, B.; Roth, W.; Steiglitz, L. *J. Organomet. Chem.* **1970**, *22*, C17.

(12) Laubereau, P. G.; Burns, J. H. *Inorg. Chem.* **1970**, *9*, 1091.

(13) Shannon, R. D. *Acta Cryst.* **1976**, *A 32*, 751.

(14) Bursten, B. E.; Rhodes, L. F.; Strittmatter, R. J. *J. Am. Chem. Soc.* **1989**, *111*, 2756-2758.

(15) Brennan, J. G.; Green, J. C.; Redfern, C. M. *J. Am. Chem. Soc.* **1989**, *111*, 2373-2377.

(16) Lauher, J. W.; Hoffmann, R. *J. Am. Chem. Soc.* **1976**, *98*, 1729-1742.

(17) Rogers, R. D.; Bynum, R. V.; Atwood, J. L. *J. Am. Chem. Soc.* **1978**, *100*, 5238-5239.

(18) Kopf, J.; Vollmer, H.-J.; Kaminsky, W. *Cryst. Struct. Commun.* **1980**, *9*, 985-990.

(19) Diamond, G. M.; Green, M. L. H.; Popham, N. A.; Chernega, A. N. *J. Chem. Soc., Dalton Trans.* **1993**, 2535-2536.

(20) Atwood, J. L.; Smith, K. D. *J. Am. Chem. Soc.* **1973**, *95*, 1488.

(21) Siegert, F. W.; Meijer, H. J. d. *J. Organomet. Chem.* **1968**, *15*, 131-137.

(22) Apostolidis, C.; Kanellakopulos, B.; Maier, R.; Rebizant, J.; Ziegler, M. L. *J. Organomet. Chem.* **1990**, *396*, 315-326.

(23) Apostolidis, C.; Kanellakopulos, B.; Maier, R.; Rebizant, J.; Ziegler, M. L. *J. Organomet. Chem.* **1991**, *409*, 243-254.

(24) Lucas, C. R.; Green, M. L. H.; Forder, R. A.; Prout, K. W. *J. Chem. Soc., Chem. Commun.* **1973**, 97.

(25) Petersen, J. L.; Dahl, L. F. *J. Am. Chem. Soc.* **1975**, *97*, 6416-6422.

(26) Petersen, J. L.; Dahl, L. F. *J. Am. Chem. Soc.* **1975**, *97*, 6422-6433.

(27) Green, J. C.; Payne, M. P.; Teuben, J. H. *Organometallics* **1983**, *2*, 203-210.

(28) Maginn, R. E.; Manastyrsky, S.; Dubeck, M. *J. Am. Chem. Soc.* **1963**, *85*, 672-676.

(29) Fagan, P. J.; Manriquez, J. M.; Marks, T. J.; Day, C. S.; Vollmer, S. H.; Day, V. W. *Organometallics* **1982**, *1*, 170-180.

(30) Blake, P. C.; Lappert, M. F.; Taylor, R. G.; Atwood, J. L.; Hunter, W. E.; Zhang, H. *J. Chem. Soc., Chem. Commun.* **1986**, 1394-1395.

(31) Zalkin, A.; Stuart, A. L.; Andersen, R. A. *Acta. Cryst.* **1988**, *C44*, 2106-2108.

(32) Beshouri, S. M., Unpublished results

(33) Arney, D. S.; Burns, C. J. *J. Am. Chem. Soc.* **1993**, *115*, 9840-9841.

(34) Kot, W.; Shalimoff, G.; Edelstein, N.; Edelman, M.; Lappert, M. F. *J. Am. Chem. Soc.* **1988**, *110*, 986-987.

(35) Bursten, B. E.; Strittmatter, R. J. *Angew. Chem., Int. Ed. Engl.* **1991**, *30*, 1069-1085.

Chapter One: Dicyclopentadienyluranium(III) Chemistry

Inorganic uranium compounds exist in oxidation states 3 through 6; however, organometallic chemistry of uranium has chiefly focused on the uranium(IV) compounds. From the first organometallic uranium complex, Cp_3UCl ($Cp = C_5H_5$), prepared by Wilkinson in 1956[1], through uranocene, prepared by Streitwieser in 1968[2], to $Cp^*_2UCl_2$ ($Cp^* = C_5Me_5$), prepared by Marks in 1978[3], the most prominent and well studied organouranium compounds have been in the +4 oxidation state.

This is not to say that other oxidation states have been ignored. A few U(VI) organometallic complexes are known, $Cp^*_2U(NPh)_2$ being the most prominent.[4] Several U(V) organometallic compounds of the type Cp_3UNR (R = $SiMe_3$, CMe_3, or aryl) are known.[5-7] Many uranium(III) compounds have also been prepared, but most of these are $Cp_3U(L)$ where L is a Lewis base.[8-10] Compounds of the type Cp_2UX (X = halide or other one electron ligand) are known only for the bulky Cp^*[11,12] and Cp" [13] (Cp" = 1,3-$(Me_3Si)_2C_5H_3$) ligands. Unfortunately, the Cp^*_2UX (X = halide or other one electron ligand) complexes are insoluble in aliphatic hydrocarbon solvents. The $Cp"_2UX$ complexes, on the other hand, are hydrocarbon soluble and fairly easily prepared. Additionally, the Cp" ligand, unlike Cp*, is anisotropic and its NMR spectra can potentially yield more information.

The $[Cp"_2UX]_2$ dimers in which X = Cl, Br, and I have been reported previously,[13] and a number of additional $Cp"_2UX$ complexes had been synthesized by Beshouri.[14] In addition, Stewart had made some of the analogous $Cp^‡_2UX_2$ and $[Cp^‡_2UX]_2$ complexes ($Cp^‡$ = 1,3-$(Me_3C)_2C_5H_3$, X = Cl, Me).[15] Initially, we hoped to extend the $[Cp^‡_2UX]_2$ series to include all of the halides and examine the behavior of the $[Cp"_2UX]_2$ and $[Cp^‡_2UX]_2$ dimers in solution. Additionally, we wanted to compare the reactivity of compounds bearing the $Cp^‡$ ligand to the analogous Cp" and Cp* complexes.

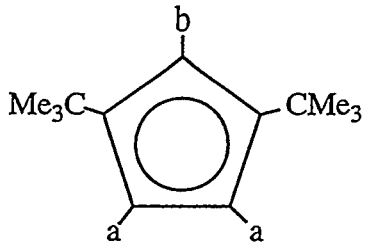

Cp‡

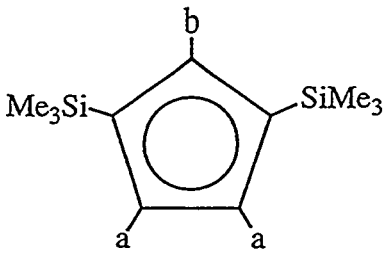

Cp"

1a: Dicyclopentadienyluranium(IV) Dihalides and Related Complexes

In order to synthesize the desired U(III) bridging halides, $[Cp"_2UX]_2$ and $[Cp^{‡}_2UX]_2$, where X = F, Cl, Br, I, the corresponding U(IV) dihalides had to be prepared. The dichlorides were prepared by treating UCl_4 with $Cp^{‡}_2Mg$ or $Cp"_2Mg$ in diethyl ether followed by crystallization from hexane as shown in eq 1a.1 Both dichlorides, $Cp"_2UCl_2$ (**1**)[13] and $Cp^{‡}_2UCl_2$ (**2**)[15], have been previously prepared.

$$UCl_4 + Cp^{‡}_2Mg \longrightarrow Cp^{‡}_2UCl_2\ (\mathbf{1}) + MgCl_2$$
$$UCl_4 + Cp"_2Mg \longrightarrow Cp"_2UCl_2\ (\mathbf{2}) + MgCl_2 \qquad (1a.1)$$

The molecular structure of **2** is shown in Figure 1a.1, and interesting bond lengths and distances are given in Table 1a.1. The molecule is a monomer with crystallographic C_2 symmetry and staggered cyclopentadienyl ligands. The bulky $SiMe_3$ groups are close to eclipsed, and both Cp" ligands point towards the front of the bent metallocene wedge, defining the b proton as the front of the Cp" (or $Cp^{‡}$) ligand and the a protons as the back. In comparison to $Cp^*_2UCl_2$,[16] the U-Cl bond length in **2** is 0.01 Å shorter and the U-$\langle C_{ring}\rangle$ distance in **2** is 0.04 Å longer; however, these numbers are not statistically significant. The only major difference is in the Cp-U-Cp bond angle

which is 132° in $Cp^*_2UCl_2$, presumably larger than in 2 due to nonbonded Me-Me contacts between the two Cp* ligands at the back of the metallocene wedge.

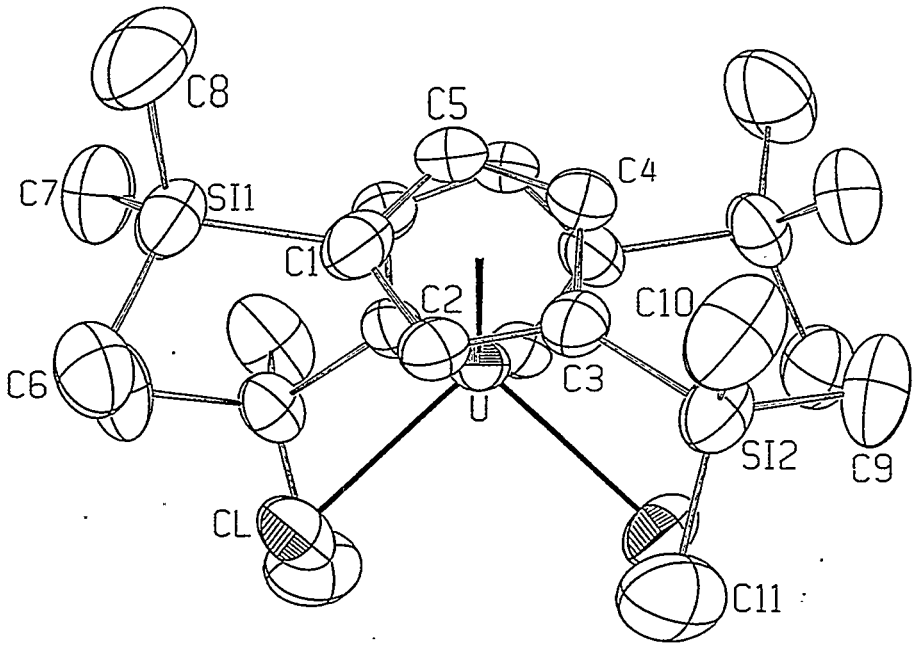

Figure 1a.1: An ORTEP of Cp''_2UCl_2 (2) with 50% thermal ellipsoids

Table 1a.1: Some distances and angles in Cp''_2UCl_2 (2)

Distances		Angles	
U-Cl	2.573(1) Å	Cp-U-Cp'	124.7°
U-⟨C_{ring}⟩	2.71(2) Å	Cl-U-Cl'	95.2(2)°
U-Cp	2.42 Å		

In this table, and in all other tables, Cp is the centroid of the cyclopentadienyl ligand.

The diiodides and dibromides were synthesized by treating the dichlorides, **1** and **2**, with trimethylsilyl halide in diethyl ether (eq 1a.2). Like the dichlorides, the diiodides and dibromides are quite soluble in hexane from which they were crystallized. Compounds **4** and **6** were previously prepared by treating **2** with BBr_3 and BI_3, respectively.[13]

$$Cp^{\ddagger}_2UCl_2 + Me_3SiX \longrightarrow Cp^{\ddagger}_2UX_2 \text{ (3, X=Br; 5, X = I)} + Me_3SiCl \quad \text{(1a.2)}$$

$$Cp''_2UCl_2 + Me_3SiX \longrightarrow Cp''_2UX_2 \text{ (4, X=Br; 6, X = I)} + Me_3SiCl$$

However, this sythetic route did not yield the corresponding difluorides. The failure to prepare difluorides by this route appears to contradict the thermochemistry for this system. For UF_4, the F_3U-F bond strength is 147 kcal/mol versus the Cl_3U-Cl bond strength of 100 kcal/mol, and for Me_3SiF, the Si-F bond strength is 135 kcal/mol versus the Me_3Si-Cl bond strength of 98 kcal/mol. This reaction is expected to be exothermic by about 10 kcal/mol. However, the assumption that the difference between the U-X energies in the tetrahalides is the same as the difference between the U-X energies in the metallocenes is poor. In the tetrahalides, especially UF_4, the inductive effect of the halide ligands will greatly increase the ionic contribution to the bonding similar to the trend in the C-F bond strengths of fluoromethanes.

The fluorides were prepared in a manner analogous to the synthesis of Cp_2MF_2 where M = Ti, Zr, or Hf.[17] Treating $Cp^{\ddagger}_2UMe_2$[15] with BF_3•OEt_2 in diethyl ether gave $Cp^{\ddagger}_2UF_2$ (**7**), and treating $Cp''_2U(NMe_2)_2$[18] with BF_3•OEt_2 in diethyl ether gave Cp''_2UF_2 (**8**) (eq 1a.3).

$$Cp^{\ddagger}_2UMe_2 + BF_3{\bullet}OEt_2 \longrightarrow Cp^{\ddagger}_2UF_2\ (7) + MeBF_2 \qquad (1a.3)$$

$$Cp"_2U(NMe_2)_2 + BF_3{\bullet}OEt_2 \longrightarrow Cp"_2UF_2\ (8) + Me_2NBF_2$$

Table 1a.2: ^1H NMR values for the dicyclopentadienyluranium dihalides. The Full Width at Half Maximum (FWHM) of the NMR peaks are given in parentheses in Hz.

	δ of Me_3X (X=C or Si)	δ of a_2 protons	δ of b proton	Color
$Cp^{\ddagger}_2UF_2$ (7)	-1.38(24)	-16.55(36)	-9.61(30)	yellow
$Cp^{\ddagger}_2UCl_2$ (1)	0.31(5)	-40.91(14)	97.36(15)	red
$Cp^{\ddagger}_2UBr_2$ (3)	1.54(15)	-43.85(45)	105.56(38)	red
$Cp^{\ddagger}_2UI_2$ (5)	3.69(13)	-46.20(43)	108.31(64)	orange
$Cp"_2UF_2$ (8)	-0.76(2)	-14.61(9)	-16.14(13)	green
$Cp"_2UCl_2$ (2)	-2.60(5)	-34.24(15)	90.46(24)	orange
$Cp"_2UBr_2$ (4)	-1.60(8)	-36.23(24)	98.29(30)	orange
$Cp"_2UI_2$ (6)	-0.12(10)	-37.80(60)	101.30(60)	purple

The NMR values for the dihalides are listed in Table 1a.2. The difluorides differ from the other halides in a number of ways. First, while all of the heavier halides are red or orange, **7** is bright green and **8** is yellow. Second, their solubilities differ from the other halides; **7** is much more hexane soluble, and **8** is much less hexane soluble than any of the other dihalides. Finally, the ^1H NMR spectra of the difluorides are very different from that of the other dihalides. In the other halides, the chemical shift of the b proton varies between 90 and 108 ppm, and the chemical shift of the a proton varies between -34 and -46 ppm. For the difluorides, the magnitude of the chemical shift is much smaller, and the sign of the chemical shift of b is different.

The chemical shift of a proton in a paramagnetic complex can be written as shown in eq 1a.4 where δ_{dia} is the chemical shift of the same proton in an analogous

$$\delta_{para} = \delta_{dia} + \Delta_{dip} + \Delta_{con} \qquad (1a.4)$$

diamagnetic complex, a thorium complex in this case.[15] The contact term, Δ_{con}, is due to unpaired spin density at the proton (eq 1a.5) where the symbols have their usual

$$\Delta_{con} = \frac{1}{\mu_0} \cdot \frac{A_c}{\hbar \gamma_N \mu_b} \cdot \frac{g_J - 1}{g_J} \chi \qquad (1a.5)$$

meanings.[15] The dipolar term, Δ_{dip}, is due to the anisotropy of the magnetic field of the paramagnetic metal center as shown in eq 1a.6 where x,y, and z are the Cartesian

$$\Delta_{dip} = \frac{1}{2Nr^3} \cdot \frac{2}{3} \left\{ \chi_x \left[3\left(x^2/r^2\right) - 1 \right] + \chi_y \left[3\left(y^2/r^2\right) - 1 \right] + \chi_z \left[3\left(z^2/r^2\right) - 1 \right] \right\} \qquad (1a.6)$$

coordinates of the proton relative to the metal center at the origin, r is the distance from the proton to the metal center, and χ_x, χ_y and χ_z are the values of the magnetic susceptibility along the x, y and z axes, respectively.[19] In these complexes, the dipolar term is expected to dominate even for the ring protons since, in f-metal complexes, the contact term falls off rapidly with distance.[20] The chemical shift of a proton depends mainly on two factors: its position relative to the metal center (x, y, z, and r), and the electronic structure of the metal center (χ_x, χ_y, χ_z).

The difference in the NMR spectra of the difluorides relative to the other dihalides suggested that the difluorides possibly have a different molecular structure than the other dihalides; that is, x, y, and z of eq 1a.6 are different. To examine this possibility, the crystal structure of Cp''_2UF_2 was determined. An ORTEP drawing of **8** is shown in Figure 1a.2, and the important bonds and angles are give in Table 1a.3.

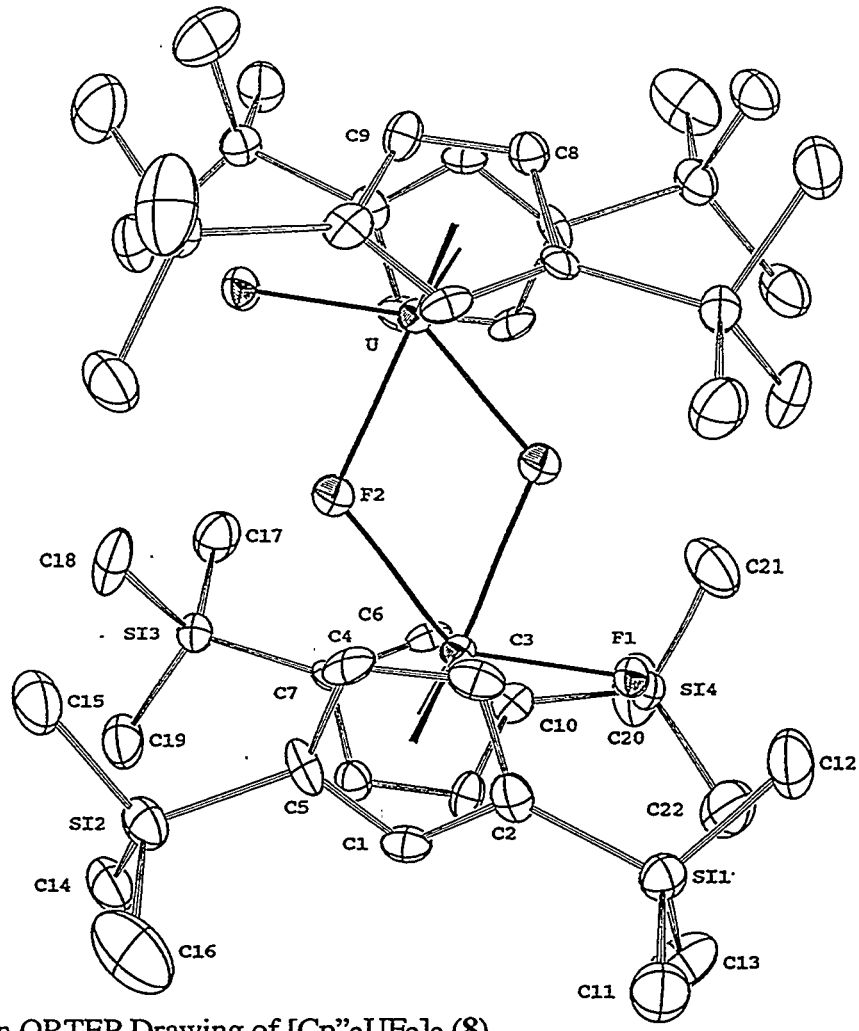

Figure 1a.2: An ORTEP Drawing of $[Cp''_2UF_2]_2$ (**8**)

Table 1a.3: Some distances and angles in $[Cp''_2UF_2]_2$ (**8**)

Distances		Angles	
U-F1	2.073(5) Å	Cp1-U-Cp2	126.3°
U-F2'	2.343(5) Å	F1-U-F2	75.6(2)°
U-F2	2.297(5) Å	F1-U-F2'	138.9(2)°
U-Cp1	2.48 Å	U-F2-U'	116.7(2)°
U-Cp2	2.47 Å	F2-U-F2'	63.3(2)°
U-U	3.9504(7) Å		
U-$\langle C_{ring} \rangle$	2.76(4) Å		

As seen in Figure 1a.2, the molecule is a dimer with inversion symmetry. In comparison to other known $[Cp"_2UX]_2$ dimers, the U-U distance is longer than that of $[Cp"_2UO]_2$ (3.39 Å), but shorter than that of $[Cp"_2UCl]_2$ or $[Cp"_2UBr]_2$ which are 4.36 Å and 4.34 Å, respectively.[13] The U-Cp centroid distances and average U-C_{ring} distances are very similar in all of these complexes although the uranium oxidation state is different.

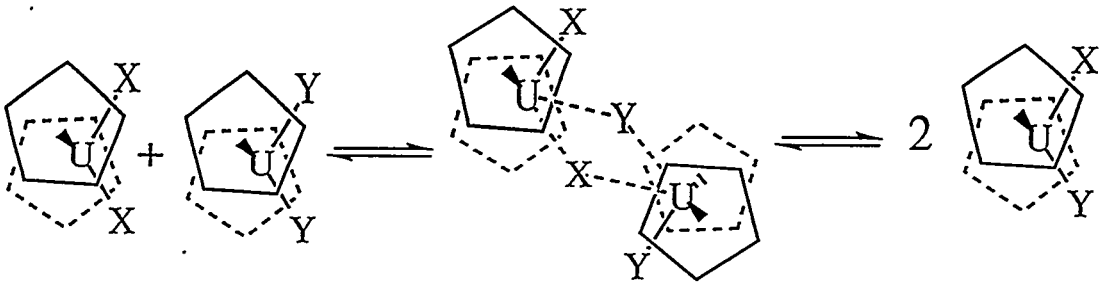

Scheme 1a.1: Potential Mechanism for Halide Exchange in U(IV) Metallocenes

The most interesting aspect of the crystal structure of **8** is that the molecule is a dimer. Uranium(IV) metallocenes are known to readily exchange ligands. For example, mixing $Cp^*_2UCl_2$ with $Cp^*_2UMe_2$ results in the formation of $Cp^*_2U(Me)Cl$.[21] The crystal structure of **8** suggests a possible transition state for this reaction. A potential mechanism for this exchange process is given in Scheme 1a.1.

For comparison, the crystal structure of **7** was also determined. A drawing of the molecule is given in Figure 1a.3, and interesting distances and angles are given in Table 1a.4. Unlike **8**, **7** is monomeric in the solid state. The molecule has crystallographically imposed C_2 symmetry, and the CMe_3 groups of the $Cp^‡$ ligands are eclipsed. Surprisingly, the U-F bond length for the terminal fluoride in **8** is slightly shorter than the U-F bond length in **7**, and the U-Cp distances and angles in the two molecules are almost identical. Dimerization does not seem to perturb the geometry of **8** to any great extent. The biggest difference between the two U(IV) fluorides is the conformation of the CMe_3 and $SiMe_3$ groups. In **7**, the b-protons of both ligands point

to the open part of the bent metallocene wedge, while in **8**, one set of b-protons points towards the front of the wedge and one set points towards the back.

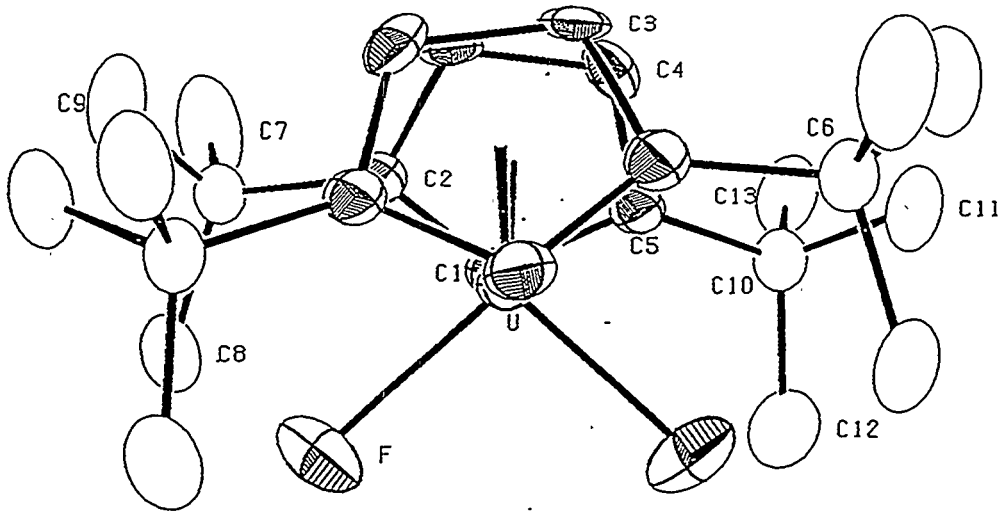

Figure 1a.3: An ORTEP drawing of $Cp^{\ddagger}_2UF_2$ (7)

Table 1a.4: Some distances and angles in $Cp^{\ddagger}_2UF_2$ (7)

Distances		Angles	
U-F1	2.086(2) Å	Cp-U-Cp	125.3°
U-$\langle C_{ring} \rangle$	2.74(3) Å	F-U-F	95.4(2)°
U-Cp	2.46 Å		

While the structures of the molecules differ in the solid state, it was thought that, in solution, their structures might be similar which would account for the differences between the NMR spectra. To investigate this possibility, the variable temperature NMR behavior of **7** and **8** was examined. A plot of the chemical shifts of the protons of **8**

versus 1/T is shown in Figure 1a.4. At -100 °C, four $SiMe_3$ peaks of equal area with chemical shifts of 41.54, 32.72, 29.85, and -33.02 ppm can be observed for **8**. These peaks coalesce to a single peak at -40 °C. The observation of four chemically inequivalent $SiMe_3$ groups is consistent with the solid state structure since the molecule possess only inversion symmetry.

The average of the chemical shifts of the $SiMe_3$ groups at low temperature is not close to the chemical shift of the $SiMe_3$ groups above the coalescence temperature. In other words, **8** does not obey Curie-Weiss behavior. One explanation for this observation is that a rapid monomer-dimer equilibrium is present. Since the equilibrium constant for such an equilibrium would change with temperature ($\Delta S^\circ \neq 0$), and since the chemical shift of the monomer is unlikely to be the same as that of the dimer, the chemical shift would not vary linearly with 1/T since the monomer-dimer ratio would change with temperature. Similar behavior is observed for $(MeC_5H_4)_3Nd$[22] and $(MeC_5H_4)_3Ce$[23] in which monomers and tetramers are in equilibrium.

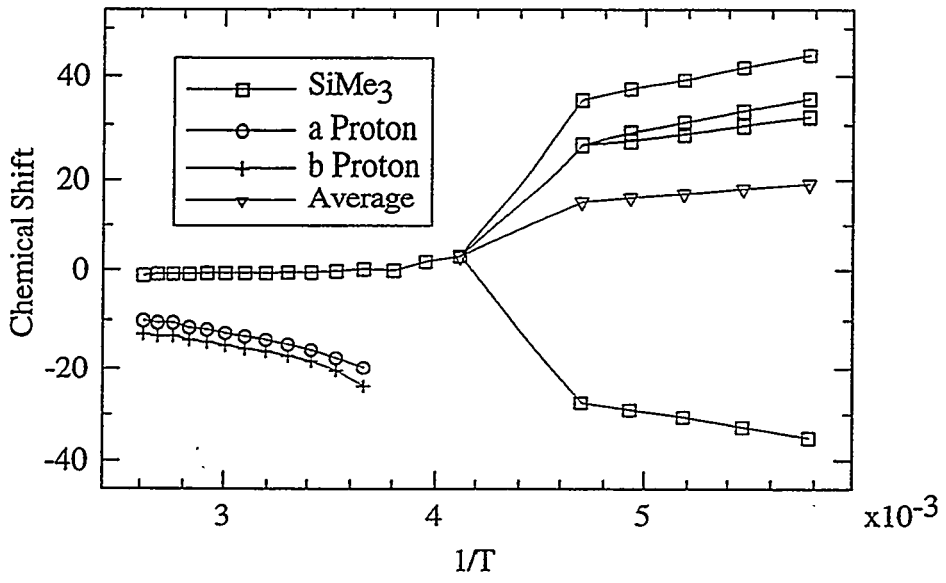

Figure 1a.4: Variable Temperature NMR Behavior of the Protons of $[Cp''_2UF_2]_2$ (**8**)

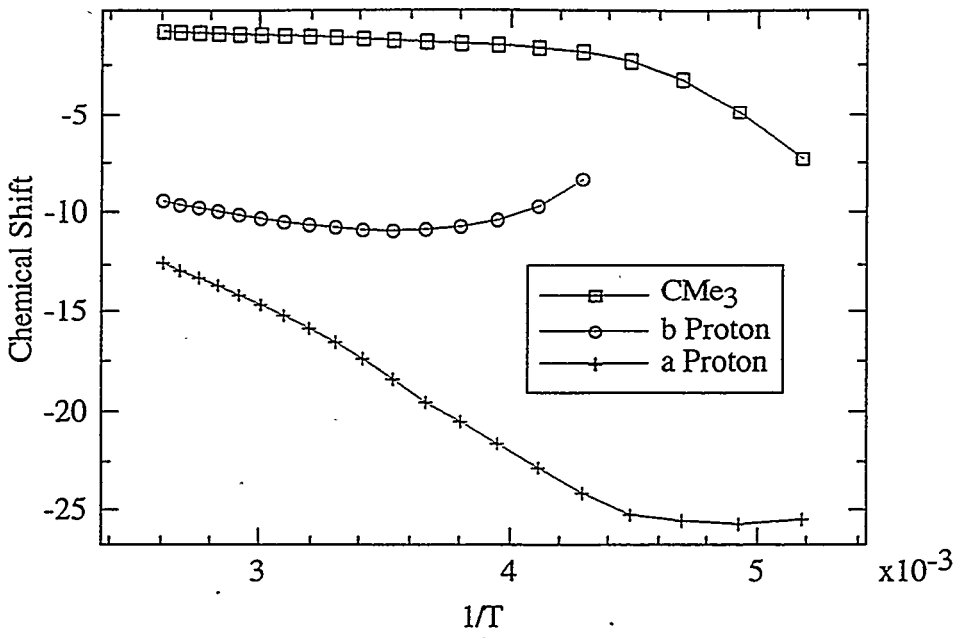

Figure 1a.5: Variable Temperature NMR Behavior of the Protons of $Cp^{\ddagger}_2UF_2$ (7)

The variable temperature NMR behavior of **7**, shown in Figure 1a.5, is slightly different. At -100 °C, two very broad resonances are observed which coalesce at -90 °C (not shown in Figure 1a.5). As seen in Figure 1a.5, the chemical shifts of the protons do not obey Curie-Weiss behavior. Again, a possible explanation is that **7** is undergoing a monomer-dimer equilibrium in solution. This explanation is supported by the observation of a similar equilibrium in Cp_3UF.[24] However, the solution structure of **7** would have to be different from that of **8** to explain the presence of two sets of inequivalent CMe_3 groups in **7** versus four sets of inequivalent $SiMe_3$ groups in **8**. Several structures could be postulated for **7**, but we cannot distinguish among them.

Table 1a.5: ^{1}H NMR values for some U(IV) metallocene complexes. FWHM values of the peaks are given in parentheses in Hz. (FWHM = Full Width at Half Maximum)

	δ of Me_3X (X=C or Si)	δ of a_2 protons	δ of b proton	δ of other protons
$Cp^{‡}_2UMe_2$	-0.64 (6)	-39.02 (9)	18.18(12)	-35.43 (14) U-Me
$Cp"_2UMe_2$	-1.19 (3)	-28.42(6)	7.61(6)	-21.03 (7) U-Me
$Cp^{‡}_2U-(CH_2SiMe_3)_2$	-0.50(15)	-30.89(30)	11.93(25)	2.80(9) CH_2SiMe_3 -55.93(45) CH_2SiMe_3
$Cp^{‡}_2U(Me)Cl$	3.46(4) -3.82(4)	-29.52(12) -41.78(10)	55.6(12)	-52.42(20) U-Me
$Cp"_2U(Me)Cl$	0.14(3) -3.77(3)	-25.62(8) --32.00(8)	46.82(9)	-49.90(20) U-Me
$Cp^{‡}_2U(OMe)_2$	-1.56(5)	-25.89(8)	-9.02(5)	37.12(5) U-OMe
$Cp"_2U(OMe)_2$	-1.24(3)	-25.09(4)	-10.75(4)	46.32(4) U-OMe
$Cp"_2U(NMe_2)_2$	0.07(3)	-10.82(11)	-5.70(6)	9.82(5) NMe_2

Since **8** has terminal and bridging fluoride ligands, the site exchange between them is an interesting possibility. Unfortunately, the resonance of a nucleus bound directly to a paramagnetic metal is expected to be very broad and difficult to detect making ^{19}F NMR useless. For this reason, the NMR behavior of the analogous dimethoxides, $Cp^{‡}_2U(OMe)_2$ (**9**), and $Cp"_2U(OMe)_2$ (**10**) was examined. It seemed possible that **10**, at least, could dimerize in the same manner as **7**. At room temperature, the ^{1}H NMR spectra of **9** and **10** resemble those of the difluorides in that the chemical shifts for the a_2 and b protons are small. The ^{1}H NMR values for **9** and **10** and for some other U(IV) metallocenes is given in Table 1a.5. $Cp"_2UMe_2$ and $Cp"_2U(Me)Cl$ were first made by Beshouri [14] and $Cp"_2U(NMe_2)_2$[18] was briefly mentioned by Lappert and coworkers.

The variable temperature NMR behavior of **9** and **10** is shown in Figures 1a.6 and 1a.7, respectively. The protons of both compounds show Curie-Weiss behavior, and in both complexes, the CMe_3 or $SiMe_3$ resonances decoalesce at low temperatures; for **9**, the chemically inequivalent CMe_3 groups never grow back (presumably, the barrier is too low). In **10**, two inequivalent $SiMe_3$ groups and two inequivalent a protons are observed below the coalescence temperature of -70 °C. The barrier to site exchange is 8.5 kcal/mol when calculated using the chemical shifts of the $SiMe_3$ groups and 8.6 kcal/mol using the chemical shifts of the a protons, equal within the error of the measurement. In **9**, the peaks become broad at -100 °C. In both compounds, the methoxide and b proton resonances remain sharp throughout the temperature range examined. These observations are not consistent with a monomer-dimer equilibrium. Rather, they suggest that the molecules remain monomeric, and that the molecules have C_2 symmetry at low temperature. The C_2 symmetry makes the methoxide groups and b protons equivalent, but only makes two of the four $SiMe_3$ or CMe_3 groups equivalent.

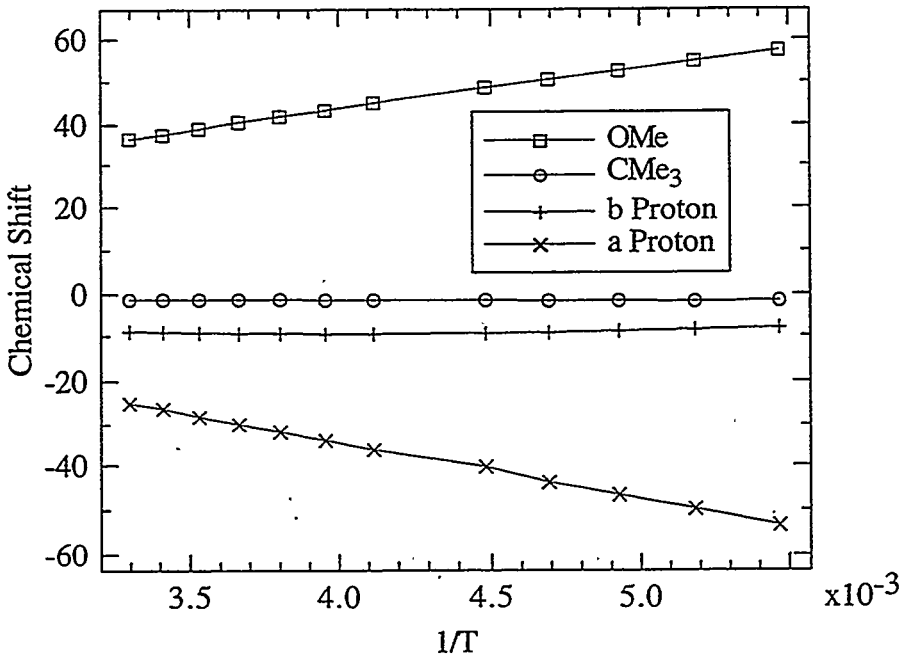

Figure 1a.6: Variable temperature NMR behavior of $Cp^{\ddagger}_2U(OMe)_2$ (**9**)

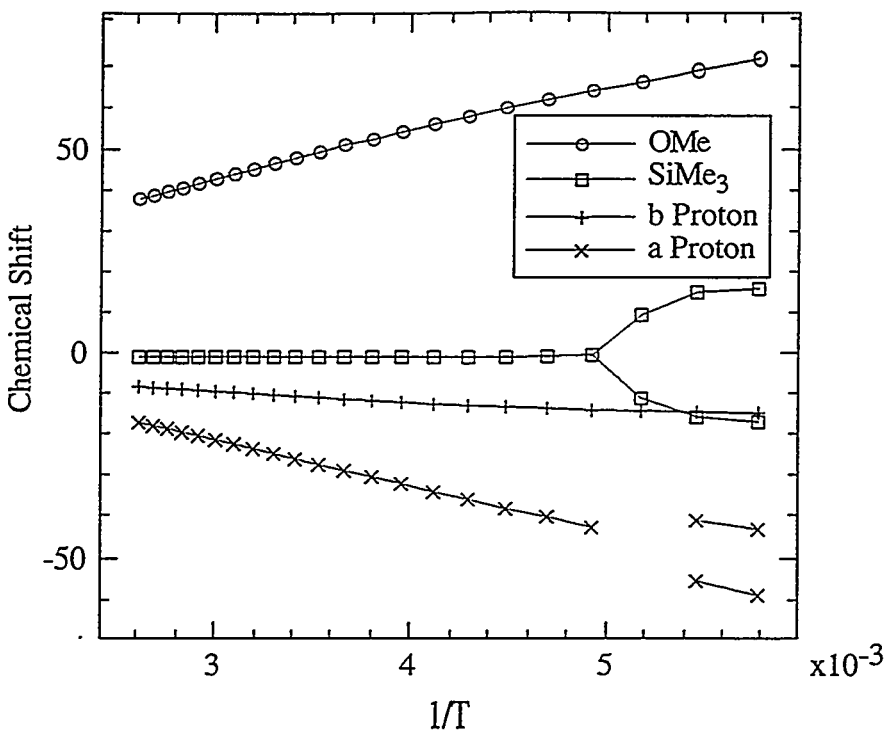

Figure 1a.7: Variable temperature NMR behavior of Cp"$_2$U(OMe) (**10**)

The evidence is consistent with a monomeric solution structure for the methoxides. Since these molecules have chemical shifts for the a_2 and b protons similar to those of the difluorides, the molecular structure of the difluorides is probably not responsible for their anomalous NMR spectra. The difference must then result from a difference in the electronic structures of the molecules. To examine this possibility, the variable temperature magnetic susceptibilities, χ, of Cp‡$_2$UCl$_2$ (**1**) and Cp‡$_2$UF$_2$ (**7**) were measured. Plots of $1/\chi$ versus T for **1** and **7** are shown in Figures 1a.8 and 1a.9, respectively. The magnetic moment was calculated using the Curie-Weiss equation, eq 1a.7.

$$\chi = C/(T-\theta)$$
$$\mu_{eff} = (8C)^{1/2} \qquad \text{(1a.7)}$$

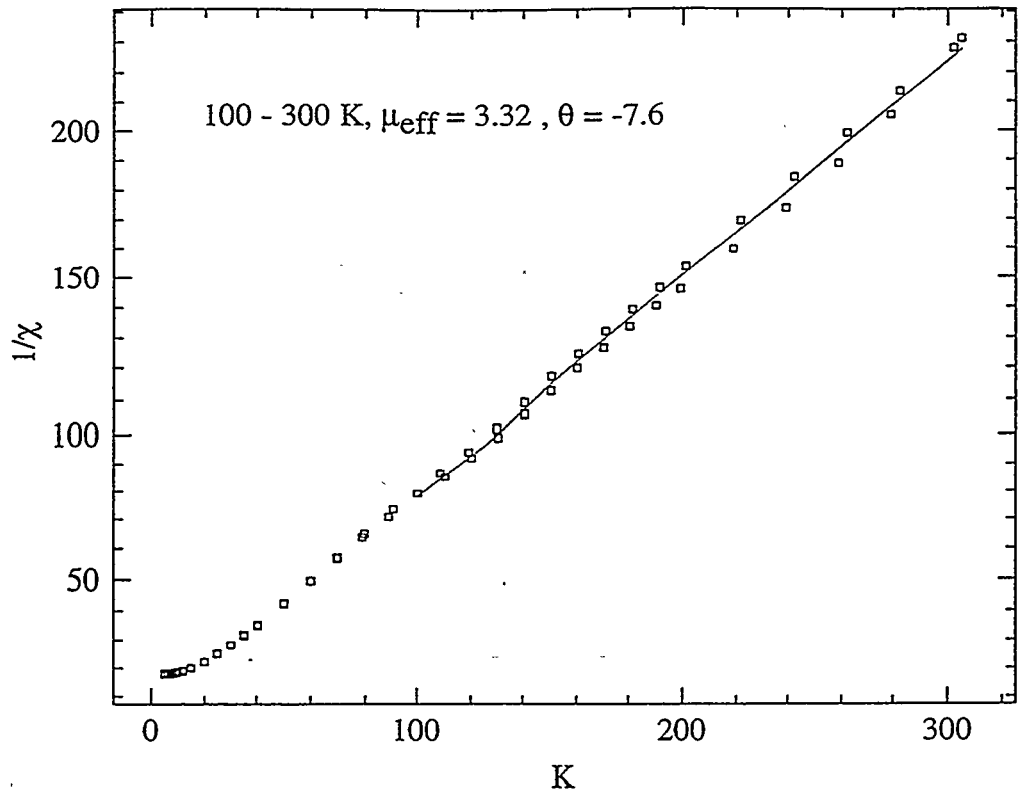

Figure 1a.8: Curie-Weiss plot of the magnetic susceptibility of $Cp^{\ddagger}_2UCl_2$ (**1**). The solid line is a linear least squares fit to the data.

Uranium(IV) is an f^2 ion and should have a $^3H_4$ ground state. Given the low symmetry of these complexes, this J = 4 manifold is expected to split into 9 singlets (J_z = -4,-3,...3,4) by the crystal field.[25] Only the lowest few states are expected to contribute to the magnetism of these complexes at room temperature because the splitting of the $^3H_4$ manifold is expected to be greater than 200 K.[25] In UF_4, the splitting is calculated to be 1775 cm^{-1}.[26] Therefore it is the χ_x, χ_y, and χ_z values of the low-lying states which contribute to the dipolar shift in the NMR spectra of these compounds. The different J_z states have different magnetic moments, and more importantly, different anisotropies.

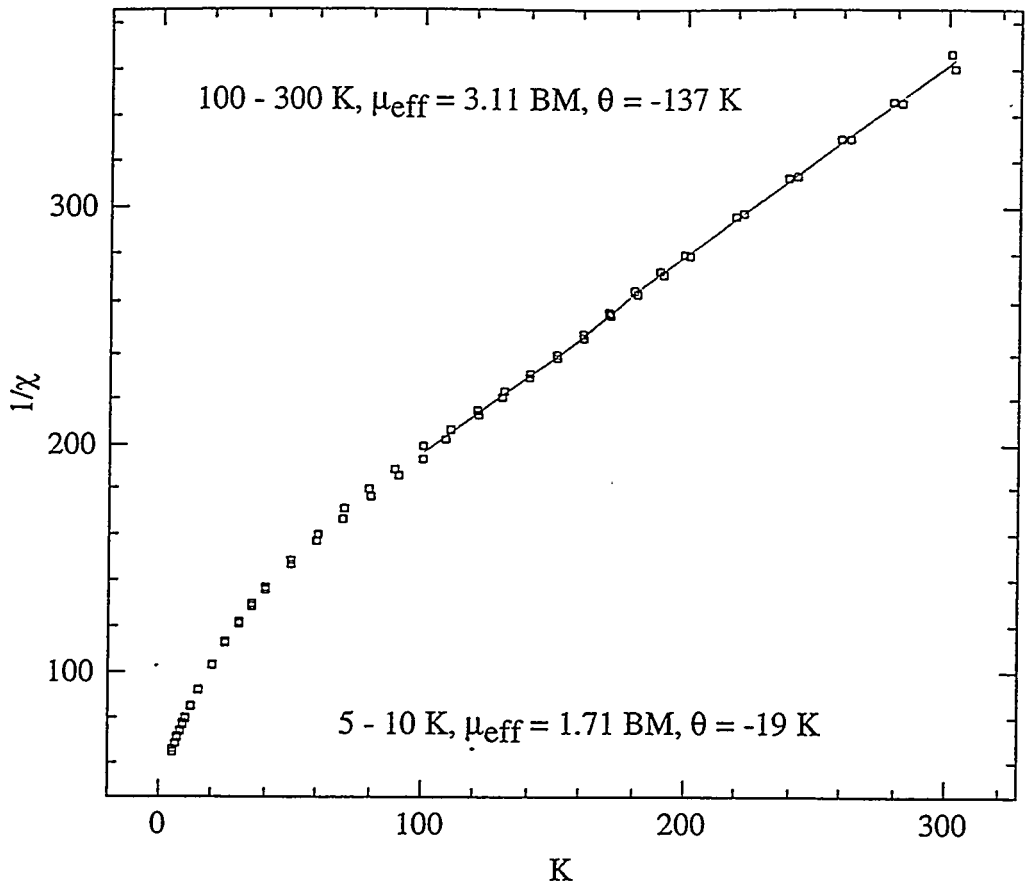

Figure 1a.9: Curie-Weiss plot of the magnetic susceptibility of $Cp^{\ddagger}_2UF_2$ (**7**). Solid lines are linear least squares fits to the data.

The ground states of **1** and **7** are clearly not the same. Below 10 K, **1** displays the temperature independent magnetism typical of an isolated singlet ground state found in many low symmetry U(IV) compoounds.[27] The low temperature susceptibility of **7**, on the other hand, shows that this complex has a magnetic ground state. This observation is somewhat surprising since the low symmetry of the complex removes any degeneracy in the $^3H_4$ manifold. Most likely, in **7**, the two lowest lying states are accidentally degenerate or nearly so. Due to the low symmetry of these complexes, the nature of their ground states was not investigated any further. The different electronic structure of the difluorides rather than their different molecular structure causes their NMR spectra to differ from the NMR spectra of the other dihalides.

In conclusion, the dicyclopentadienyluranium(IV) dihalides have been prepared. The NMR spectra of the difluorides are different from those of the other dihalides. Since the magnetic susceptibility of $Cp^{\ddagger}_2UF_2$ shows that its electronic structure is different from that of $Cp^{\ddagger}_2UCl_2$, the difference in the NMR spectra of the difluorides is attributed to a difference in electronic structure. The crystal structure of $[Cp''_2UF_2]_2$ shows that it is dimeric while the crystal structure of $Cp^{\ddagger}_2UF_2$ shows this complex to be monomeric. Additionally, the variable temperature spectra of $Cp^{\ddagger}_2UF_2$ and $[Cp''_2UF_2]_2$ do not obey Curie-Weiss behavior. This observation seems to imply that both difluorides exists as a mixture of monomers and dimers in solution.

1b: Dicyclopentadienyluranium(III) Bridging Halide Complexes

The initial reasons for examining the solution behavior of the dicyclopentadienyluranium(III) halides were to determine whether the molecules have the same structure in solution as in the solid state and whether the halides would exchange in solution. The syntheses of $[Cp"_2UX]_2$ [13] where X = Cl, Br, and I, and of $[Cp^{‡}_2UCl]_2$ [28] have been described previously. All of the bridging halides were synthesized by the same route, shown in eq 1b.1. The ^1H NMR values for the dimers are given in Table 1b.1. All of the molecules are dimeric in the gas phase by mass spectroscopy.

$$Cp^{‡}_2UX_2 + t\text{-BuLi} \xrightarrow{-LiX} [Cp^{‡}_2UX]_2 \text{ (}\mathbf{11}\text{, X=F; }\mathbf{13}\text{, X=Cl; }\mathbf{15}\text{, X=Br; }\mathbf{17}\text{, X = I)} \quad (1b.1)$$

$$Cp"_2UX_2 + t\text{-BuLi} \xrightarrow{-LiX} [Cp"_2UX]_2 \text{ (}\mathbf{12}\text{, X=F; }\mathbf{14}\text{, X=Cl; }\mathbf{16}\text{, X=Br; }\mathbf{18}\text{, X = I)}$$

Table 1b.1: Room temperature ^1H NMR values of U(III) halide dimers. The FWHM of each peak is given in Hz in parentheses.

Compound	Number	δ of Me_3X (X=C or Si)	δ of a_2 protons	δ of b proton
$[Cp^{‡}_2UF]_2$	**11**	-11.78(51)	Unobserved	
$[Cp^{‡}_2UCl]_2$	**13**	-6.66(36)	-51.62(400)	61.98(400)
$[Cp^{‡}_2UBr]_2$	**15**	-5.37(34)	-62.77(200)	76.64(300)
$[Cp^{‡}_2UI]_2$	**17**	-4.32(38)	-68.5(250)	86.9(400)
$[Cp"_2UF]_2$	**12**	-10.84(28)	Unobserved	
$[Cp"_2UCl]_2$	**14**	-9.01(11)	-2.61(140)	29.76(190)
$[Cp"_2UBr]_2$	**16**	-8.30(13)	-5.09(160)	35.49(120)
$[Cp"_2UI]_2$	**18**	-7.08(15)	-3.17(140)	41.62(170)

To determine whether the solution and solid state structures of the U(III) halide dimers are the same, the solid state structures of the complexes must be known. Lappert and coworkers determined the structures of $[Cp''_2UCl]_2$ (**14**) and $[Cp''_2UBr]_2$ (**16**).[13] The molecules are isostructural and have crystallographic C_i symmetry as shown in Figure 1b.1.

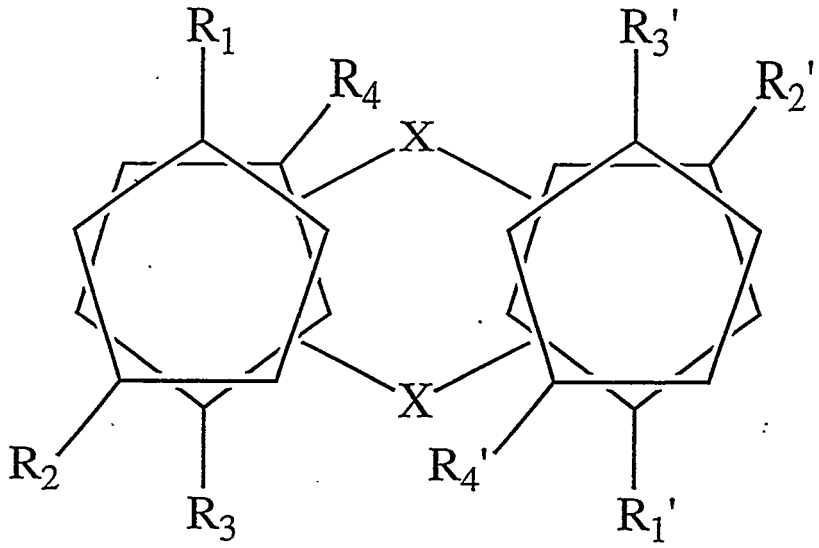

Figure 1b.1: Solid state structure of $[Cp''_2UX]_2$ (X = Br(**16**), Cl(**14**)) showing inversion symmetry. R is $SiMe_3$.

The only other U(III) bridging halide dimer which was structurally characterized is $[Cp^{\ddagger}_2UCl]_2$ (**13**).[28] Its solid state structure is different from that of $[Cp''_2UCl]_2$. The dimer, **13** has crystallographic 2-fold symmetry, but has D_2 idealized symmetry as shown in Figure 1b.2. The most important difference between the structures of **13** and **14** is the U-U distance which is almost 0.2 Å longer in **13** presumably due to the presence of 4 R groups (R_2) pointing towards the center of the dimer in **13** versus 2 (R_4) pointing towards the center in **14**.

The bridging fluoride, $[Cp''_2UF]_2$ (**12**) was also characterized by x-ray crystallography. The compound crystallizes with two crystallographically independent but virtually identical molecules in the asymmetric unit. An ORTEP diagram of one of the molecules is shown in Figure 1b.3, and important distances and angles are given in Table 1b.2. This molecule possess a solid state structure somewhat different from **14** or **16**. While all of these molecules have inversion symmetry, the idealized symmetry of **12** is C_{2h} as shown in Figure 1b.4. As in **13**, the biggest difference between the structure of **12** and that of **14** or **16** is the U-U distance which is over one angstrom shorter in **12**. The shortening of the U-U distance is presumably what forces the molecule to adopt a C_{2h} geometry rather than the C_i geometry seen in **14** and **16**.

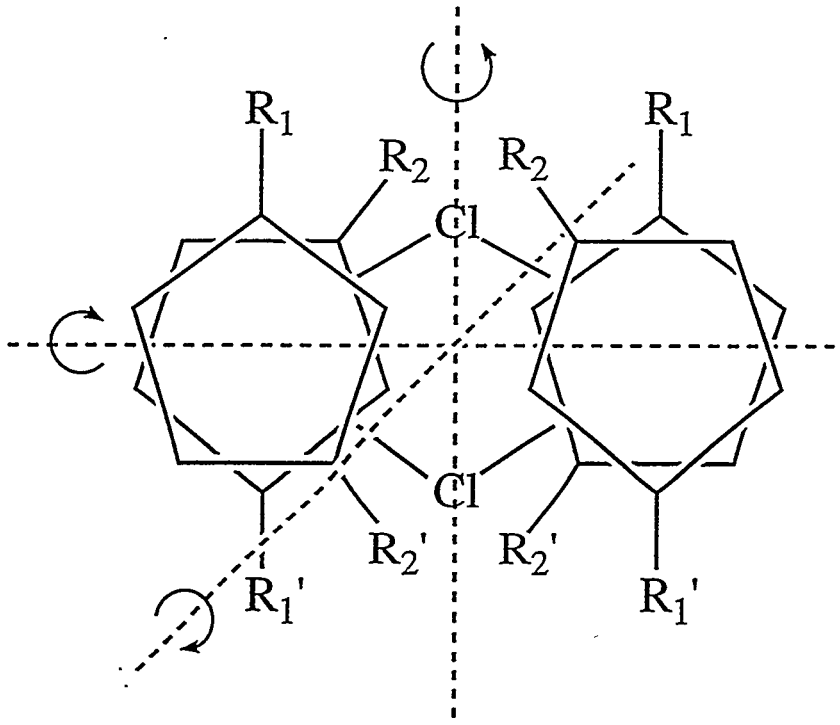

Figure 1b.2: Solid State Structure of $[Cp^{\ddagger}_2UCl]_2$ (**13**) Showing Idealized D_2 Symmetry. R is CMe_3.

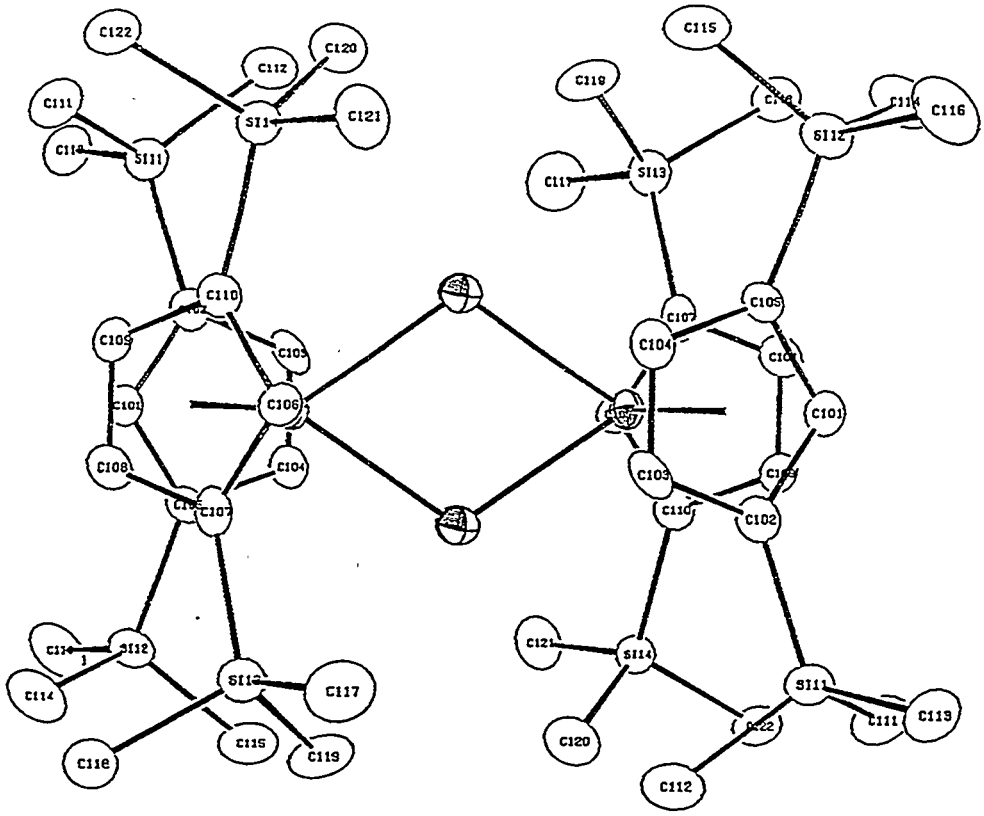

Figure 1b.3: An ORTEP drawing of $[Cp''_2UF]_2$ (**12**) with 50% thermal ellipsoids

Table 1b.2: Some distances and angles in $[Cp''_2UF]_2$ (**12**)

Molecule 1		Molecule 2	
U1-U1	2.8446(4) Å	U2-U2	3.8508(4) Å
U1-F1	2.331(3) Å	U2-F2	2.334(3) Å
U1-F1'	2.332(3) Å	U2-F2'	2.333(3) Å
U1-Cp11	2.49 Å	U2-Cp21	2.49 Å
U2-Cp12	2.49 Å	U2-Cp22	2.49 Å
U1-$\langle C_{ring} \rangle$	2.766(8) Å	U2-$\langle C_{ring} \rangle$	2.768(9)
F1-U1-F1	68.9(1)°	F2-U2-F2	68.8(1)°
U1-F1-U1`	111.1(1)°	U2-F2-U2	111.2(1)°
Cp11-U1-Cp12	130.4°	Cp21-U-Cp22	129.7°

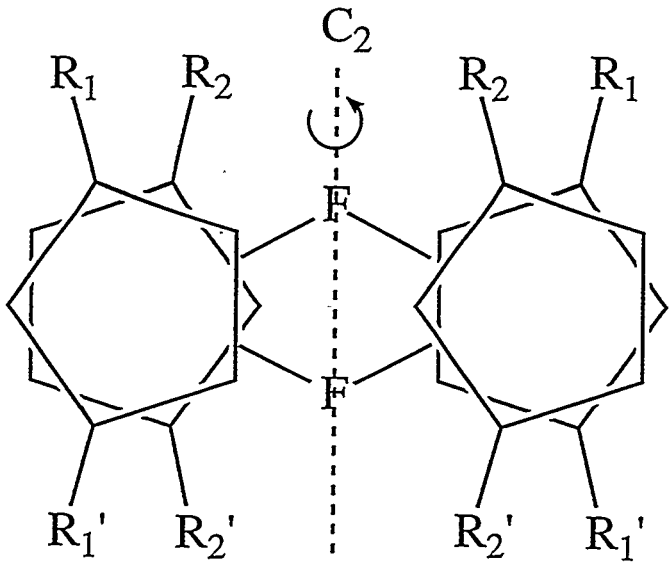

Figure 1b.4: Idealized C_{2h} symmetry of $[Cp"_2UF]_2$ (**12**)

If the molecules have the same structure in solution as shown in the crystal structures, then, at low temperatures, four distinct $SiMe_3$ groups should be seen in the NMR spectra of **14**, **16**, and presumably **18** since, in the solid state, these complexes have C_i symmetry. Complexes **12**, **13**, and, presumably, **15** and **17** should all have 2 inequivalent sets of R groups at low temperature since these molecules are all in point groups with four symmetry operations. In every case in which the solid state structure is known and where the ring rotation can be frozen out, the low temperature spectrum is consistent with the solid state structure. For **18**, apparently, the coalescence temperature is lower than -95 °C since only one $SiMe_3$ resonance was observed down to this temperature. Plots of δ versus 1/T are shown in Figures 1b.5 - 1b.12.

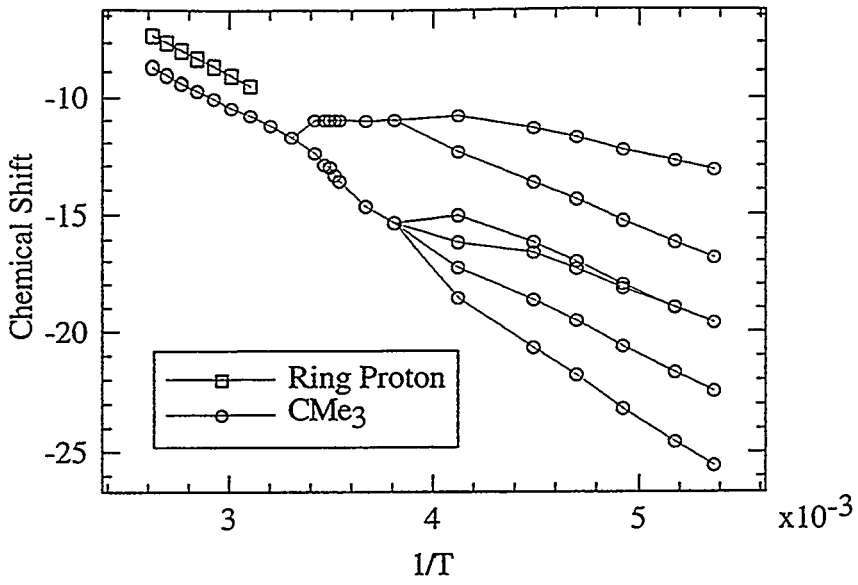

Figure 1b.5: Chemical shift of the protons of $[Cp^{\ddagger}_2UF]_2$(**11**) versus temperature (whether the ring proton is a_2 or b is not known)

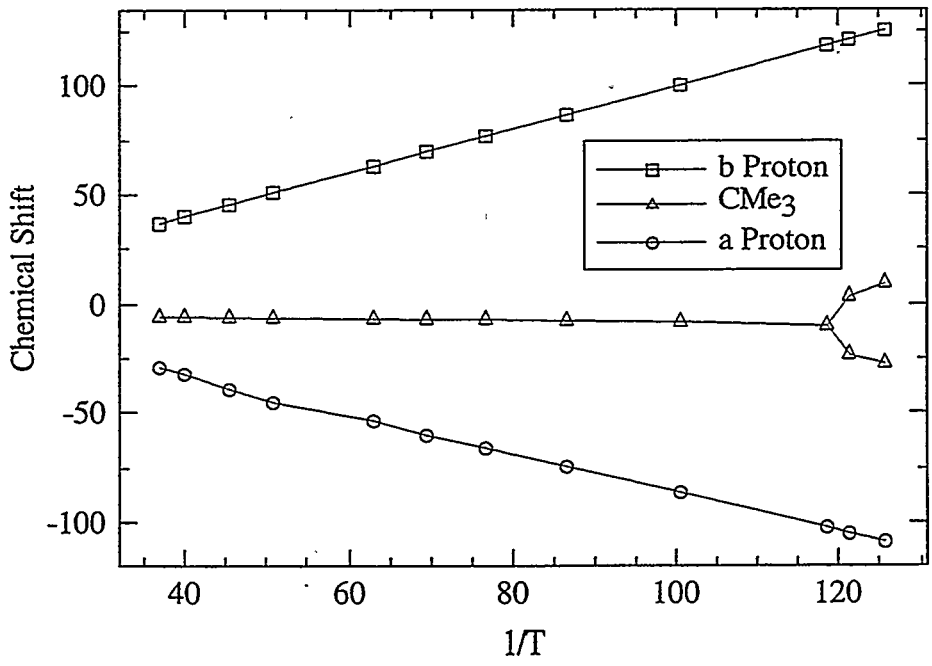

Figure 1b.6: Chemical shift of the protons of $[Cp^{\ddagger}_2UCl]_2$(**13**) versus temperature

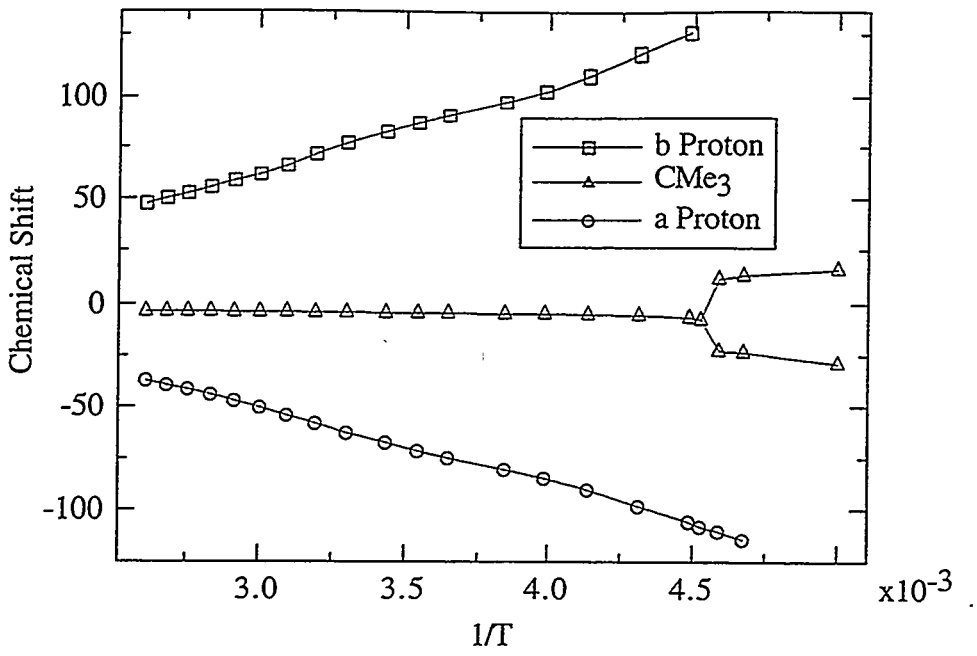

Figure 1b.7: Chemical shift of the protons of $[Cp^{\ddagger}_2UBr]_2$(**15**) versus temperature

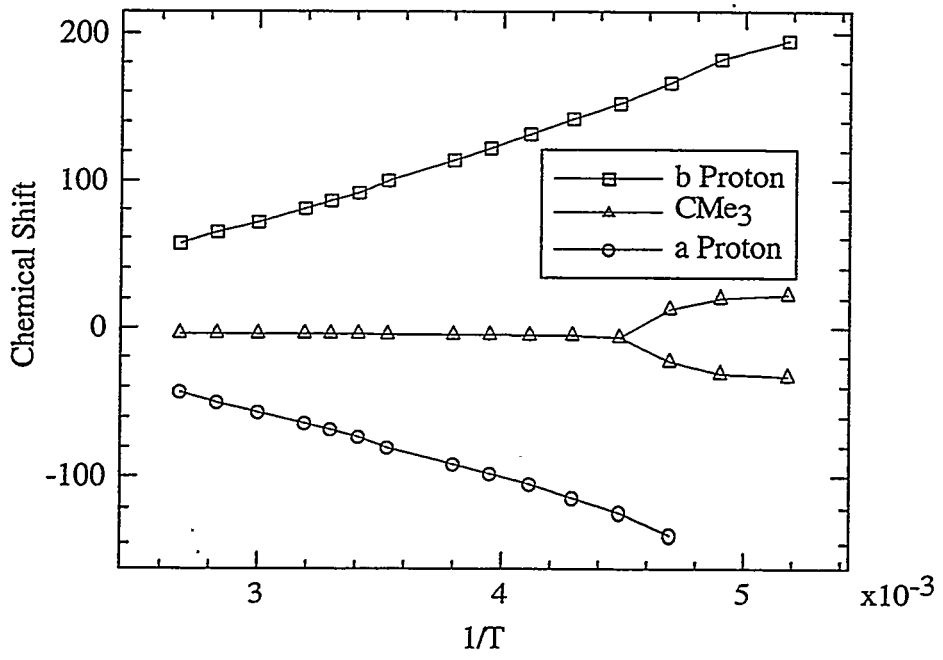

Figure 1b.8: Chemical shift of the protons of $[Cp^{\ddagger}_2UI]_2$(**17**) versus temperature

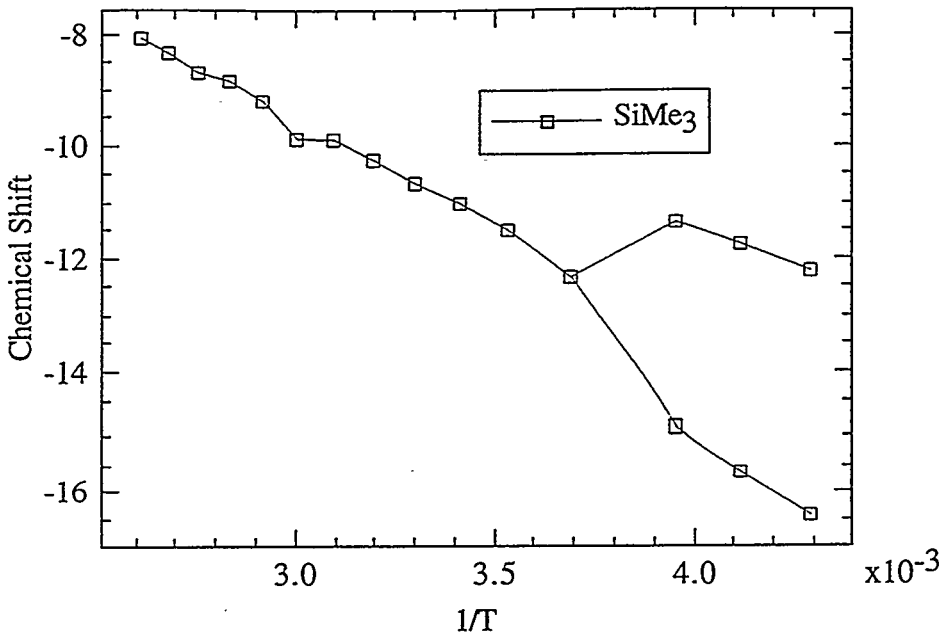

Figure 1b.9: Chemical shift of the protons of $[Cp''_2UF]_2$ (**12**) versus temperature. The resonances of the a_2 and b protons are not observed.

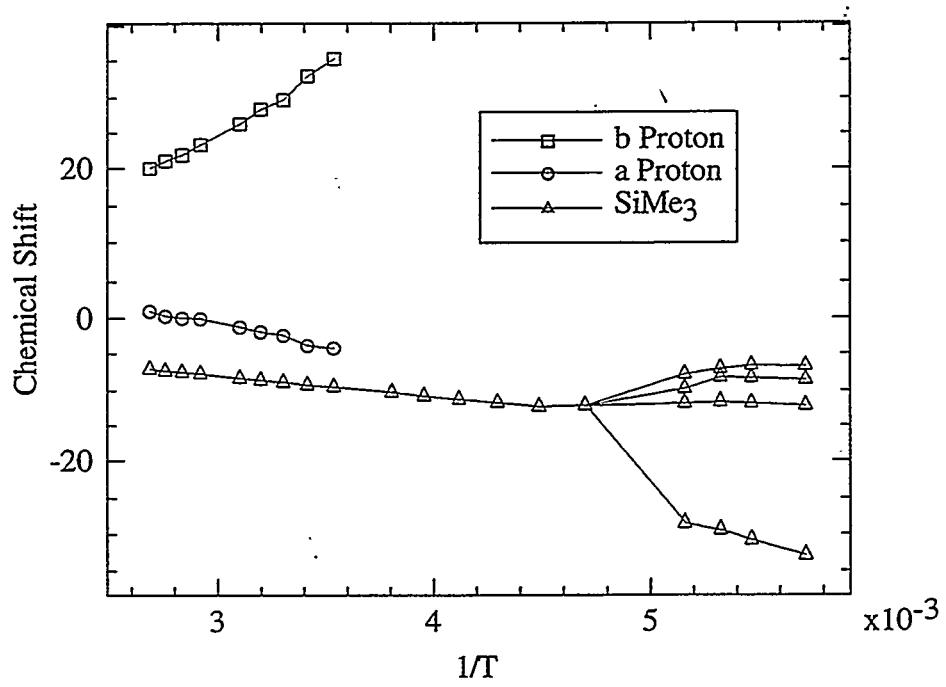

Figure 1b.10: Chemical shift of the protons of $[Cp''_2UCl]_2$(**14**) versus temperature

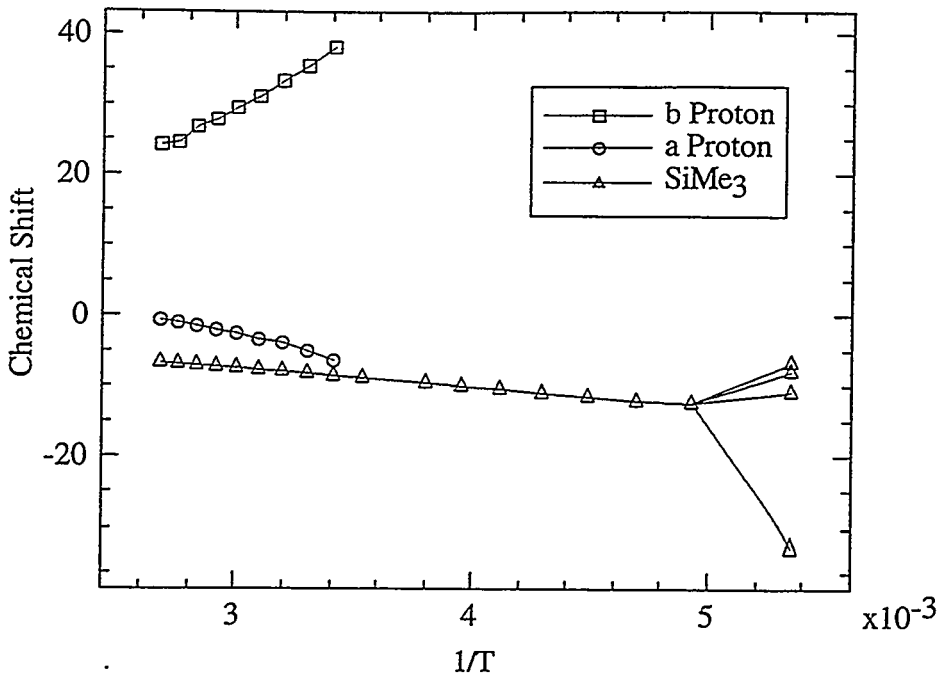

Figure 1b.11: Chemical shift of the protons of $[Cp"_2UBr]_2$(**16**) versus temperature

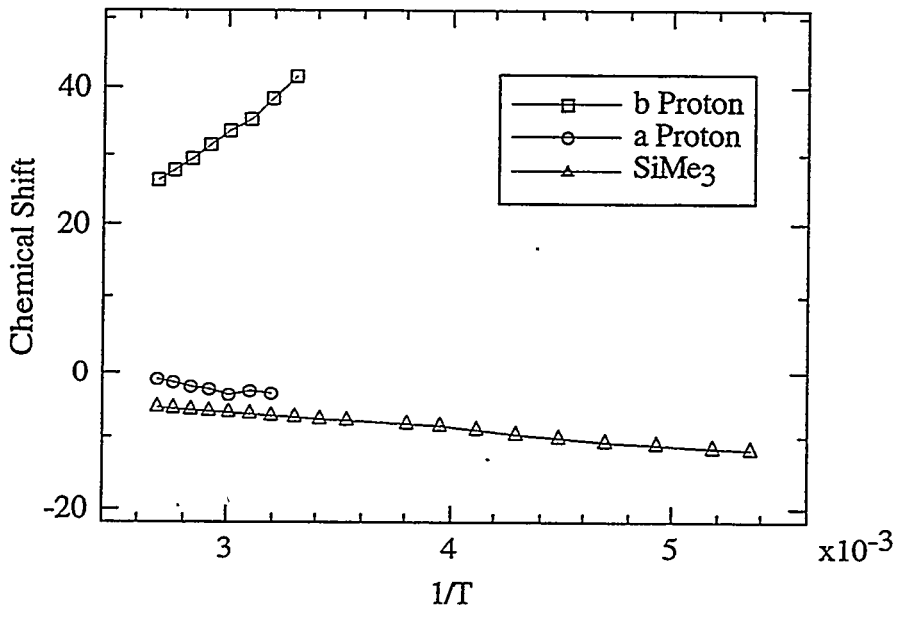

Figure 1b.12: Chemical shift of the protons of $[Cp"_2UI]_2$(**18**) versus temperature

From the variable temperature NMR behavior in the U(III) dimers, two trends are apparent. First, the fluorides are quite different from the other halides. Second, apart from the fluoride dimers, for the set of halide complexes with the same Cp ligand, the low temperature structures are all the same. Surprisingly, in the Cp" ligand series, the barrier to site exchange, as judged by the coalescence temperature, appears to *decrease* from Cl to I while in the $Cp^{\ddagger}$ ligand series, the barrier to site exchange appears to *increase* from Cl to I. The barriers to site exchange and the coalescence temperatures are listed in Table 1b.3. The reasons for this behavior will be discussed in a later section (**1e**).

Table 1b.3. Barriers to ring site exchange in dicyclopentadienyluranium(III) halides in kcal/mol. Coalescence temperatures, in °C, are in parentheses. For $[Cp"_2UBr]_2$ and $[Cp"_2UCl]_2$, the barrier was estimated using the outer two peaks of the 4 inequivalent $SiMe_3$ resonances.

	Barrier	T_c		Barrier	T_c
$[Cp"_2UF]_2$	12.4	-2	$[Cp^{\ddagger}{}_2UF]_2$	13.5	30
$[Cp"_2UCl]_2$	8.9	-60	$[Cp^{\ddagger}{}_2UCl]_2$	8.2	-70
$[Cp"_2UBr]_2$	7.9	-80	$[Cp^{\ddagger}{}_2UBr]_2$	8.9	-52
$[Cp"_2UI]_2$		< -95	$[Cp^{\ddagger}{}_2UI]_2$	8.9	-50

The low temperature spectrum of $[Cp^{\ddagger}{}_2UF]_2$ (**11**) is strange. The presence of six inequivalent CMe_3 groups cannot be accounted for by a single dimeric structure. Two causes for such a low temperature spectrum are possible. The first possibility is that the molecule is not a dimer, but a trimer with C_2 symmetry. This explanation seems plausible in light of the fact that $[Cp^*{}_2UCl]_3$ is a trimer with crystallographic C_2 symmetry. Alternatively, **11** could be present as a mixture of rotamers, one with C_i

symmetry having 4 inequivalent CMe_3 groups, and one with either C_{2h} or D_2 symmetry having 2 inequivalent CMe_3 groups. This latter explanation seems somewhat less likely since different rotamers have not been observed previously for these molecules. The obvious way to answer the question would be to determine the solid state structure of the complex. Unfortunately, **11** does not crystallize well, and macroscopic crystals could not be obtained. Finally, the protons of all of the dimers obey Curie-Weiss behavior. This implies that no monomer-dimer equilibrium is present.

To further establish that the U(III) halides complexes are dimeric in solution, crossover experiments in which two different halide complexes are mixed in solution were carried out. When dissolved in C_7D_8, the dimers scrambled in solution to give a mixture as shown in Eq 1b.2 by the time an NMR spectrum was taken. Unfortunately, because the $SiMe_3$ or CMe_3 peaks overlap in the ^1H NMR spectra of these complexes, it

$$[Cp^{\#}{}_2UX]_2 + [Cp^{\#}{}_2UY]_2 \rightleftharpoons Cp^{\#}{}_4U_2(\mu\text{–}X)(\mu\text{–}Y) \qquad K \approx 4 \qquad \text{(1b.2)}$$

homohalide dimers heterohalide dimer

X and Y are different halides *e.g.* X = Cl and Y = Br. $Cp^{\#}$ is either Cp" or Cp‡

was not possible to determine K accurately. When a 1:1 ratio of starting halides was used, an approximately 1:1:2 ratio of starting halide dimers to heterohalide dimer was obtained. Based on the assumptions that $\Delta H^0 = 0$ for this reaction, that the internal entropy of the molecules remains the same, and that the molecules are going from idealized D_{2h} symmetry for the homohalide dimers to C_{2h} for the heterohalide dimers,

$$\Delta S^0 = 2\Delta S^0_{int(XY)} - 2R\ln 2 - (\Delta S^0_{int(X2)} - R\ln 4 + \Delta S^0_{int(Y2)} - R\ln 4)$$

$$= R\ln 4$$

and, therefore, $K = \exp(-\Delta G^0/RT) = \exp(T\Delta S^0/RT) = \exp(RT\ln 4 / RT) = 4$. [29] If the actual symmetry of the molecules is used rather than the idealized symmetry, the result is the same.

The mixed halide bridged dimer is observable in solution throughout the temperature range accessible for C_7D_8. This observation implies that the molecules are present as dimers at all temperatures in agreement with the observed Curie-Weiss behavior of the chemical shifts of these dimers. The chemical shifts of the homohalide bridged dimers in the cross-over experiment are identical to those of the homohalide bridged dimers alone.

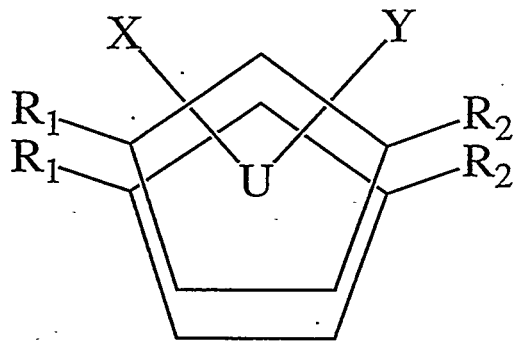

Figure 1b.13: A bent metallocene with diastereotopic R groups (R = $SiMe_3$ or CMe_3). X and Y are different ligands.

While the heterohalide bridged dimer was observable at all temperatures, the behavior of its NMR spectrum was surprising. As shown in Figure 1b.13, in a bent metallocene in which X and Y are inequivalent, the $SiMe_3$ or CMe_3 groups of the ligand are diastereotopic; however, in the heterohalide bridged dimers, these groups become equivalent at slightly elevated temperatures. The ubiquitous variable temperature plots for the heterohalide bridged dimers are given in Figures 1b.14 through 1b.24.

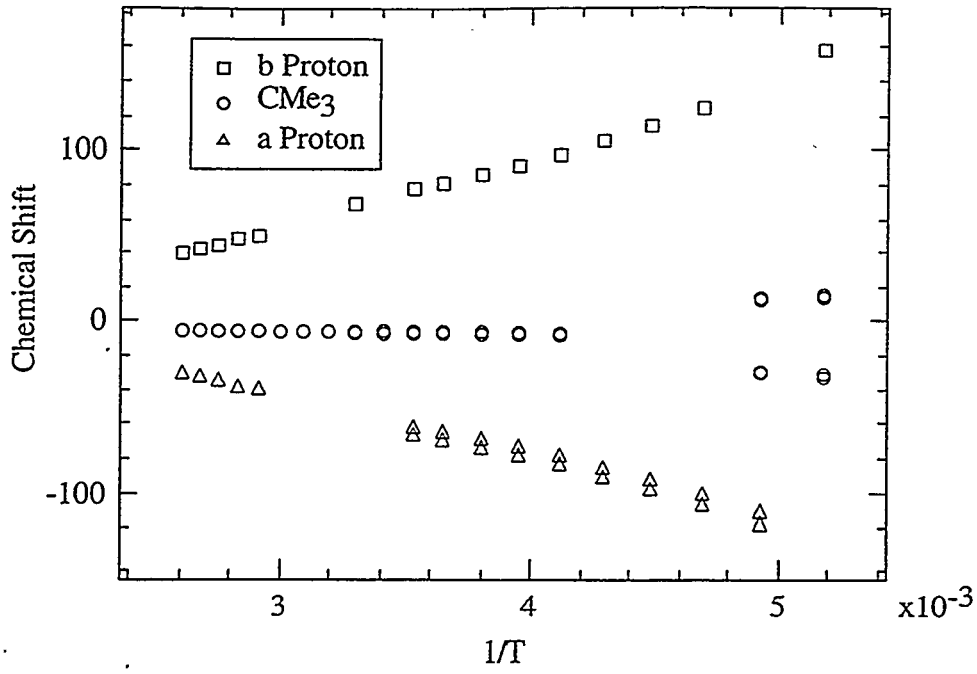

Figure 1b.14: Chemical shift of all protons of $Cp^{\ddagger}_4U_2(\mu\text{-Cl})(\mu\text{-Br})$ versus temperature

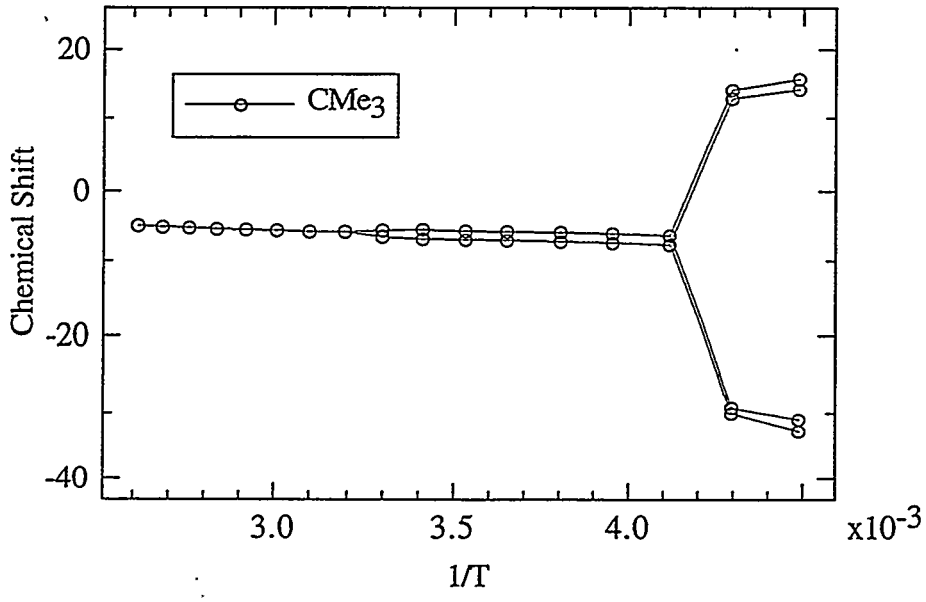

Figure 1b.15: Chemical shift of the CMe_3 protons of $Cp^{\ddagger}_4U_2(\mu\text{-Cl})(\mu\text{-Br})$ versus temperature

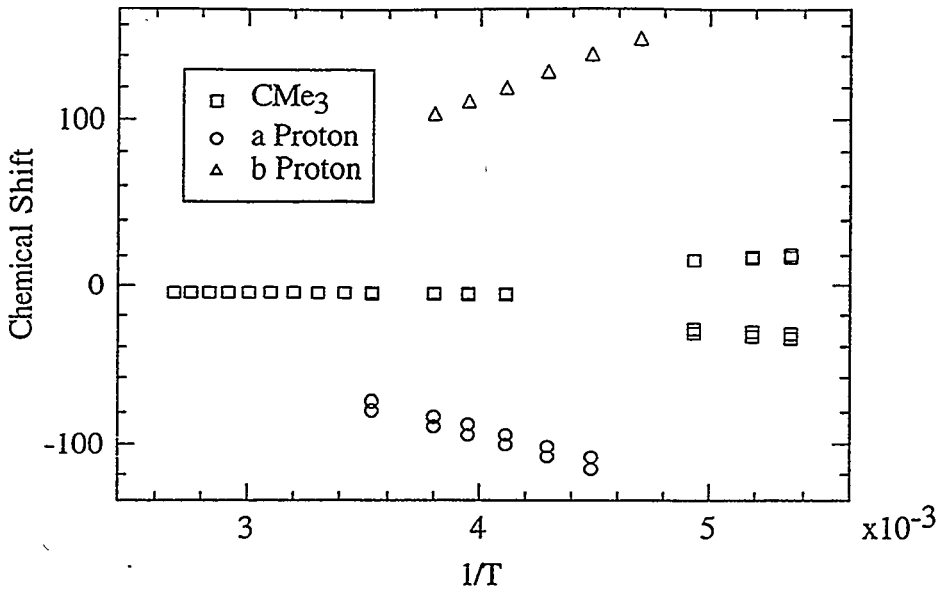

Figure 1b.16: Chemical shift of all protons of $Cp^{\ddagger}_4U_2(\mu\text{-I})(\mu\text{-Br})$ versus temperature

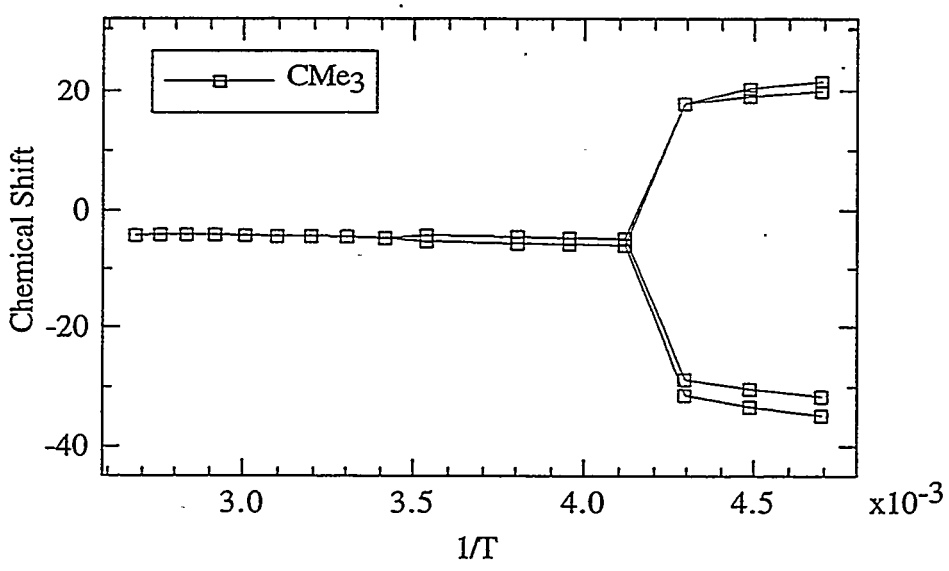

Figure 1b.17: Chemical shift of the CMe_3 protons of $Cp^{\ddagger}_4U_2(\mu\text{-I})(\mu\text{-Br})$ versus temperature

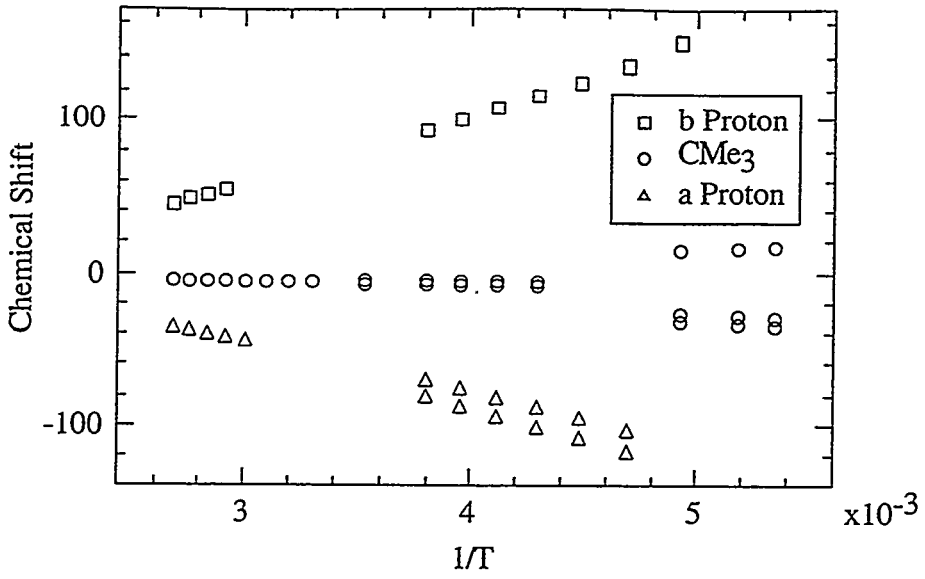

Figure 1b.18: Chemical shift of all protons of $Cp^{\ddagger}_4U_2(\mu\text{-I})(\mu\text{-Cl})$ versus temperature

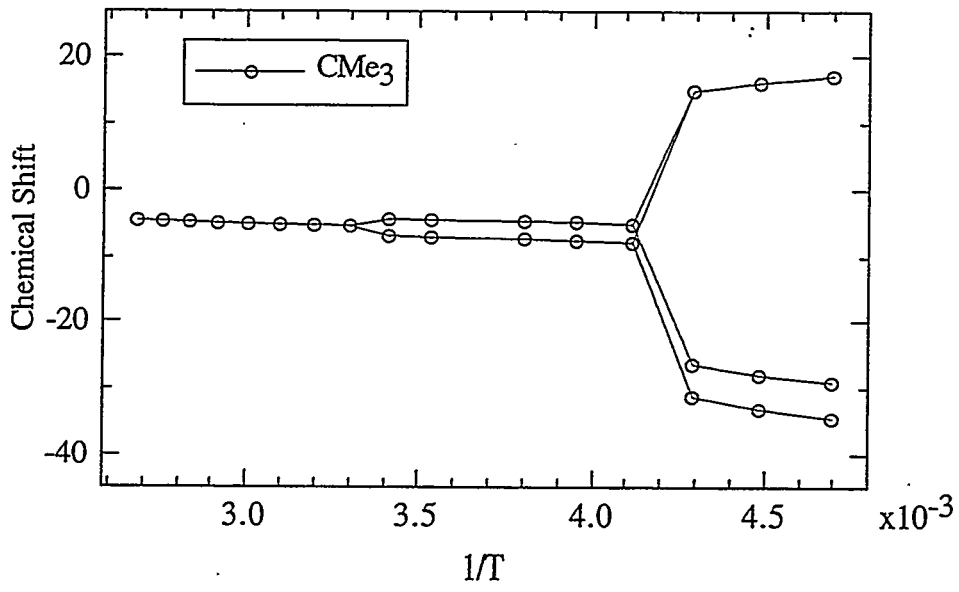

Figure 1b.19: Chemical shift of the CMe_3 protons of $Cp^{\ddagger}_4U_2(\mu\text{-I})(\mu\text{-Cl})$ versus temperature

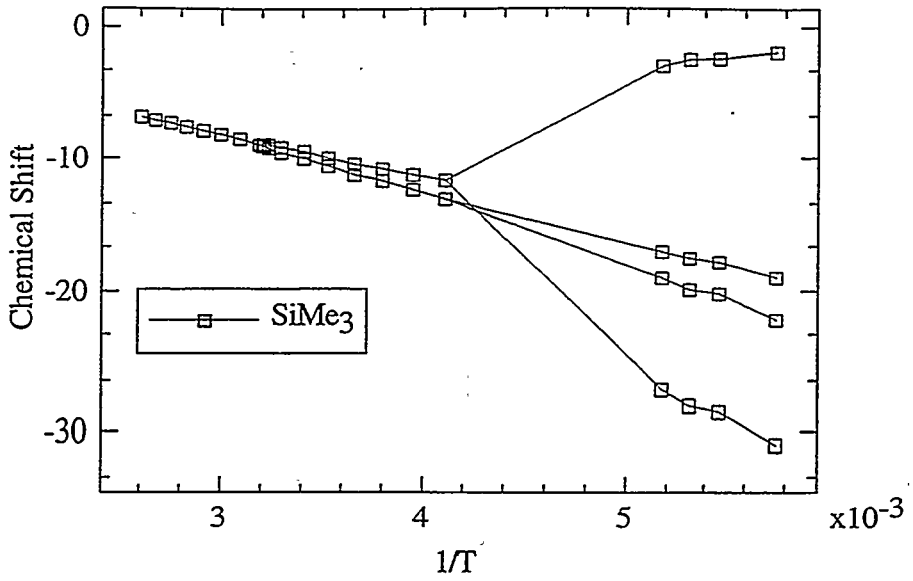

Figure 1b.20: Chemical shift of the $SiMe_3$ protons of $Cp''_4U_2(\mu\text{-}I)(\mu\text{-}F)$ versus temperature

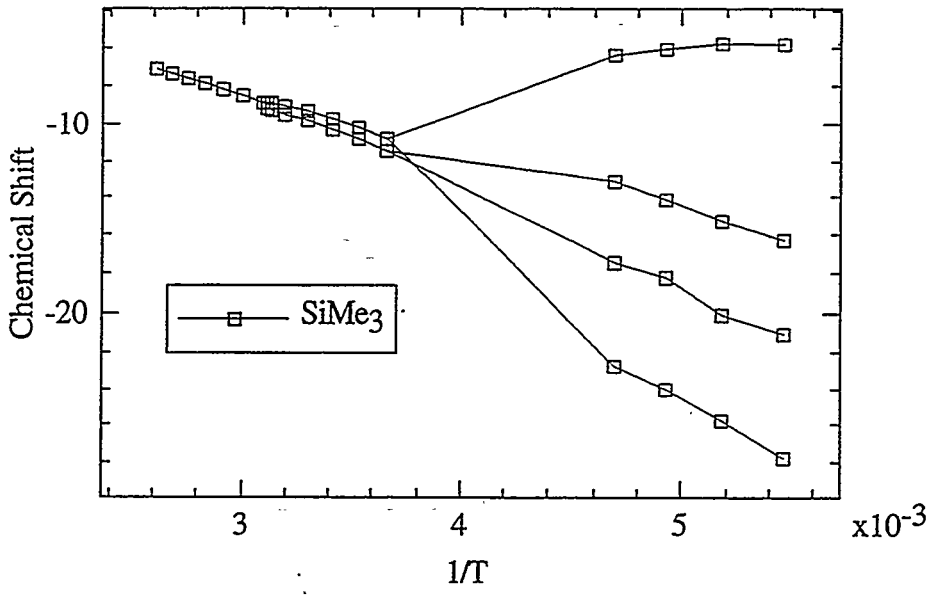

Figure 1b.21: Chemical shift of the $SiMe_3$ protons of $Cp''_4U_2(\mu\text{–}Br)(\mu\text{-}F)$ versus temperature

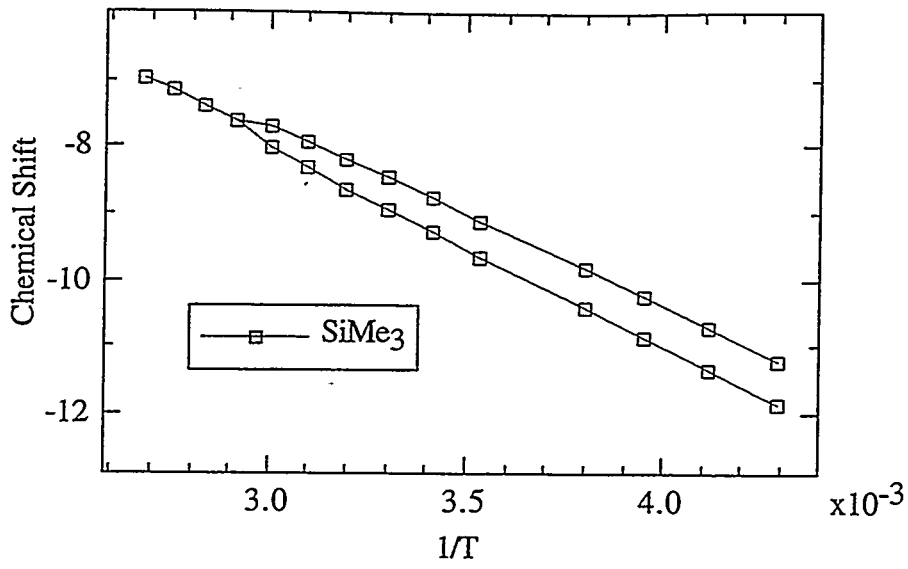

Figure 1b.22: Chemical shift of the $SiMe_3$ protons of $Cp''_4U_2(\mu\text{–}Br)(\mu\text{-}Cl)$ versus temperature

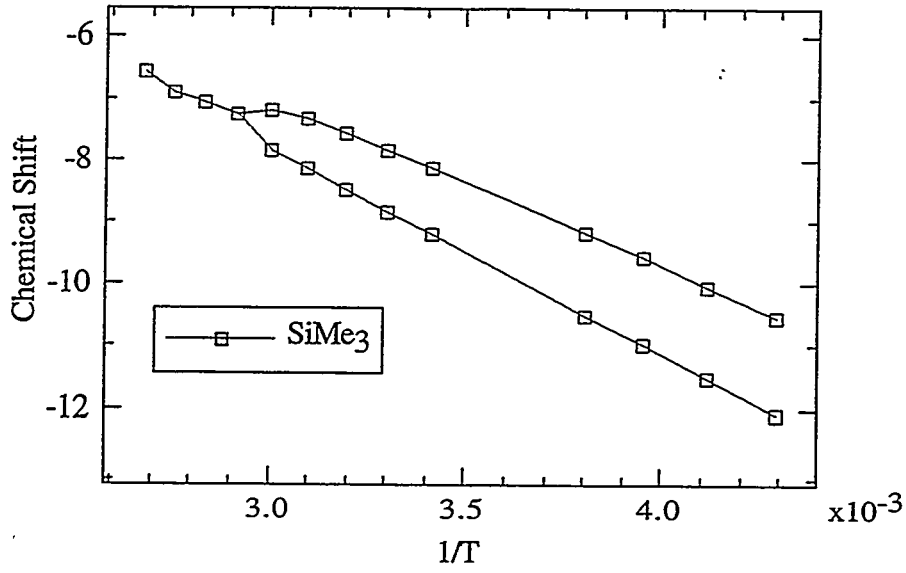

Figure 1b.23: Chemical shift of the $SiMe_3$ protons of $Cp''_4U_2(\mu\text{–}I)(\mu\text{-}Cl)$ versus temperature

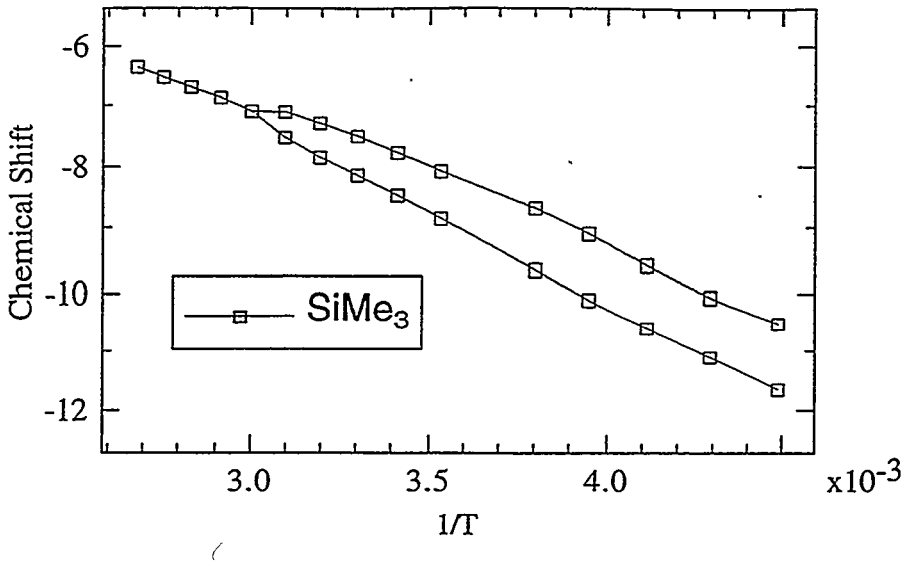

Figure 1b.24: Chemical shift of the $SiMe_3$ protons of $Cp''_4U_2(\mu\text{–I})(\mu\text{-Br})$ versus temperature

Table 1b.4: Barrier to coalescence of the diastereotopic protons of $Cp^{\ddagger}_4U_2(X,Y)$ dimers. The coalescence temperature is in parentheses.

	CMe_3 Protons				a_2 Protons			
	X = Cl		X = Br		X = Cl		X = Br	
	Barrier	T_c	Barrier	T_c	Barrier	T_c	Barrier	T_c
Y = Br	15.0	40°			15.2	60°		
Y = I	13.6	30°	13.6	20°	13.7	50°	13.7	40°

Table 1b.5: Barrier to coalescence of the diastereotopic $SiMe_3$ protons of $Cp''_4U_2(X,Y)$ dimers. The coalescence temperature is in parentheses

	X = F		X = Cl		X = Br	
	Barrier	T_c	Barrier	T_c	Barrier	T_c
Y = Br	15.7	50°	16.7	70°		
Y = I	15.6	40°	16.2	70°	16.0	60°

Table 1b.6. Barriers to ring site exchange in dicyclopentadienyluranium(III) heterohalides in kcal/mol. The coalescence temperatures, in °C, are in parentheses.

	Barrier	T_c		Barrier	T_c
$Cp''_2U_2(\mu\text{-Br}, \mu\text{-Cl})$	NA		$Cp^{\ddagger}_2U_2(\mu\text{-Br}, \mu\text{-Cl})$	9.0	-50°
$Cp''_2U_2(\mu\text{-Br}, \mu\text{-I})$	NA		$Cp^{\ddagger}_2U_2(\mu\text{-Br}, \mu\text{-I})$	9.2	-50°
$Cp''_2U_2(\mu\text{-I}, \mu\text{-Cl})$	NA		$Cp^{\ddagger}_2U_2(\mu\text{-I}, \mu\text{-Cl})$	8.7	-50°
$Cp''_2U_2(\mu\text{-Br}, \mu\text{-F})$	11.0	-10°	$Cp''_2U_2(\mu\text{-I}, \mu\text{-F})$	9.9	-30°

The presence of distinct resonances for the 2 homohalide bridged dimers and for the heterohalide bridged dimer at all temperatures rules out the possibility that an intermolecular process makes these protons equivalent. The dimers cannot be separating into monomers and then recombining. If this were the case, only one R group resonance would be observed since all of the molecules in solution would be in rapid equilibrium. The mechanism responsible for making the diastereotopic protons equivalent must be intramolecular.

In order for the diastereotopic protons of the heterohalide bridged dimers to become equivalent, the molecule must "gain" a mirror plane as shown in Figure 1b.25. The molecule can "gain" a mirror in two ways. Either the inequivalent R groups of the Cp ligand or the X and Y halide must change sites rapidly on the NMR time scale. The only way for the R groups of the Cp ligand to change sites is to change the face of the Cp ligand coordinated to the uranium center. This process seemed unlikely, but, to investigate this hypothesis, the variable temperature NMR behavior of a monomeric metallocene $Cp^{\ddagger}_2U(Me)(Cl)$ (**19**) was examined and is shown in Figure 1b.25. Not surprisingly, the CMe_3 and a protons of **19** do not coalesce at temperatures up to 100 °C. The fact that none of the diastereotopic protons of **19** coalesce at NMR accessible

temperatures shows that the $Cp^{\ddagger}$ ligands are not changing the face coordinated to the metal center and that the X and Y ligands are not exchanging sites.

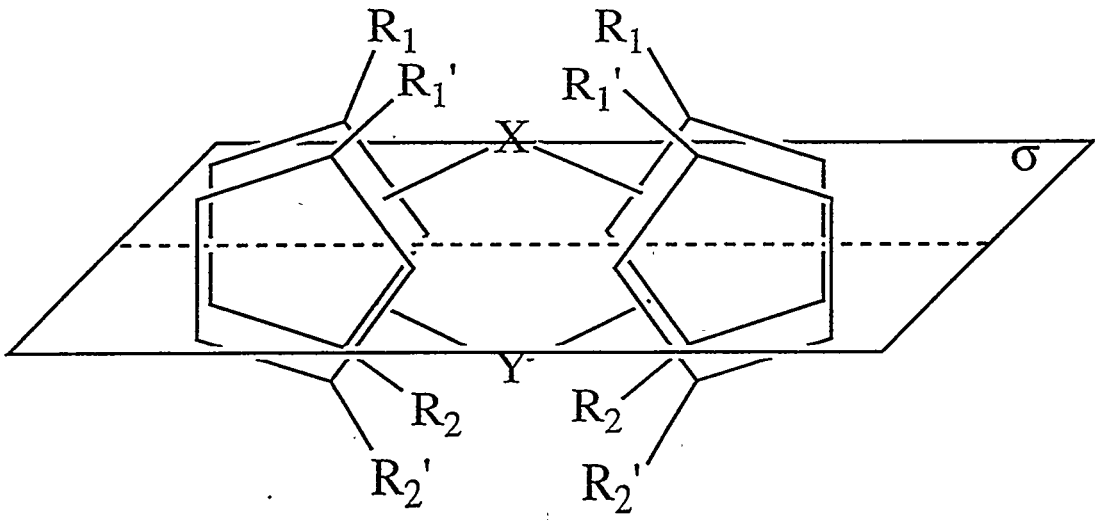

Figure 1b.25: A mirror plane which makes R_1 and R_2 equivalent in a heterohalide dimer

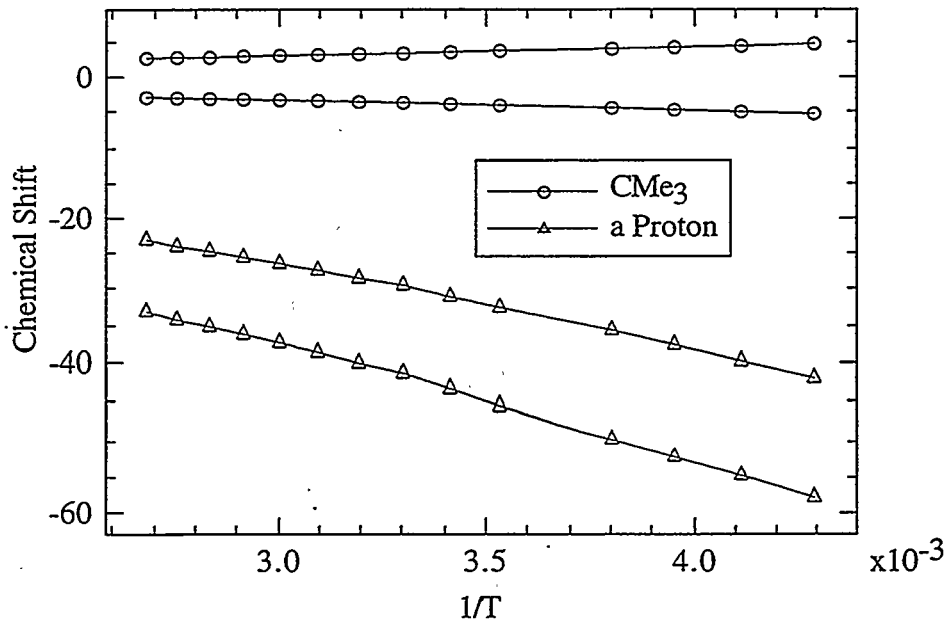

Figure 1b.26: Chemical shifts of the diastereotopic protons of (**19**) versus temperature

Since the diastereotopic protons of a monomeric metallocene do not coalesce, it seems likely that the process which allows these protons to become equivalent in the U(III) heterohalide bridged dimers is site exchange between the two halides as shown in Scheme 1b.1. Note that this mechanism only makes the R groups of the left half of the dimer equivalent, so X-Y site exchange must be occurring twice as fast as the observed rate for the diastereotopic protons to become equivalent. Correcting the $\Delta G^{\ddagger}$ values in Tables 1b.5 and 1b.6 for the faster rate of the X-Y site exchange reduces the $\Delta G^{\ddagger}$ values by 0.4 kcal/mole.

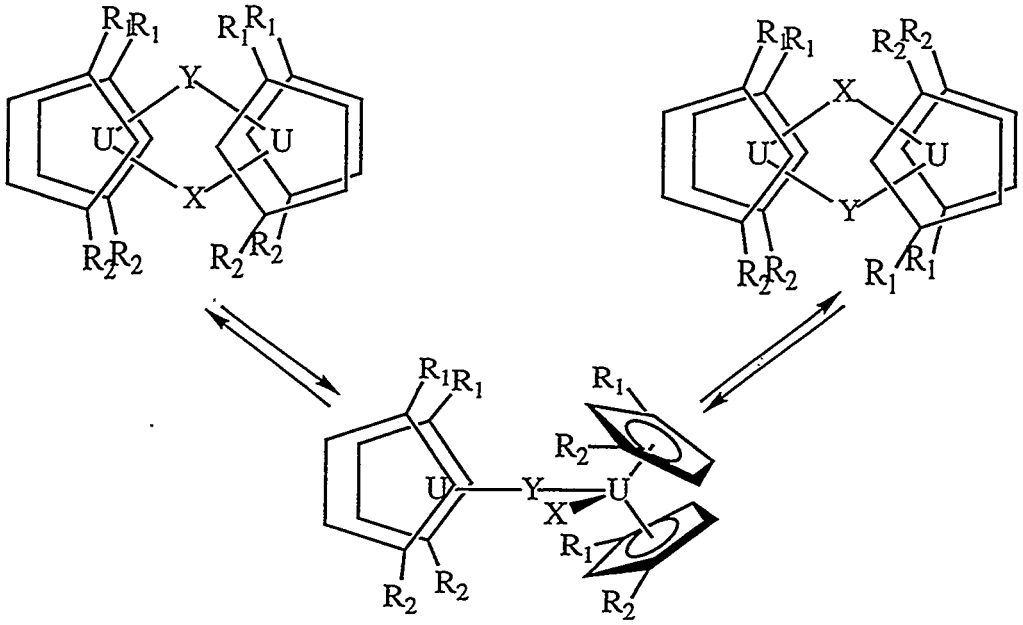

Scheme 1b.1: Heterohalide site exchange

The "one-legged" transition state in Scheme 1b.1 has some precedent. The complexes $[Cp^*_2YbMe]_2$,[30] $[Cp^*_2YMe]_2$,[31] $[Cp^*_2YCl]_2$,[32] and $[Cp^*_2LuMe]_2$[31] adopt this structure in the solid state. At low temperatures (< 200 K), these molecules show the expected 1:1:2 pattern of Cp* resonances which coalesce at higher temperatures. Unfortunately, whether the coalescence is due to intramolecular or intermolecular

processes is not known, so the barriers to site exchange can not be compared to those of the heterohalide bridged dimers.

The trend in barriers to halide site exchange can be explained if the larger halide is assumed to be the bridging halide in the transition state. This seems likely since a larger halide bridge will minimize steric interactions between the two metallocenes fragments in the transition state. Additionally, the shorter the terminal halide to uranium bond, the smaller the interaction between the terminal halide and the other metallocene fragment in the transition state. Since the uranium terminal halide bond lengths in Cp''_2UX_2 complexes are 2.073, 2.573, 2.734(1), and 2.953(2) Å for X = F, Cl, Br, and I, respectively,[13] the barrier should be much lower when fluoride is the terminal ligand rather than chloride or bromide. This hypothesis is consistent with the data in Tables 1b.4 and 1b.5.

One final note on the low temperature behavior of the $Cp''_4U_2(\mu\text{-}F,\mu\text{-}I)$ and $Cp''_4U_2(\mu\text{-}F,\mu\text{-}Br)$ dimers. In the slow exchange limit for ring rotation, these molecules have 4 inequivalent sets of $SiMe_3$ protons. This observation implies that the molecules have the C_{2h} symmetry seen in $[Cp''_2UF]_2$ rather than the C_i symmetry seen in $[Cp''_2UBr]_2$. Additionally, the barrier to ring rotation in these molecules is quite a bit higher than that in $[Cp''_2UBr]_2$. The values are given in Table 1b.7.

In conclusion, the U(III) halide complexes studied appear to be dimeric in solution at all temperatures studied. Their solution structure is consistent with the known solid state structures. The halides dimers quickly exchange in solution to give a mixture of homohalide bridged dimers and heterohalide bridged dimers. The halides of the heterohalide bridged dimers exchange sites rapidly on the NMR time scale at somewhat elevated temperatures.

1c: Dicyclopentadienyluranium Hydroxide and Oxide Complexes

Metal hydroxide and oxide complexes have long been of interest in our group (likely due to the fact that they turn up in every alkyl complex), so the behavior of the dicyclopentadienyluranium(III) hydroxide complexes were examined. Only two examples of organouranium(IV) hydroxide compounds exist: Cp_3UOH[27] and $(RC_5H_4)_3UOH$ (R = CMe_3 or $SiMe_3$).[33] No organouranium(III) hydroxide compounds have been reported. Organouranium oxides are more common. Some examples include $[(RC_5H_4)_3U]_2O$ (R = Me,[6] R = $SiMe_3$[34]) and the very interesting terminal oxo compounds $Cp^*_2U(O)OR$ and $Cp^*_2U(O)NR$ (R = 2,6-*i*-$Pr_2C_6H_3$). [35] In addition, $[(RC_5H_4)_2U(\mu\text{-}O)]_3$ can be prepared by thermolysis of $(RC_5H_4)_3UOH$ (R = CMe_3 or SiMe3). [33] Again, no organouranium(III) oxo compounds have been reported.

Although the dicyclopentadienyluranium(III) halides were easy to synthesize, they did not provide useful routes to the hydroxides. A similar complex, $[Cp"_2CeOH]_2$, was obtained by treating $Cp"_3Ce$ with water in tetrahydrofuran.[10] As shown by Beshouri, this route also works for the synthesis of $[Cp"_2UOH]_2$ (**19**) which can be crystallized from hexane.[14] Since the analogous $Cp^{\ddagger}_3U$ is difficult to prepare, $[Cp^{\ddagger}_2UOH]_2$ (**20**) was synthesized from water and the hydride, $[Cp^{\ddagger}_2UH]_2$ (**21**), which was obtained by treating $Cp^{\ddagger}_2UMe_2$ with hydrogen. The reduction of uranium(IV) alkyl complexes with hydrogen has been seen previously for $Cp^*_2UR_2$ and $Cp^*_2UR(Cl)$ complexes.[11,36] The routes to the hydroxide complexes are given in Scheme 1c.1. The complexes **19**, **20**, and **21** are all dimeric in the gas phase as determined by mass spectroscopy.

$$3\ Cp''_2UCl_2 + 6\ K \rightarrow 2\ Cp''_3U + 6\ KCl + U\ (metal)$$

$$2\ Cp''_3U + 2\ H_2O \rightarrow [Cp''_2UOH]_2\ (\mathbf{19}) + 2\ Cp''H$$

$$Cp^{\ddagger}_2UCl_2 + 2\ MeLi \rightarrow Cp^{\ddagger}_2UMe_2 + 2\ LiCl$$

$$2\ Cp^{\ddagger}_2UMe_2 + 3\ H_2 \rightarrow [Cp^{\ddagger}_2UH]_2\ (\mathbf{21}) + 4\ CH_4$$

$$[Cp^{\ddagger}_2UH]_2 + 2\ H_2O \rightarrow [Cp^{\ddagger}_2UOH]_2\ (\mathbf{20}) + 2\ H_2$$

Scheme 1c.1: Synthesis of dicyclopentadienyluranium(III) hydroxides

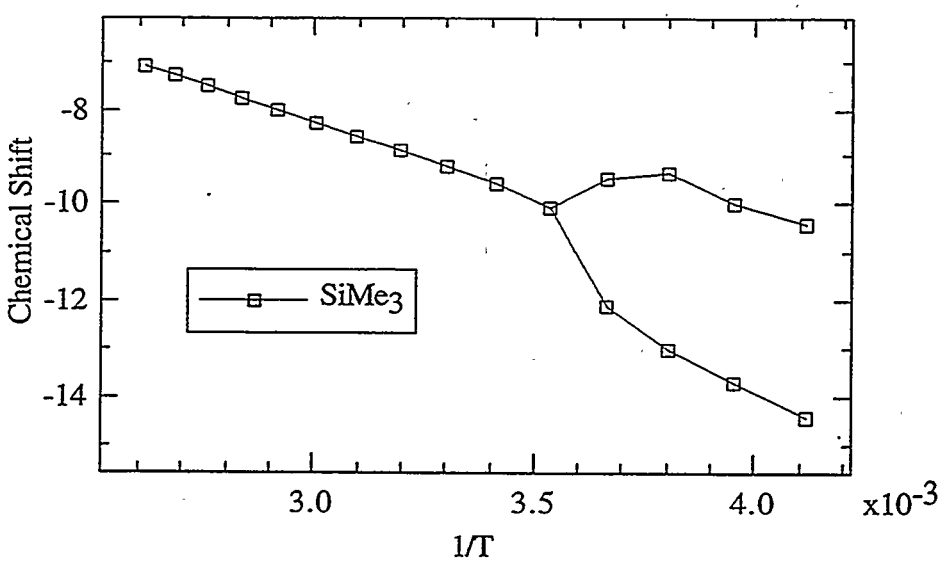

Figure 1c.1: Chemical shift of the $SiMe_3$ protons of $[Cp''_2UOH]_2$ (**19**) versus temperature

The variable temperature NMR spectra of the new U(III) complexes were examined and are shown in Figures 1c.1 - 1c.3. The barriers to site exchange for the R groups in $[Cp''_2UOH]_2$ is 12.4 kcal/mol at 0 °C, and in $[Cp^{\ddagger}_2UOH]_2$, the barrier is 13.0 kcal/mol at 30 °C based upon the outer two lines of the low temperature spectrum. These values are similar to those of the analogous fluoride complexes, $[Cp''_2UF]_2$ and $[Cp^{\ddagger}_2UF]_2$, which are 12.4 kcal/mol at –2 °C and 13.5 kcal/mol at 30 °C, respectively. The similarity between the barriers to site exchange in the fluorides and hydroxides is not surprising since the U-F and U-OH bond lengths are similar in $[Cp''_2UF]_2$ and

$[Cp''_2UOH]_2$. Therefore, analogous fluoride and hydroxide dimers are expected to have similar U-U distances and Cp ring conformations. The chemical shifts of the protons of these complexes all obey Curie-Weiss behavior.

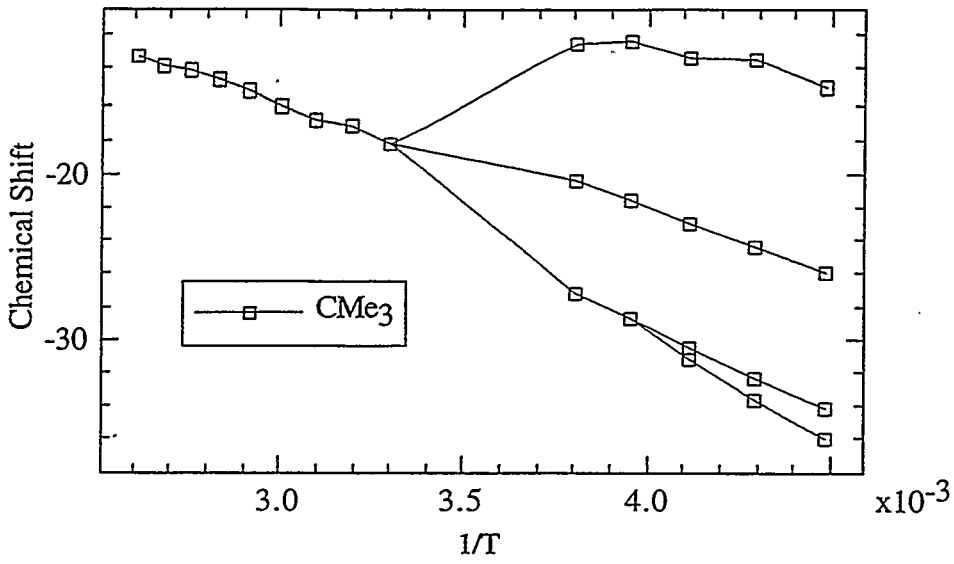

Figure 1c.2: Chemical shift of the CMe_3 protons of $[Cp^{\ddagger}_2UH]_2$ (**21**) versus temperature

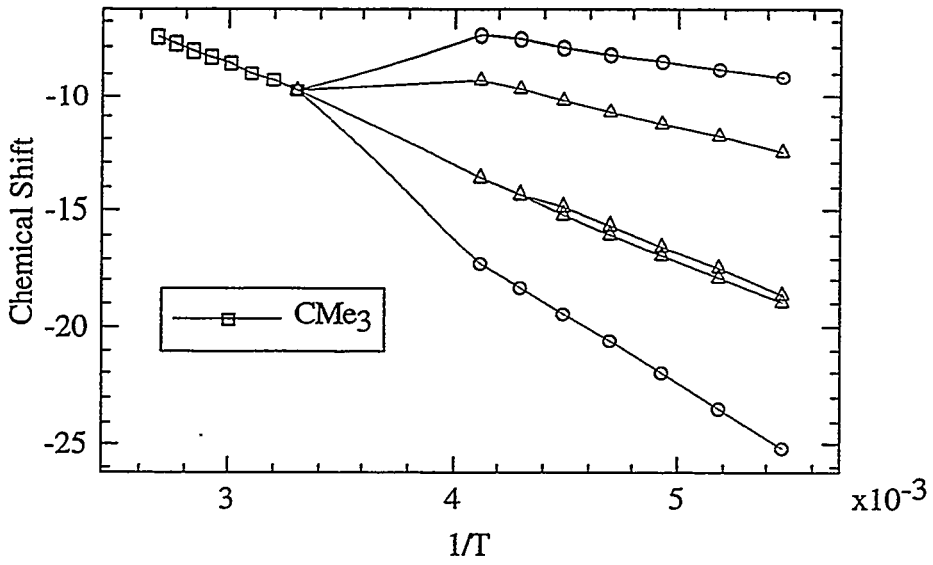

Figure 1c.3: Chemical shift of the CMe_3 protons of $[Cp^{\ddagger}_2UOH]_2$ (**20**) versus temperature

As in the halide dimers, we were interested to know whether the hydroxide dimer would exchange with other U(III) dimers in solution. Surprisingly, a mixture of $[Cp"_2UOH]_2$ and $[Cp"_2UCl]_2$ in C_7D_8 did not show any additional resonances attributable to the mixed bridge species $Cp"_4U_2(\mu\text{-Cl}, \mu\text{-OH})$. Given the difference in size between hydroxide and chloride, it seemed possible, but unlikely, that the difference in bonding between hydroxide and chloride made $Cp"_4U_2(\mu\text{-Cl}, \mu\text{-OH})$ less stable than the heteroligand bridged complexes. To minimize this difference in bonding, a crossing experiment between $[Cp"_2CeOH]_2$ and $[Cp"_2UOH]_2$ was attempted. Like the crossing experiment with $[Cp"_2UCl]_2$, no new resonances attributable to the mixed metal hydroxide dimer, $Cp"_4CeU(\mu\text{-OH})_2$, were observed. Additionally, no new resonances were seen when a mixture of $[Cp"_2CeOH]_2$ and $[Cp"_2LaOH]_2$ was heated to 100 °C for a few hours.

When the mixtures for the crossover experiments were heated, the resonance due to $[Cp"_2UOH]_2$ (**19**) disappeared and two new peaks appeared in the NMR spectrum. The new compound was thought to be $[Cp"_2UO]_2$ (**22**). This hypothesis was confirmed by the independent synthesis of $[Cp"_2UO]_2$ from $Cp"_2UMe_2$ and water by Blosch.[37] In addition, $[Cp^{\ddagger}_2UOH]_2$ decomposes in solution. This product too was shown by Blosch to be $[Cp^{\ddagger}_2UO]_2$ (**23**) by independent synthesis from $Cp^{\ddagger}_2UMe_2$ and water.[37]

The NMR spectra of the oxide complexes, **22** and **23**, are virtually identical and show that both molecules adopt the C_{2h} geometry at room temperature as shown in Figure 1c.4. The NMR spectrum can be assigned based upon the peak area and the NMR shifts of the protons by comparing them to the $Cp"_2UX_2$ and $Cp^{\ddagger}_2UX_2$ complexes assuming that dipolar shifts are dominant (Table 1c.1). The variable temperature NMR spectra of **22** and **23** show that these complexes obey Curie-Weiss behavior, and have very high barriers to ring rotation. For **22**, the barrier to R group site exchange is 16.9 kcal/mol at 110 °C. For **23**, the coalescence temperature greater than 110 °C, and the barrier is greater than 16.6 kcal/mol.

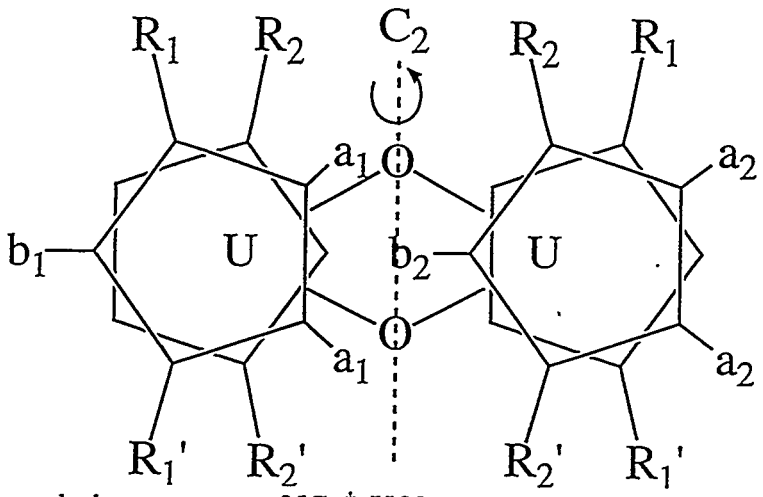

Figure 1c.4: The solution structure of $[Cp^{‡}_2UO]_2$ and $[Cp''_2UO]_2$. R = CMe_3 or $SiMe_3$

Table 1c.1: Assignment of the NMR spectra of $[Cp''_2UO]_2$ and $[Cp^{‡}_2UO]_2$ in ppm.

	a_1	b_2	R_2	R_1	a_2	b_1
$[Cp''_2UO]_2$	79.92	82.45	-0.72	-13.16	-81.75	-85.27
$[Cp^{‡}_2UO]_2$	81.52	78.17	0.98	-16.94	-97.85	-89.01

Table 1c.2: Distances and angles in $[Cp^{‡}_2UO]_2$ and $[Cp''_2UO]_2$

$[Cp^{‡}_2UO]_2$		$[Cp''_2UO]_2$[38]	
U-U	3.3904(7) Å	U-U	3.3927(9) Å
U-O	2.118(7) Å	U-O	2.096(6) Å
U-O'	2.121(7) Å	U-O'	2.129(5) Å
U-Cp1	2.53 Å	U-Cp1	2.50 Å
U-Cp2	2.52 Å	U-Cp2	2.49 Å
U-$\langle C_{ring}\rangle$	2.80(4) Å	U-$\langle C_{ring}\rangle$	2.7(2)°
Cp1-U-Cp2	124°	Cp1-U-Cp2	123°
O-U-O	73.8(3)°	O-U-O	73.2(2)°
U-O-U	106.2(3)°	U-O-U	106.8(2)°

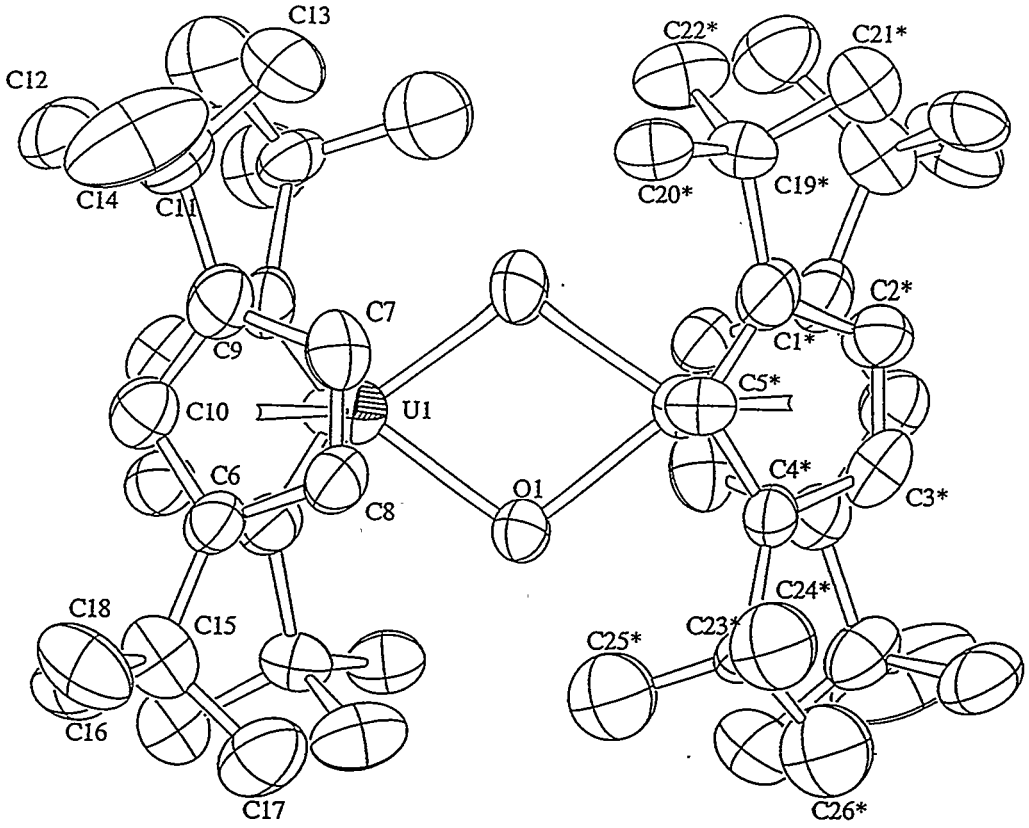

Figure 1c.5: An ORTEP drawing of $[Cp^{\ddagger}_2UO]_2$ with 50% thermal ellipsoids.

Since the structure of **22** had been determined previously,[38] the crystal structure of **23** was determined for comparison and is shown in Figure 1c.5. Interesting distances and angles are given in Table 1c.2 along with those of **22** for comparison. One of the CMe_3 groups of **23** is disordered and only one set of the disordered atoms is shown in Figure 1c.5. The solid state structures of **22** and **23** are virtually identical, and, based upon the similarity of the NMR spectra, the solution structures are also identical. The geometries of the molecules are controlled by the short U-O bond lengths and corresponding short U-U distances which force the ligands to adopt the observed C_{2h} geometry.

$$[Cp''_2UOH]_2\ (\mathbf{19}) \rightarrow [Cp''_2UO]_2\ (\mathbf{22}) + H_2 \qquad (1c.1)$$

The conversion of **19** to **22** (eq 1c.1) is surprising and warranted further investigation into the reaction mechanism. Kinetic data for this reaction from 380 to 303 K is given in Table 1c.3, and an Eyring plot using this data is shown in Figure 1c.6. The decomposition obeyed first order kinetics cleanly at all temperatures as shown in Figure 1c.7 for decomposition at 98 °C. The product, $[Cp''_2UO]_2$ (**22**) was formed at the same rate the reactant decomposed, and no induction period was seen in the formation of **22** (Figure 1c.8). During kinetics runs in the NMR probe, hydrogen was observed in the NMR spectrum.

Table 1c.3: Kinetic Data for the Decomposition of $[Cp''_2UOH]_2$ (**19**)

Compound	T (K)	k (s^{-1})
$[Cp''_2UOH]_2$	380	$(3.66 \pm 0.03)\times10^{-3}$
$[Cp''_2UOH]_2$	373	$(1.77 \pm 0.01)\times10^{-3}$
$[Cp''_2UOH]_2$	371	$(1.46 \pm 0.08)\times10^{-3}$
$[Cp''_2UOH]_2$	362	$(5.82 \pm 0.3)\times10^{-4}$
$[Cp''_2UOH]_2$	353	$(2.63 \pm 0.2)\times10^{-4}$
$[Cp''_2UOH]_2$	341	$(8.37 \pm 0.9)\times10^{-5}$
$[Cp''_2UOH]_2$	319	$(5.80 \pm 0.6)\times10^{-6}$
$[Cp''_2UOH]_2$	303	$(7.96 \pm 0.3)\times10^{-7}$
$[Cp''_2UOH]_2$+ DHA	373	$(1.65 \pm 0.2)\times10^{-3}$
$[Cp^{\ddagger}_2UOH]_2$	373	$(2.82 \pm 0.1)\times10^{-4}$
$[Cp''_2UOD]_2$	380	$(8.99 \pm 0.1)\times10^{-4}$

$k_H/k_D = 4.1$ (1) at 107 °C

$k_H/k_D = 6.0$ (2) at 25 °C (assuming $\Delta S^{\ddagger}_{OH} = \Delta S^{\ddagger}_{OD}$)

$\Delta H^{\ddagger} = 24.2 \pm 0.1$ kcal/mol

$\Delta S^{\ddagger} = -6.8 \pm 0.3$ e.u.

DHA is dihydroanthracene

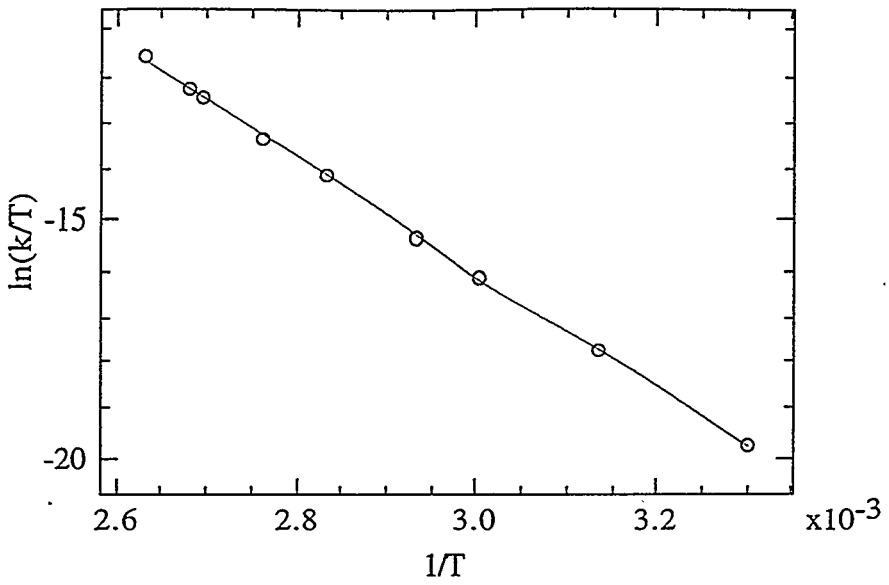

Figure 1c.6: An Eyring plot for the decomposition of $[Cp''_2UOH]_2$

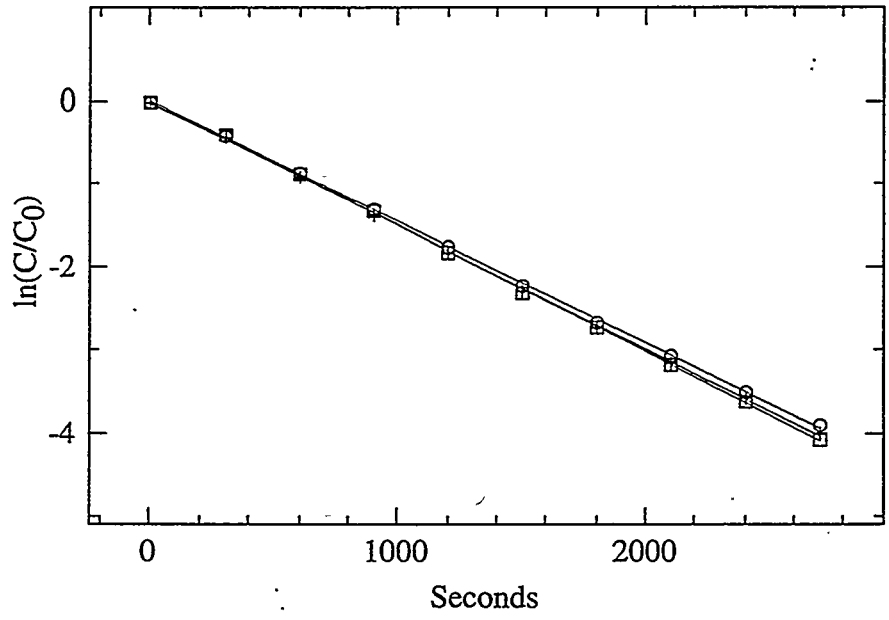

Figure 1c.7: Decomposition of **19** at 98 °C showing first order kinetics (3 runs)

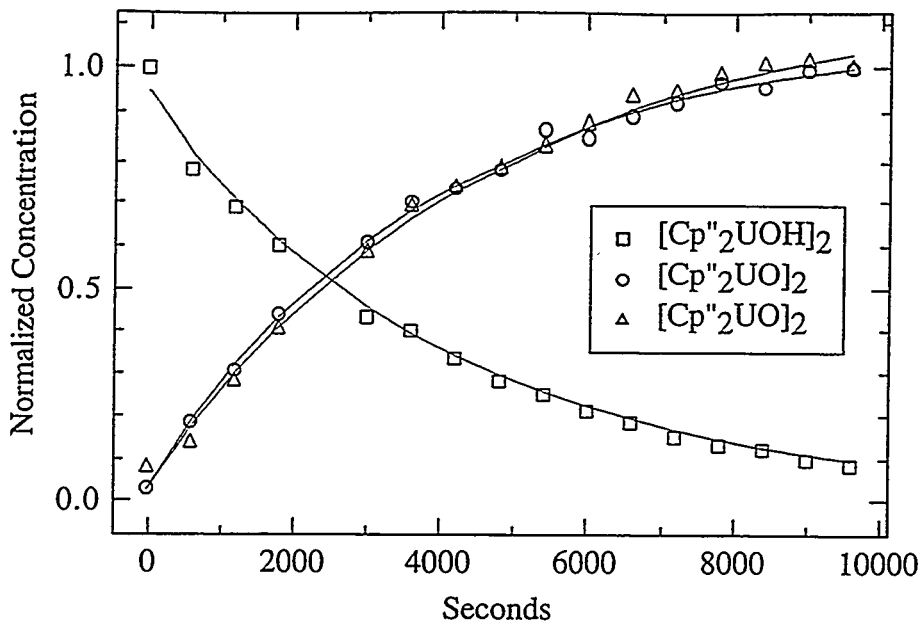

Figure 1c.8: Plot showing disappearance of $[Cp"_2UOH]_2$ (**19**) and appearance of $[Cp"_2UO]_2$ (**22**) at 80 °C. Solid lines are least squares fits to $C=C_0e^{-kT}$ for the disappearance of **19**, and $C=C_0(1-e^{-k(t+t_0)})$ for the appearance of **22**.

When $[Cp"_2UOD]_2$ was examined, a small amount of H_2 and HD was observed, presumably due to exchange with adventitious water in the solvent or on the walls of the NMR tube. The kinetic isotope effect at 107 °C is 4.1(1) which is calculated to be 6.0(2) at 25 °C. If the $[Cp"_2UOD]_2$ samples were allowed to sit before the kinetics experiment was started, more H_2 and HD was observed, and the rate of decomposition was faster than if the kinetics run was started immediately. When the decomposition of a mixture of $[Cp"_2UOH]_2$ and $[Cp"_2UOD]_2$ was examined, a large amount of H_2 and only a small amount of HD was observed. The HD presumably comes from the mixed isomer resulting from the reaction of adventitious water and $[Cp"_2UOD]_2$ as noted previously. When the decomposition was carried out in the presence of 5 to 7 equivalents of dihydroanthracene (DHA) as a radical trap, the rate of decomposition did not change, and no anthracene was produced.

These observations strongly imply that the decomposition is intramolecular, proceeds with the loss of hydrogen, and does not involve radicals. Additionally, the large kinetic isotope effect (KIE) requires that O-H bond breaking occurs during or before the rate limiting step of the reaction. Two mechanisms can be postulated for the elimination of H_2 from the complex: concerted, shown in Figure 1c.9; and stepwise, shown in Figure 1c.10.

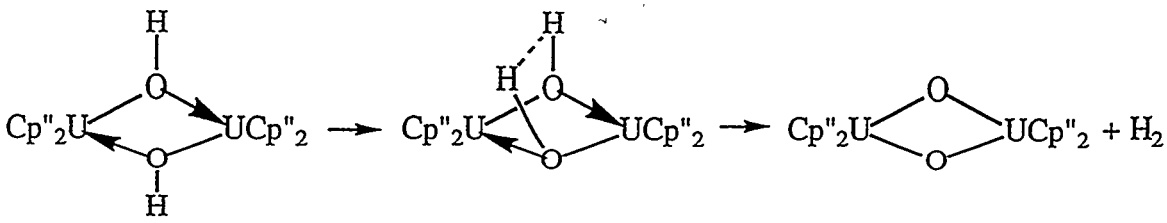

Figure 1c.9: Concerted Elimination of H_2 from **19**

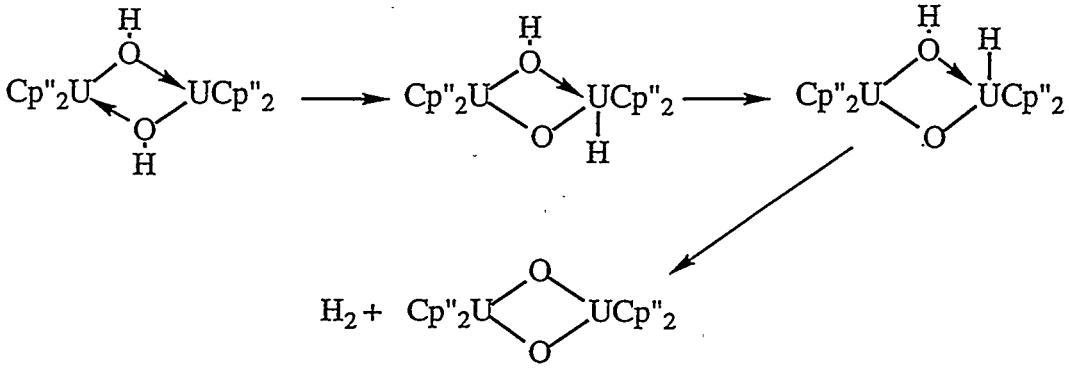

Figure 1c.10: Stepwise Elimination of H_2 from **19**

One possible way to differentiate between the two mechanisms is by comparing the observed kinetic isotope effect (KIE) and activation parameters to those known for similar reactions. The observed KIE is similar to KIEs observed for α-elimination and α-migration reactions. For the decomposition of $CpTa(CH_2CMe_3)_2Cl_2$ to $CpTa(CHCMe_3)Cl_2$, $\Delta S^{\ddagger}$ varies from -4 e.u. to -36 e.u. depending upon the solvent, and the KIE when the neopentyl ligands are deuterated in the α-position is 5.4 ± 0.5 at 36 °C.[39] For the decomposition of Cp^*WMe_5 to $Cp^*WMe_3(CH_2)$, $\Delta S^{\ddagger}$ is -1 e.u., and

the KIE is 6 ± 1 at 25 °C when the methyl groups are deuterated.[40] More similarly, for the migration of the α-hydroxyl proton in $Re(OH)(EtCCEt)_3$, $\Delta S^{\ddagger}$ is -25 e.u., and the KIE is 5 ±1, presumably at 25°C.[41] Unfortunately, it is difficult to say exactly what to expect for the KIE of a concerted elimination of H_2.[42] However, given the similarity of the KIE and activation parameters to those reported for α-elimination reactions, the decomposition of **19** presumably follows the stepwise mechanism.

The analogous compound $[Cp^{\ddagger}_2UOH]_2$ decomposes more slowly than $[Cp"_2UOH]_2$, but presumably by the same mechanism. The slower rate of decomposition is likely due the different ring conformations in the two compounds. $[Cp"_2UOH]_2$ has the same C_{2h} symmetry as $[Cp"_2UO]_2$, so no change in Cp conformation is needed in going from reactant to product. As seen in its low temperature NMR spectrum, $[Cp^{\ddagger}_2UOH]_2$ does not have the same C_{2h} symmetric ring conformation as $[Cp^{\ddagger}_2UO]_2$. The decomposition of $[Cp^{\ddagger}_2UOH]_2$ will have a higher barrier to decomposition since the Cp ring conformation must change during the reaction.

In conclusion, the bridging hydroxide, $[Cp"_2UOH]_2$ (**19**) has a solution structure similar to the analogous fluoride $[Cp"_2UF]_2$ (**12**). Unlike **12**, **19** does not exchange with other halides in solution. The bridging hydroxide $[Cp^{\ddagger}_2UOH]_2$ (**20**) has a low temperature NMR spectrum similar to that of the fluoride $[Cp^{\ddagger}_2UF]_2$; however, neither solid state structure is known. When heated, both **19** and **20** decompose to form the bridging oxide complexes, $[Cp"_2UO]_2$ (**22**) and $[Cp^{\ddagger}_2UO]_2$ (**23**), which have the same C_{2h} symmetric solid state and solution structure. The decomposition of **19** has been studied in detail and is thought to proceed by α-migration of one of the hydroxyl protons followed by the α-elimination of hydrogen. The rate of decomposition of **20** is lower than that of **19** presumably due to the reorganization of the Cp ligands of **20** needed in the transition state.

1d: X-Ray Absorption Spectroscopy of Dicyclopentadienyluranium Complexes

The inability to grow x-ray quality crystals of $[Cp^{\ddagger}_2UX]_2$ (X = H, OH, and F) limited the interpretation of the low temperature NMR spectra of these complexes. Since the spectra did not resemble that of any other U(III) complex, we were not certain of the conformations of the Cp rings or even the nuclearity (dimer versus trimer) of these complexes. One way to address the question of nuclearity was to examine the U-U distance in these complexes using extended x-ray absorption fine structure spectroscopy (EXAFS). The U - U distance in a trimer is expected to be quite a bit longer than in a dimer because the U - X - U angle can be close to linear in a trimer. For comparison, the average U - U distance in $[Cp^*_2UCl]_3$ is 5.66 Å versus 4.36 Å in $[Cp^{\ddagger}_2UCl]_2$.[11,28] In order to probe the reliability of the bond lengths determined by EXAFS, several complexes which had been crystallographically characterized were examined.[43]

In addition, since the edge-shift of the x-ray absorption is dependent upon the shielding of the electron, we were interested to see whether changing the ligands in these complexes would have any effect upon the energy of the x-ray absorption. The L_{III} x-ray absorption spectrum of $[Cp^{\ddagger}_2UCl]_2$, is shown in Figure 1d.1. The L_{III} electrons are the $2p_{3/2}$ electrons. The edge shifts for the complexes relative to a 0.2 M water solution of UO_2Cl_2 are given in Table 1d.1. The standard deviation of the edge shift was found to be 0.23 eV by comparing the edge shifts for successive scans of one sample ($[Cp^{\ddagger}_2UF]_2$).

The edge shift reflects the change in the binding energy of the L_{III} electrons. A more negative shift indicates a smaller binding energy. As seen in Table 1d.1, the edge shifts of the U(III) complexes are more negative than the U(IV) complexes consistent with greater screening of the L_{III} electrons in the U(III) complexes due to the extra 5f electron. While there does appear to be trend among the binding energies of the U(IV)

complexes, the energies would have to be different by more than 0.7 eV (3σ) for the difference to be meaningful.

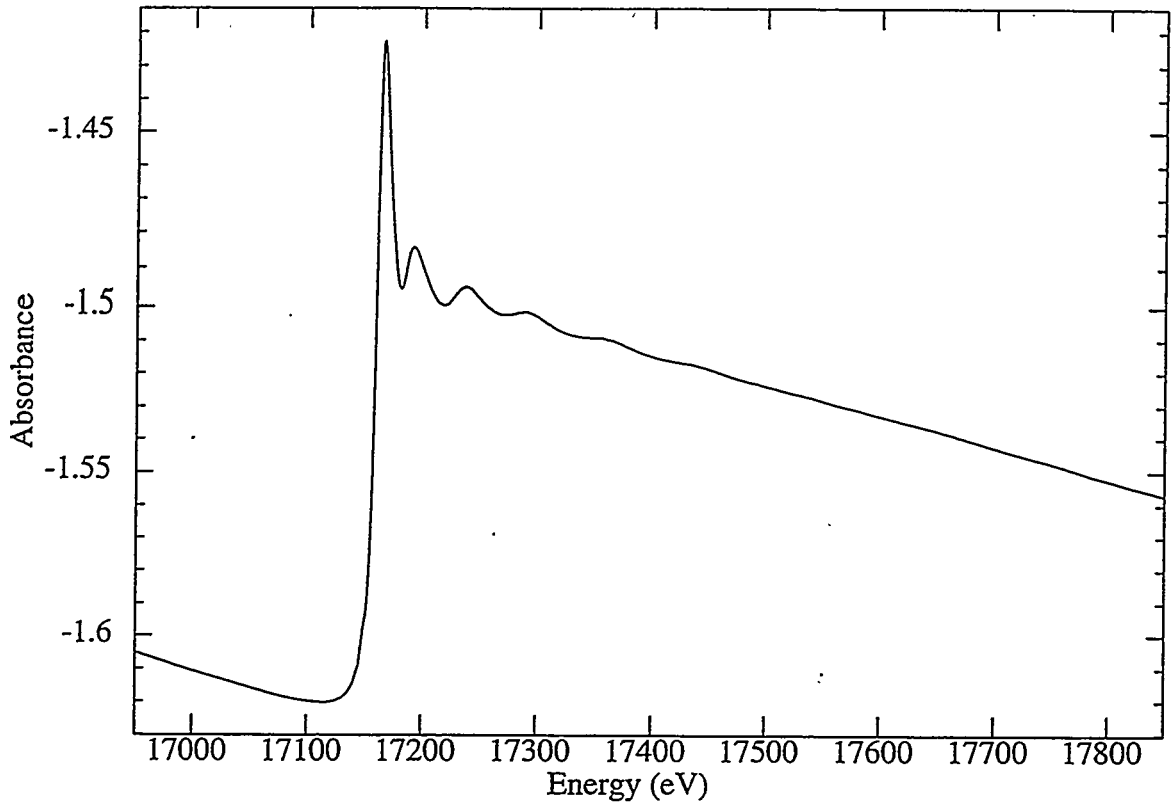

Figure 1d.1: The L_{III} x-ray absorption spectrum of $[Cp^{\ddagger}_2UCl]_2$

The binding energies of the U(IV) and U(III) complexes with the same halide but different Cp ligands are very similar for all of the complexes except the U(IV) dichlorides and the U(III) fluorides. In addition, no trend in binding energies versus Cp ligand exists among these compounds. At least towards the binding energies of the uranium L_{III} electrons, the Cp" and $Cp^{\ddagger}$ ligands are identical. The difference between the two Cp ligands is therefore entirely steric.

Table 1d.1: Binding energies of the U L_{III} electrons in eV of some dicyclopentadienyl-uranium complexes relative to a 0.2 M UO_2Cl_2 solution. The standard deviation of the edge shift is 0.23 eV.

Compound	Edge Shift (eV)	Compound	Edge Shift (eV)
$[Cp^{‡}_2UO]_2$	-2.0		
$Cp^{‡}_2UF_2$	-2.4	$[Cp"_2UF_2]_2$	-2.6
$Cp^{‡}_2UCl_2$	-2.9	$Cp"_2UCl_2$	-2.4
$Cp^{‡}_2UBr_2$	-3.5	$Cp"_2UBr_2$	-3.7
$Cp^{‡}_2UI_2$	-3.6	$Cp"_2UI_2$	-3.6
$[Cp^{‡}_2UOH]_2$	-6.4		
$[Cp^{‡}_2UF]_2$	-5.0	$[Cp"_2UF]_2$	-5.9
$[Cp^{‡}_2UCl]_2$	-6.3	$[Cp"_2UCl]_2$	-6.4
$[Cp^{‡}_2UBr]_2$	-5.7	$[Cp"_2UBr]_2$	-5.6

EXAFS spectroscopy gives information about the atomic number, distance, and number of the atoms neighboring the atom being examined (uranium in this case). The analysis of a complex yields different shells of coordinating atoms. A shell is described by the atomic number of the atoms comprising it, number of atoms in the shell (coordination number, CN), the distance of the atoms from the central atom (radius, R), and by the Debye-Waller factor (σ) which represents both the static and thermal disorder of the atoms in the shell. The Debye-Waller factor is analogous to the thermal parameter in crystallography.

The analysis was carried out using the EXAFS theoretical phases and amplitudes calculated using FEFF6[44] with atom positions based on known crystal structures.[28,38] When the crystal structure was not known, the atomic positions of the Cp_2U unit were

taken from the crystal structure of the most similar complex, and the U-X distances were changed according to the relative radii of X. Full experimental details are given in the experimental section.

Plots of the EXAFS spectra, theoretical fits, and their Fourier transforms are given in Figures 1d.2 -1d.12. The spectra are plotted against k which is the energy in $Å^{-1}$ of the ejected L_{III} electron determined by subtracting the energy of the L_{III} edge from the energy of the x-rays. The EXAFS, χ, are weighted by k^3 to give features at higher k similar amplitude to low k features. The results of the analyses of the EXAFS spectra are given in Tables 1d.2 and 1d.3. Note that, just as in crystallography, the number in parentheses in the EXAFS distance column is the standard deviation of that parameter in the fit relative to the data; however, empirically, the error in distances determined by EXAFS is about 0.01 - 0.02 Å based upon comparisons to crystallographically determined structures.

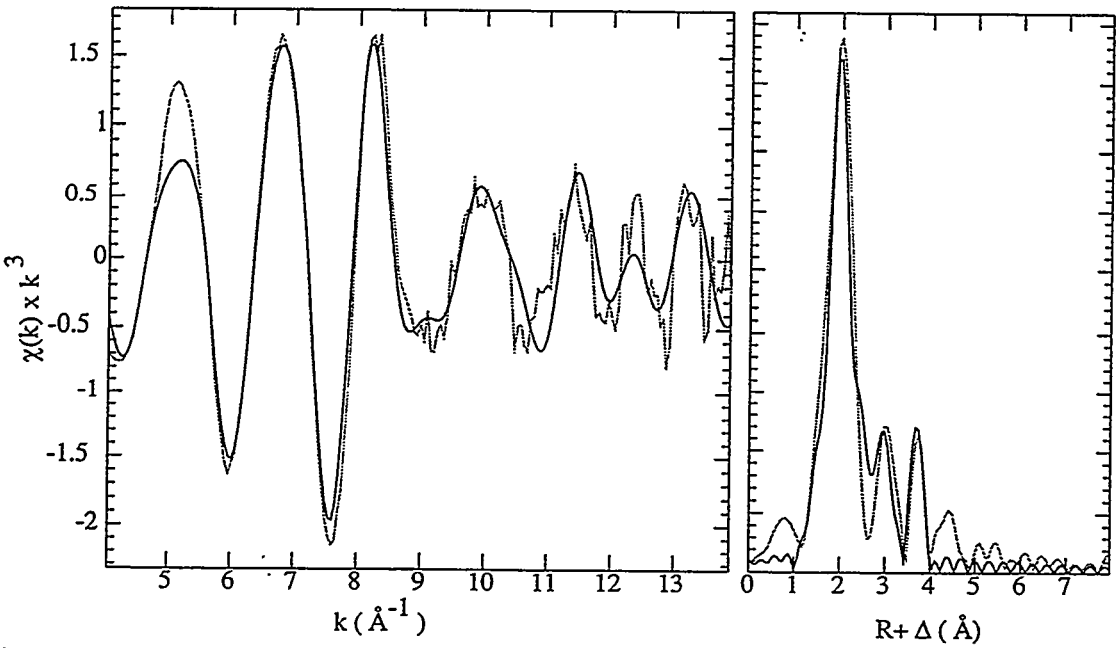

Figure 1d.2: EXAFS spectrum (gray), fit (black), and Fourier transform of $[Cp"_2UF]_2$

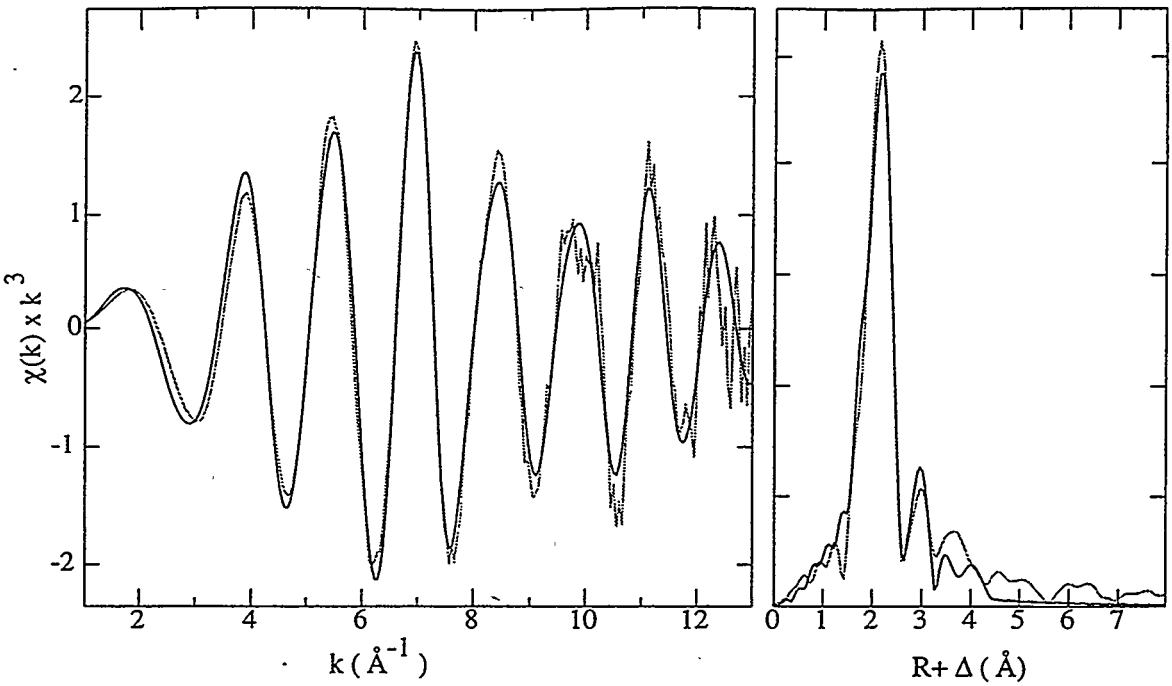

Figure 1d.3: EXAFS spectrum (gray), fit (black), and Fourier transform of $[Cp''_2UCl]_2$

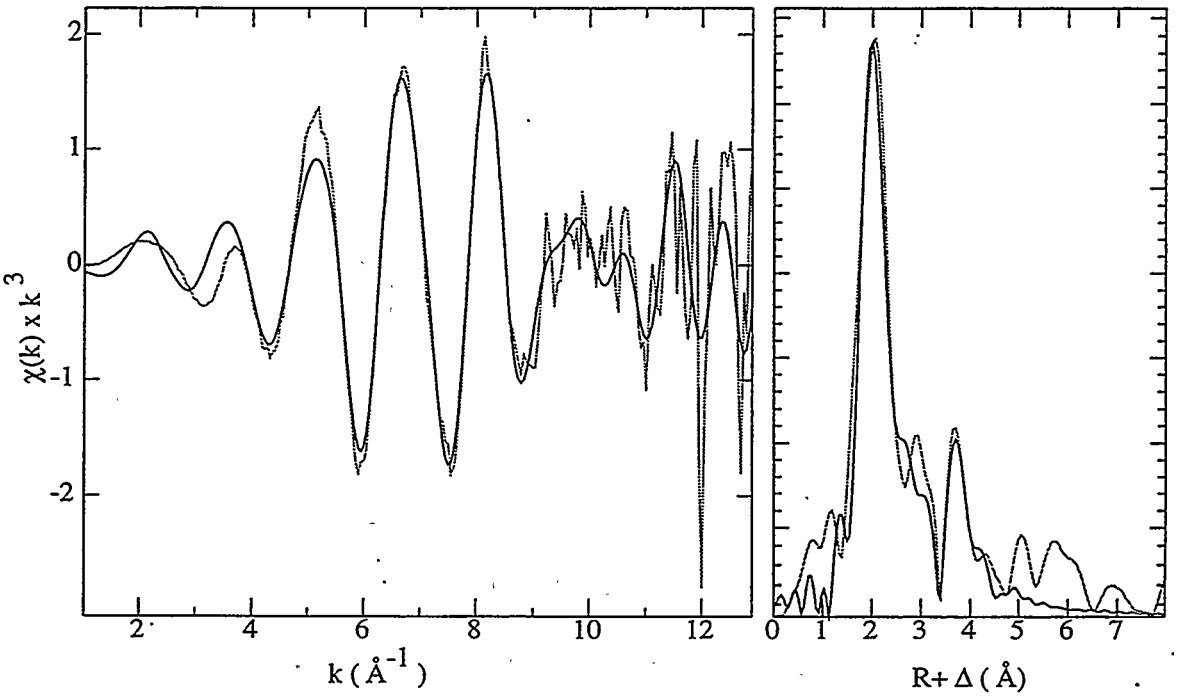

Figure 1d.4: EXAFS spectrum (gray), fit (black), and Fourier transform of $[Cp^{\ddagger}_2UOH]_2$

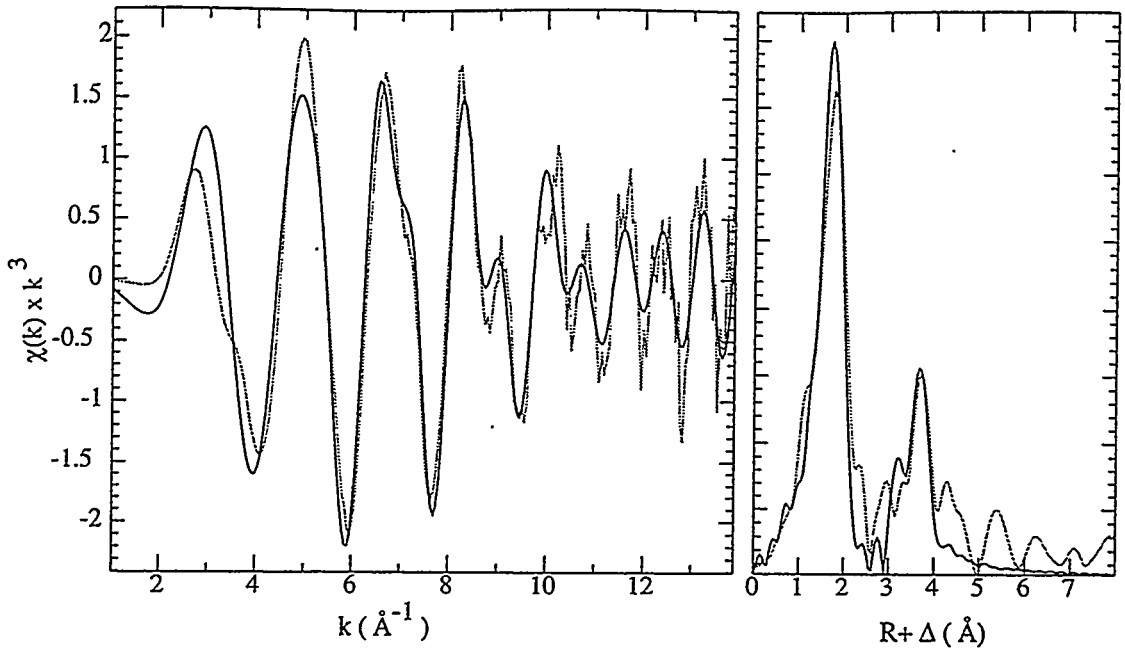

Figure 1d.5: EXAFS spectrum (gray), fit (black), and Fourier transform of $[Cp^{\ddagger}_2UF]_2$

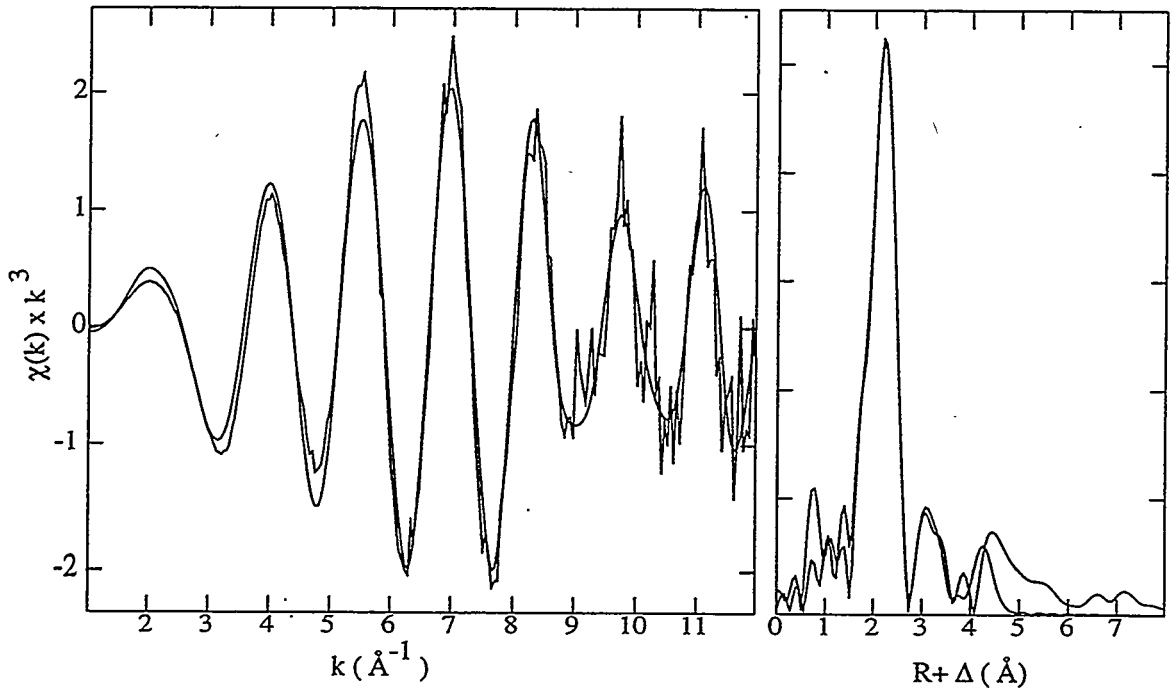

Figure 1d.6: EXAFS spectrum (gray), fit (black), and Fourier transform of $[Cp^{\ddagger}_2UCl]_2$

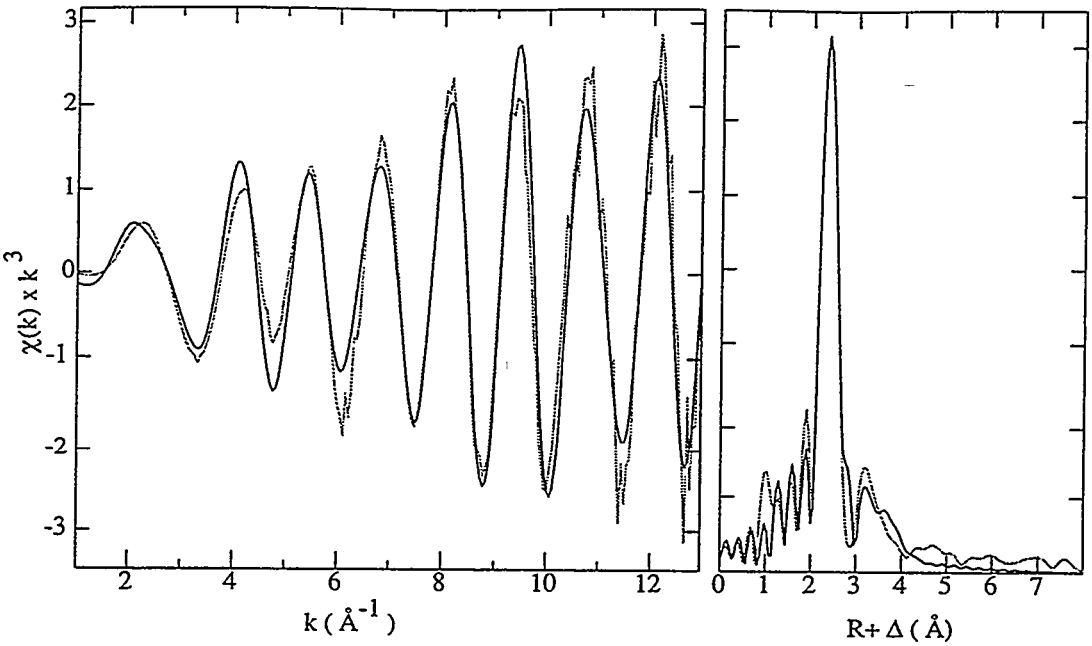

Figure 1d.7: EXAFS spectrum (gray), fit (black), and Fourier transform of $[Cp^{\ddagger}_2UBr]_2$

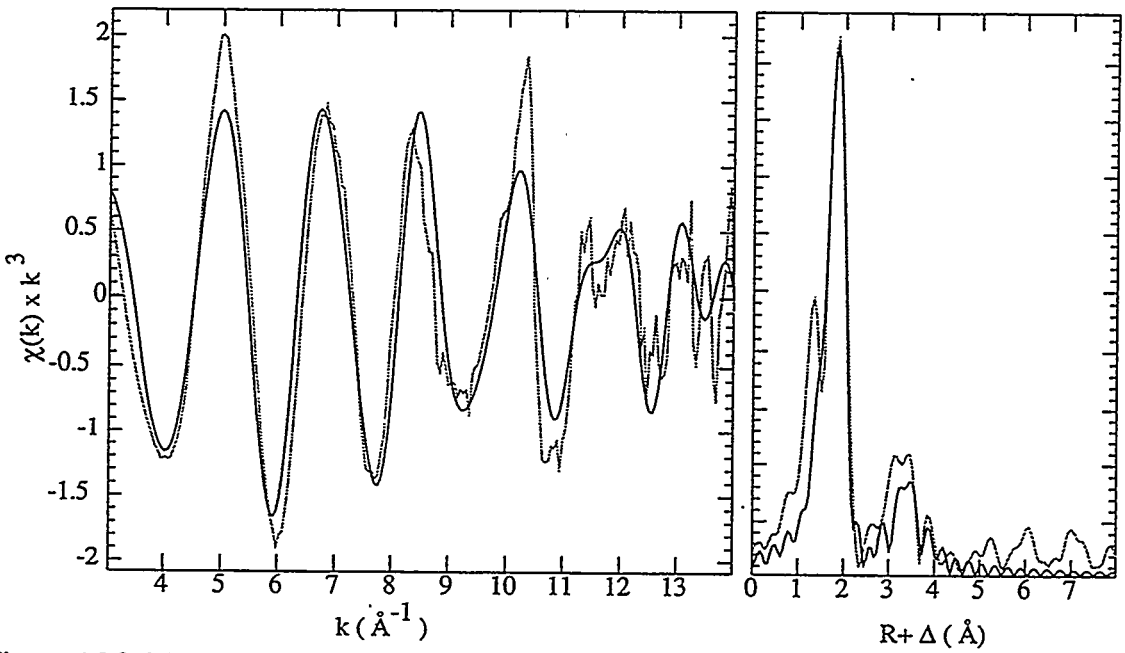

Figure 1d.8: EXAFS spectrum (gray), fit (black), and Fourier transform of $[Cp"2UF_2]_2$

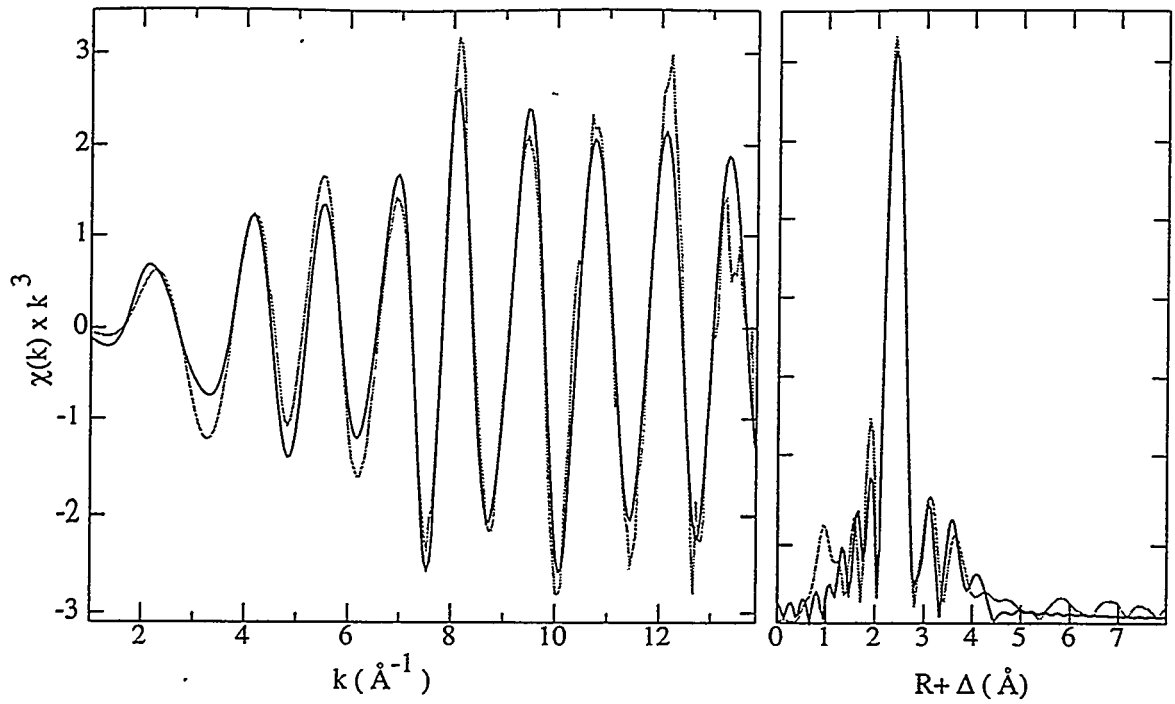

Figure 1d.9: EXAFS spectrum (gray), fit (black), and Fourier transform of $[Cp"2UBr]_2$

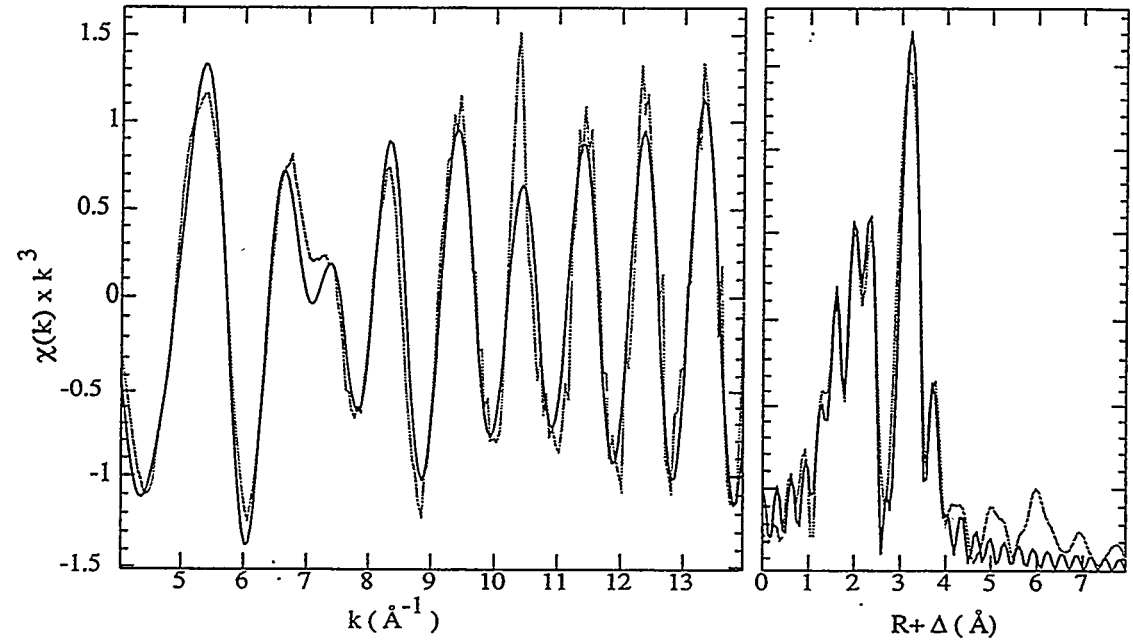

Figure 1d.10: EXAFS spectrum (gray), fit (black), and Fourier transform of $[Cp^{\ddagger}_2UO]_2$

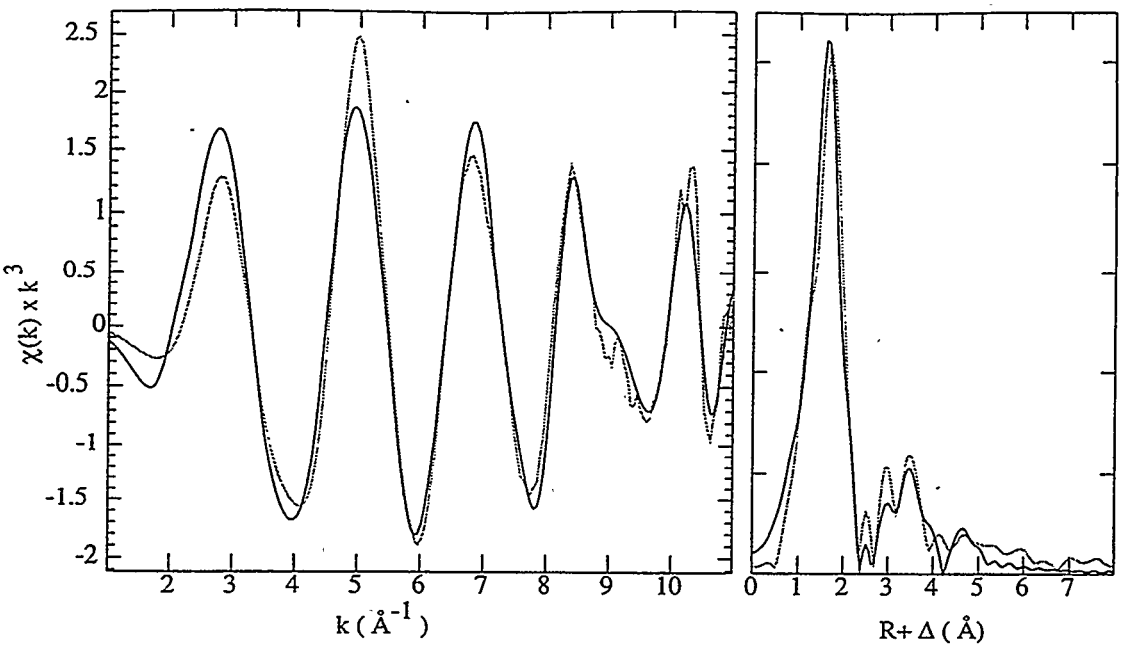

Figure 1d.11: EXAFS spectrum (gray), fit (black), and Fourier transform of $Cp^{\ddagger}_2UF_2$

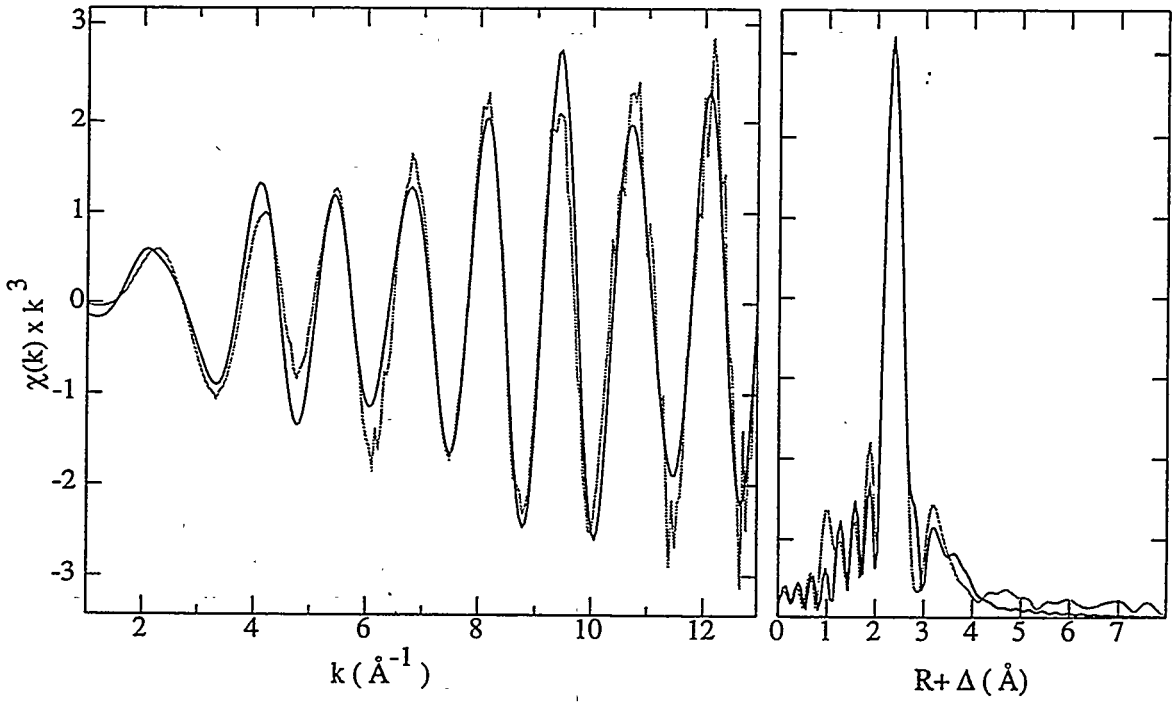

Figure 1d.12: EXAFS spectrum (gray), fit (black), and Fourier transform of $Cp^{\ddagger}_2UBr_2$

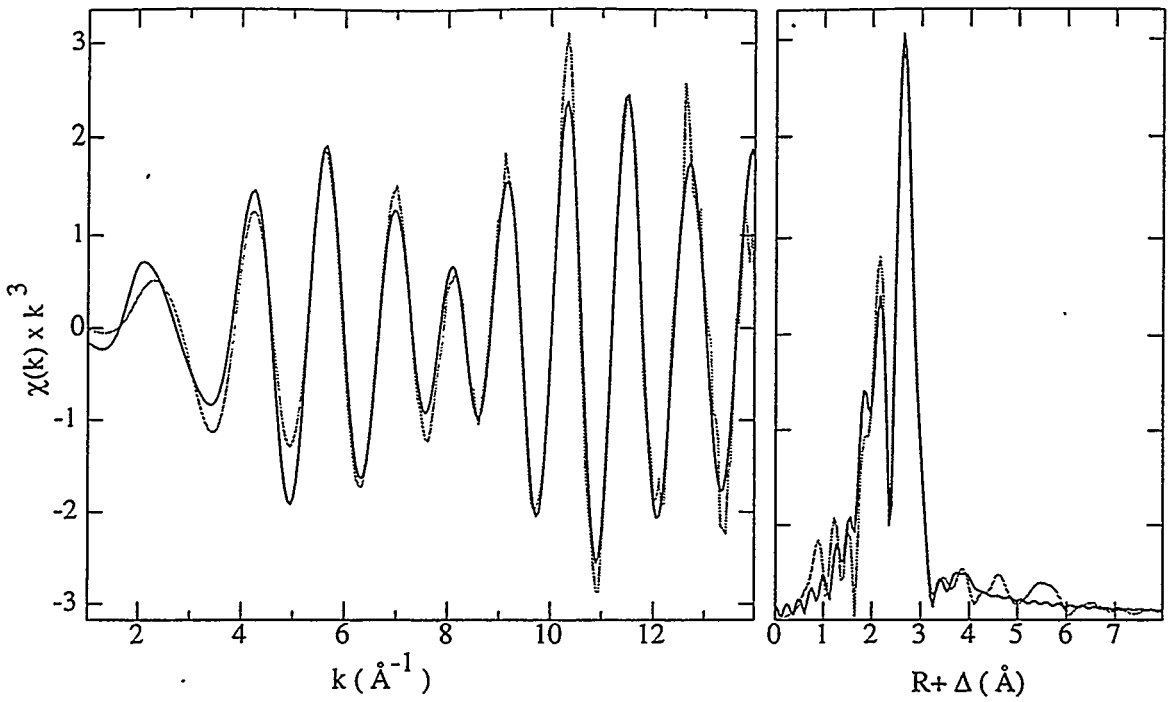

Figure 1d.13: EXAFS spectrum (gray), fit (black), and Fourier transform of $Cp^{\ddagger}_2UI_2$

The quality of the EXAFS data varies somewhat due to a number of factors including the nature of the sample (heavier atom neighbors scatter electrons better and give more intense data at high k), the quality of the x-ray beam at the time of acquisition, and the number of scans averaged to give the spectrum. In general, if the beam was not noisy, the average of two scans gave a fairly good EXAFS spectrum. The U-U distances obtained from EXAFS are generally in good agreement with those obtained by crystallography. In the case of $[Cp''_2UF_2]_2$, the agreement is poor; however, the EXAFS spectrum of this compound is poor.

Table 1d.2: EXAFS Data for Dicyclopentadienyluranium(III) Complexes

Shell	Coordination Number (CN)	Debye-Waller Factor (σ)	Distance by EXAFS (Å)	Distance by Crystallography (Å)
$[Cp''_2UF]_2$				
U-F	2	0.0056	2.353(5)	2.331(3)
U-C_{ring}	10	0.0143	2.862(8)	2.767(8)
U-C_{ring} (MS)	20	0.0001	3.418(6)	
U-U	1	0.0077	3.934(9)	3.8446(4)
U-Si	4	0.0244	4.17(3)	
$[Cp''_2UCl]_2$				
U-C_{ring}	10	0.0059	2.719(2)	2.78(2)
U-C_{ring} (MS)	20	0	3.416(6)	
U-Si	4	0.0147	4.21(1)	
U-U	1	0.0016	4.33(2)	4.357(1)
$[Cp^{\ddagger}_2UOH]_2$				
U-O	2	0.0052	2.375(6)	
U-C_{ring}	10	0.0102	2.864(8)	
U-C_{ring} (MS)	20	0.0030	3.38(1)	
U-U	1	0.0013	3.89(3)	
U-C_{tert}	4	0.0010	3.84(2)	
U-C_{Me}	4	0.0014	4.06(4)	
U-C_{Me}	4	0.0054	4.44(4)	
$[Cp^{\ddagger}_2UF]_2$				
U-F	2	0.0057	2.264(6)	
U-C_{ring}	4	0.0067	2.428(8)	
U-U	1	0.0027	3.891(5)	
U-C_{tert}	4	0.0019	3.860(8)	
$[Cp^{\ddagger}_2UCl]_2$				
U-C_{ring}	10	0.0062	2.759(3)	2.78(4)
U-C_{ring}(MS)	20	0.0007	3.419(7)	
U-C_{tert}	4	0.0097	3.86(3)	
U-C_{Me}	4	0.019	4.02(6)	
U-U	1	0.0055	4.57(1)	4.540(1)
$[Cp^{\ddagger}_2UBr]_2$				
U-C_{ring}	10	0.0111	2.828(4)	
U-Br	2	0.0099	2.993(5)	
U-C_{ring} (MS)	20	0.0005	3.411(8)	
U-C_{tert}	4	0.0034	3.834(8)	
U-C_{Me}	4	0.0079	4.04(2)	
U-U	1	0.0080	4.65(2)	

Table 1d.3: EXAFS Data for Dicyclopentadienyluranium(IV) Complexes

Shell	Coordination Number (CN)	Debye-Waller Factor (σ)	Distance by EXAFS (Å)	Distance by Crystallography (Å)
$[Cp''_2UF_2]_2$				
U-F	3	0.0060	2.316(5)	2.2(1) (average of 3 U-F distances)
U-C_{ring}	10	0.0515	2.60(3)	2.76(1)
U-U	1	0.0048	3.741(8)	3.9504(7)
U-Si	2	0.0055	4.12(1)	
Cp''_2UBr_2				
U-C_{ring}	10	0.0121	2.708(7)	2.71(1)
U-Br	2	0.0046	2.742(2)	2.734(1)
U-C_{ring} (MS)	20	0.0001	3.409(8)	
U-Si	4	0.0082	4.175(8)	
U-C_{Me}	6	0.0017	4.72(2)	
$[Cp^{\ddagger}_2UO]_2$				
U-O	1	0.0080	2.15(1)	2.118(7)
U-O	1	0.0080	2.33(1)	2.121(7)
U-C_{ring}	10	0.0145	2.823(6)	2.80(5)
U-U	1	0.0029	3.399(3)	3.3904(7)
U-C_{Me}	4	0.0064	4.25(1)	
$Cp^{\ddagger}_2UF_2$				
U-C_{ring}	10	0.0113	2.335(3)	2.74(3)
U-C_{tert}	4	0.0010	3.874(8)	
U-C_{Me}	8	0.0063	4.104(8)	
U-C_{Me}	4	0.0027	5.29(2)	
$Cp^{\ddagger}_2UBr_2$				
U-C_{ring}	10	0.0155	2.710(8)	
U-Br	2	0.0052	2.744(2)	
U-C_{tert}	4	0.0009	3.817(7)	
U-C_{Me}	8	0.0080	3.98(1)	
$Cp^{\ddagger}_2UI_2$				
U-C_{ring}	10	0.0104	2.728(3)	
U-I	2	0.0051	2.975(1)	
U-C_{tert}	4	0.0021	3.817(7)	
U-C_{Me}	4	0.0041	3.98(1)	

For the most part, the distances for the U-$C_{Cp\ ring}$ and U-X where X is the other ligand on uranium agree with the crystallography only when X is much heavier than C. The problem is that low atomic number (Z) scattering atoms have the greatest EXAFS amplitude in the low k region of the spectrum. If X is a light atom, such as O or F, both the U-C_{ring} distance and the U-X distance are somewhat similar, so both shells of atoms make very similar contributions to the EXAFS spectrum. When a fit of the EXAFS spectrum was attempted including both the U-C_{ring} and the U-X contributions, the Debye-Waller factors of the shells were strongly correlated. Either the Debye-Waller parameters of both shells became very small, or the Debye-Waller factor for one of the shells became very large. If this problem with the Debye-Waller factors occurred, the shell which gave the best fit to the observed spectrum was retained and the other shell was discarded. In many of the compounds, EXAFS data for both U-C_{ring} and U-X is not reported because of this problem.

When X is much heavier than carbon, as in Br and I, the amplitude of its contribution to the EXAFS spectrum is larger than the contribution from carbon at higher k, as shown the deconvolution of the fit of the EXAFS spectrum of Cp"2UBr_2 in Figure 1d.14. In this case, both the U-C_{ring} and U-Br distance can be determined. In general, due to the large number of carbon atoms in these complexes, the utility of EXAFS in determining bond lengths to other atoms coordinated to the uranium center is limited to heavier atoms.

In the cases where the U-X bond length could be determined, the agreement with crystallographic data was good. Where crystallographic data was not available, the bond lengths are similar to bond lengths in analogous complexes. For example, in $Cp^{\ddagger}_2UBr_2$ and $Cp^{\ddagger}_2UI_2$, the U-X bond lengths of 2.744(2) Å and 2.975(3) Å, respectively, are close to the U-X bond lengths found in $Cp"_2UBr_2$ and $Cp"_2UI_2$ of 2.734(1) Å and 2.953(2) Å, respectively.[18]

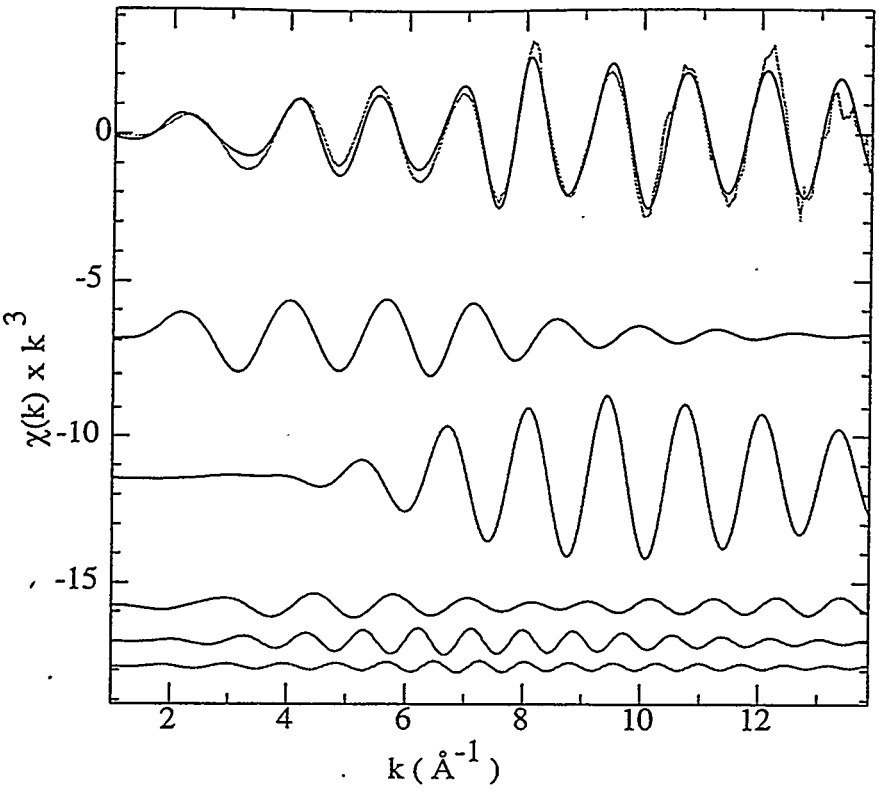

Figure 1d.14: Deconvolution of the fit of the EXAFS spectrum of $Cp"_2UBr_2$

Upper Plots:	Spectrum (in gray), fit (in black)
Second Plot:	C_{ring} scattering
Third Plot:	Br scattering
Fourth Plot:	C_{ring}-C_{ring} multiple scattering
Fifth Plot:	Si scattering
Sixth Plot:	C_{Me} scattering

Despite the fact that the EXAFS spectra did not always yield useful information on the nearest coordination shells of the uranium center, useful information was obtained from the U-U distances. As noted earlier, the low temperature NMR spectra of $[Cp^{‡}_2UX]_2$ complexes where X = H, F, or OH were confusing, and it was not clear whether the molecules exist as trimers or as a mixture of rotamers. The identical U-U distance of 3.89 Å in both $[Cp^{‡}_2UF]_2$ and $[Cp^{‡}_2UOH]_2$ implies that they have the same symmetrically bridged dimeric structure seen in $[Cp"_2UF]_2$. A trimer or a dimer in which only one of the fluorides or hydroxides was bridging would have a U-U distance

of about twice the U-F distance depending upon the U-F-U angle, that is, about 4.6 Å. In $[Cp^*_2UCl]_3$, the U-U distance is 5.67 Å compared to the U-Cl distance of 2.90 Å.

In summary, EXAFS spectroscopy on these complexes gives useful information on the U-U distance in dimers. Additionally, when obtainable, the U-Cp distances and distances to other ligands of the complexes are in good agreement with those determined by crystallography. However, because of complications due to the similar atomic number and bond distance of the Cp carbon atoms, the latter bond distances are not always available.

1e: Ring Conformations and Barriers to Site Exchange ("Ring Rotation") in Uranium Metallocenes

In the preceding sections, the crystal structures and NMR behavior of a number of complexes were reported. The observations were not commented upon previously since it was difficult to make any generalizations based upon any of these small subsets of structural data. From the combined structural and solution data, a number of trends become obvious. The conformations of the $Cp^{\ddagger}$ and Cp" rings observed in these compounds can be placed into the three categories shown in Figure 1e.1. A few complexes have ring orientations in which the C_{2v} structure has the rings slightly twisted with respect to each other but not to the extent of the C_2 structure; note that in the C_2 structure two R groups lie between the X ligands. This additional structure is labeled C_{2v}/C_2; note that in this structure, the R groups do not lie between the X ligands. A list of known crystal structures and ring conformations is given in Table 1e.1 along with the Van der Waals radius of X, when known, and the U-U distance in dimers.

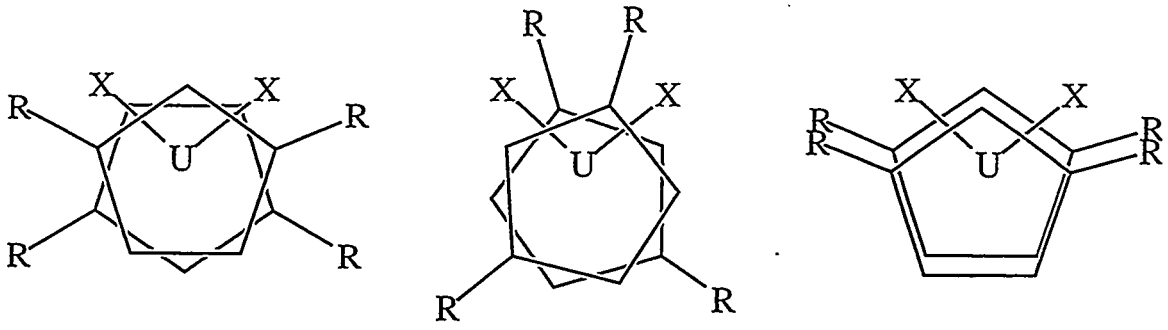

Figure 1e.1 Observed conformations of Cp" and $Cp^{\ddagger}$ rings in bent metallocene complexes. R = $SiMe_3$ or CMe_3.

Table 1e.1: Conformations of bent metallocenes containing the Cp" or Cp‡ ligand

Compound	Conf.	Radius of X[45]	U-X Dist.	U-U Dist.	M - Cp Dist.	Cp-U-Cp Angle	Exch. Barrier
$Cp^{‡}_2UF_2$	C_{2v}	1.35	2.09		2.46	125.3	
$Cp"_2UCl_2$	C_{2v}	1.8	2.573		2.42	124.7	
$[Cp^{‡}_2UH]_2$	C_s ?	1.2					13.2
$[Cp^{‡}_2UF]_2$	C_s ?	1.35					13.5
$[Cp^{‡}_2UOH]_2$	C_s ?	1.4					13.5
$[Cp^{‡}_2UCl]_2$	C_{2v}/C_2	1.8	2.86	4.54	2.52	120	8.4
$[Cp^{‡}_2UBr]_2$	C_{2v}/C_2	1.95					9.0
$[Cp^{‡}_2UI]_2$	C_{2v}/C_2 ?	2.15					8.9
$Cp"_2UMe_2$	C_2	2.0	2.42		2.44	131	
$Cp"_2U(OMe)_2$	C_2						8.5
$Cp"_2UI_2$[18]	C_2	2.15	2.953				
$Cp"_2UBr_2$[18]	C_{2v}/C_2	1.95	2.734				
$[Cp"_2UF_2]_2$	C_s	1.35	2.3	3.95	2.48	126.3	10.0
$[Cp"_2UF]_2$	C_s	1.35	2.33	3.85	2.49	130	12.4
$[Cp"_2UCl]_2$[13]	C_s	1.8	2.81	4.36	2.49	131	8.9
$[Cp"_2UBr]_2$[13]	C_s	1.95	2.93	4.33			7.9
$[Cp"_2UI]_2$ [13]	C_s ?	2.15					
$[Cp"_2UO]_2$[38]	C_s	1.4	2.12	3.39	2.49	123	16.9
$[Cp"_2UOH]_2$	C_s ?	1.4	2.30	3.85	2.49	128	12.4
$Cp"_2UCl_2^-$ Ph_4P^+[18]	C_2	1.8	2.67				
$[Cp^{‡}_2UO]_2$	C_s	1.4	2.12	3.39	2.52	124	>16.6

In order to make sense of the conformations of the Cp ligands it is necessary to consider the different steric interactions in the molecules. First, in all of the molecules, the ligand R groups must be in the neighborhood of X. In monomers, depending on the size of X, the ligands adopt either a C_{2v} geometry or a C_2 geometry. If X is small, the steric interaction between X and the R group of the Cp ligand is also small, and the Cp ligands can adopt the C_{2v} geometry. As X gets larger, then the R groups cannot adopt

the C_{2v} geometry since this will result in an unfavorable interaction between the R group and the X group. Rather, the ligands adopt the C_2 conformation in which the R groups of one Cp ligand straddle one of the X ligands to minimize steric interactions.

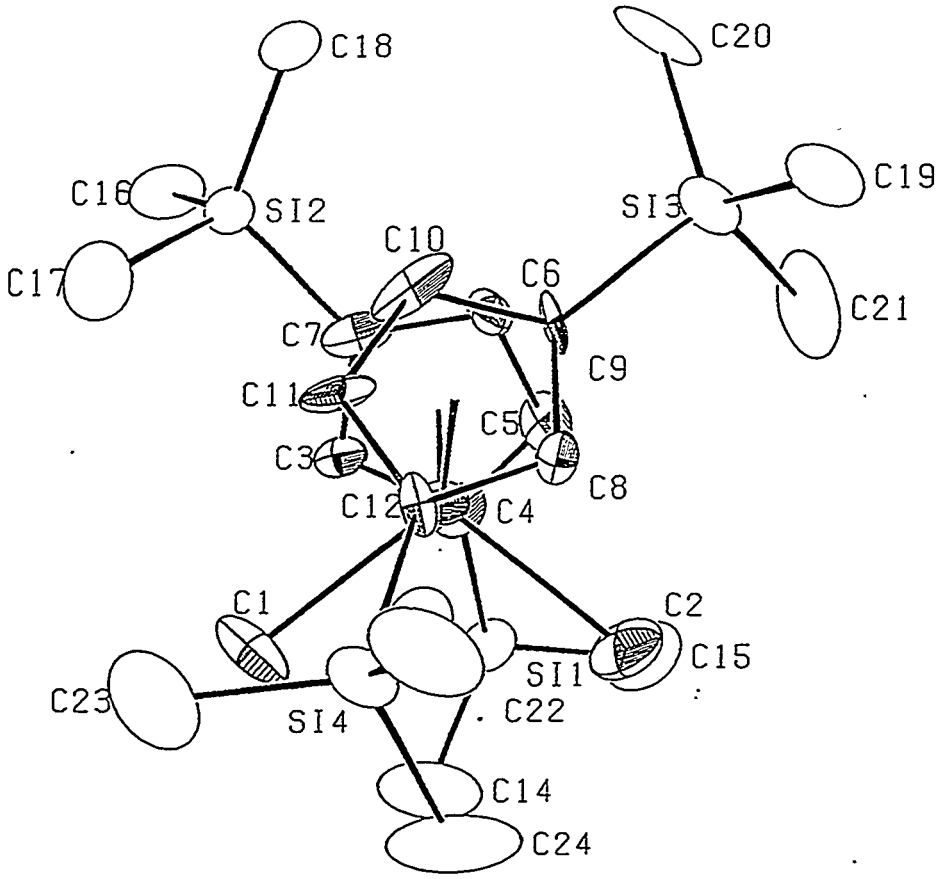

Figure 1e.2: An ORTEP diagram of Cp"$_2$UMe$_2$ with 50% thermal ellipsoids

Table 1e.2: Some distances and angles in Cp"$_2$UMe$_2$

Distances		Angles	
U-C1	2.42(2) Å	Cp1-U-Cp2	130.8°
U-Cp	2.44 Å	C1-U-C2	105.0(7)°
U-$\langle C_{ring} \rangle$	2.72(3) Å		
U-C2	2.42(2) Å		
U-Cp2	2.44 Å		

An example of a complex with the C_2 conformation is $Cp"_2UMe_2$ shown in Figure 1e.2. Distances and angles are given in Table 1e.2. Few compounds with uranium to carbon sigma bonds have been structurally characterized. However, the 2.42(2) Å U-Me bond length in $Cp"_2UMe_2$ is similar to the 2.465(7) U-Me bond length in $Li\{U(Me)[OCH(CMe_3)_2]_4\}$,[46] to the 2.422(8) Å U-Me bond length in $MeU[OC(CMe_3)_3]_3$,[47] and to the 2.48(3) Å U-C σ-bond length in Cp_3U(2-methyl-allyl).[48] In comparison to $Cp"_2UCl_2$, the Me-U-Me angle is 10° wider than the Cl-U-Cl angle due to the presence of the bulky $SiMe_3$ between the methyl groups. The C_2 geometry of $Cp"_2UMe_2$ also allows the metallocene to bend less than in the C_{2v} $Cp"_2UCl_2$.

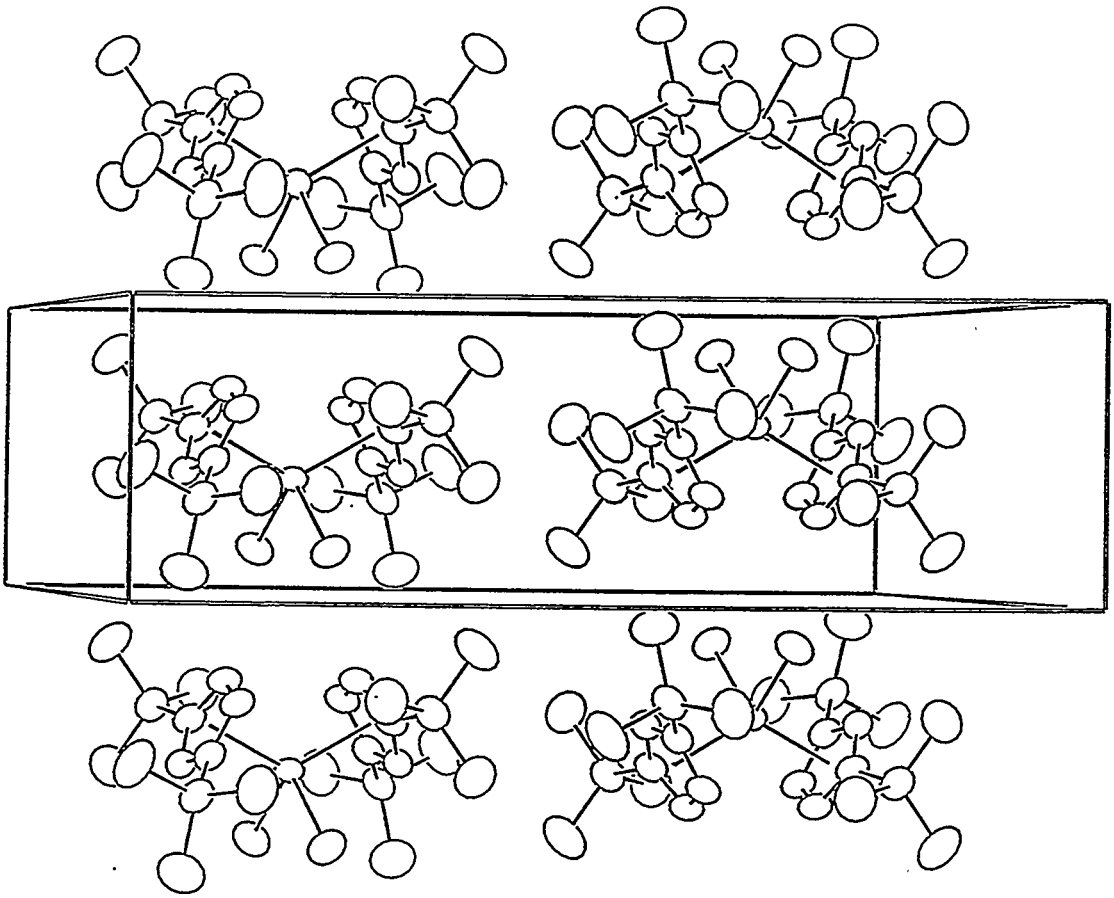

Figure 1e.3: Packing of $Cp"_2UCl_2$

It seems strange that all of the monomers do not adopt the C_2 conformation since, regardless of the size of X, this conformation minimizes repulsions between X and the Cp ligand. One explanation is that Cp"$_2$UCl$_2$, Cp$^{\ddagger}_2$UCl$_2$, and Cp$^{\ddagger}_2$UF$_2$ adopt the C_{2v} geometry in the solid state to maximize dipole interactions. In all of the crystal structures of these molecules, the metallocenes are aligned along the short b axis of the unit cell with a U - U separation equal to the length of the b axis as shown in Figure 1e.3. Presumably packing in this way maximizes the interactions between the molecular dipoles. By adopting the C_{2v} structure, the molecules can get closer together than if they had the C_2 structure. This explanation is supported by the conformation of the Cp"$_2$UCl$_2$ anion in the [Cp"$_2$UCl$_2$]$^-$ [PPh$_4$]$^+$ structure. In this case, the anionic metallocene fragments are not aligned, and the ligands adopt the expected C_2 structure. In addition to explaining the C_{2v} conformation of Cp$^{\ddagger}_2$UF$_2$, the dipole interaction hypothesis also explains the low solubility of this complex in hydrocarbons.

In the dimers, the interaction between the Cp ligands on opposite metal centers is also important. When this interaction dominates, the ligands adopt the C_s conformation, and the dimer either has the C_{2h} geometry of [Cp"$_2$UO]$_2$ or the C_i geometry of [Cp"$_2$UCl]$_2$. This intermetallocene interaction is more important than the interaction of the ligand with X in all of the [Cp"$_2$UX]$_2$ dimers and when the uranium centers are close together as in [Cp$^{\ddagger}_2$UO]$_2$. In the case of [Cp$^{\ddagger}_2$UCl]$_2$, the Cp ligands adopt a geometry between C_{2v} and C_2. This conformation suggests that the geometry of the CMe$_3$ groups is influenced by both the X ligand and by the other metallocene fragment of the dimer. Since the Cp-CMe$_3$ distance is shorter than the Cp-SiMe$_3$ distance, the influence of the other metallocene fragment of the dimer does not force the Cp‡ containing molecules to adopt the C_s geometry until the U-U distance is very short, as in [Cp$^{\ddagger}_2$UO]$_2$.

The conformations are responsible for the NMR behavior of the complexes. For the monomers, when X is large, the site exchange can be stopped at low temperature, and the two inequivalent CMe$_3$ or SiMe$_3$ groups in the C_2 conformation can be

observed. In $Cp''_2U(OMe)_2$, this barrier is 8.5 kcal/mol. The barrier is presumably due to the interaction of the $SiMe_3$ group with the OMe ligand.

In the dimers, two possible cases exist depending upon whether the metallocenes adopt a C_s or C_{2v}/C_2 conformation. In the C_{2v}/C_2 conformation, seen in $[Cp^{\ddagger}_2UCl]_2$, the R groups of the ligands do not need to interact with the front of the other metallocene in the dimer when changing sites, as shown in Figure 1e.3. The most important result of

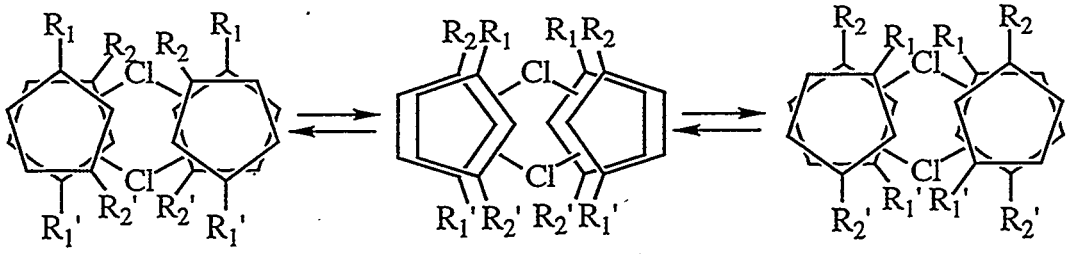

Figure 1e.3 Site Exchange in $[Cp^{\ddagger}_2UCl]_2$ (**13**)

this observation is that in $[Cp^{\ddagger}_2UX]_2$ dimers with this conformation, the barrier to site exchange will not depend greatly on the U-U distance. Rather, the barrier will depend on the size of the bridging ligand. This is consistent with the trend in ring rotation barriers in the $[Cp^{\ddagger}_2UX]_2$ series $\Delta G^{\ddagger}_I > \Delta G^{\ddagger}_{Br} > \Delta G^{\ddagger}_{Cl}$.

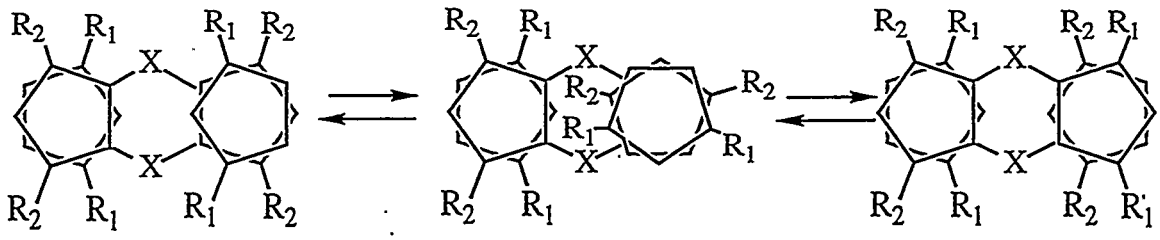

Figure 1e.4 Site Exchange in Dimers with the C_s Ring Conformation

On the other hand, when the ring conformation is C_s, the barrier to ring rotation is strongly dependent upon the U-U distance since the bulky R groups must rotate past

the other metallocene unit of the dimer as shown in Figure 1e.4. This rotation mechanism is consistent with the trend observed in site exchange barriers: $[Cp"_2UO]_2$ > $[Cp"_2UOH]_2 \approx [Cp_2UF]_2 > [Cp"_2UCl]_2 \approx [Cp"_2UBr]_2 > [Cp"_2UI]_2$.

The only molecules which do not obey these rules are $[Cp^{\ddagger}_2UF]_2$ and $[Cp^{\ddagger}_2UOH]_2$. At low temperatures, these molecules display several inequivalent CMe_3 resonances. Since EXAFS data show that the U-U distances in these molecules are consistent with a dimeric structure, the most likely explanation of the observed behavior at low temperature is that more than one conformer exists in solution. In $[Cp^{\ddagger}_2UF]_2$, at low temperatures, 6 inequivalent CMe_3 groups are present, in $[Cp^{\ddagger}_2UOH]_2$, 5 are present (two overlap). The presence of two rotamers, with one having the $[Cp"_2UCl]_2$ structure with 4 inequivalent CMe_3 groups and one having either the $[Cp^{\ddagger}_2UCl]_2$ structure can account for these observations. Since the U - U distance in $[Cp^{\ddagger}_2UF]_2$ and $[Cp^{\ddagger}_2UOH]_2$ is somewhere between that of $[Cp^{\ddagger}_2UCl]_2$ and that of $[Cp^{\ddagger}_2UO]_2$, rotamers with the C_{2v}/C_2 conformation of $[Cp^{\ddagger}_2UCl]_2$ and the C_s conformation of $[Cp^{\ddagger}_2UO]_2$ might both be stable.

The conformations of metallocenes containing the $Cp^{\ddagger}$ or Cp" ligands are due to two factors: first, the interaction between the $SiMe_3$ or CMe_3 groups and the other ligands bonded to the metal center and second, the interaction between metallocene units in dimers. The ligand site exchange barriers determined by variable temperature ^1H NMR spectroscopy reflect the different conformations.

References

(1) Reynolds, L. T.; Wilkinson, G. *J. Inorg. Nucl. Chem.* **1956**, *2*, 246-253.

(2) Streitwieser Jr., A.; Müller-Westerhoff, U. *J. Am. Chem. Soc.* **1968**, *90*, 7364.

(3) Manriquez, J. M.; Fagan, P. J.; Marks, T. J. *J. Am. Chem. Soc.* **1978**, *100*, 3939-3941.

(4) Arney, D. S. J.; Burns, C. J.; Smith, D. C. *J. Am. Chem. Soc.* **1992**, *114*, 10068-10069.

(5) Brennan, J. G.; Andersen, R. A. *J. Am. Chem. Soc.* **1985**, *107*, 514.

(6) Brennan, J. G. Ph. D. Thesis, University of California, Berkeley, 1985.

(7) Rosen, R. K. Ph. D. Thesis, University of California, Berkeley, 1989.

(8) Kanellakopolous, B.; Fischer, E. O.; Dornberger, E.; Baumgärtner, F. *J. Organomet. Chem.* **1970**, *24*, 507.

(9) Brennan, J. G.; Stults, S. D.; Andersen, R. A.; Zalkin, A. *J. Am. Chem. Soc.* **1988**, *110*, 4554.

(10) Stults, S. D. Ph. D. Thesis, University of California, Berkeley, 1988.

(11) Fagan, P. J.; Manriquez, J. M.; Marks, T. J.; Day, C. S.; Vollmer, S. H.; Day, V. W. *Organometallics* **1982**, *1*, 170-180.

(12) Duttera, M. R.; Fagan, P. J.; Marks, T. J.; Day, V. W. *J. Am. Chem. Soc.* **1982**, *104*, 865-867.

(13) Blake, P. C.; Lappert, M. F.; Taylor, R. G.; Atwood, J. L.; Hunter, W. E.; Zhang, H. *J. Chem. Soc., Chem. Commun.* **1986**, 1394-1395.

(14) Beshouri, S., Unpublished Results

(15) Stuart, T., Unpublished Results

(16) Spirlet, M. R.; Rebizant, J.; Apostolidis, C.; Kanellakopolous, B. *Acta. Cryst.* **1992**, *C48*, 2135-2137.

(17) Druce, P. M.; Kingston, B. M.; Lappert, M. F.; Spalding, T. R.; Srivastava, R. C. *J. Chem. Soc. (A)* **1969**, 2106-2110.

(18) Blake, P. C.; Lappert, M. F.; Taylor, R. G.; Atwood, J. L.; Zhang, H. *Inorg. Chim. Acta* **1987**, *129*, 12-20.

(19) Bleaney, B. *J. Magn. Resonance* **1972**, *8*, 91-100.

(20) von Ammon, R.; Fischer, R. D. *Angew. Chem. internat. Edit.* **1972**, *11*, 675-692.

(21) Fagan, P. J.; Manriquez, J. M.; Maata, E. A.; Sayam, A. M.; Marks, T. J. *J. Am. Chem. Soc.* **1981**, *103*, 6650-6667.

(22) Jahn, W.; Yünlu, K.; Oroschin, W.; Amberger, H.-D.; Fischer, R. D. *Inorg. Chim. Acta* **1984**, *95*, 85-104.

(23) Stults, S. D.; Andersen, R. A.; Zalkin, A. *Organometallics* **1990**, *9*, 115-122.

(24) Fischer, R. D.; von Ammon, R.; Kanellakopulos, B. *J. Organomet. Chem.* **1970**, *25*, 123.

(25) Edelstein, N. M.; Goffart, J. In *The Chemistry of the Actinide Elements*; J. J. Katz, G. T. Seaborg and L. R. Morss, Eds.; Chapman and Hall: New York, 1986; Vol. 2; pp 1361-1387.

(26) Carnall, W. T.; Liu, G. K.; Williams, C. W.; Reid, M. F. *J. Chem. Phys.* **1991**, *95*, 7194-7203.

(27) Kannellakopolous, B. In *Organometallics of the f-Elements*; T. J. Marks and R. D. Fischer, Eds.; D. Reidel Publishing Company: Dordrecht: Holland, 1978; pp 1-36.

(28) Zalkin, A.; Stuart, A. L.; Andersen, R. A. *Acta. Cryst.* **1988**, *C44*, 2106-2108.

(29) Lowry, T. H.; Richardson, K. S. *Mechanism and Theory in Organic Chemistry;* Third ed.; Harper & Row: New York, 1987.

(30) Matsunaga, P. T. Ph. D. Thesis, U. C., Berkeley, 1991.

(31) Watson, P. L. *J. Am. Chem. Soc.* **1983**, *105*, 6491-6493.

(32) Evans, W. J.; Peterson, T. T.; Rausch, M. D.; Hunter, W. E.; Zhang, H.; Atwood, J. L. *Organometallics* **1985**, *4*, 554-559.

(33) Berthet, J.-C.; Ephritikhine, M.; Lance, M.; Nierlich, M.; Vigner, J. *J. Organomet. Chem.* **1993**, *460*, 47-53.

(34) Berthet, J.-C.; Maréchal, J.-F. L.; Nierlic, M.; Lance, M.; Vigner, J.; Ephritikhine, M. *J. Organomet. Chem.* **1991**, *408*, 335-341.

(35) Arney, D. S.; Burns, C. J. *J. Am. Chem. Soc.* **1993**, *115*, 9840-9841.

(36) Fagan, P. J.; Manriquez, J. M.; Maatta, E. A.; Seyam, A. M.; Marks, T. J. *J. Am. Chem. Soc.* **1981**, *103*, 6650-6667.

(37) Blosch, L., Unpublished Results

(38) Zalkin, A.; Beshouri, S. *Acta Cryst.* **1988**, *C44*, 1826-1827.

(39) Wood, C. D.; McLain, S. J.; Schrock, R. R. *J. Am. Chem. Soc.* **1979**, *101*, 3210 - 3222.

(40) Liu, A. H.; Murray, R. C.; Dewan, J. C.; Santarsiero, B. D.; Schrock, R. R. *J. Am. Chem. Soc.* **1987**, *109*, 4282-4291.

(41) Tahmassebi, S. K.; Conry, R. R.; Mayer, J. M. *J. Am. Chem. Soc.* **1993**, *115*, 7553-7554.

(42) Limbach, H.-H.; Hennig, J.; Gerritzen, D.; Rumpel, H. *Faraday Discuss Chem. Soc.* **1982**, *74*, 229-243.

(43) *X-Ray Absorption: Principles, Applications, Techniques of EXAFS, SEXAFS, and XANES*; Koningsberger, D. C.; Prins, R., Eds.; John Wiley & Sons: New York, 1988.

(44) Rehr, J. J.; Zabinsky, S. I.; Albers, R. D. *Phys. Rev. Lett.* **1992**, *69*, 3397.

(45) Pauling, L. *The Nature of the Chemical Bond*; Cornell University Press: Ithaca, New York, 1960.

(46) Stewart, J. L.; Andersen, R. A. *J. Chem. Soc., Chem. Commun.* **1987**, 1846 - 1847.

(47) Stewart, J. L. Ph. D. Thesis, University of California, Berkeley, 1988.

(48) Halstead, G. W.; Baker, E. C.; Raymond, K. N. *J. Am. Chem. Soc.* **1975**, *97*, 3049.

Chapter Two: Tris-cyclopentadienyl Complexes

Unlike the chemistry of dicyclopentadienyluranium(III), the chemistry of triscyclopentadienyluranium base adducts has been extensively studied.[1-4] The electronic structure of $Cp_3U•L$ (L is a Lewis base) has also been studied, and the MO structures of Cp_3U and $Cp_3U•L$ have also been described.[5-9] Surprisingly, some calculations have suggested that the ground state of Cp_3U might be d^1f^2 rather than the expected f^3 configuration because the $6d_z2$ orbital does not interact with the Cp ligands and is low in energy.[6] The base adducts are calculated to have an f^3 ground state because the d_z2 orbital is destabilized by the σ-donating orbital of the base. In light of the fact that $Cp"_3Th$ has a $6d^1$ ground state and not a $5f^1$ ground state, the uranium result seems plausible.[10,11] However, while base adducts of Cp_3U are well known, base-free Cp_3U compounds are rare. Only $(Me_3CC_5H_4)_3U$,[12] $(Me_3SiC_5H_4)_3U$,[13] $(Me_4C_5H)_3U$,[14] and $Cp"_3U$[15] are known, and the ground states of none of these compounds have been examined. Since $Cp"_3U$ and $Cp"_3U(t\text{-BuNC})$ had been synthesized previously by Beshouri,[15] we thought it would be interesting to examine the magnetism and EPR spectra of these complexes to determine whether the ground state is d^1f^2 or f^3.

2a: The Ground State of Tris-cyclopentadienyluranium

$Cp"_3U$ seems to be an excellent candidate in which to study the electronic ground state of the uranium center. The compound has idealized C_{3h} symmetry in the solid state, but, unfortunately, it crystallizes in the space group $P\bar{1}$ and does not have true C_{3h} symmetry.[16] The *tert*-butyl isocyanide adduct of $Cp"_3U$ has also been made, so a uranium compound which should have an f^3 ground state is available. In addition, the

analogous neodymium complexes can be examined since all of the neodymium complexes should have an f^3 ground state.

The syntheses of the tris-cyclopentadienyl complexes are similar to the syntheses of known compounds (eq 2a.1). Like $Cp"_3Ce$, both $Cp"_3La$ and $Cp"_3Nd$ were synthesized by treating $Ln[N(SiMe_3)_3]_3$ (Ln = La, Nd) with Cp"H in toluene.[17] While this route does work to make $Cp"_3U$, it does not work well. Instead, $Cp"_2UCl_2$ was reduced by molten potassium in hexane, as in the synthesis of $Cp"_3Th$ from $Cp"_2ThCl_2$ and sodium-potassium alloy. [10] Neither of these routes gave $Cp^{‡}_3U$. It was prepared by treating $[Cp^{‡}_2UF]_2$ with $Cp^{‡}_2Mg$ in tetrahydrofuran. The tris-cyclopentadienyl compounds are all very soluble in hexane from which they were crystallized.

$$M[N(SiMe_3)_2]_3 + 3\ Cp"H \rightarrow Cp"_3M + 3\ HN(SiMe_3)_2 \quad (M = La, Nd, U)$$
$$3\ Cp"_2UCl_2 + 6\ K \rightarrow 2\ Cp"_3U + 6\ KCl + U\ (metal) \qquad (2a.1)$$
$$[Cp^{‡}_2UF]_2 + Cp^{‡}_2Mg \rightarrow Cp^{‡}_3U + MgF_2$$

The *tert*-butyl isocyanide (*t*-BuNC) and cyclohexyl isocyanide ($C_6H_{11}NC$) adducts of $Cp"_3M$ (M = La, Nd, U) were made by adding the base to a hexane solution of $Cp"_3M$. The base adducts formed immediately. Like the $Cp"_3M$ complexes, the base adducts are hexane soluble, but less so than the base-free compounds. The CN stretching absorption is a strong, sharp feature in the IR spectrum (Table 2a.1). The CN stretch in the uranium complexes is lower in frequency than the CN stretch in the lanthanide complexes due to the greater overlap of the 5f orbitals with the π^* orbitals of the isocyanide group.[18,19]

Table 2a.1: CN stretching frequencies (in cm^{-1}) of $Cp"_3M(CN\text{-}R)$ complexes

	Base Alone[20]	M = La	M = Nd	M = U
R = *tert*-butyl	2146	2178	2178	2140
R = cyclohexyl	2138		2183	2154

The variable temperature magnetic susceptibilities, χ, of $Cp"_3Nd$, $Cp"_3U$, and their isocyanide adducts were measured. Plots of $1/\chi$ versus T are given in Figure 2a.1, and the numerical results are given in Table 2a.2. The magnetic moment from 200 K to 300 K in all cases is consistent with a $^4I_{9/2}$ ground state with the various crystal field states equally populated. For the $^4I_{9/2}$ level, the theoretical value of μ_{eff} is 3.62 B.M.[21] The measured μ_{eff} values for the neodymium complexes are very similar to the free ion value since the 4f orbitals have very little overlap with the ligand orbitals.[21] In the uranium complexes, the value of μ_{eff} near room temperature is lower presumably due to covalent effects.[22] The 5f orbitals of uranium have a greater radial extent than the 4f orbitals of neodymium and interact more strongly with the ligand orbitals.[23] The low temperature magnetic moments for all of the complexes are similar except for the $Cp"_3U$ and $Cp^{\ddagger}_3U$ complexes in which μ_{eff} is somewhat greater.

Table 2a.2: Magnetic data for $Cp"_3M$ and $Cp"M{\bullet}L$ complexes

	μ_{eff} (5 K)	μ_{eff} (5→7 K)	μ_{eff} (200→300 K)
$Cp"_3Nd$	1.65	1.84	3.70
$Cp"_3Nd{\bullet}(C_6H_{11}NC)$	1.75	2.05	3.60
$Cp"_3Nd{\bullet}(t\text{-BuNC})$	1.69	1.84	3.91
$Cp"_3U$	2.03	2.17	3.32
$Cp"_3U{\bullet}(C_6H_{11}NC)$	1.76	1.87	3.25
$Cp"_3U{\bullet}(t\text{-BuNC})$	1.78	1.94	3.14
$Cp^{\ddagger}_3U$	2.13	2.36	3.37

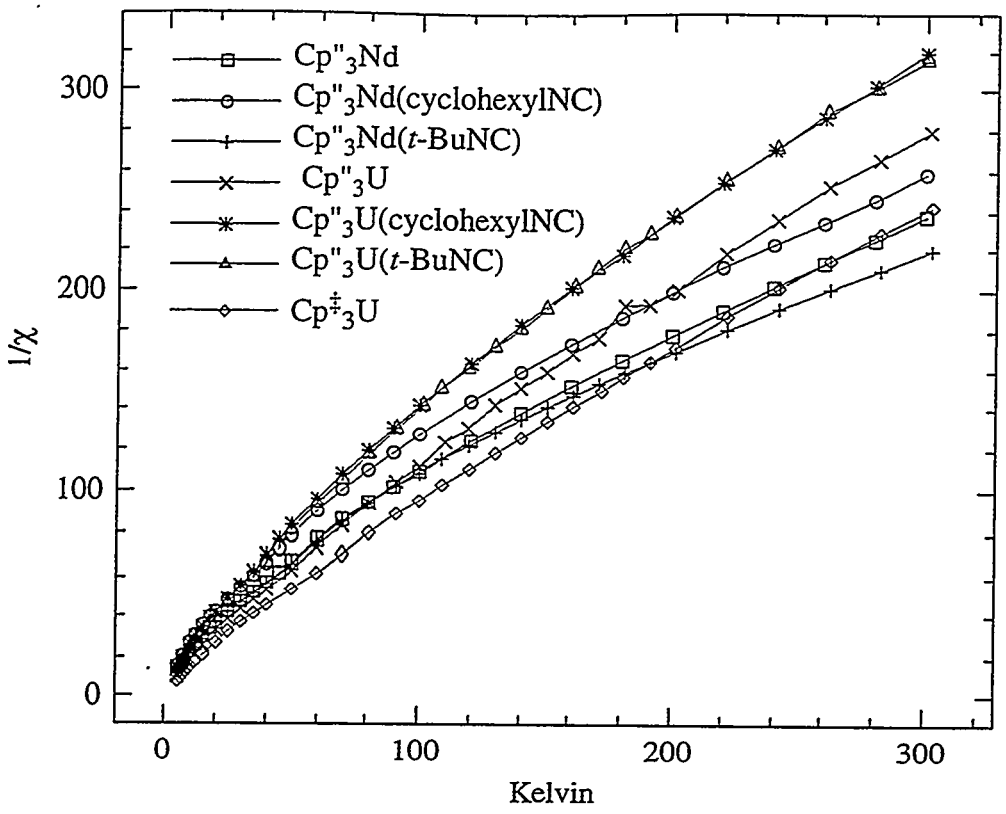

Figure 2a.1: Magnetic susceptibilities of Cp"$_3$M and Cp"$_3$M•L complexes

The EPR spectra of the tris-cyclopentadienyl complexes and their base adducts are shown in Figures 2a.2-2a.8 along with their least-squares fits. The line-shape used in fitting is that outlined by Soulie[24] which is based upon earlier work by Pilbrow.[25] In the fitting procedure, both the positions of the EPR signals and their line widths were allowed to vary. The fitting results are given in Table 2a.3. The values of μ_{eff} calculated from the EPR spectra are close to or lower than μ_{eff} determined by magnetic susceptibility for all of the complexes. One reason that μ_{eff} determined by EPR is low is that one of the g components, g_3, occurs at very high field in all of these compounds. The g_3 component is only observed for the Cp"$_3$Nd•L complexes. The fitting program obviously can not determine g_3 if it does not contribute to the spectrum over the range of

magnetic fields examined. In many cases, g_3 ends up being very small as a fitting parameter making μ_{eff} too low.

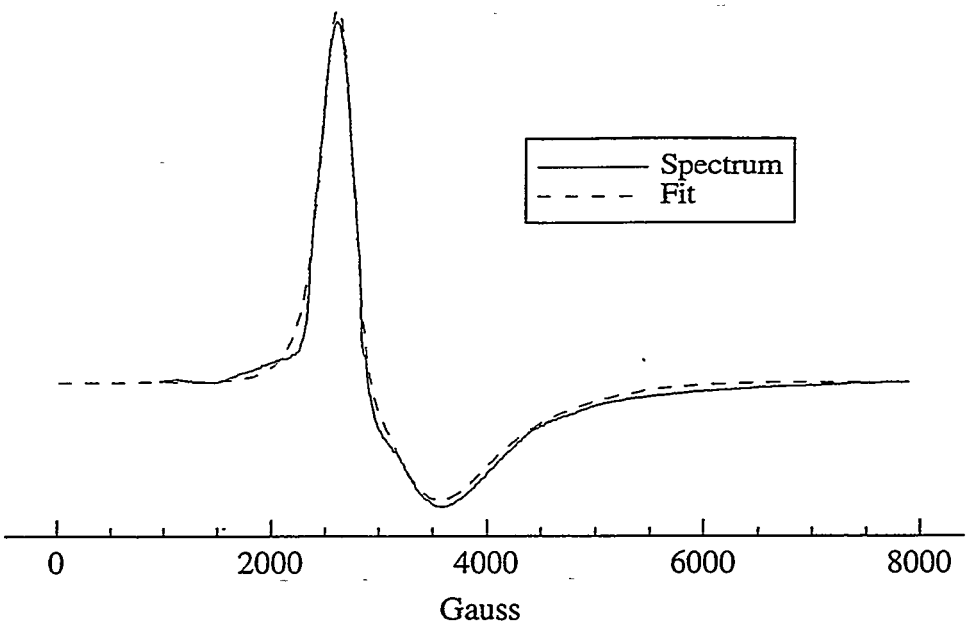

Figure 2a.2: EPR spectrum of Cp"$_3$Nd powder at 2 K

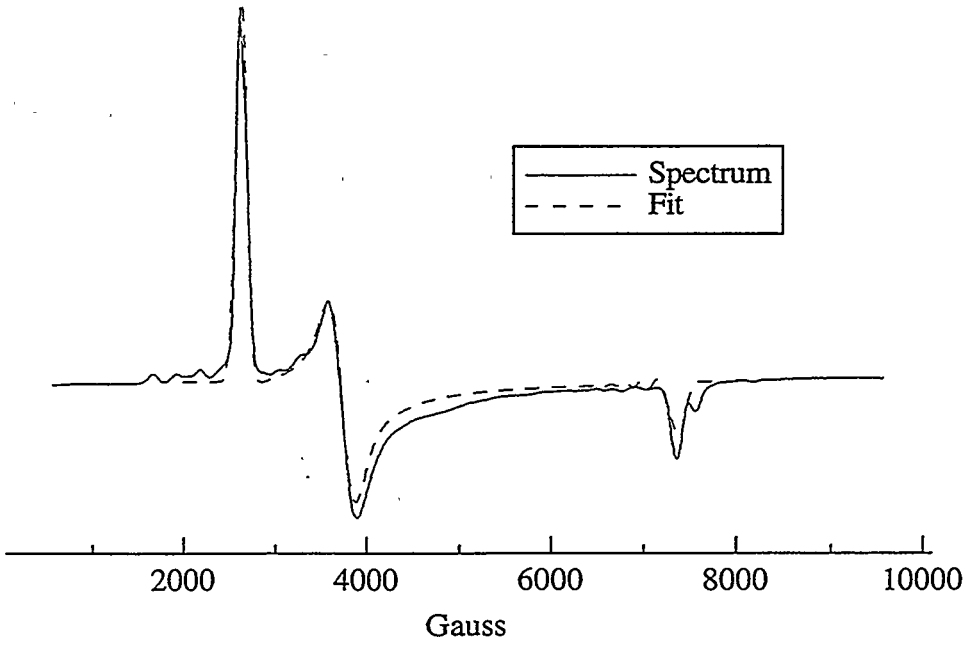

Figure 2a.3: EPR spectrum of Cp"$_3$Nd•(cyclohexyl isocyanide) powder at 2 K

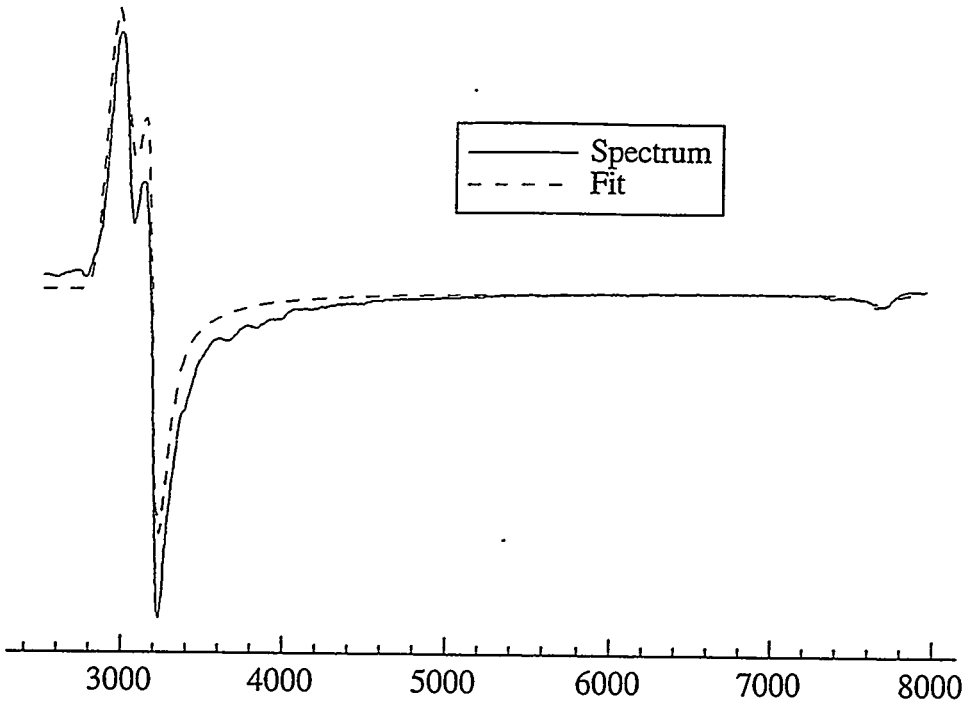

Figure 2a.4 EPR spectrum of $Cp''_3Nd\bullet(t\text{-BuNC})$ powder at 2 K

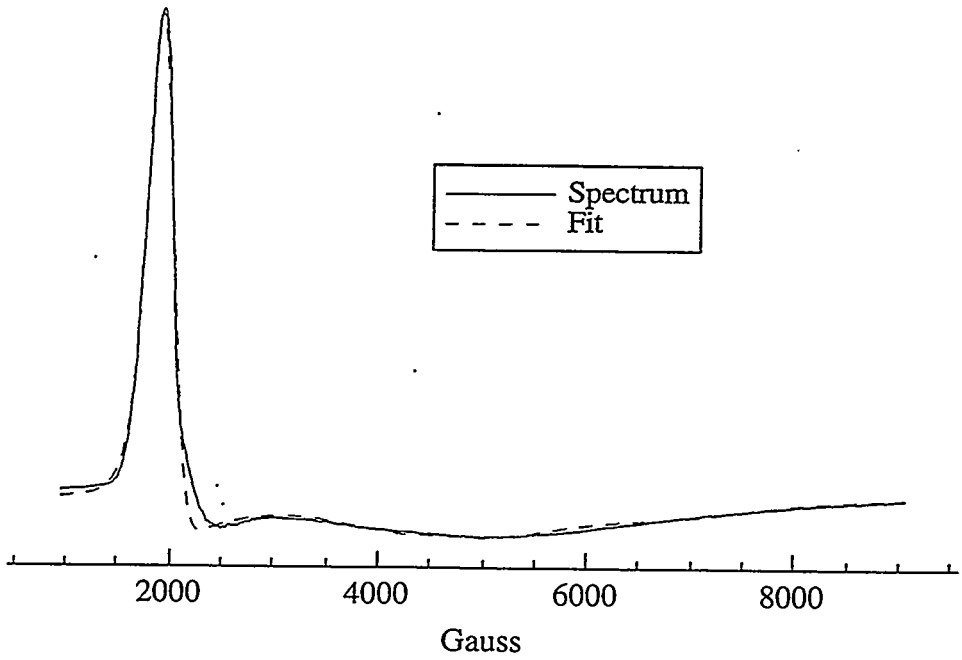

Figure 2a.5: EPR spectrum of Cp''_3U powder at 2 K

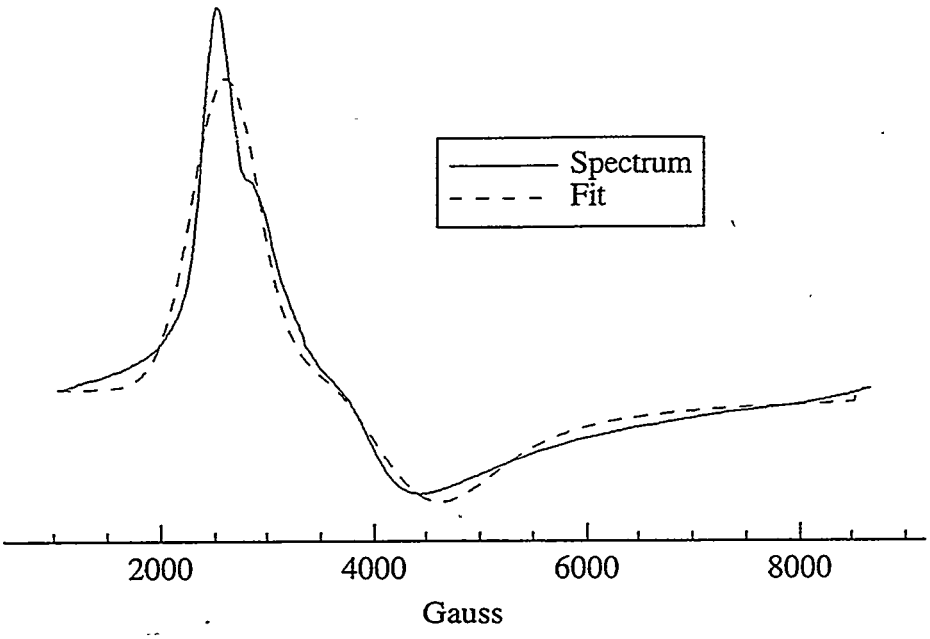

Figure 2a.6: EPR spectrum of Cp"$_3$U•(cyclohexyl isocyanide) powder at 2 K

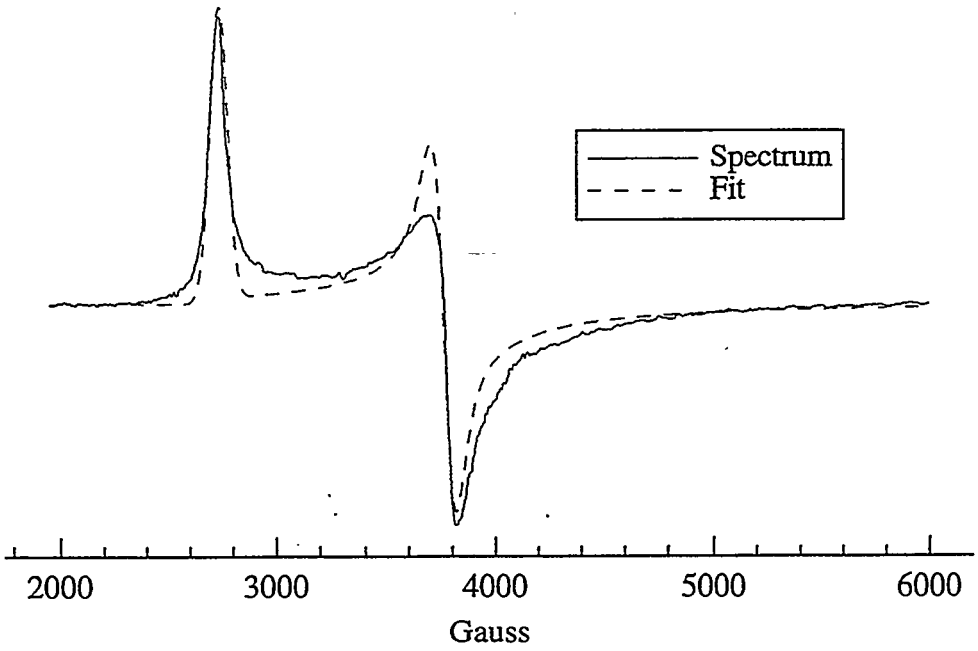

Figure 2a.7: EPR spectrum of Cp"3U•(t-BuNC) powder at 2 K

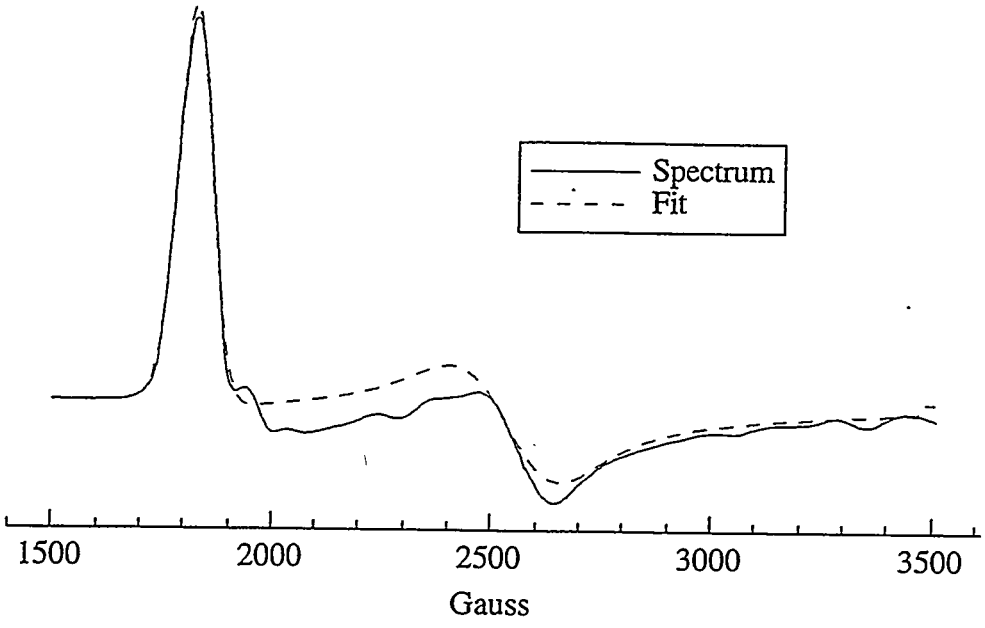

Figure 2a.8: EPR spectrum of $Cp^{\ddagger}_3U$ powder at 2 K

Table 2a.3: EPR values for Cp_3M and their base adducts determined by fitting their EPR spectra. The linewidth in GHz is in parentheses. The g values in curly brackets occur to fields not observed in the spectra (not reliable). $\mu_{eff}(calc) = (1/2)(g_1^2+g_2^2+g_3^2)^{1/2}$

	g_1	g_2	g_3	μ_{eff}(calc)	μ_{eff}(exp)
Cp"$_3$Nd	2.48(0.48)	2.08(1.29)	{0.18(0.69)}	1.62	1.65
Cp"$_3$Nd•(C_6H_{11}NC)	2.51(0.21)	1.76(0.29)	0.88(0.07)	1.60	1.75
Cp"$_3$Nd•(*t*-BuNC)	2.25(0.19)	2.08(0.11)	0.86(0.09)	1.59	1.69
Cp"$_3$U	3.41(0.50)	1.65(2.08)	0.85(0.75)	1.94	2.03
Cp"$_3$U•(C_6H_{11}NC)	2.51(0.96)	1.59(1.17)	{0.72(1.76)}	1.53	1.76
Cp"$_3$U•(*t*-BuNC)	2.41(0.12)	1.75(0.09)	{0.29(0.65)}	1.49	1.78
$Cp^{\ddagger}_3U$	3.60(0.16)	2.36(0.34)	{0.70(0.98)}	2.21	2.13

The theoretical basis for explaining the electronic spectra of lanthanide ions in C_{3v} and C_{3h} symmetry was developed by Stevens, Elliott, and Judd.[26-31] Briefly, for an f^3 ion, the ground state is $^4I_{9/2}$ due to spin-orbit coupling. The crystal field due to the surrounding ligands is a treated as a perturbation of the $^4I_{9/2}$ state. The $^4I_{9/2}$ state is 10 fold degenerate with the substates having J_z= (-9/2, -7/2, -5/2, ..., 9/2). The crystal field removes the degeneracy of the J_z states. The crystal field for a complex with C_{3h} symmetry has the form shown in eq 2a.2 where the A^m_n terms are parameters

$$V(C_{3h}) = A_2^0(3z^2 - r^2) + A_4^0(35z^2 - 30r^2z^2 + 3r^4) + A_6^0(231z^6 - 315r^2z^4 + 105r^4z^2 - 5r^6) + A_6^6(x^6 - 15x^4y^2 + 15x^2y^4 - y^6) \quad (2a.2)$$

which describe the crystal field. For our purposes, the most important term is A^6_6 term. This term allows mixing of states having $\Delta J_z = 6$. The A^0_x terms do not mix states having different values of J_z. Ignoring contributions from excited states, and limiting the discussion only to the J = 9/2 manifold, the EPR active ground states of an f^3 ion are $\Psi = |1/2\rangle$ and $\Psi = a|7/2\rangle + b|-5/2\rangle$ where the term in the ket is the J_z value of the state. The other possible ground states have $g_\perp = 0$.

In C_{3v} symmetry, the situation is similar. In this case, the crystal field is that shown in eq 2a.3 where the terms have meanings similar to 2a.2. The big difference

$$V(C_{3v}) = V(C_{3h}) + A_4^3(x^3 - 3xy^2) + A_6^3(11z^3 - 3zr^2)(x^3 - 3xy^2) \quad (2a.3)$$

between eq 2a.2 and eq 2a.3 is the presence of the A^3_x terms. These terms allow mixing of states with $\Delta J_z = 3$. For an f^3 complex with C_{3v} symmetry, only one ground state is EPR active: $\Psi = x|7/2\rangle + y|-5/2\rangle + z|1/2\rangle$. This ground state is a mixture of the two EPR active ground states for a complex with C_{3h} symmetry. If the symmetry is lower, the corresponding crystal field allows more mixing of J_z states.

For uranium(III) and neodymium(III), the form of the crystal field is identical. However, the magnitude of the A^x_y terms change from metal to metal. The A^x_y terms determine the mixing of different J_z states, so the coefficients a and b, or x, y, and z will change depending upon the crystal field parameters. However, the crystal field parameters for U(III) are about twice as large as the Nd(III) parameters, and ratios of the parameters are about the same in both cases. The result of the ratios remaining the same between the metals is that the ground states are more or less the same in analogous complexes.

Crystal field analyses based mainly upon optical spectra have been carried out on $Cp_3Nd(THF)$ and on $Cp_3Nd(C_6H_{11}NC)$ by Amberger and coworkers.[32,33] They find that the ground state in these complexes is mainly $|1/2\rangle$ character with smaller amounts of $|7/2\rangle$ and $|-5/2\rangle$ character. Since the structural features of $Cp"_3Ce(t\text{-BuNC})$ and $(MeC_5H_4)Ce(t\text{-BuNC})$ are similar,[17] $Cp"_3Nd(C_6H_{11}NC)$ and $Cp"_3Nd(t\text{-BuNC})$ are both expected to be structurally similar to $Cp_3Nd(C_6H_{11}NC)$ and therefore, should have similar crystal field parameters.

The EPR spectra are related to the ground states as shown in eq 2a.4 - 2a.6 neglecting contributions from higher energy J states.[31] Note that eq 2a.6 reduces to eq 2a.4 when $\phi = 90°$ and to eq 2a.5 when $\phi = 0°$.

g_J (Landé g value) $= 1+ [S(S+1)-L(L+1)+J(J+1)]/[2J(J+1)]$

$= 8/11$ for $^4I_{9/2}$

$\Psi = |1/2\rangle$

$$g_{\|} = g_J = 0.73$$

$$g_{\perp} = (J+1/2)g_J = 5g_J = 3.64 \qquad (2a.4)$$

$$\Psi = (\cos\theta)|7/2\rangle + (\sin\theta)|-5/2\rangle$$
$$g_{\parallel} = g_J(7\cos^2\theta - 5\sin^2\theta)$$
$$g_{\perp} = g_J[8(\sin\theta)(\cos\theta)] \qquad (2a.5)$$

$$\Psi = \cos\phi[(\cos\theta)|7/2\rangle + (\sin\theta)|-5/2\rangle] + (\sin\phi)|1/2\rangle$$
$$g_{\parallel} = g_J[g_J(7\cos^2\theta - 5\sin^2\theta)\cos^2\phi + \sin^2\phi]$$
$$g_{\perp} = g_J[8(\sin\theta)(\cos\theta)(\cos^2\phi) - 5\sin^2\phi] \qquad (2a.6)$$

Table 2a.3: Idealized axial EPR parameters for Cp_3M and $Cp_3M{\bullet}L$ complexes and corresponding ground state parameters, θ and ϕ (see eq 2a.6).

	$g_{\perp}$	$g_{\parallel}$	θ	ϕ
Cp''_3Nd	-2.28	0.70	45.86	62.92
$Cp''_3Nd(C_6H_{11}NC)$	-2.13	0.88	40.65	61.25
$Cp''_3Nd(t\text{-BuNC})$	-2.17	0.86	41.10	61.69
Cp''_3U	-2.53	0.85	40.24	65.64
$Cp''_3U(C_6H_{11}NC)$	-2.05	0.72	45.19	60.51
$Cp''_3U(t\text{-BuNC})$	-2.08	0.70	45.74	60.81
$Cp^{\ddagger}_3U$	-2.98	0.70	46.79	71.53
$Cp_3Nd(thf)$[32]	-2.755	0.152(calc)	58.52	51.40
$Cp_3Nd(C_6H_{11}NC)$[33]			56.58	54.49

Based on the assumption that all of the molecules have C_{3v} symmetry, eq 2a.6 can be used to find θ and ϕ based upon the EPR spectra. As is obvious from Table 2a.2 or from looking at the EPR spectra, none of these compounds actually have C_{3v} symmetry, so the two larger g values are averaged to obtain $g_\perp$, and the smaller g value is used for $g_\parallel$. Where $g_3 < 0.7$, it will be changed to be 0.7 (this has little effect on ϕ, but some effect on θ). The basis for changing $g_\parallel$ is that the EPR fitting program cannot determine g_3 if g_3 is at too great a magnetic field to be seen in the EPR spectrum. Therefore, the assumption is made that g_3 is at the lowest unobservable field giving it a value of 0.7. Since $g_\perp$ is negative for $Cp_3Nd(thf)$, it is assumed to be negative for all of these complexes as well. θ and ϕ can be found by calculating $g_\parallel$ and $g_\perp$ for all values of θ and ϕ using eq 2a.6 and comparing the calculated $g_\parallel$ and $g_\perp$ values to the observed ones. The g values and θ and ϕ obtained in this way are given in Table 2a.3.

From the data in Table 2a.3 it is clear that the ground state in all of these complexes is mainly $|1/2\rangle$. The % $|1/2\rangle$ character in the ground state varies from 76% for $Cp"_3U(C_6H_{11}NC)$ to 90% for $Cp^{\ddagger}_3U$. The parameter ϕ crudely shows the amount of mixing caused by the deviation from C_{3h} to C_{3v} symmetry. The closer to 90° that ϕ is, the smaller the amount of mixing caused by deviation from C_{3h} symmetry. The trend in ϕ shown in Table 2a.3 seems reasonable. $Cp^{\ddagger}$ is presumably the bulkiest ligand, so steric effects will tend to force $Cp^{\ddagger}_3U$ to most closely adopt the C_{3h} structure. Cp" is somewhat smaller, so $Cp"_3M$ can more easily distort, although for $Cp"_3Ce$, $\angle(Cp\text{-}Ce\text{-}Cp)_{ave} = 120°$. However, even in base adducts, the Cp-M-Cp angles remain near 120°; in $Cp"_3Ce(t\text{-}BuNC)$, $\angle(Cp\text{-}Ce\text{-}Cp)_{ave} = 119.5°$.[17] In the $Cp_3Nd{\bullet}L$ complexes, the smaller Cp ligand can bend back further than Cp" (in $Cp_3Pr(C_6H_{11}NC)$, $\angle(Cp\text{-}Pr\text{-}Cp)_{ave} = 117.4°$,[34] and in $Cp_3U(thf)$, $\angle(Cp\text{-}U\text{-}Cp)_{ave} = 117.6°$), [35] deviating more from C_{3h} symmetry and making ϕ smaller.

While the data derived from the EPR spectra of these complexes does seem interesting, any conclusions arrived at must be viewed cautiously. First, these

complexes do not have C_3 symmetry and crystal field parameters other than the ones discussed may be important. However, the compounds are fairly close to C_3 symmetry, so this is probably not too great a problem. Second, except for the Cp"$_3$Nd•L complexes, the EPR spectra are poor, and all three g components cannot be observed in most cases. Finally, all of the analyses of the spectra have ignored excited state contributions and changes in g due to covalency (orbital reduction factor).

In short, the electronic ground states of Cp"$_3$M (M= U and Nd) complexes and their base adducts have been examined. Variable temperature susceptibility suggest that the complexes all have an f^3 electronic ground state. The low temperature EPR spectra of these complexes have been measured. The g values are consistent with a $^4I_{9/2}$ ground state in which the lowest substate is mainly $J_z = 1/2$.

2b: Tris-cyclopentadienylzirconium

Few tris-cyclopentadienyl compounds of the d-transition metals have been described and, with the exception of the "pseudolanthanides" Cp_3Y[36]and Cp_3La[37], none of them have all three cyclopentadienyl ligands bound in an η^5-manner. The crystal structure of Cp_3Sc shows that it is a dimer with the two $(\eta^5\text{-}Cp)_2Sc$ fragments bridged by a pair of C_5H_5 groups that are η^1-bound to each Cp_2Sc fragment.[38] The crystal structure of the d^1 Cp_3Ti shows that two rings are bound in an η^5-manner and that the third is bound as η^2.[39] While the crystal structure of the d^2 Cp_3V is not known, the ^1H NMR spectrum of this paramagnetic compound shows two resonances in a 2:1 ratio.[40] The spectrum was assigned to two η^5-Cp ligands and a fluxional η^1-Cp ligand. The solid state and solution structures of Cp_3Tc and Cp_3Re also show that two rings are η^5 and one is η^1.[41-43] Curiously, the two η^5-rings are not rotating on the NMR time scale since all 5 protons are inequivalent. The η^1-ring is not fluxional since it has 3 inequivalent protons which are distinct at all temperatures studied.

In contrast to the d-metal complexes, the tris-cyclopentadienyl compounds of the f-metals (except for lutetium) all have 3 η^5-Cp ligands,[44] and unlike transition metal complexes, the f-metal complexes form base adducts.[45] As noted by Bursten, two factors are responsible for the difference in reactivity between the f and d-metal complexes.[7,8] First, the f-metals have large radii which reduces steric congestion enough to allow all three Cp ligands to coordinate in an η^5-manner. Second, the presence of the low lying f-orbitals prevents these complexes from becoming electronically saturated.

The MO description of tris-η^5-cyclopentadienyl compounds has been described by Bursten and previously by Lauher and Hoffmann.[6,9,46] For d-transition metals, the three ligands contribute 13 electrons since one ligand-based orbital of a' symmetry (in the point group C_{3h}, Figure 2b.1) has little or no overlap with s, p, or d orbitals. This

orbital is entirely ligand based and therefore relatively high in energy. Only one non-bonding metal based orbital is available, and it is largely d_z2. Any d-metal complex with more than two electrons must place electrons in M-Cp antibonding orbitals which will force the third cyclopentadienyl ligand to be something other than η^5. As previously noted, in the f-block metallocenes, electrons fill the f orbitals rather than the d orbitals. This leaves the d_z2 orbital empty, preventing electronic saturation, and allowing these complexes to form base adducts.

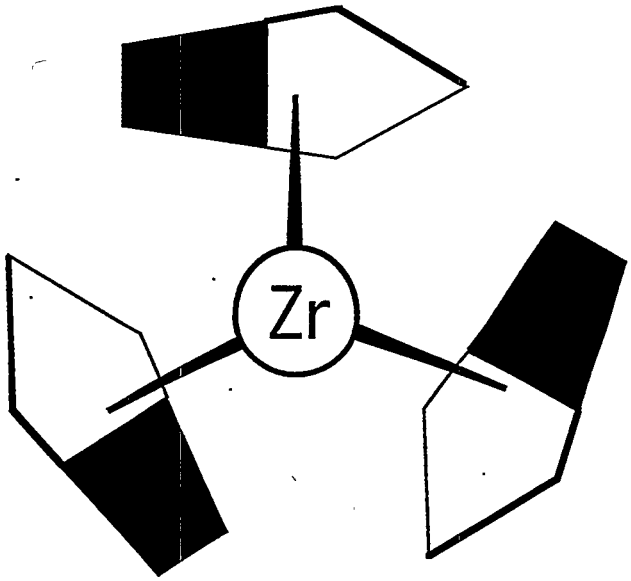

Figure 2b.1: The non-bonding a' (in C_{3h} symmetry) Cp based orbital of $(\eta^5\text{-Cp})_3Zr$. The different shadings represent different signs of the carbon π-bonding p-orbitals.

An interesting anomaly among the f-metallocenes is $[(Me_3Si)_2C_5H_3]_3Th$.[10] This complex has a $6d^1$ rather than a $5f^1$ electronic ground state and, unlike the other f-block metallocenes, does not appear to form base adducts.[11,47] The analogous lanthanide metallocene, $[(Me_3Si)_2C_5H_3]_3Ce$, has an f^1 electronic ground state and forms base adducts.[17,47] We were interested in comparing the reactions of this $6d^1$ actinide metallocene to that of a transition metallocene with a d^1 electronic ground state to investigate the influence of the electronic ground state upon the reactivity. In order to do this, we had to prepare a compound with three η^5-Cp ligands. Since zirconium(IV)

complexes which have three η^5-Cp ligands were known[9,48,49] and since Cp_3Ti was also known,[50] it seemed likely that $(\eta^5\text{-Cp})_3Zr$ could be synthesized.

Cp_3Zr was synthesized by reducing Cp_4Zr[48] with potassium graphite[51] in toluene from which it was crystallized as shiny, brown, hexagonal plates. Cp_3Zr was also made by reducing Cp_4Zr with sodium naphthalide in tetrahydrofuran. However, while it was possible to prepare Cp_3Zr pure by the former method, the latter always gave Cp_3Zr contaminated with 5-10 % Cp_3ZrH.[52] In general, it was very difficult to obtain pure Cp_3Zr since even the potassium graphite reduction often gave Cp_3Zr contaminated with Cp_3ZrH. The purity was determined by treating a C_6D_6 solution with CCl_4 and comparing the integration of the cyclopentadienyl resonance before addition of CCl_4 (due to Cp_3ZrH) to the integration of the cyclopentadienyl resonance after addition (due to Cp_3ZrCl from the reaction of Cp_3Zr and Cp_3ZrH with CCl_4). The purity of paramagnetic Cp_3Zr could not be determined directly since we were unable to find its NMR resonance. Attempts to reduce Cp_4Zr with *t*-BuLi in a manner similar to the reduction of Cp_3UCl[12,53-55] or Cp_2ZrX_2[56] gave only Cp_3ZrH, presumably by β-hydride elimination.

The EPR spectrum of Cp_3Zr at room temperature in 2-methyltetrahydrofuran was observed with $g_{iso} = 1.977$ and six satellites having $A_{iso} = 115$ MHz (41 Gauss) due to coupling to ^{91}Zr. As a frozen glass, the spectral parameters are $g_{\|}=1.999$ and $g_{\perp}=1.970$, as shown in Figure 2b.2. These g values are consistent with the MO model. For an electron in a d_{z2} orbital, spin-orbit coupling cannot change the value of $g_{\|}$ from that of a free electron, but spin-orbit coupling to the empty d_{xz} and d_{yz} orbitals can reduce to value of $g_{\perp}$.[57] The magnetic moment of Cp_3Zr was determined by variable temperature magnetic susceptibility and was found to be 1.64 B. M. from 5 to 300 K.

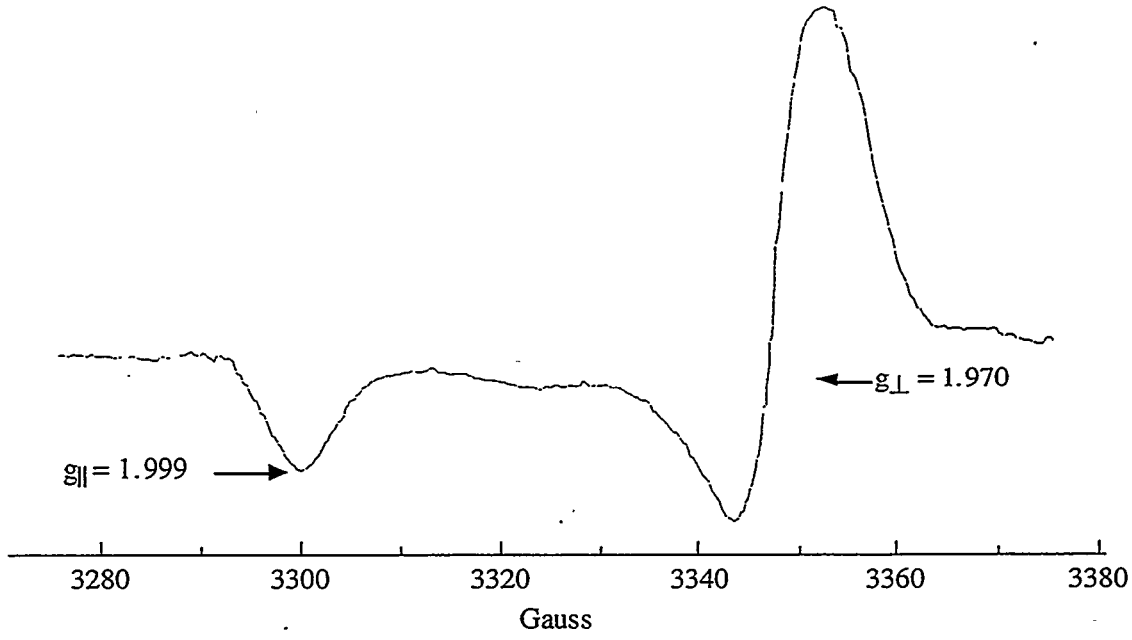

Figure 2b.2. EPR spectrum of Cp_3Zr in 2-MethylTHF at 70 K

The solid state structure of Cp_3Zr is shown in Figure 2b.3. Interesting distances and angles are given in Table 2b.1. The molecule possesses crystallographic $\bar{6}$ (C_{3h}) symmetry and is monomeric. The nearest intermolecular Zr-H and Zr-C distances are 4.29 Å and 5.00 Å, respectively. Surprisingly, the average Zr-C distance is 2.58 Å, the same as the average Zr-C distance for the three η^5-Cp ligands in Cp_4Zr.[48]

Table 2b.1: Selected Distances and Angles in Cp_3Zr

Zr - C1	2.592(3) Å	C1 - C2	1.420(5) Å
Zr - C2	2.564(3) Å	C2 - C3	1.395(5) Å
Zr - C3	2.590(4) Å	C1 - C1'	1.376(7) Å
C1 - H1	0.95(4) Å	C1'-C1-C2	108.4(2)°
C2 - H2	0.97(3) Å	C1-C2-C3	106.8(3)°
C3 - H3	0.84(5) Å	C2-C3-C2	109.2(4)°

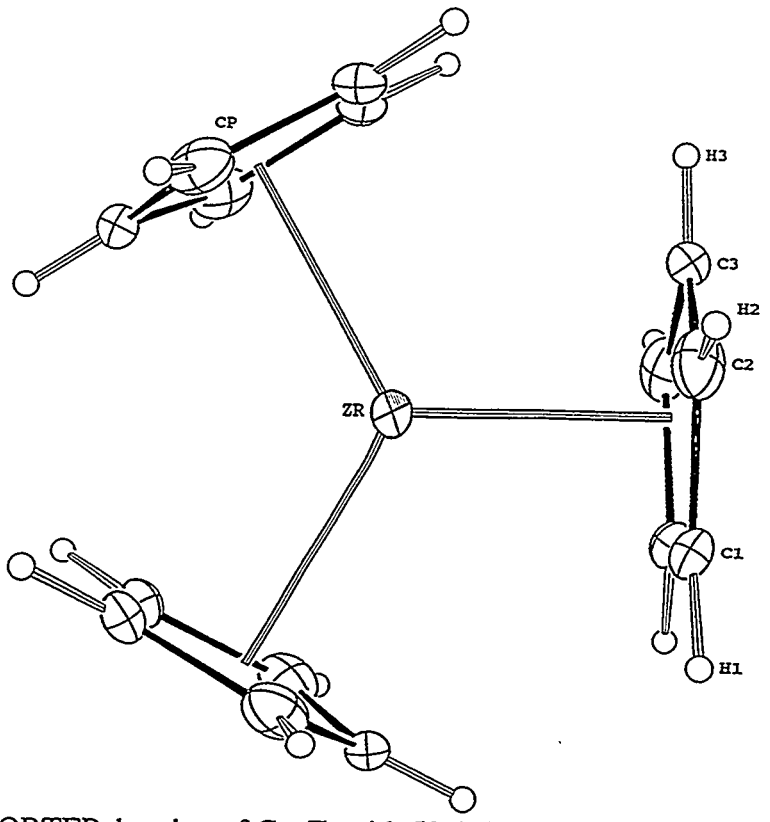

Figure 2b.3. An ORTEP drawing of Cp_3Zr with 50% thermal ellipsoids

As noted above, the Cp rings of Cp_3Zr are postulated to have a high-lying non-bonding orbital of a' symmetry which is not stabilized by the metal center.[9] The Cp rings of Cp_3Zr are distorted in a manner consistent with this lack of stabilization. This orbital (Figure 2b.1) possesses a node between C1 and C2, the presence of which is reflected in the longer C1-C2 distance of 1.420(5) Å relative to the shorter C2-C3 and C1-C1' distances of 1.395(5) Å and 1.376(7) Å, respectively. In the analogous Cp^*_3Sm[58] (Cp* is Me_5C_5) which crystallizes in the same space group also at a site of $\bar{6}$ symmetry, the Cp* ligands are not distorted in this manner, consistent with stabilization of this orbital by the $f_{y(3x2-y2)}$ orbital as predicted by Bursten and Strittmatter.[6,9] While other tris-cyclopentadienyl compounds have been characterized by crystallography, these compounds do not have pentasubstituted Cp rings.[59] Incomplete substitution of the Cp ring removes the degeneracy in the e_2 orbital, and distorts the ligand.[60,61]

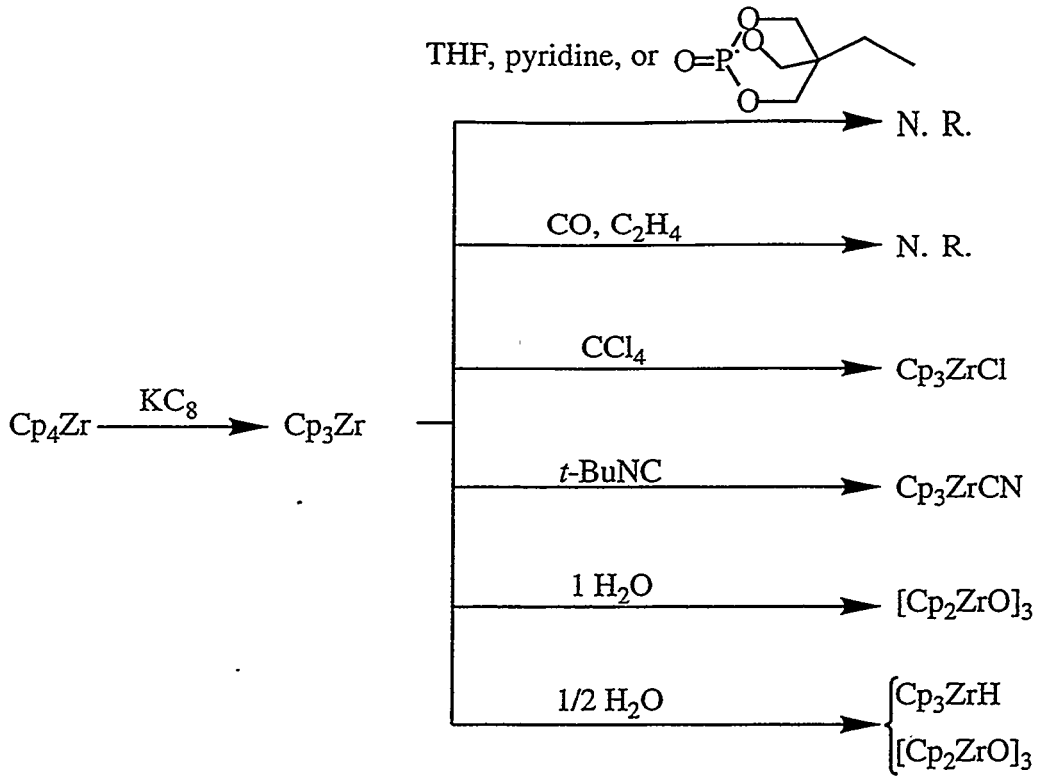

Figure 2b.4: Some reactions of Cp_3Zr (N. R. stands for no reaction).

Some reactions of Cp_3Zr are shown in Figure 2b.4. We were unable to isolate or obtain evidence for the existence of base adducts of Cp_3Zr with THF, pyridine, or $OP(OCH_2)_3CEt$. In addition, Cp_3Zr did not appear to react with carbon monoxide or ethylene. In all cases, only Cp_3Zr was recovered as determined by EPR spectroscopy. NMR spectroscopy showed no evidence of diamagnetic zirconium species in any of these reactions. While Cp_3Zr did not form base adducts, it did react with CCl_4 and *t*-BuNC to form the oxidation products Cp_3ZrCl and Cp_3ZrCN, respectively. When treated with one equivalent of water in benzene, Cp_3Zr gave $[Cp_2ZrO]_3$[62] and CpH. When treated with half an equivalent of water, Cp_3Zr gave a mixture of $[Cp_2ZrO]_3$[62] and Cp_3ZrH[52] presumably by the series of steps shown in eq 2b.1. The postulated formation of $[Cp_2ZrO]_2$ from Cp_3ZrOH is very similar to the observed formation of $[(Me_3SiC_5H_4)_2UO]_3$ from $(Me_3SiC_5H_4)_3UOH$.[63]

$$2\ Cp_3Zr + H_2O \rightarrow Cp_3ZrH + \{Cp_3ZrOH\}$$
$$\{Cp_3ZrOH\} \rightarrow 1/3\ [Cp_2ZrO]_3 + CpH \qquad (2b.1)$$

Steric effects cannot account for the inability of Cp_3Zr to form base adducts since Zr(IV) compounds which have three η^5-Cp ligands plus an additional ligand bonded to the Zr center are known. In addition, Zr(III) should be larger than Zr(IV) for a given coordination number. Rather, the lack of reactivity is most likely due to its electronic structure.

When a Lewis base interacts with Cp_3Zr, the d_{z^2} orbital is destabilized becoming the σ^* orbital with respect to the incoming ligand. Since the unpaired electron must occupy this orbital when Cp_3Zr interacts with a Lewis base, the interaction with the incoming ligand becomes much less favorable. However, the unpaired electron does not prevent single-electron reactions. When the ligand is a one electron donor, as is the case for H, OH, CN, and Cl, the unpaired electron in the a' (d_{z^2} parentage) orbital can share the bonding orbital with the electron from ligand leaving the antibonding orbital unoccupied.

To help judge whether the reactivity of Cp_3Zr is a result of its electronic structure, or if similar tris-cyclopentadienyl transition metal complexes reacte analogously, the behavior of Cp_3Ti was briefly examined. The reactivity of Cp_3Ti,[50,64,65] as shown in Figure 2b.5, is quite different from that of Cp_3Zr. While Cp_3Zr does not react with CO, Cp_3Ti is known to form $Cp_2Ti(CO)_2$ when treated with CO.[50] Additionally, although Cp_3Ti reacts with CCl_4 and *t*-BuNC, the products are Cp_2TiCl_2 and $[Cp_2TiCN]_4$,[66] respectively. Treatment of Cp_3Ti with one-half of an equivalent of water produced $(Cp_2Ti)_2(\mu\text{-}O)$ cleanly.[67] The reactivity of Cp_3Ti is consistent with a bent metallocene in which the η^2-Cp ligand behaves like a weakly bound alkyl group.

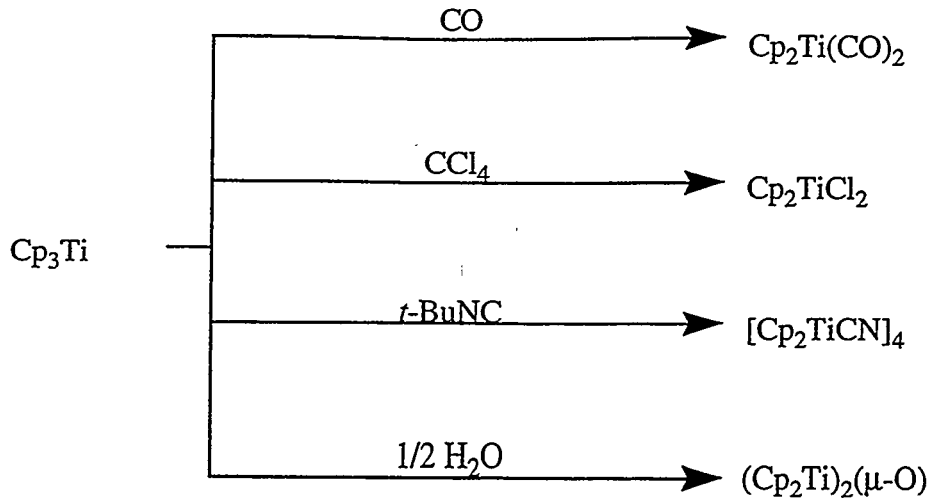

Figure 2b.5. Some reactions of Cp_3Ti

The synthesis, structure, and chemical behavior of Cp_3Zr have been described. Its reactivity is controlled by the presence of an electron in the d_{z2} orbital. Since $[(Me_3Si)_2C_5H_3]_3Th$ reacts similarly,[47] and since its electronic ground state is also d^1, it seems likely that electronic structure controls the reactivity in this case as well. Cp_3Ti, which also has a single d electron but does not have the same molecular structure, reacts differently. In light of the similarity between Cp_3Zr and $[(Me_3Si)_2C_5H_3]_3Th$, perhaps, in this case, it is useful to think of zirconium as "a little thorium".

2c: Exchange Coupling in $(Cp_2Ti)_2(\mu\text{-}O)$

Wieghardt has recently published a paper on dititanium(III)-μ-oxo compounds with nearly linear oxo bridges, $(Me_3tacn)_2Ti_2(X)_4(\mu\text{-}O)$ where X is Cl, NCS, or NCO, and Me_3tacn is N,N,N-trimethyl-1,4,7-triazacyclononane.[68,69] These d^1-d^1 dinuclear complexes are weakly antiferromagnetically coupled with a coupling constant of *ca.* -7 cm^{-1}. A model has been advanced to explain the small coupling in these compounds. The single d-electron on each octahedral titanium(III) center occupies a d_{xy} orbital (taking the Ti - Ti direction as z). These orbitals are orthogonal to the 2p orbitals of the bridging oxygen atom so no antiferromagnetic coupling can occur by superexchange through the oxygen orbitals. In order to account for the observed magnetic behavior, they postulate that the weak antiferromagnetic coupling results from overlap of the two d_{xy} orbital through space, and that this interaction is greater than the ferromagnetic potential exchange between the electrons. Wieghardt notes that $(Cp_2Ti)_2(\mu\text{-}O)$ also contains two d^1-metal centers connected by a nearly linear oxo bridge, but that no magnetic studies have been described.

While examining the chemistry of Cp_3Ti (previous section), it was discovered that $(Cp_2Ti)_2(\mu\text{-}O)$ can be easily made from water and Cp_3Ti. The new synthesis gives $(Cp_2Ti)_2O$ in high purity which is an essential prerequisite for examining magnetic behavior. The original synthesis of $(Cp_2Ti)_2O$ was the reaction between titanocene and nitrous oxide.[70,71] The khaki-green material was said to be explosively pyrophoric. The identity of the compound was inferred by the molecular ion in the mass spectrum and a g-value of 1.975 in the EPR spectrum of a toluene solution at room temperature. The crystal structure of $(Cp_2Ti)_2O$ was recently determined.[72] The crystal structure shows that the two metallocene units are perpendicular to each other giving the molecule idealized D_{2d} symmetry. The Ti-O distance is 1.838(1) Å and the Ti-O-Ti angle is 170.9(4) °, values similar to those in Wieghardt's compounds.

$(Cp_2Ti)_2O$ was prepared by the reaction of Cp_3Ti with one-half of an equivalent of water in tetrahydrofuran at -78 °C. Crystallization from toluene gives green plates which are brown when powdered. The powdered compound is very air sensitive, but not pyrophoric. To show that the bridging oxygen came from the added water, the ^{18}O labeled compound was prepared using ^{18}O enriched water. Mass spectroscopy confirms the incorporation of the labeled oxygen. The isotopically labeled compound has a new absorption in the infrared spectrum at 725 cm^{-1} assignable to the Ti-^{18}O-Ti asymmetric stretch. In the unlabelled compound, the Ti-O absorption is found at 780 cm^{-1}, but it is partially obscured by the C-H out of plane wagging absorptions of the C_5H_5 ligands.[73] In order to verify that this compound was the same as that which was characterized by crystallography, the unit cell of a single crystal was determined and found to be identical to the published unit cell.[72]

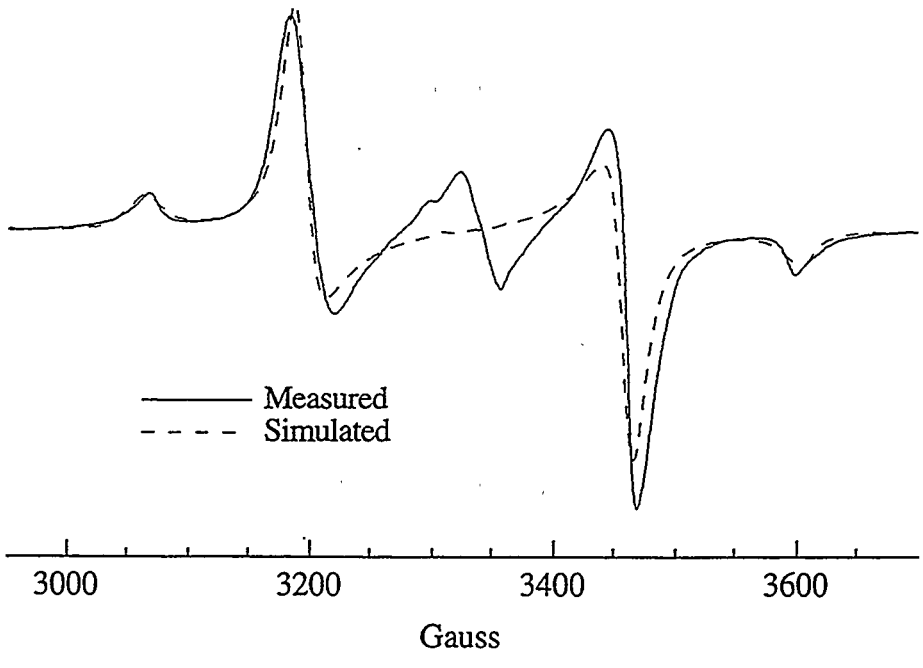

Figure 2c.1: EPR spectrum of $(Cp_2Ti)(\mu\text{-}O)$ in toluene at 2 K.

EPR spectroscopy shows that $(Cp_2Ti)_2O$ has a triplet ground state. As a powder, the room temperature EPR spectrum of $(Cp_2Ti)_2O$ is extremely broad and isotropic with a g value of 1.977. At 2 K, the spectrum is still isotropic with a g value of 1.979, and a half-field signal is observed at g = 3.974. As a toluene glass at 2 K, $(Cp_2Ti)_2O$ gives the triplet spectrum shown in Figure 3c.1 which corresponds to the values $g_{\|} = 1.979$, $g_{\perp} = 1.981$ and $|D| = 0.0249\ cm^{-1}$. The additional signal seen at g = 1.975 in Figure 3c.1 is thought to be due to oxidized or hydrolyzed $(Cp_2Ti)_2(\mu\text{-}O)$ (due to filtering the EPR sample through a Kimwipe in the glove box) since this signal's intensity varies between EPR samples prepared from the same batch of $(Cp_2Ti)_2O$.

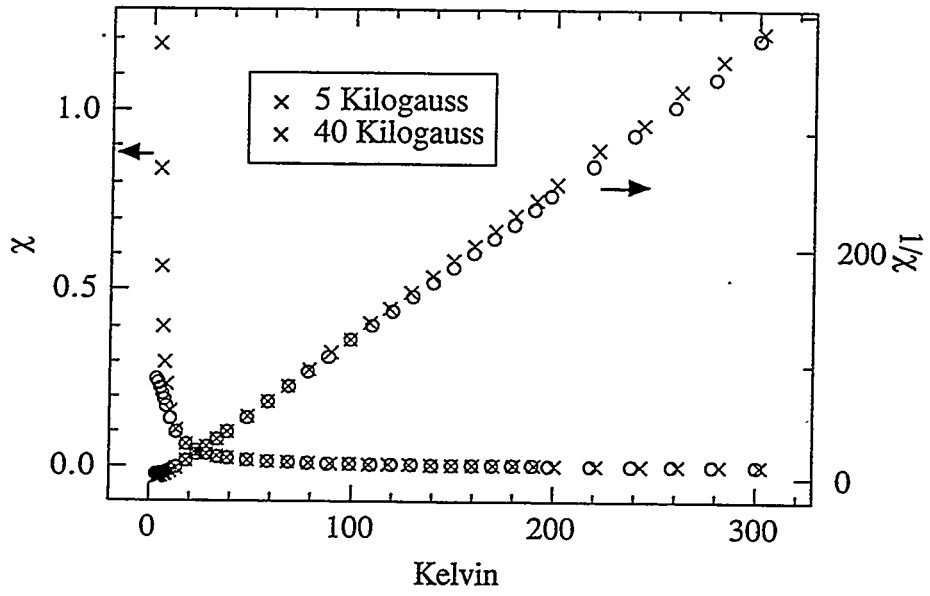

Figure 2c.2: Variable temperature susceptibility of $(Cp_2Ti)(\mu\text{-}O)$

The variable temperature magnetic susceptibility was measured from 5 to 300 K at 0.5 and 4 T and is shown in Figure 2c.2. Below 20 K, the susceptibility is field dependent. We believed that the field dependence arose from saturation magnetization due to intermolecular ferromagnetic coupling, so we examined the magnetization at 5, 10, and 20 K as a function of applied field as shown in Figure 2c.3. At 20 K, the

magnetization increases almost linearly with applied field as expected for a paramagnetic system in which intermolecular interactions are weak. However, at lower temperatures, the magnetization no longer increases linearly with applied field indicating that intermolecular ferromagnetic interactions are lowering the internal field of the sample and therefore, the observed magnetization.[74]

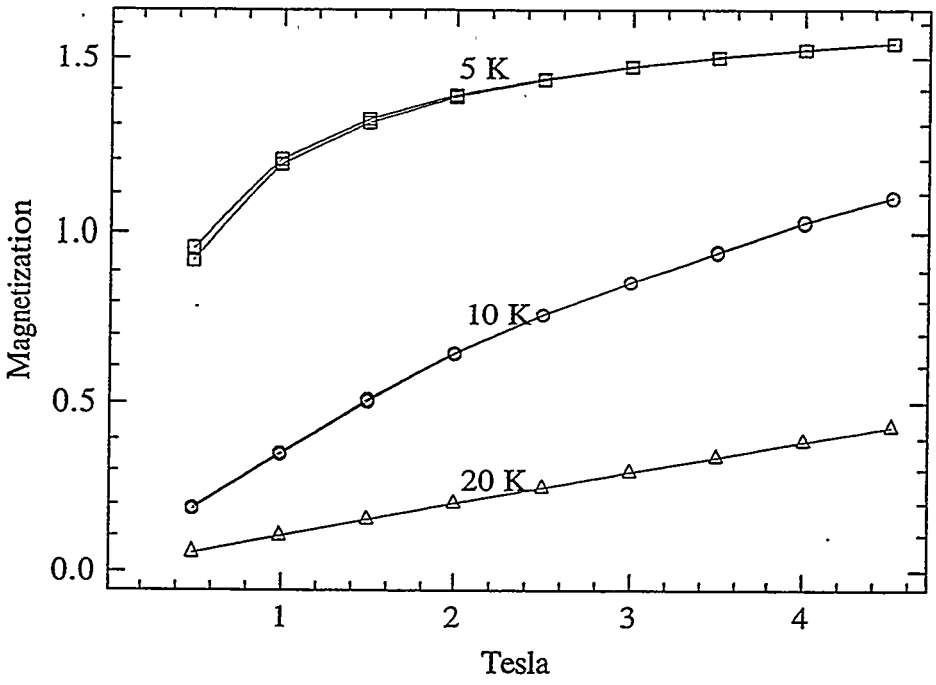

Figure 2c.3: Magnetization of $(Cp_2Ti)(\mu\text{-}O)$ at different fields (1 Tesla = 10^4 Gauss)

$$\chi = \frac{2Ng^2\mu_b^2}{kT(3+\exp(-2J/kT))} + N\alpha \qquad (2c.1)$$

Above 20 K, the susceptibility is independent of the applied field, and a least squares fit of the data using the Curie-Weiss equation gives $\mu_{eff} = 2.47$, and $\theta = 8.3$ K per dinuclear molecule; the positive sign of θ is consistent with an intermolecular ferromagnetic interaction.[74,75] Because of the field dependence of the susceptibility,

only the 0.5 T data from 10 to 300 K was used for fitting. The Bleaney-Bowers equation (eq 2c.1), where χ is per dinuclear molecule,[74] gives only a mediocre least squares fit (χ^2(of fit)=6.6 x 10^6) with g = 1.979 (fixed, from the EPR spectrum), J = 22 cm^{-1}, Nα = 357 x 10^{-6} cm^3/mol, and the other symbols have their usual meaning.[74,76]

$$\chi = \frac{\chi'}{1-(2zJ'/Ng^2\mu_b^2)\chi'} \qquad (2c.2)$$

The intermolecular ferromagnetic interaction was treated using the Weiss Molecular Field approximation (eq 2c.2)[75,77] where z is number of neighbors, J' is the intermolecular coupling constant between the z nearest neighbors, and χ' is the Bleaney-Bowers equation. A much better fit is obtained (χ^2(of fit) = 1.3 x 10^4) with the parameters g = 1.979(fixed, from the EPR spectrum), J = 11 cm^{-1}, zJ'= 3.2 cm^{-1}, and Nα = -28 x 10^{-6} cm^3/mol.[78] From the value of θ, the Weiss constant, can be calculated to be 6 K from eq 2c.3 where S = 1 for each dinuclear molecule. This value agrees well with the θ = 8.3 K determined by fitting $1/\chi$ with the Curie-Weiss equation. Since the Weiss Molecular Field approximation is only valid above this temperature, we did not try to fit the data below 10 K to this model. The variable temperature susceptibility and the least squares fits are shown in Figure 2c.4, and μ_{eff} and the least squares fits versus temperature are shown in Figure 2c.5.

$$\theta = \frac{2J'zS(S+1)}{3k} \qquad (2c.3)$$

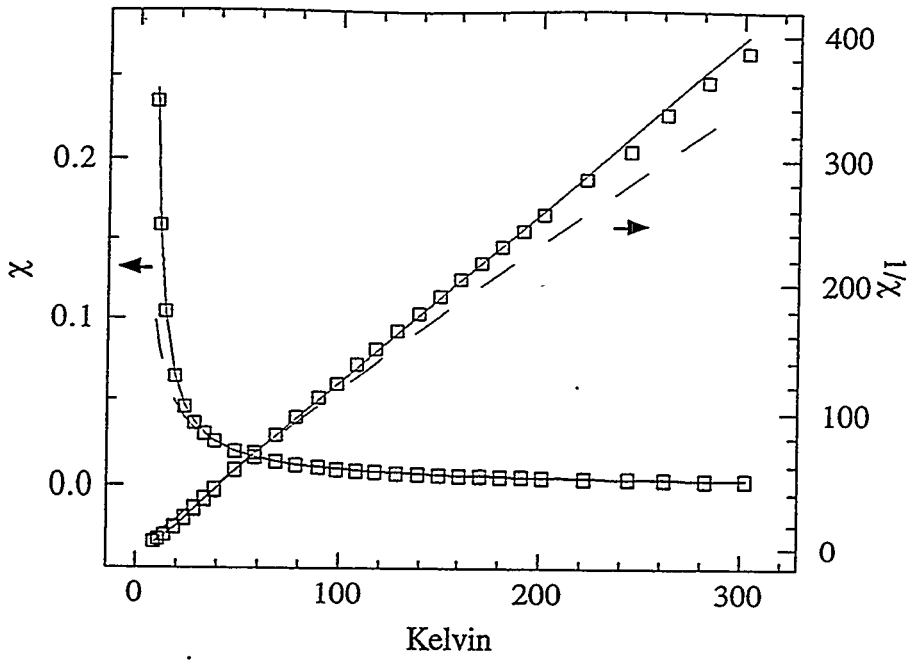

Figure 2c.4: Modeling the magnetic susceptibility of $(Cp_2Ti)(\mu\text{-}O)$. Dotted line: Bleaney-Bowes equation. Solid line: Bleaney-Bowers equation with Weiss Molecular Field approximation.

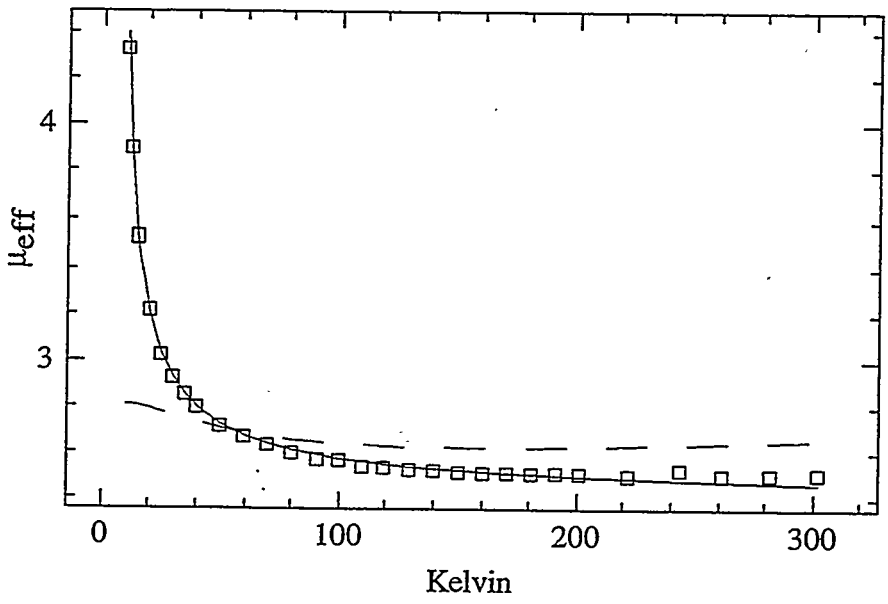

Figure 2c.5: Modeling the magnetic moment of $(Cp_2Ti)(\mu\text{-}O)$. Dotted line: Bleaney-Bowers equation. Solid line: Bleaney-Bowers equation with Weiss Molecular Field approximation.

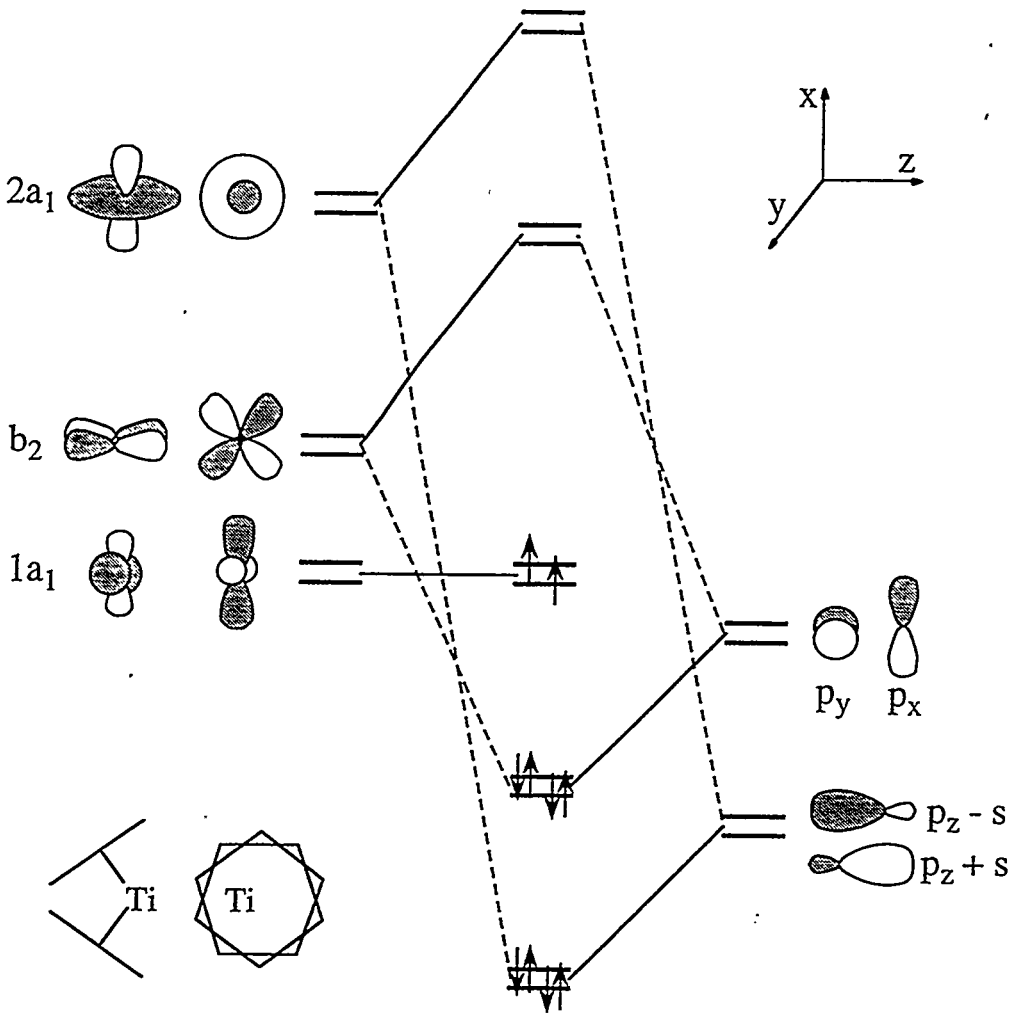

Figure 2c.6: Qualitative MO diagram for $(Cp_2Ti)(\mu\text{-}O)$

As far as we know, this is the only bimetallic titanocene compound in which the titanium centers are coupled ferromagnetically. Stucky has studied a large number of titanocene dimers and has found antiferromagnetic coupling in all cases which they explain mainly by superexchange involving the bridging ligand.[79-84] In the case of $(Cp_2Ti)_2O$, as in Wieghardt's oxo bridged dimer, no superexchange pathway exists. As shown in Figure 2c.6, the $2p_x$ and $2p_y$ orbitals on the oxo bridge are orthogonal to the $1a_1$ orbitals of each titanocene fragment. Since $1a_1$ has little or no electron density along the z axis[46,85], it cannot interact effectively with either the 2s or $2p_z$ orbitals of the oxo

bridge. Additionally, the two $1a_1$ orbitals cannot interact through space. In $(Cp_2Ti)_2O$ the $1a_1$ orbitals are rotated by 90° relative to each other and should have little overlap. Since no mechanism exists for coupling the electrons of the titanium centers in $(Cp_2Ti)_2O$, the coupling is ferromagnetic due to potential exchange. [86-88] In Wieghardt's bridging oxo dimer, the lack of a superexchange pathway did not result in antiferromagnetic coupling presumably due to overlap of the two d_{xy} orbitals through space; nonetheless, the magnitude of the coupling was small.[68,69]

In summary, the variable temperature magnetism and low temperature EPR of $(Cp_2Ti)(\mu\text{-}O)$ were examined. The titanium centers are found to be ferromagnetically coupled with $J = 11\ cm^{-1}$. This observation is in contrast to the *anti*-ferromagnetic coupling in all of the other titanocene dimers. The difference in coupling is due to the fact that no ligand mediated superexchange pathway exists between the titanium centers of $(Cp_2Ti)_2(\mu\text{-}O)$.

References

(1) Reynolds, L. T.; Wilkinson, G. *J. Inorg. Nucl. Chem.* **1956**, *2*, 246-253.

(2) Marks, T. J.; Streitwieser Jr., A. In *The Chemistry of the Actinide Elements*; J. J. Katz, G. T. Seaborg and L. R. Morss, Eds.; Chapman and Hall: London, 1986; Vol. 2; pp 1547-1587.

(3) Marks, T. J. In *The Chemistry of the Actinide Elements*; J. J. Katz, G. T. Seaborg and L. R. Morss, Eds.; Chapman and Hall: London, 1986; Vol. 2; pp 1588-1628.

(4) *Organometallics of the f-Elements*; Marks, T. J.; Fischer, R. D., Eds.; D. Reidel Publishing Company: Dordrecht, 1979, pp 517.

(5) Tatsumi, K.; Nakamura, A. *J. Organomet. Chem.* **1984**, *272*, 141-154.

(6) Bursten, B. E.; Rhodes, L. F.; Strittmatter, R. J. *J. Am. Chem. Soc.* **1989**, *111*, 2756-2758.

(7) Bursten, B. E.; Rhodes, L. F.; Strittmatter, R. J. *J. Am. Chem. Soc.* **1989**, *111*, 2758-2766.

(8) Bursten, B. E.; Strittmatter, R. J. *Angew. Chem., Int. Ed. Engl.* **1991**, *30*, 1069-1085.

(9) Strittmatter, R. J.; Bursten, B. E. *J. Am. Chem. Soc.* **1991**, *113*, 552 - 559.

(10) Blake, P. C.; Lappert, M. F.; Atwood, J. L.; Zhang, N. *J. Chem. Soc., Chem. Commun.* **1986**, 1148-1149.

(11) Kot, W.; Shalimoff, G.; Edelstein, N.; Edelman, M.; Lappert, M. F. *J. Am. Chem. Soc.* **1988**, *110*, 986-987.

(12) Brennan, J. G. Ph. D. Thesis, U. C. Berkeley, 1985.

(13) Zalkin, A.; Brennan, J. G.; Andersen, R. A. *Acta Cryst.* **1988**, *C44*, 2104-2106.

(14) Parry, J.; Carmona; E.; Coles, S.; Hursthouse, M. *J. Am. Chem. Soc.* **1995**, *117*, 2649-2650.

(15) Beshouri, S. B., Unpublished results

(16) Beshouri, S. B.; Hollander, F. J., Unpublished Results

(17) Stults, S. D.; Andersen, R. A.; Zalkin, A. *Organometallics* **1990**, *9*, 115.

(18) Brennan, J. G.; Stults, S. D.; Andersen, R. A.; Zalkin, A. *Organometallics* **1988**, *7*, 1329.

(19) Brennan, J. G.; Andersen, R. A.; Robbins, J. L. *J. Am. Chem. Soc.* **1986**, *108*, 335.

(20) Ugi, I.; Meyr, R. *Chem. Ber.* **1960**, *93*, 239-248.

(21) van Vleck, J. H. *The Theory of Electric and Magnetic Susceptibilities*; Oxford University Press: London, 1932.

(22) Kanellakopolous, B. In *Organometallics of the f-Elements*; T. J. Marks and R. D. Fischer, Eds.; D. Reidel Publishing Company: Dordrecht, 1978; pp 1 - 36.

(23) Carnall, W. T.; Crosswhite, H. M. In *The Chemistry of the Actinide Elements*; J. J. Katz, G. T. Seaborg and L. R. Morss, Eds.; Chapman and Hall: London, 1986; Vol. 2; pp 1235-1277.

(24) Soulie, E. J.; Lesieur, P. C. *J. Chem. Soc., Faraday Trans. I* **1989**, *85*, 4053-4062.

(25) Pilbrow, J. R. *Transition Ion Electron Paramagnetic Resonance*; Clarendon Press: Oxford, 1990, p 717.

(26) Stevens, K. W. H. *Proc. Phys. Soc. A* **1952**, *65*, 209-215.

(27) Elliot, R. J.; Stevens, K. W. H. *Proc. R. Soc. A* **1952**, *215*, 437-453.

(28) Elliot, R. J.; Stevens, K. W. H. *Proc. R. Soc. A* **1953**, *218*, 553-566.

(29) Elliot, R. J.; Stevens, K. W. H. *Proc. R. Soc. A* **1953**, *219*, 387-404.

(30) Judd, B. R. *Proc. R. Soc. A* **1955**, *227*, 552-560.

(31) Judd, B. R. *Proc. R. Soc. A* **1955**, *232*, 458-474.

(32) Reddmann, H.; Schultze, H.; Amberger, H.-D.; Shalimoff, G. V.; Edelstein, N. M. *J. Organomet. Chem.* **1991**, *411*, 331-345.

(33) Amberger, H.-D.; Schultze, H.; Edelstein, N. M. *Spectrochimica Acta* **1986**, *42A*, 657-667.

(34) Burns, J. H.; Baldwin, W. H. *J. Organomet. Chem.* **1976**, *120*, 361-368.

(35) Wasserman, H. J.; Zozulin, A. J.; Moody, D. C.; Ryan, R. R.; Salazar, K. V. *J. Organomet. Chem.* **1983**, *254*, 305-311.

(36) Adam, M.; Behrens, U.; Fischer, R. D. *Acta Cryst.* **1991**, *C47*, 968-971.

(37) Eggars, S. H.; Kopf, J.; Fischer, R. D. *Organometallics* **1986**, *5*, 383-385.

(38) Atwood, J. L.; Smith, K. D. *J. Am. Chem. Soc.* **1973**, *95*, 1488.

(39) Lucas, C. R.; Green, M. L. H.; Forder, R. A.; Prout, K. W. *J. Chem. Soc., Chem. Commun.* **1973**, 97.

(40) Siegert, F. W.; de Lifde Meijer, H. J. *J. Organomet. Chem.* **1968**, *15*, 131-137.

(41) Apostolidis, C.; Kanellakopulos, B.; Maier, R.; Rebizant, J.; Ziegler, M. L. *J. Organomet. Chem.* **1990**, *396*, 315-326.

(42) Apostolidis, C.; Kanellakopolus, B.; Rebizant, J.; Ziegler, M. L. *J. Organomet. Chem.* **1991**, *411*, 171.

(43) Apostolidis, C.; Kanellakopulos, B.; Maier, R.; Rebizant, J.; Ziegler, M. L. *J. Organomet. Chem.* **1991**, *409*, 243-254.

(44) Eggars, S. H.; Kopf, J.; Fischer, R. D. *Acta. Cryst.* **1987**, *C43*, 2288-2290.

(45) Fischer, R. D. In *Organometallics of the f-Elements*; T. J. Marks and R. D. Fischer, Ed.; D. Reidel Publishing Company: Dordrecht, Holland, 1979.

(46) Lauher, J. W.; Hoffmann, R. *J. Am. Chem. Soc.* **1976**, *98*, 1729-1742.

(47) Kot, W. Chemistry Thesis, U. C. Berkeley, 1991.

(48) Rogers, R. D.; Bynum, R. V.; Atwood, J. L. *J. Am. Chem. Soc.* **1978**, *100*, 5238-5239.

(49) Kopf, J.; Vollmer, H.-J.; Kaminsky, W. *Cryst. Struct. Commun.* **1980**, *9*, 985-990.

(50) Fischer, E. O.; Löchner, A. *Z. Naturforsch.* **1960**, *15b*, 266.

(51) Schwindt, M. A.; Lejon, T.; Hegedus, L. B. *Organometallics* **1990**, *9*, 2814-2819.

(52) Lokshin, B. V.; Klemenkova, Z. S.; Ezernitskaya, M. G.; Strunkina, L. I.; Brainina, E. M. *J Organomet Chem* **1982**, *235*, 69 - 75.

(53) Brennan, J. G.; Andersen, R. A.; Zalkin, A. *Inorg. Chem.* **1986**, *25*, 1756-1760.

(54) Marks, T. J.; Seyam, A. M.; Kolb, J. R. *J. Am. Chem. Soc.* **1973**, *95*, 5529 - 5539.

(55) Weydert, M. Ph. D. Thesis, U. C. Berkeley, 1993.

(56) Wielstra, Y.; Gambarotta, S.; Meetsma, A. *Organometallics* **1989**, *9*, 2948 - 2952.

(57) McGarvey, B. R. In *Transition Metal Chemistry, a Series of Advances*; R. L. Carlin, Ed.; Marcel Dekker, Inc.: New York, 1966; Vol. 3; pp 90-201.

(58) Evans, W. J.; Gonzales, S. L.; Ziller, J. W. *J. Am. Chem. Soc.* **1991**, *113*, 7423-7424.

(59) Schumann, H.; Glanz, M.; Hemling, H. *J. Organomet. Chem.* **1993**, *445*, C1-C3.

(60) Davies, A. G.; Jeffery, P. G.; Lusztyk, E.; Lusztyk, J. *J. Chem. Soc. Perkin Trans. II* **1982**, 737-743.

(61) Davies, A. G.; Lusztyk, E.; Lusztyk, J. *J. Chem. Soc. Perkin Trans. II* **1982**, 729-736.

(62) Fachinetti, G.; Floriani, C.; Chiesi-Villa, A.; Guastini, G. *J. Am. Chem. Soc.* **1979**, *101*, 1767-1775.

(63) Berthet, J.-C.; Ephritikhine, M.; Lance, M.; Nierlich, M.; Vigner, J. *J. Organomet Chem.* **1993**, *460*, 47-53.

(64) Canty, A. J.; Coutts, R. S. P.; Wailes, P. C. *Aust. J. Chem.* **1968**, *21*, 807 - 810.

(65) Siegert, F. W.; Meijer, H. J. D. L. *J. Organomet. Chem.* **1969**, *20*, 141 -145.

(66) Schinnerling, P.; Thewalt, U. *J. Organomet. Chem.* **1992**, *431*, 41 - 45.

(67) Lukens, W. W.; Andersen, R. A. *Inorg. Chem.* **1995**, *34*, 3440-3443.

(68) Bodner, A.; Jeske, P.; Weyhermuller, T.; Wieghardt, K.; Dubler, E.; Schmalle, H.; Nuber, B. *Inorg. Chem.* **1992**, *31*, 3737-3748.

(69) Jeske, P.; Wieghardt, K.; Nuber, B. *Inorg. Chem.* **1994**, *33*, 47-53.

(70) Bottomley, F.; Brintzinger, H. H. *J. C. S., Chem. Commun.* **1978**, 234 -235.

(71) Bottomley, F.; Lin, I. J. B.; Mukaida, M. *J. Am. Chem. Soc.* **1980**, *102*, 5238 - 5242.

(72) Honold, B.; Thewalt, U.; Herberhold, M.; Alt, H. G.; Kool, L. B.; Rausch, M. D. *J. Organomet. Chem.* **1986**, *314*, 105 - 111.

(73) Cotton, F. A.; Marks, T. J. *J. Am. Chem. Soc.* **1969**, *91*, 7281 - 7285.

(74) Carlin, R. L.;von Duyneveldt, A. J. *Magnetic Properties of Transition Metal Compounds*; Springer-Verlag: New York, 1977.

(75) Smart, J. S. *Effective Field Theories of Magnetism*; W. B. Saunders and Co.: Philadelphia, 1966.

(76) The effect of the zero field splitting was not included since a zero field splitting of 0.025 cm^{-1} will not affect the susceptibility until the temperature is in the range of D/k = 0.036 K.

(77) O'Connor, C. J. In *Progress in Inorganic Chemistry*; S. J. Lippard, Ed.; John Wiley and Sons: New York, 1982; Vol. 29; pp 203 - 285.

(78) As noted by a reviewer for the $(Cp_2Ti)(O)$ manuscript, the error in J obtained from the susceptibility is somewhat large since the data is not fit below 10 K and due to the presence of the intermolecular exchange. However, the ground state is clearly S = 1 even in the absence of intermolecular effects as evidenced by the strong triplet EPR spectrum observed at 2 K.

(79) Fieselmann, B. F.; Hendrickson, D. N.; Stucky, G. D. *Inorg. Chem.* **1978**, *17*, 1841-1848.

(80) Sekutowski, D.; Jungst, R.; Stucky, G. D. *Inorg. Chem.* **1978**, *17*, 1848 - 1855.

(81) Fieselmann, B. F.; Hendrickson, D. N.; Stucky, G. D. *Inorg. Chem.* **1978**, *17*, 2078 - 2084.

(82) Kramer, L. S.; Clauss, A. W.; Francesconi, L. C.; Corbin, D. R.; Hendrickson, D. N.; Stucky, G. D. *Inorg. Chem.* **1981**, *20*, 2070-2077.

(83) Francesconi, L. C.; Corbin, D. R.; Clauss, A. W.; Hendrickson, D. N.; Stucky, G. D. *Inorg. Chem.* **1981**, *20*, 2059 - 2069.

(84) Francesconi, L. C.; Corbin, D. R.; Clauss, A. W.; Hendrickson, D. N.; Stucky, G. D. *Inorg. Chem.* **1981**, *20*, 2078 - 2083.

(85) Petersen, J. L.; Dahl, L. F. *J. Am. Chem. Soc.* **1975**, *97*, 6416-6422.

(86) Anderson, P. W. In *Magnetism*; G. T. Rado and H. Suhl, Eds.; Academic Press Inc: New York, 1963; Vol. I; pp 25 - 81.

(87) Bencini, A.; Gatteschi, D. *EPR of Exchange Coupled Systems*; Springer-Verlag: New York, 1990.

(88) Hotzelmann, R.; Wieghardt, K.; Florke, U.; Haupt, H.; Weatherburn, D. C.; Bonovoisin, J.; Blondin, G.; Girerd, J. *J. Am. Chem. Soc.* **1992**, *114*, 1681 - 1696.

Chapter Three: Decamethyltitanocene Chemistry

Unlike some of the chemistry in the preceding sections, the chemistry of titanocenes and pentamethyltitanocenes is well known and well developed. The first titanocene, Cp_2TiCl_2, was, of course, first made by Wilkinson.[1] The development of the pentamethylcyclopentadienyl chemistry of titanium is largely due to Brintzinger and Bercaw.[2,3] The titanium(III) chemistry studied in this chapter was largely developed by Teuben and co-workers.[4] They found that the Cp* ligand allows the preparation of monomeric titanium(III) complexes. These complexes were of interest to us because their electronic spectra could possibly provide useful information about the π-bonding in these complexes.[5,6]

3a: A π-Bonding Spectrochemical Series in Cp^*_2TiX

Cp^*_2TiX complexes (X is a monodentate, one-electron ligand such as a halide, amide, alkoxide, or alkyl group) appear to be ideal for the study of ligand π-bonding. They are monomeric, unlike Cp_2TiX. They have a single electron in the a_1 orbital making electronic spectroscopy simple, unlike Cp_2VX in which both the a_1 and b_2 orbitals are singly occupied.[7,8] They have an empty b_2 orbital available for π-bonding, unlike Cp_2MX_2. Finally, the bonding in bent metallocenes is well understood.

The best known bonding model, the Lauher-Hoffmann model, is shown in Figure 3a.1 using an alternative coordinate system.[10-15] The coordinate system used here (due to Petersen and Dahl), varies from the usual coordinate system as shown in Figure 3a.2. Choosing this alternative coordinate system minimizes the mixing of d_{z2}

and d_{x2-y2} orbitals. This metallocene bonding model is supported by two papers by Petersen and Dahl in which single crystal EPR spectroscopy showed that the unpaired electron in $(\eta^5\text{-}MeC_5H_4)_2VCl_2$ and Cp_2VS_5 occupies an orbital that is perpendicular to the plane formed by the metal and the two Cp centroids and is largely of d_{z2} parentage (in this coordinate system).[9,16] In Cp^*_2TiX, the unpaired electron resides in the low-lying a_1 orbital which is largely d_{z2}. The empty b_2 orbital can interact with the p_z orbital of the X ligand to form a π-bond.

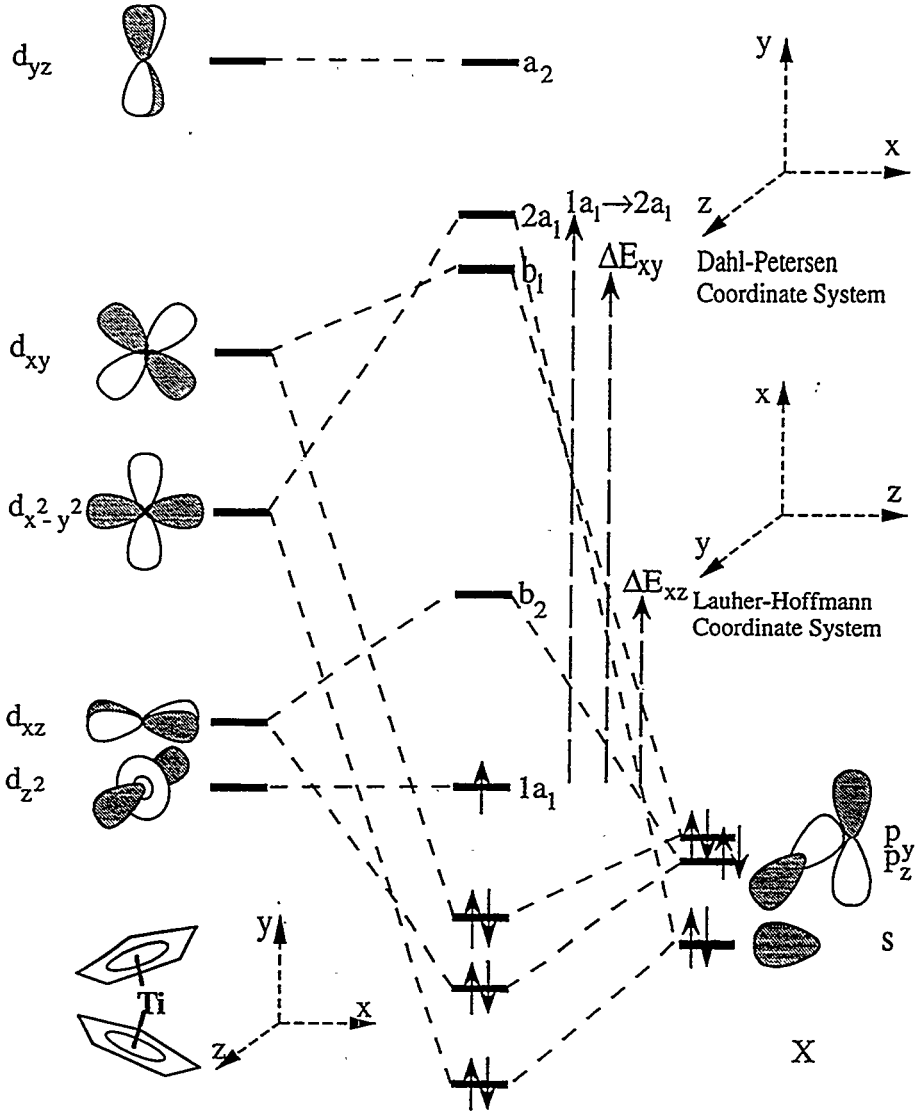

Figure 3a.1: Qualitative MO drawing for Cp_2TiX (after Lauher and Hoffmann)[9]

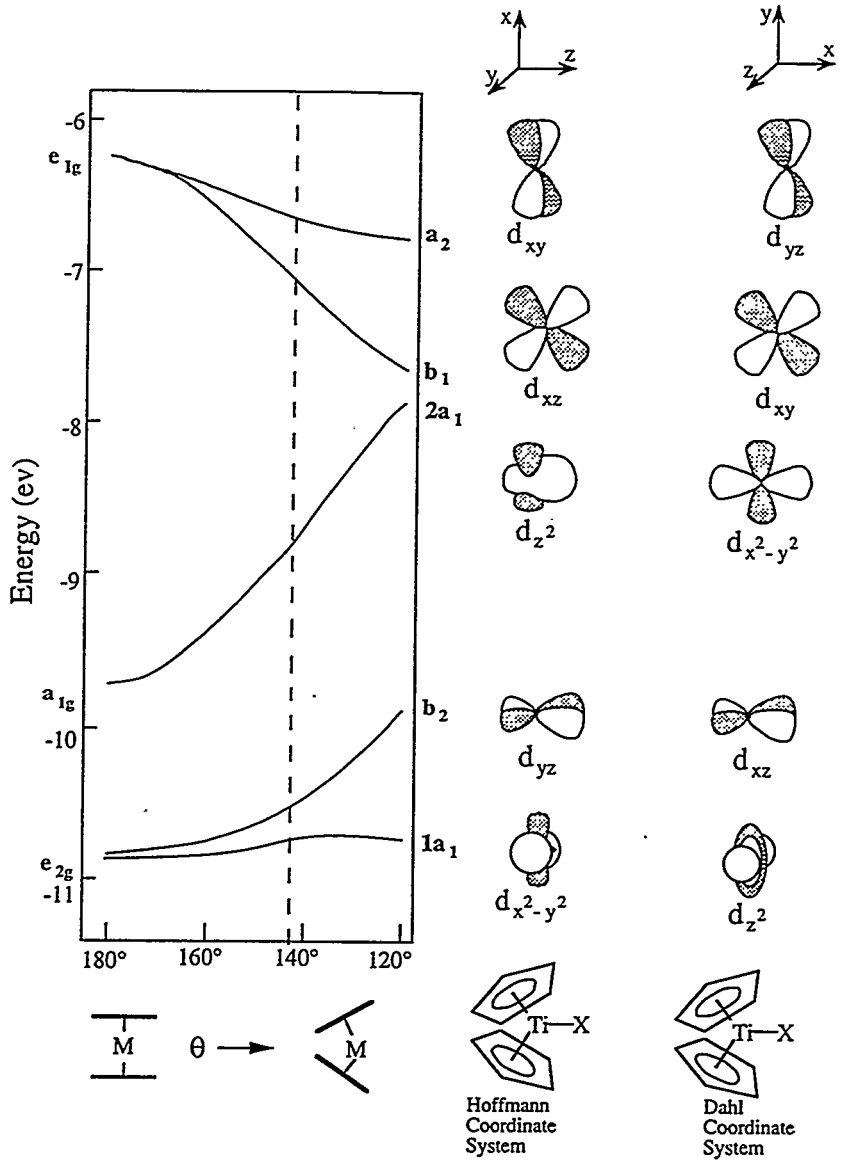

Figure 3a.2: Walsh diagram for metallocenes (after Lauher and Hoffmann)

The syntheses of the titanium complexes were straightforward. Teuben showed that Cp^*_2TiCl is a useful synthon for the preparation of Cp^*_2TiX complexes by chloride metathesis.[4,17] This synthetic route was used to prepare additional examples of Cp^*_2TiX (X = F, N(Et)Ph, N(Me)H, OMe, or OPh) in which X is a potential π-donor ligand. The brown-purple methoxide and phenoxide and the lilac colored

methylamide are soluble in hexane from which they were crystallized. The N-H stretching frequency of the methylamide is a sharp, low intensity feature found at 3370 cm^{-1} in the solid state.

The fluoride Cp^*_2TiF was prepared in two steps. First, the difluoride $Cp^*_2TiF_2$ was prepared using the method used by Lappert to make Cp_2TiF_2: the reaction of $Cp^*_2TiMe_2$ with $BF_3{\bullet}OEt_3$ in diethyl ether.[18] Curiously, the difluoride is almost identical in color and solubility to $Cp^*_2TiMe_2$; consequently, the reaction proceedes with little color change. Reduction of the difluoride with potassium-graphite[19] gave Cp^*_2TiF as green crystals from hexane. Recently, Cp^*_2TiF has also been prepared by the reaction of Cp^*_2TiCl with Me_3SnF.[20]

The solid state structure of $Cp^*_2TiN(Me)H$ is shown in Figure 3a.3, and is almost identical to that of the amide $Cp^*_2TiNH_2$.[21] Useful bonding parameters are listed in Table 3a.1. The most interesting aspect of the crystal structure is the orientation of the methylamide ligand which adopts the least sterically favorable conformation. In $Cp^*_2TiNH_2$, the amide group adopts a similar conformation. The methylamide group lies just slightly out of the plane formed by the titanium atom and the two ligand centroids with a Cp1-Ti-N-C21 torsion angle of 13.5°. The interaction of the amide methyl group with the Cp* ligand bends the amide group "down" opening the Ti-N-Me angle to 145° rather than the 120° expected for an sp^2 hybridized nitrogen atom. In $Cp^*_2TiNH_2$, the Ti-N-H angle is only 126°. Stabilization of the nitrogen lone pair by interaction with the empty b_2 orbital is presumably the reason that the methylamide ligand adopts this conformation. A similar explanation was given for the orientation of the methylamide ligand in the solid state structure of $Cp^*_2Hf(H)N(Me)H$.[22]

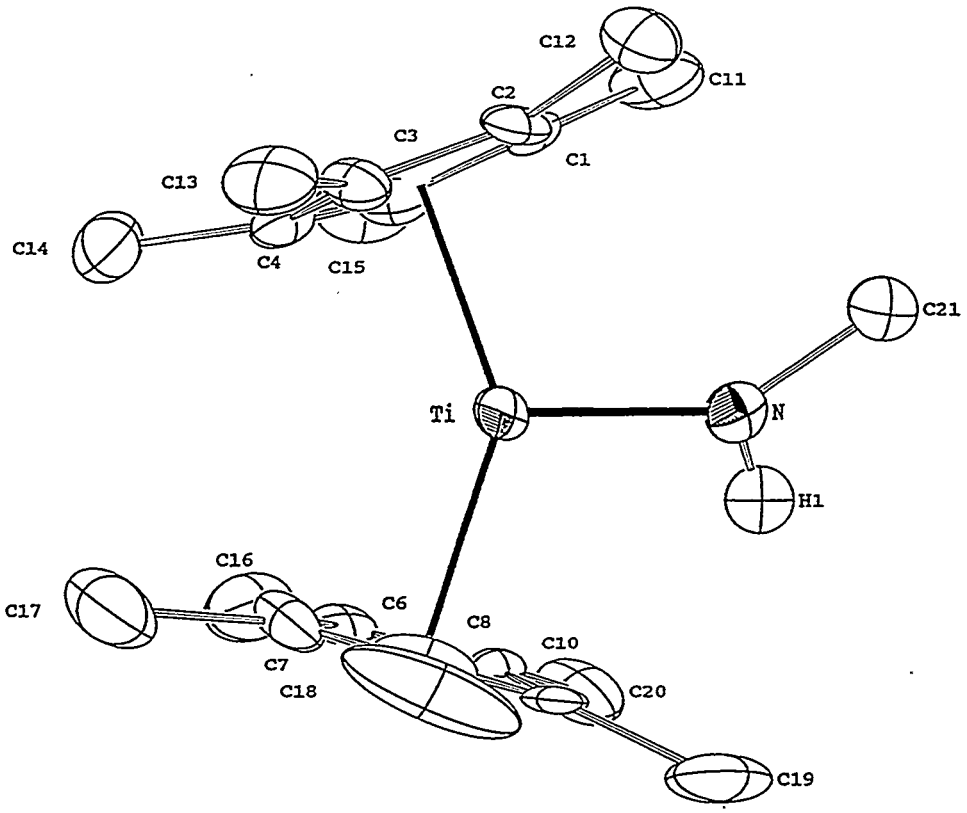

Figure 3a.3: An ORTEP drawing of $Cp^*_2TiN(Me)H$ with 50% thermal ellipsoids

Table 3a.1 Distances and angles in $Cp^*_2TiN(Me)H$

Distances		Angles	
Ti-N	1.955(5) Å	Cp1-Ti-Cp2	141.7°
Ti-Cp1	2.084 Å	Cp1-Ti-N-C21	13.5°
Ti-Cp2	2.094 Å	N-Ti-Cp1	110.4°
Ti-$\langle C_{ring} \rangle$	2.41(2) Å	N-Ti-Cp2	107.9°
N-H1	0.77(7) Å	C21-N-H1	105(5)°
N-C21	1.446(8) Å	Ti-N-H1	110(5)°
		Ti-N-C21	144.9(5)°

In contrast to the orientation of the amide group in Cp*2TiN(Me)H, the crystal structure of $Cp^*_2TiN(Me)Ph$[23] shows that the N-methylanilide ligand is perpendicular to the Cp^*_2Ti fragment with a Cp(centroid)-Ti-N-Me torsion angle of *ca.* 90° preventing the nitrogen lone pair from acting as a π-donor to the empty b_2 orbital. In $Cp^*_2TiNH_2$ and $Cp^*_2TiN(Me)H$, the conformation of the amide group relative to Cp^*_2Ti implies maximum Ti-N π-bonding while in $Cp^*_2TiNMePh$, the conformation of the amide group implies minimal π-bonding. The Ti-N bond distances are consistent with this hypothesis. In $Cp^*_2TiNH_2$ and $Cp^*_2TiN(Me)H$, the Ti-N bond distances are 1.944(2) Å and 1.955(2) Å, respectively, while the Ti-N bond distance of $Cp^*_2TiN(Me)Ph$ is 2.054(2) Å. Other than the orientation of the amide ligand and the short Ti-N bond length, the crystal structure is unremarkable. The other structural features are similar to related crystallographically characterized Cp^*_2TiX compounds.[4,17,21,23]

The crystal structure analysis of Cp^*_2TiF revealed two crystallographically independent but virtually identical molecules in the asymmetric unit, one of which is shown in Figure 3a.4. The important bond parameters for both independent molecules are listed in Table 3a.2. The Ti-F bond lengths are short at 1.845(4) Å and 1.838(4) Å. However, as seen in Figure 3a.4, the fluorine atoms have large thermal parameters making the bond lengths seem shorter. The bonds lengths corrected for the thermal motion using the RMS displacements are 1.860 Å and 1.855 Å, respectively.[24] The corrected bond distances are 0.5 Å shorter than the Ti-Cl distance of 2.363(1) Å in Cp^*_2TiCl[4] in agreement with difference in the size of chloride and fluoride.[25] Like $Cp^*_2TiN(Me)H$, the rest of the structure of Cp^*_2TiF is similar to the other known Cp^*_2TiX structures.[4,17,21,23]

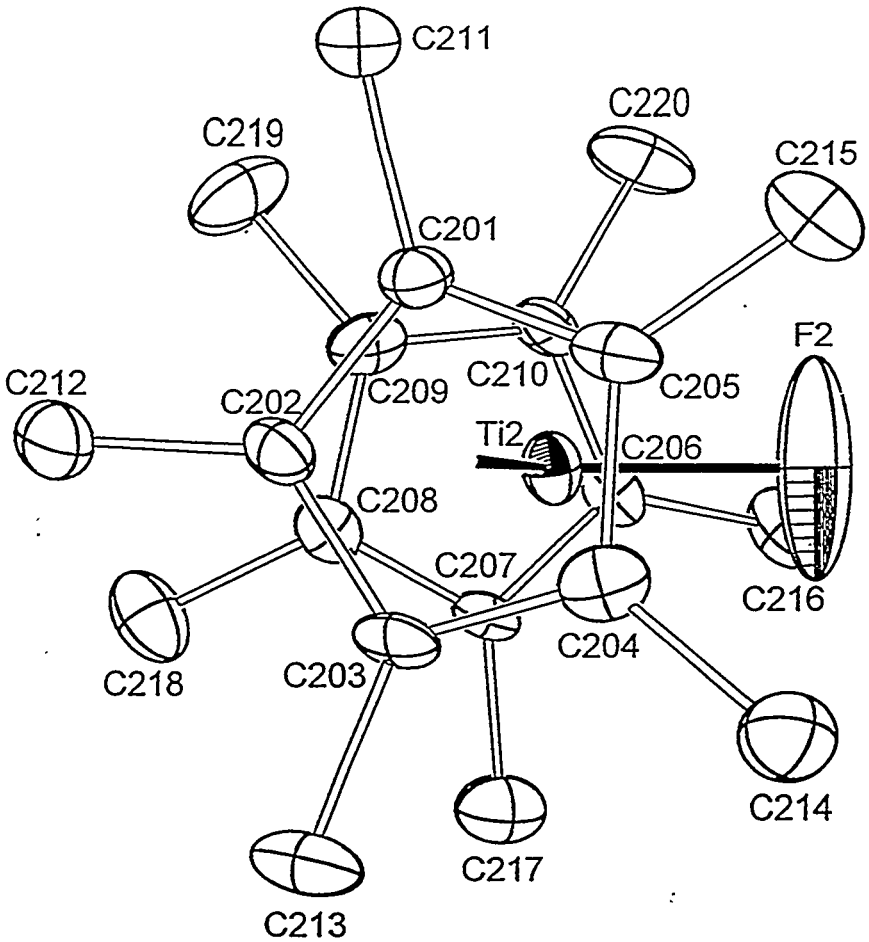

Figure 3a.4: An ORTEP drawing of Cp^*_2TIF with 50% thermal ellipsiods

Table 3a.2: Selected Distances and Angles in Cp^*_2TiF

Molecule 1		Molecule 2	
Ti1-F1	1.845(4) Å	Ti2-F2	1.838(4) Å
Ti1-$\langle C_{ring} \rangle$	2.38(2) Å	Ti2-$\langle C_{ring} \rangle$	2.38(2) Å
Ti1-Cp1	2.06 Å	Ti2-Cp3	2.05 Å
Ti1-Cp2	2.06 Å	Ti2-Cp4	2.05 Å
Cp1-Ti1-Cp2	144.1°	Cp3-Ti2-Cp4	145.6°
Cp1-Ti1-F1	107.3°	Cp3-Ti2-F2	106.3°
Cp2-Ti1-F1	108.5°	Cp4-Ti2-F2	108.0°

The EPR spectra of the new compounds and several known Cp^*_2TiX compounds [4,5,17] were measured as methylcyclohexane solutions at room temperature and as frozen glasses. The EPR results are listed in Table 3a.3. For Cp^*_2TiBr and Cp^*_2TiI, the the EPR parameters were obtained from the simulated spectra. The EPR spectra and simulations for some complexes are shown in Figures 3a.5 - 3a.8. A typical spectrum, that of $Cp^*_2TiN(Me)H$ is shown in Figure 3a.9.

Table 3a.3: EPR data for Cp^*_2TiX compounds. Where present, the ligand hyperfine coupling constant is given in MHz in parentheses.

Compound	g_{ave} (a)	g_z (b)	g_x (b)	g_y (b)
Cp^*_2TiH	(c)	1.997(39)	1.981	1.780
Cp^*_2TiI	1.939	1.997	1.973(36)	1.852
$Cp^*_2TiCH_2Ph$	1.948	1.996	1.870	1.978
$Cp^*Ti(\eta^6\text{-}H_2CC_5Me_4)$	1.950	1.997	1.985	1.880
$Cp^*_2TiCH_2CMe_3$	1.951	1.998	1.984	1.881
Cp^*_2TiBr	1.953	1.996(12)	1.980(21)	1.883
$Cp^*_2Ti(n\text{-}Pr)$	1.953	1.998	1.984	1.884
Cp^*_2TiCl	1.956	1.999	1.984	1.889
Cp*2TiN(Me)Ph	1.958	1.999	1.981	1.937
$Cp^*_2TiN(Et)Ph$	1.955	1.998	1.980	1.895
Cp^*_2TiMe	1.958	1.998	1.981	1.898
$Cp^*_2TiNMe_2$	1.962	1.998	1.979	1.924
Cp^*_2TiF	1.972	1.998(37)	1.982	1.938
Cp^*_2TiEt	1.972	2.000	1.982	1.974
Cp^*_2TiOPh	1.974	1.999	1.983	1.945
Cp^*_2TiOMe	1.977	1.999	1.981	1.956
$Cp^*_2TiNH_2$	1.979	1.998	1.981	1.962
$Cp^*_2TiN(H)Me$	1.980	1.998	1.980	1.965

a) The averaged g-values in solution at room temperature
b) The anisotropic g-values from frozen solutions (*ca.* 80 K)
c) Unobserved

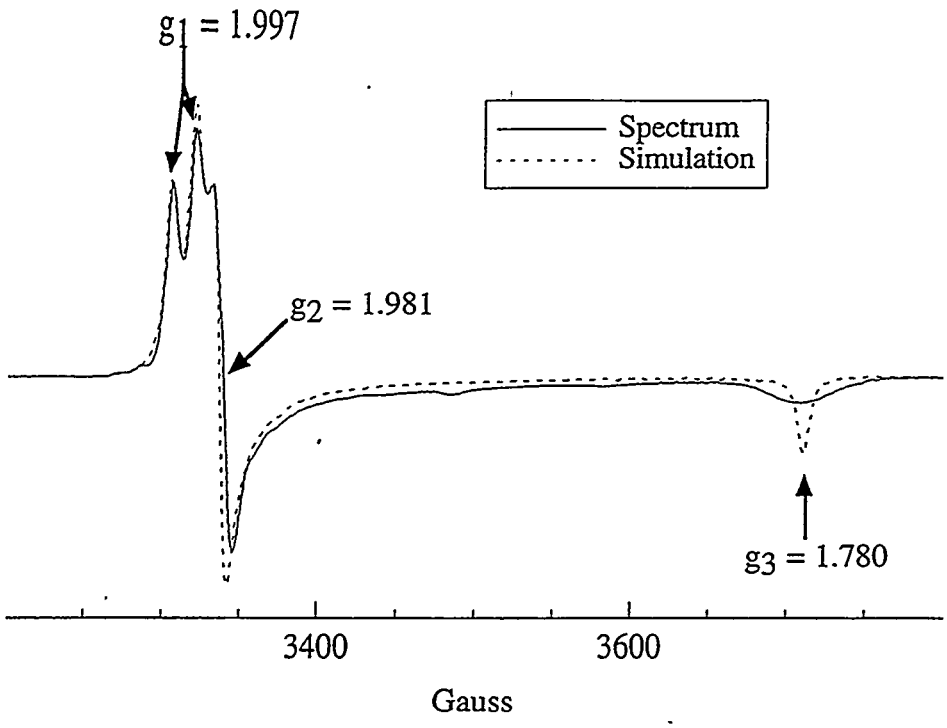

Figure 3a.5: EPR spectrum of Cp^*_2TiH in methylcyclohexane at 80 K (Note that the EPR simulation does not allow the peak width to vary between peaks)

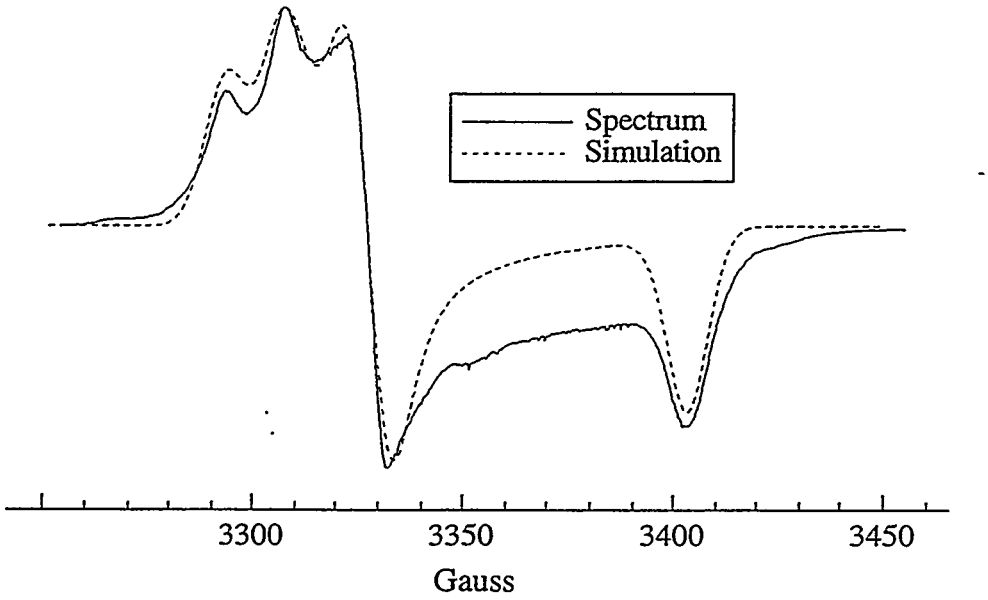

Figure 3a.6: EPR spectrum of Cp^*_2TiF in methylcyclohexane at 80 K

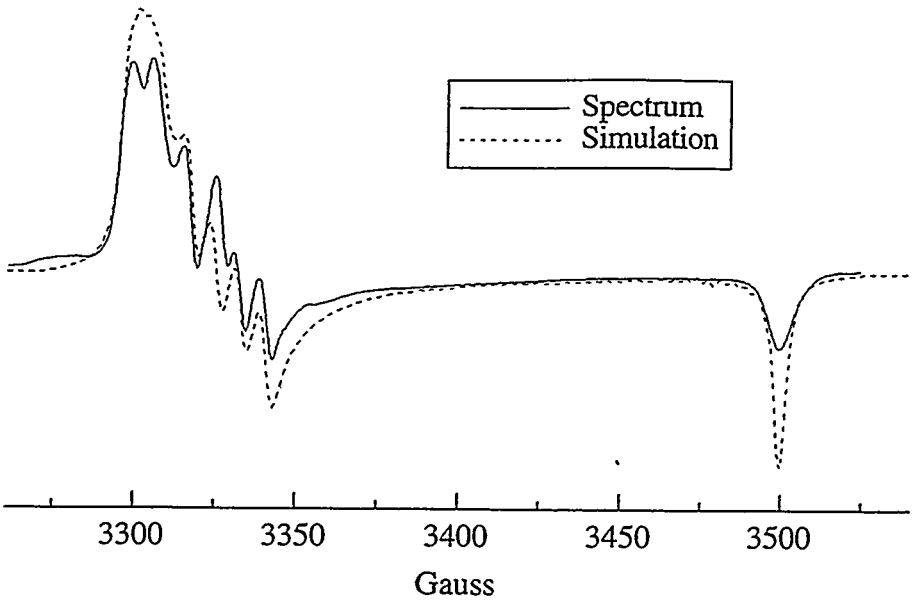

Figure 3a.7: EPR spectrum of Cp^*_2TiBr in methylcyclohexane at 80 K

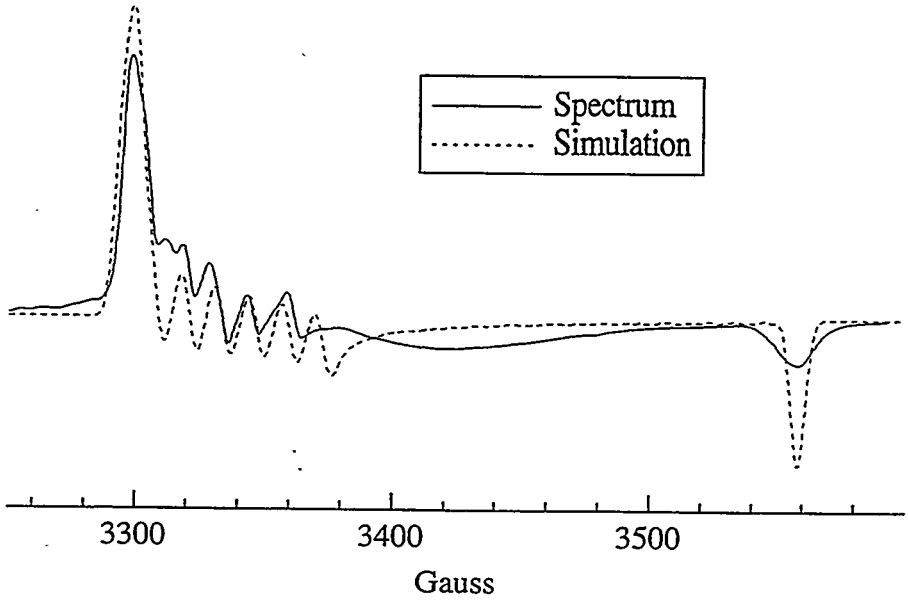

Figure 3a.8: EPR spectrum of Cp^*_2TiI in methycyclohexane at 80 K

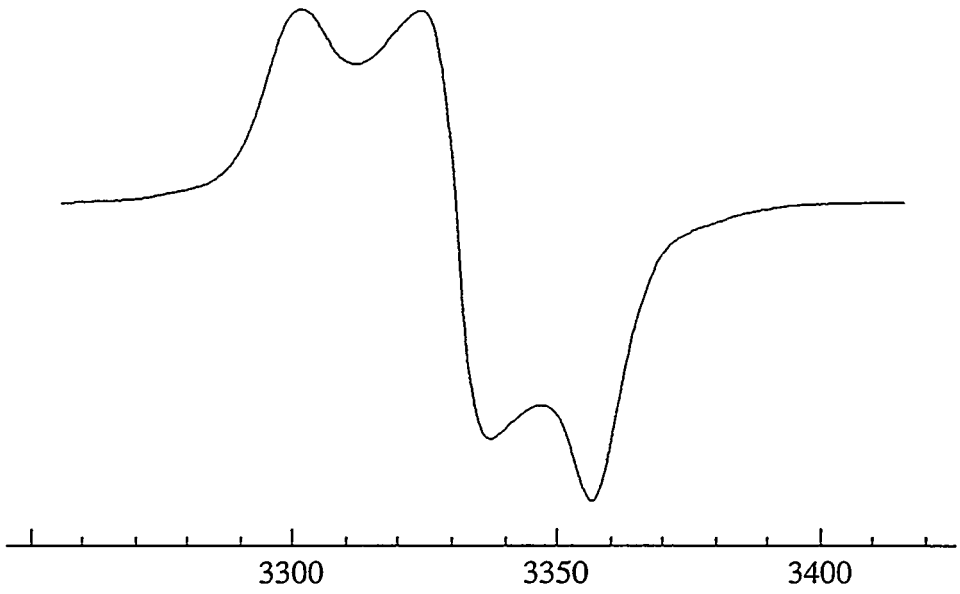

Figure 3a.8: EPR spectrum of $Cp^*_2TiN(Me)H$ in methylcyclohexane at 80 K

At room temperature, complexes with ligands usually thought of as good π-donors (OR, NR_2) have g_{av} values greater than those of complexes whose ligands are thought to be poor π-donors. We were unable to observe either titanium or ligand hyperfine coupling at room temperature in any of these complexes, in agreement with earlier studies.

The EPR spectra of these compounds as frozen glasses are more informative than the room temperature spectra. The most striking aspect of these spectra is their similarity. All of the compounds show two peaks at lower fields with g values of about 1.999 and 1.981. The g value of the other peak varies widely following the trend seen in g_{ave}. Finally, like the spectra of Cp^*_2TiBr and Cp^*_2TiI,[5] the spectra of Cp^*_2TiH and Cp^*_2TiF display ligand hyperfine coupling at low temperature.

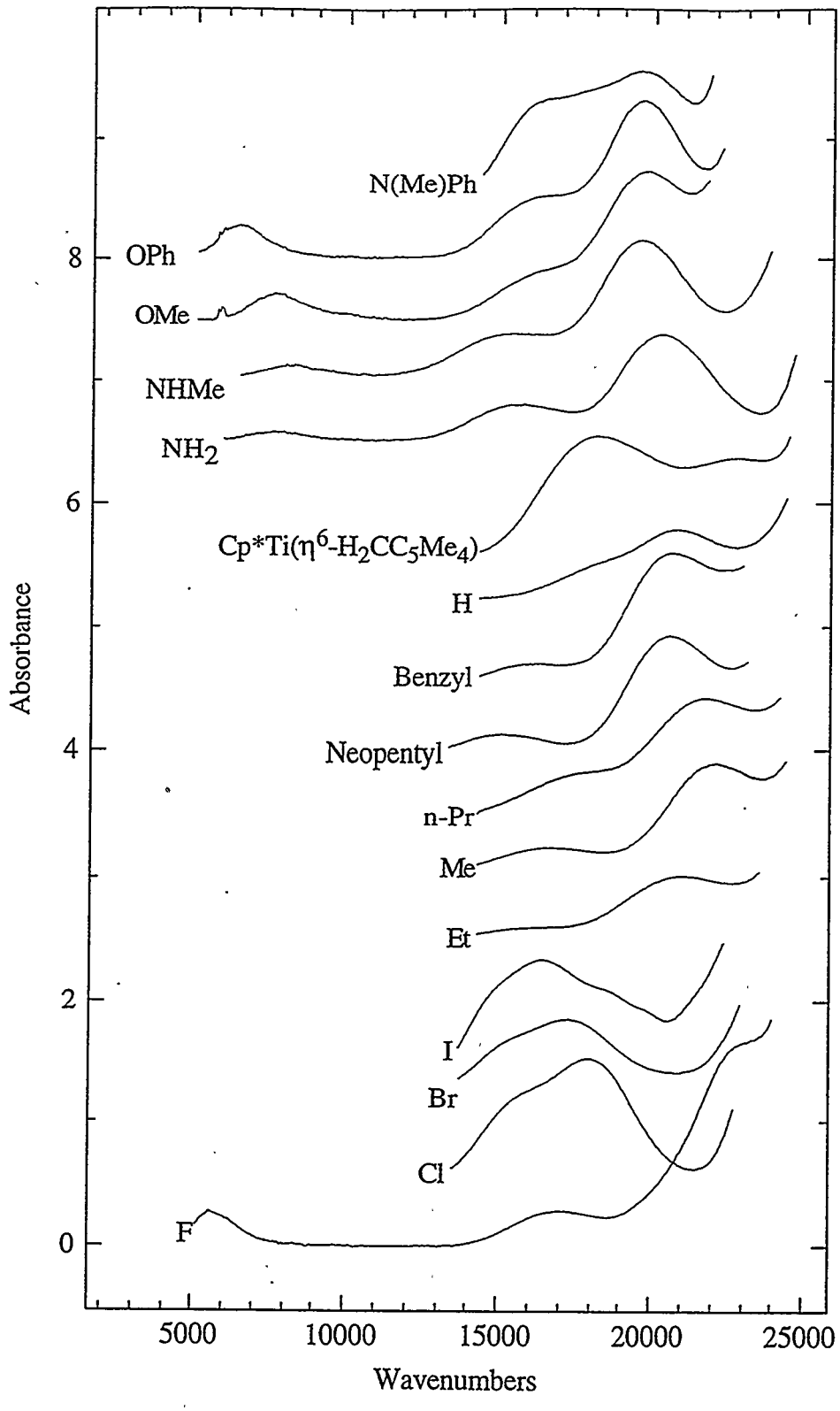

Figure 3a.10: Electronic spectra of Cp^*_2TiX molecules (X is given near the spectrum)

Table 3a.4: Electronic transitions of Cp^*_2TiX complexes in cm^{-1}. The molar extinction coefficients are given in L cm^{-1} mol^{-1} in parentheses.

Compound	$1a_1 \rightarrow 2a_1$	$1a_1 \rightarrow b_2$ (ΔE_{xz})	$1a_1 \rightarrow b_1$ (ΔE_{xy})
Cp^*_2TiH	20976 (131)		18272 (69)
Cp^*_2TiI	16065 (135)		14610 (51)
$Cp^*_2TiCH_2Ph$	20203 (173)		16017 (42)
$Cp^*Ti(h^6\text{-}Me_4C_5CH_2)$	23030 (180)		17816 (180)
$Cp^*_2TiCH_2CMe_3$	20340 (182)		15190 (29)
$Cp^*_2Tin\text{-}Pr$	21702 (189)		17342 (63)
Cp^*_2TiBr	17260 (131)		15023 (40)
Cp^*_2TiCl	18118 (110)		15426 (59)
$Cp^*_2TiN(Me)Ph$	19465 (247)		15893 (121)
Cp^*_2TiMe	21781 (170)		16665 (50)
Cp^*_2TiEt	20826 (122)		15895 (21)
Cp^*_2TiF	23231 (167)	5738 (23)	17124 (29)
Cp^*_2TiOPh	19596 (134)	6464 (29)	15980 (51)
Cp^*_2TiOMe	19607 (128)	7700 (21)	16155 (47)
$Cp^*_2TiNH_2$	20369 (90)	7633 (6)	15422 (34)
$Cp^*_2TiN(Me)H$	19593 (114)	8180 (8)	15159 (40)

The electronic spectra of several Cp^*_2TiX were measured at room temperature as 10^{-3} to 10^{-2} M solutions in methylcyclohexane. Some spectra are shown in Figure 3a.10. The spectra were fit sums sums of Gaussian curves, and the energies of the peaks determined in this way are listed in Table 3a.4. In the visible region, two peaks are present for all complexes: a more intense peak at higher energy and a less intense peak at lower energy. In the near infrared, weak transitions were observed for a few of the compounds. The near IR peak varies in energy from 5630 cm^{-1} for Cp^*_2TiF to 8220 cm^{-1} for $Cp^*_2N(Me)H$. At 77 K, Cp^*_2TiEt has an absorption at 8460 cm^{-1}. No near infrared absorption was observed for many of the compounds.

As noted previously, the unpaired electron occupies the $1a_1$ orbital which is largely d_z2 with a small amount $d_{x^2-y^2}$ character. This orbital is non-bonding and interacts only weakly with the X ligand in Cp^*_2TiX.[10] The LUMO, b_2, is mainly d_{xz} character, and, in the absence of π-effects, is close to $1a_1$ in energy. When X is a π-donor, b_2 is the π-accepting orbital and is destabilized as the ligand π-donating orbital is stabilized. By comparing the energy of the $1a_1 \rightarrow b_2$ transition for a series of complexes to the energy of this transition in a complex with a σ-only ligand, Cp^*_2TiH, the relative strength of the π-interaction in these complexes can be determined. Since b_2 is π-antibonding, the actual strength of the π-interactions will be somewhat less than the energy determined in this way.

For a Cp^*_2TiX complex, three d-d absorptions are expected: $1a_1 \rightarrow b_2$, $1a_1 \rightarrow b_1$, and $1a_1 \rightarrow 2a_1$ in order of increasing energy (see Figure 3a.1). The $1a_1 \rightarrow a_2$ transition should be similar in energy to the $1a_1 \rightarrow b_1$ and $1a_1 \rightarrow 2a_1$ transitions but is electric dipole forbidden and not observed. The absorptions observed in the optical spectra can be assigned in a straightforward manner. First, the lowest energy absorption, which is only observed when X is a strong π-donor, is assigned to the $1a_1 \rightarrow b_2$ transition. When X is not a good π-donor, the $1a_1 \rightarrow b_2$ absorption is too low in energy for us to observe directly. The absorptions observed in the visible region of the spectrum are the $1a_1 \rightarrow b_1$ and $1a_1 \rightarrow 2a_1$ transitions. The more intense, higher energy peak is assigned to the $1a_1 \rightarrow 2a_1$ transition. Its greater intensity is due to the fact that the $2a_1$ orbital is

σ-antibonding towards the X ligand of Cp^*_2TiX. The ligand character in this orbital gives this transition some charge transfer character.[26] The weaker visible absorption is the $1a_1 \rightarrow b_1$ transition. The b_1 orbital is somewhat Ti-Cp* antibonding and also can act as a π-acceptor if the X ligand of Cp^*_2TiX has a p_y orbital capable of acting as a π-donor (*e.g.* $Cp^*_2TiN(Me)Ph$).

While the energy $1a_1 \rightarrow b_2$ transition could not be measured directly in all cases, its energy can be determined by a combination of EPR and visible spectroscopy. As shown by McGarvey, the deviation the g_i values from g_0 is due to coupling of excited states into the ground state is shown in eq 3a.1 where i is x, y or z; λ is the spin-orbit

$$g_i = g_0 - 2\lambda \sum_n \frac{\langle 0|L_i|n\rangle\langle n|L_i|0\rangle}{E_n - E_0} \qquad (3a.1)$$

coupling constant, $E_n - E_0$ is the difference in energy of the orbitals, and the sum is over all orbitals containing d-character.[6] For bent metallocenes, Petersen and Dahl have shown that the relationship of the g values to the energies of the excited states is as shown in eq 3a.2 where λ is the observed spin-orbit coupling constant,

$$g_x = g_0 - \frac{2\lambda(a\sqrt{3} + b)^2}{\Delta E_{yz}} \qquad g_y = g_0 - \frac{2\lambda(a\sqrt{3} - b)^2}{\Delta E_{xz}} \qquad g_z = g_0 - \frac{8\lambda b^2}{\Delta E_{xy}} \qquad (3a.2)$$

g_0 is 2.002 (the value of g for a free electron), ΔE_{yz}, ΔE_{xy} and ΔE_{xz} are the energies of the excited states of d_{yz}, d_{xy}, and d_{xz} character, that is, the a_2, b_2, and b_1 orbitals,

respectively, and a and b are the coefficients of d_{z^2} and $d_{x^2-y^2}$ in the ground state, $\Psi = a|d_{z^2}\rangle + b|d_{x^2-y^2}\rangle$. [9,16] Since we did not measure ΔE_{yz}, only the last two relationships are used. Note that in eq 3a.2, while no orbital reduction factor is used, the value of λ is allowed to vary to account for covalency.

Using eq 3a.2 rather that eq 3a.1 involves two main assumptions. First, only the unoccupied d orbitals contribute to the change in g. Since the d orbitals are involved in bonding, some low lying orbitals will also have d character and could potentially change the value of g. However, these orbitals are much further in energy from $1a_1$ and contain little d-orbital character, and so, are not expected to change g to any great extent.

The other assumption is that the b_1 and b_2 orbitals have the same amount of d character. Since these orbitals are involved in bonding to the Cp* versus the X ligands, this assumption could possibly be bad.[27] Using eq 3a.3, where the κ^2 terms are

$$g_y = g_0 - \frac{2\lambda(a\sqrt{3}-b)^2}{\Delta E_{xz}}\kappa_y^2 \qquad g_z = g_0 - \frac{8\lambda b^2}{\Delta E_{xy}}\kappa_z^2 \qquad (3a.3)$$

the orbital reduction factiors, can accounted for the different amount of d-character in the b_1 and b_2 orbitals. Unfortunately, the presence of the κ^2 terms introduces too many variables to determine using only the two equations of 3a.2. By choosing a new set of parameters, a', b', and λ' as shown in eq 3a.4, a relationship similar to eq 3a.2 can be

$$\frac{a'}{b'} = \frac{1}{\sqrt{3}}\left[1+\sqrt{\frac{\kappa_y^2}{\kappa_z^2}\left(a\sqrt{3}/b-1\right)}\right] \qquad \lambda' = \frac{\lambda b^2 \kappa_z^2}{b'^2} \qquad a'^2+b'^2=1 \qquad (3a.4)$$

$$g_y = g_0 - \frac{2\lambda'(a'\sqrt{3}-b')^2}{\Delta E_{xz}} \qquad g_z = g_0 - \frac{8\lambda' b'^2}{\Delta E_{xy}} \qquad (3a.5)$$

used, eq 3a.5. It must be noted that a', b', and λ' have no real physical meaning, but are closely related to a, b, and λ. When κ_y^2 is equal to κ_z^2, a' and b' become a and b, respectively. PES studies on the similar Cp_2VX (X=halide, alkyl) have shown that the amount of ligand character in the b_2 orbital is very small.[28] The consequence of this observation is that the second assumption is probably not too bad, so a', b', and λ' are interchangable with a, b, and λ. If g_y, ΔE_{xz}, g_z, and λ' are known, eq 3a.5 can be used to obtain the energy of the b_2 orbital relative to $1a_1$.

To use eq 3a.5 to obtain the energy of the b_2 orbital, the EPR spectra, as well as the electronic spectra must be assigned. The high field g component of the EPR spectra, g_3, has already been assigned to g_y by Mach and Raynor.[5] Since b' is expected to be quite small, g_z is the low field component, closest to g_0. The remaining, middle component is g_x.

In the compounds for which g_y, g_z, ΔE_{zx}, and ΔE_{xy} are observed, the values of a', b', and λ' can be determined directly. The results are shown in Table 3a.5. The values of a' and b' vary only slightly among these complexes, and the value of a'^2/b'^2 is similar to that seen by Petersen and Dahl for Cp_2VX_2 complexes.[9,16] The fact that a'

and b' have the same sign shows that $1a_1$ resides mainly in the yz plane (the d_z2 orbital is compressed along the x axis, see the $1a_1$, d_z2 orbital in Figure 3a.2). In contrast, Petersen and Dahl found that in the Cp_2VX_2 complexes, a and b have opposite signs, so that $1a_1$ is mainly in the xz plane.[9,16] However, for Cp_2VCO, the ratio a^2/b^2 was about the same as this ratio in Cp_2VX_2, but the signs of a and b were the same.[29] This contradiction was explained by noting that in Cp_2VCO, as in the trivalent decamethyltitanocenes, the change in sign of b reflects a decrease in electron density along the x-axis minimizing a destabilizing interaction with the σ-orbital of the ligand.

Table 3a.5: Values of a', b', and λ' determined from the electronic and EPR spectra

	a'	b'	λ' (cm^{-1})
Cp^*_2TiF	0.96	0.29	99
Cp^*_2TiOPh	0.97	0.26	92
Cp^*_2TiOMe	0.97	0.26	89
$Cp^*_2TiNH_2$	0.95	0.30	84
$Cp^*_2TiN(Me)H$	0.95	0.30	83

Unlike the values of a' and b', the value of λ' changes with the ligand. The greater the ligand electronegativity,[30] the higher the value of λ'. As seen in Figure 3a.11, this relationship is roughly linear. The less electronegative ligands have a more covalent interaction with the titanium center, decreasing λ' for the unpaired electron. The highest calculated value of λ' is 98 cm^{-1}, for Cp^*_2TiF, considerably reduced from the free-ion value of 154 cm^{-1} for Ti(III) in the gas phase.[31]

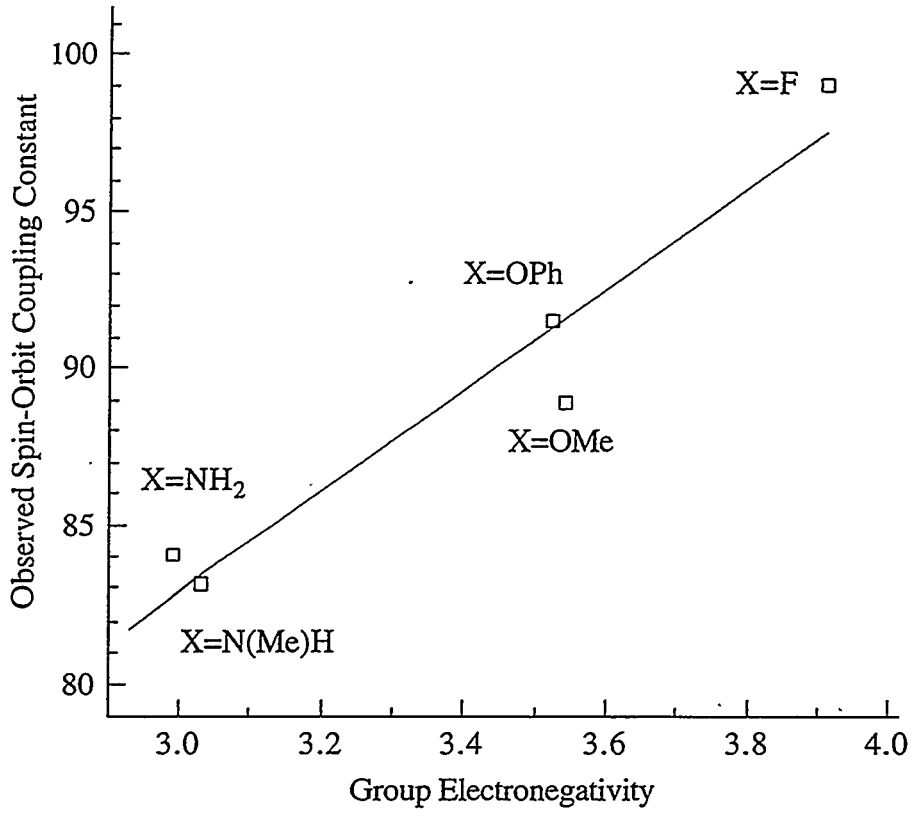

Figure 3a.11: Observed spin-orbit coupling constant for Cp*2TiX complexes

The transition energy ΔE_{xz} was calculated using the g values from the EPR spectra, the value of ΔE_{xy}, and the λ' values obtained from fitting the linear relationship shown in Figure 3a.11. The results, along with the calculated values of a' and b' are listed in Table 3a.6. The values of ΔE_{xz} calculated from the EPR spectra agree with those obtained from the near infrared spectra.

Table 3a.6: Calculated values for Cp^*_2TiX complexes. The energies are in cm^{-1}.

	b'	a'	ΔE_{xz} (calc)	ΔE_{xz} (obs)	ΔE_{xz} relative to Cp^*_2TiH
Cp^*_2TiH	0.57	0.82	447		0
Cp^*_2TiI	0.36	0.93	1537		1090
$Cp^*_2TiCH_2Ph$	0.40	0.92	1601		1154
$Cp^*Ti(\eta^6\text{-}Me_4C_5CH_2)$	0.39	0.92	1794		1348
$Cp^*_2TiCH_2CMe_3$	0.32		2157		1710
$Cp^*_2Tin\text{-}Pr$	0.34	0.94	2096		1649
Cp^*_2TiBr	0.38	0.92	1923		1476
Cp^*_2TiCl	0.27	0.96	2852		2405
$Cp^*_2TiN(Me)Ph$	0.28	0.96	4870		4423
Cp^*_2TiMe	0.33	0.94	2410		1963
Cp^*_2TiF	0.30	0.96	5622	5738	5175
Cp^*_2TiOPh	0.26	0.97	6445	6463	5998
Cp^*_2TiOMe	0.26	0.97	7995	7700	7549
$Cp^*_2TiNH\text{-}$	0.31	0.95	7479	7633	7032
$Cp^*_2TiN(Me)H$	0.30	0.95	8217	8180	7770
Cp^*_2TiEt	0.33	0.94	8695	8460(a)	8248

a) Not used in determining the k^2 relationship.

The amount of destabilization of b_2 caused by the π-donor ligand was calculated by comparing ΔE_{xz} to the value of ΔE_{xz} in a compound which possess a σ-only ligand: Cp^*_2TiH. A potential problem exists, however, in that Lauher and Hoffmann have predicted that the hydride ligand will not lie on the x axis.[10] This distortion would increase the value of ΔE_{xz} for Cp^*_2TiH from a true σ-only value. However, more recent calculations have suggested that the hydride ligand does lie along the x axis.[32] The relatively high value of b' for this complex was disturbing

since this observation implies that the bonding in Cp*TiH is somewhat different from the other metallocenes.

Since we thought that a geometric distortion (bending of the hydride ligand) was responsible for the difference in bonding suggested by the high value of b' in Cp^*_2TiH, we determined its crystal structure. An ORTEP drawing of Cp^*_2TiH is given in Figure 3a.12, and bond distances and angles are given in Table 3a.7. Like Cp^*_2TiF, two crystallographically independent, but virtually identical, molecules exist in the asymmetric unit. The hydride hydrogen atoms in both molecules were located and refined isotropically, all of the other hydrogen atoms were located and refined positionally with a global thermal parameter. The hydride ligand does indeed lie on the psuedo 2-fold axis of the molecule, but the Cp*-Ti-Cp* angle is much greater than that of other decamethyltitanocenes. The smaller steric demand of the hydride ligand allows the metallocene angle to increase relative to other Cp^*_2TiX complexes.

The large value of the Cp*-Ti-Cp* angle is somewhat surprising in light of the metallocene angle in other hydride complexes. The metallocene angles in the d^0 metallocenes Cp_2TaH_3 and Cp_2NbH_3 are 139.9° and 141.6°, respectively.[33] The metallocene angle in d^2 Cp_2MoH_2 is larger at 145.8°.[34] Finally, the metallocene angle in d^4 $(EtMe_4C_5)(C_5H_5)ReH$ is largest at 161.6°.[35] The trend in bending angles can be explained by referring to Figure 3a.2. Since both the $1a_1$ and b_2 orbitals fall in energy when the metallocene angle increases, when these orbitals are occupied, as in Cp_2MoH_2 and in $(EtMe_4C_5)CpReH$, the metallocene angle should increase. Since the $1a_1$ and b_2 are unoccupied in Cp^*_2TiH, the large metallocene angle must be due to steric repulsions between methyl groups of the Cp* ligands at the back of the metallocene wedge. It is still surprising that this angle is so much larger than in other decamethyltitanocene complexes.

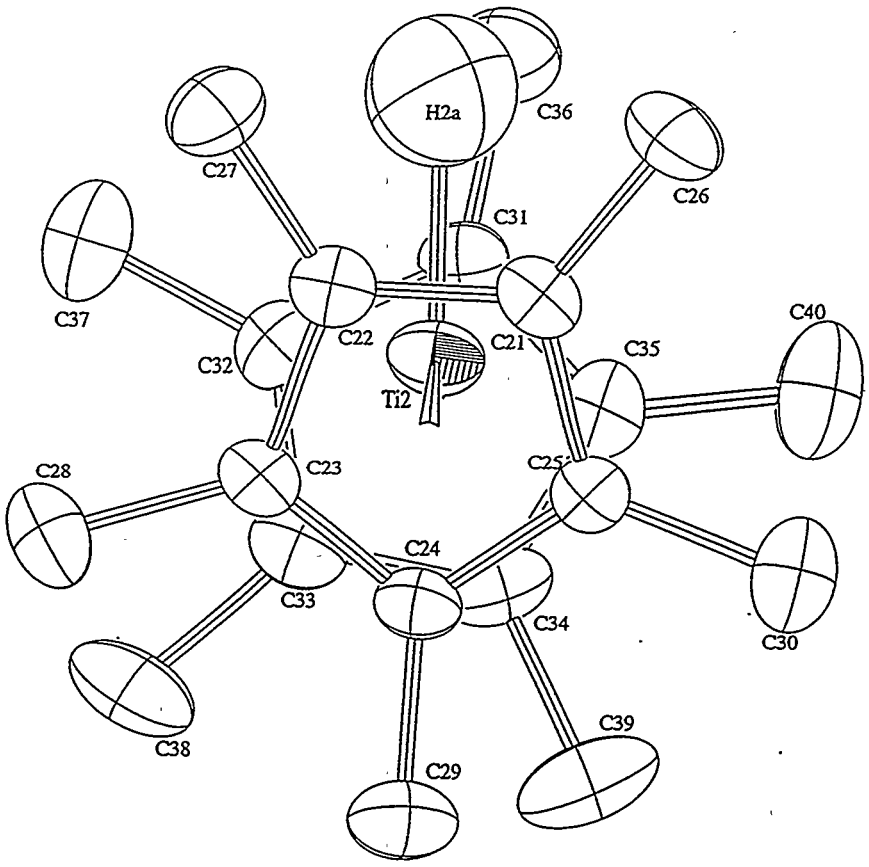

Figure 3a.12: An ORTEP drawing of Cp^*_2TiH with 50% thermal ellipsoids

Table 3a.7: Selected distances and angles in Cp^*_2TiH

Molecule 1		Molecule 2	
Ti1-H1a	1.69(5) Å	Ti2-H2a	1.84(4) Å
Ti1-$\langle C_{ring} \rangle$	2.36(1) Å	Ti2-$\langle C_{ring} \rangle$	2.36(1) Å
Ti1-Cp1	2.03 Å	Ti2-Cp3	2.03 Å
Ti1-Cp2	2.03 Å	Ti2-Cp4	2.04 Å
Cp1-Ti1-Cp2	152.3°	Cp3-Ti2-Cp4	152.0°
Cp1-Ti1-H1a	103°	Cp3-Ti2-H2a	106°
Cp2-Ti1-H1a	104°	Cp4-Ti2-H2a	101°

The larger Cp*-Ti-Cp* angle in Cp^*_2TiH is the geometric distortion responsible for the higher value of b' in this complex. As seen in Figure 3a.2, as the titanocene angle increases, the d_z2 and $d_{x^2-y^2}$ orbitals become closer in energy and will interact more strongly, giving $1a_1$ more $d_{x^2-y^2}$ character relative to the other complexes. The greater hybridization of the $1a_1$ orbital will increase b' and decrease a' for Cp^*_2TiH.

The trend in π-bond strengths of the halides are found to be F > Cl > Br > I. This trend has been observed previously in other analyses of bonding in bent metallocenes and has been attributed to strong overlap between the p-orbitals of the halide and the d orbitals of the bent metallocene fragment.[36,37] While this trend appears to contradict the spectrochemical series, this is actually not the case. It is well known that the splitting in octahedral metal complexes, 10Dq, is a combination of σ and π effects. Specifically, $10Dq = 3e_\sigma(L) - 4e_\pi(l)$ where e_σ and e_π are angular overlap parameters which reflect the σ and π donor ability of ligands.[26] For π donors, such as halides, both e_σ and e_π are positive. Fluoride is both a strong σ and a strong π donor. As one descends the periodic table, both e_σ and e_π decrease. In octahedral Cr(III) complexes, the π-bonding trend is also F > Cl > Br > I.[26] In Cp^*_2TiX, fluoride is a good π-donor, only slightly weaker than phenoxide.

A potential problem exists in the analysis of the halides since the observed spin-orbit coupling could increase due to ligand character in the metallocene d-orbitals. This effect would decrease g_y by increasing λ_{eff} rather than by decreasing b_2 making the heavier halides seem like poorer π-donors than they actually were. For Cp^*_2TiI

with $\zeta_I = 5069\ cm^{-1}$,[38] this effect would be greatest, but since $3g_{av} - g_y$ (that is, $g_x + g_y$) is approximately the same for all of these compounds, λ_{eff} seems not to vary greatly among these compounds. In addition, based upon the small values observed for the ligand hyperfine coupling, little ligand character is present in the $1a_1$ orbital.[39] This observation is in agreement with the previously mentioned PES studies on Cp_2VX in which little ligand orbital character was seen in the b_2 orbital.[28]

In conclusion, the origin of the shifts in the g values of trivalent decamethyltitanocenes is explained in terms of the model developed by Petersen and Dahl.[9,16] The major factor contributing to the change in the g value is spin-orbit coupling to the low lying b_2 orbital. Since the energy of b_2 is closely related to the π-donor ability of the X ligand in these Cp^*_2TiX compounds, a combination of the electonic spectra and the g values from the EPR spectra allows the π-bond strengths of these compounds to be estimated.

3b: Agostic Interactions in Cp^*_2TiX Complexes

Agostic interactions are well known in organometallic chemistry and are thought to be important in a number of processes including olefin polymerization. Among Ti(III) complexes, Cp^*_2TiEt is reported to have a β-agostic ethyl group on the basis of its IR spectrum.[17] Since, as shown in the preceding section, EPR is very sensitive to the energies of the low lying excited states in Cp^*_2TiX complexes, this method seemed to be well suited to studying agostic interactions in these compounds.

As shown in Figure 3b.1, a β-agostic interaction of a ligand with the titanium center will raise the energy of the b_2 orbital. This change in energy is reflected in the EPR spectrum by a shift of the g_y component to lower field resulting in a higher g_y value. For example, in Cp^*_2TiEt, g_y is 1.974 while, in Cp^*_2TiMe, g_y is 1.898. Since the energy of the b_2 orbital relative to the $1a_1$ orbital can be calculated from the EPR and electronic spectra of these complexes, the energy of b_2 in a complex with an agostic ligand can be compared to that of a similar complex without an agostic interaction.

The difference in energy between $1a_1$ and b_2 is greater than the actual strength of the agostic interaction for two reasons. First, b_2 is the antibonding orbital, and the stabilization of the bonding orbital will be less than the destabilization of the antibonding orbital. Second, if the σ-bond of the ligand moves off of the C_2 axis of the metallocene, b_2 will be destabilized by σ-bonding as well as by the agostic interaction. Note that for Cp^*_2TiEt, the $1a_1 \rightarrow 2a_1$ separation is about 1000 cm^{-1} lower than in Cp^*_2TiMe showing that the ethyl group is interacting more weakly with the $2a_1$ orbital

presumably because is has moved off of the C_2 axis of the metallocene. In addition, the destabilization of b_2 reflects only the electronic contribution to the agostic interaction. The electronic contribution is greater than the net interaction since it does not reflect destabilization due to steric crowding or strain caused by bending the ligand.

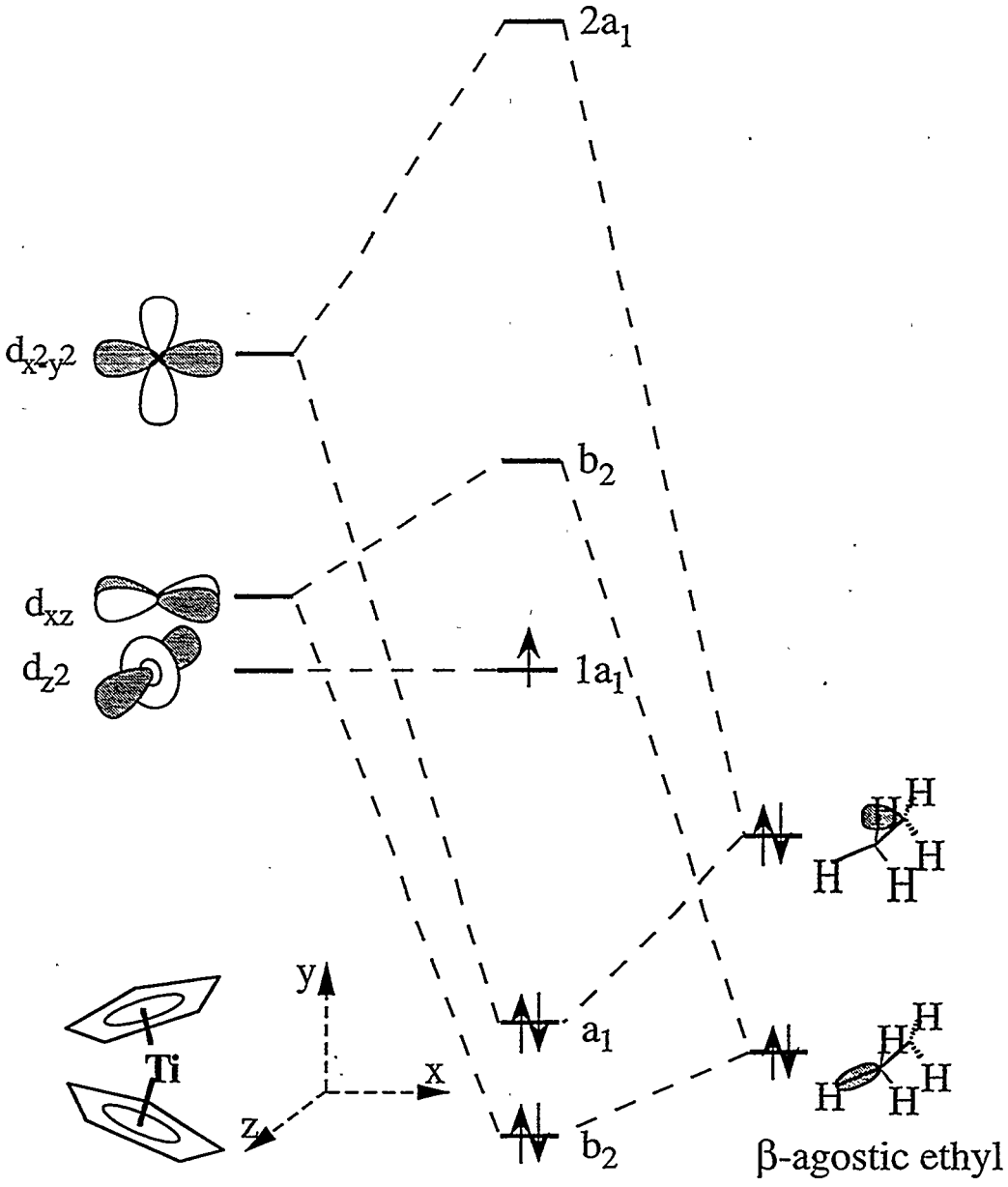

Figure 3b.1: Destabilization of the b_2 (d_{xz}) orbital by a β-agostic interaction. Note that the symmetry labels for C_{2v} symmetry have been included for consistency. The actual symmetry is C_s or C_1.

In the Cp^*_2TiX system, no other alkyl ligands appear to have agostic interactions based upon their EPR spectra.[17] All of the other alkyl ligands function as σ-donors only. While b_2 in Cp^*_2TiMe is somewhat destabilized relative to the other alkyl complexes, no corroborating evidence, such as low frequency C-H absorptions in the IR, exists to support an α-agostic interaction in this complex.

Another complex which appears to have a β-agostic ligand is $Cp^*_2TiN(Me)Ph$. In the crystal structure of this compound, $\angle Ti\text{-}N\text{-}C_{Me}$ = 110.8(2)° and $\angle Ti\text{-}N\text{-}C_{Ph}$ = 131.6(1)° while in the n-butyl isocyanide adduct of $Cp^*_2TiN(Me)Ph$, $\angle Ti\text{-}N\text{-}C_{Me}$ = 121.2(4)° and $\angle Ti\text{-}N\text{-}C_{Ph}$ = 125.6(4)°.[23] In addition, weak absorptions are seen at 2570 cm^{-1} and 2620 cm^{-1} in the IR spectrum, typical of agostic C-H bonds.[40] In $Cp^*_2TiN(Me)Ph$, the X ligand does appear to lie on the C_2 axis of the metallocene, so the destabilization of b_2 is due entirely to the agostic interaction.

Surprisingly, the g_{ave} values for Cp^*_2TiEt and $Cp^*_2TiN(Me)Ph$ are not equal to the averages of the g components at low temperature. This observation implies that some change in the electronic structure of the complexes occurs between ~100 K and 300 K. Since only these complexes have different g_{ave} values at different temperatures, the change is likely due to the presence (or absence) of the agostic interaction as argued below. Presumably, molecules having an agostic interaction are in equilibrium with molecules without one as shown in eq 3b.1.

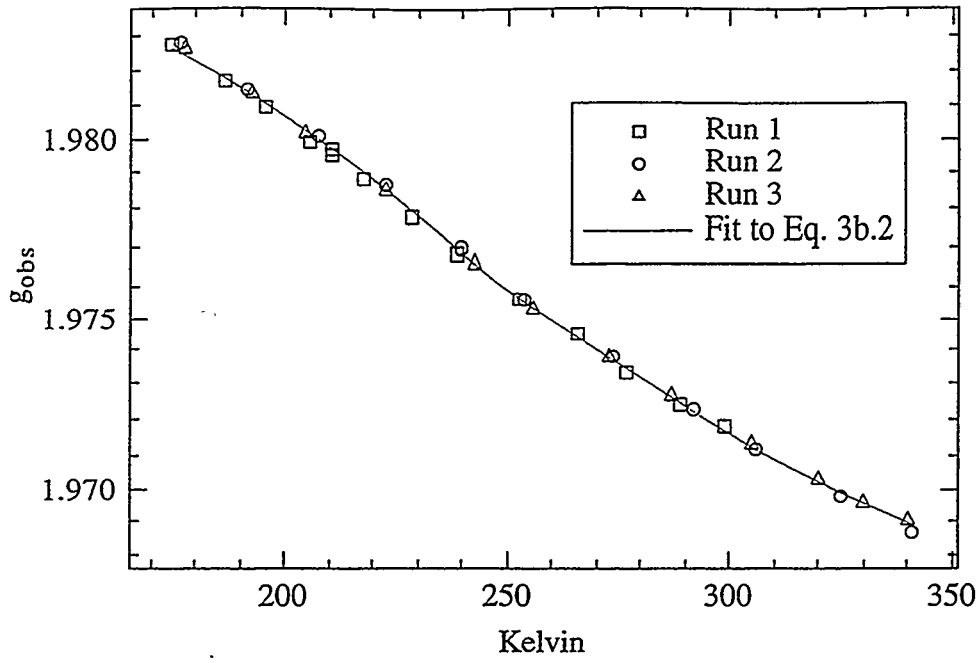

Figure 3b.2: Variable temperature EPR behavior of Cp^*_2TiEt

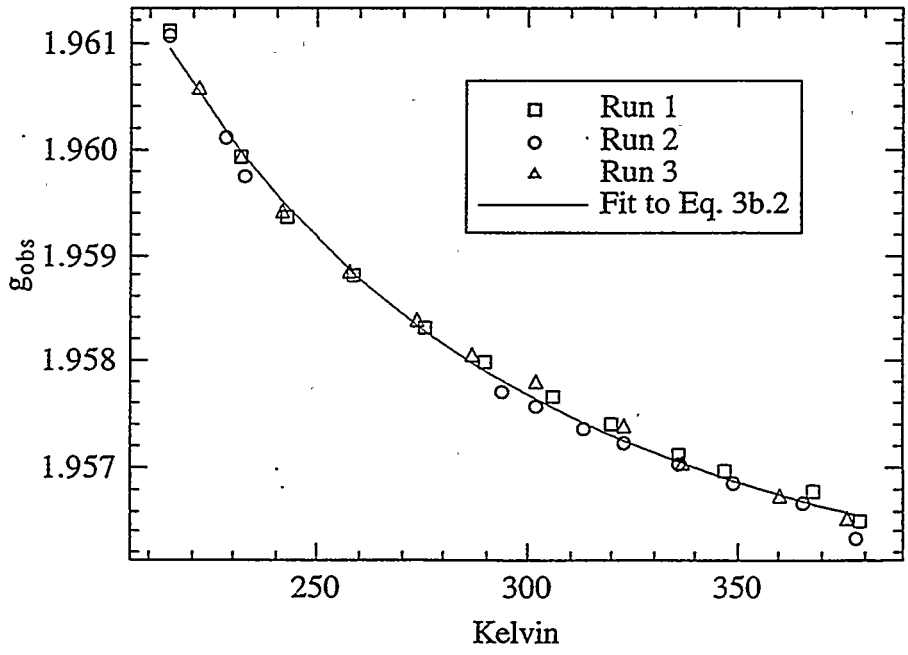

Figure 3b.3: Variable temperature EPR behavior of $Cp^*_2TiN(Me)Ph$

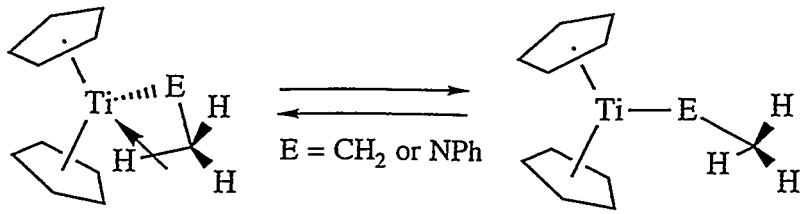

agostic anagostic (3b.1)

$$g_{obs} = \frac{1}{K+1}\left(g_{agostic} + Kg_{anagostic}\right) \quad (3b.2)$$

$$K = e^{-(\Delta H^0 - T\Delta S^0)/RT}$$

Fitting the g_{ave} values of these complexes at different temperatures using eq 3b.2 will give the values of the three unknowns: ΔH^0, ΔS^0 , and $g_{anagostic}$. The value of $g_{angostic}$ is assumed to be the average of the g components in the frozen glass spectrum. Plots of g_{ave} versus T for Cp^*_2TiEt and $Cp^*_2N(Me)Ph$ are shown in Figures 3b.2 and 3b.3, respectively. For Cp^*_2TiEt, the variable temperature EPR data from -98 °C to 68 °C yield ΔH^0 = 1.93(3) kcal/mol, ΔS^0 = 6.3(2) e.u. and $g_{anagostic}$ = 1.9570(7). For $Cp^*_2TiN(Me)Ph$ from -58 °C to 105 °C, the values are ΔH^0 = 1.5(1) kcal/mol, ΔS^0 = 7.9(5) e.u., and $g_{anagostic}$ = 1.9545(3). The data are for three separate runs for each complex and assume an error of 1×10^{-4} in g ($\sigma(g_{ave})$ for spectra acquired at the same temperature).

The entropy difference between the agostic and anagostic molecules is the same in both cases. The entropy difference is $R\ln(\sigma)$ where σ is the product of the symmetry numbers of the anagostic molecule versus the agostic molecule.[41] Assuming that all of

the ligands are freely rotating, then the anagostic molecule has C_{2v} symmetry ($\sigma = 2$) while the agostic molecule has C_s symmetry ($\sigma = 1$). Additionally, in the agostic molecule, a 3-fold methyl rotation and a 2-fold Ti-Et rotation are being stopped. The symmetry difference σ is $3 \times 2 \times 2$ and $R\ln\sigma$ is 4.9 in rough agreement with the observed ΔS^0.

The $g_{anagostic}$ values for Cp^*_2TiEt and $Cp^*_2TiN(Me)Ph$ are very similar to the g_{av} values of Cp^*_2TiMe (1.958) and $Cp^*_2TiN(Et)Ph$ (1.955) as expected. The $g_{anagostic}$ values can be used to estimate the g_y value for the anagostic form of the molecules by assuming that g_z and g_x are the same in both conformations. For Cp^*_2TiEt and $Cp^*_2TiN(Me)Ph$, the g_y values for the non-agosic conformation are 1.890 and 1.884, respectively. If the optical spectra are known for the agostic and anagostic conformers, the change in the $1a_1 \rightarrow b_2$ energy between them can be estimated. This energy gives the electronic contribution to the agostic interaction.

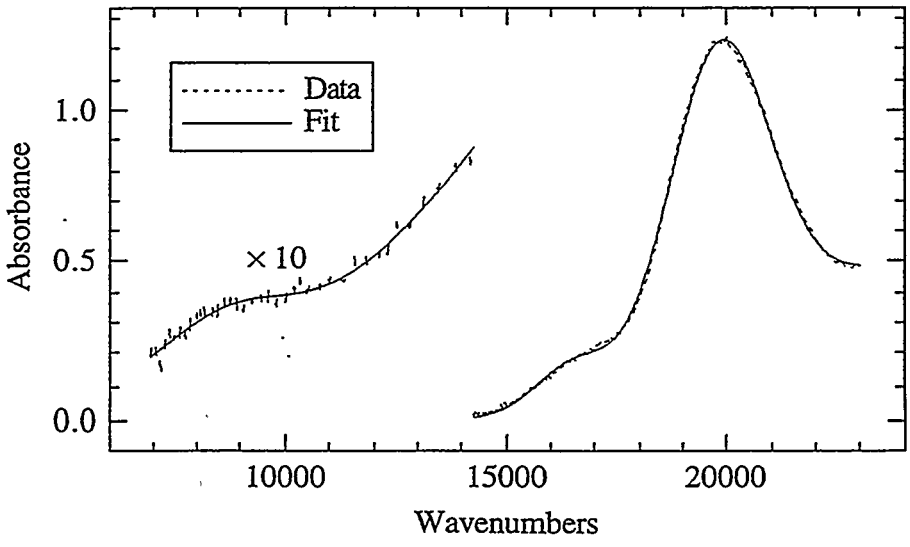

Figure 3b.4: Electronic spectrum of Cp^*_2TiEt in C_7D_8 at 77 K

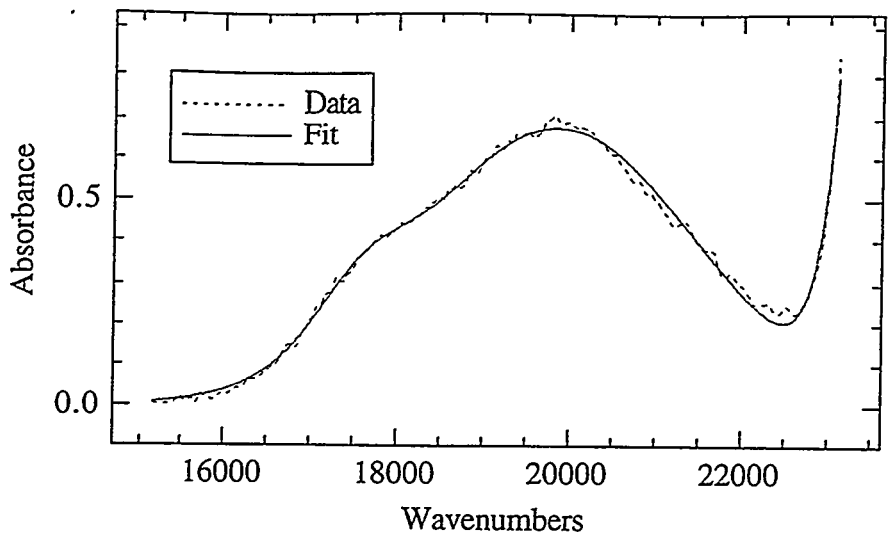

Figure 3b.5 Electronic spectrum of $Cp^*_2TiN(Me)Ph$ in MCH at 77K

From ΔH^0 and ΔS^0, at 20°C the equilibrium constants for Cp^*_2TiEt and $Cp^*_2TiN(Me)Ph$ are 0.87 and 4.1, respectively. The equilibrium constants help to explain why no $1a_1 \rightarrow b_2$ transition is observed for Cp^*_2TiEt or $Cp^*_2TIN(Me)Ph$ at room temperature. For $Cp^*_2TiN(Me)Ph$, most of the molecules have no agostic interaction and for Cp^*_2TiEt around 45% have no agostic interaction . By measuring the electronic spectrum at lower temperature, we hoped to observe the $1a_1 \rightarrow b_2$ transition. While the transferability of solution data to a frozen glass is somewhat questionable, at 77 K, the equilibrium constants for Cp^*_2TiEt and $Cp^*_2TiN(Me)Ph$ are 8×10^{-5} and 3×10^{-3}, respectively. Spectra acquired at this temperature are expected to be due only to the agostic species. The spectrum of Cp^*_2TiEt in toluene-d_8 at 77 K is shown in Figure 3b.4, and that of $Cp^*_2TiN(Me)Ph$ is shown in Figure 3b.5. The energies of the electronic transitions for the complexes at 77 K and at room temperature is given in Table 3b.1. Unfortunately, the $1a_1 \rightarrow b_2$ transition for

$Cp^*_2TiN(Me)Ph$ was not observed due to the presence of C-H or C-D stretch overtones from the solvent. However, this energy can be obtained from the EPR spectrum using the methodology outlined in the previous section.

Table 3b.1: Transition energies for Cp^*_2TiEt, Cp*2TiMe, and $Cp^*_2TiN(Me)Ph$ in cm^{-1}

	T in K	b'	a'	ΔE_{xy} (obs)	ΔE_{xz} (calc)	ΔE_{xz} vs Cp^*_2TiH in kcal/mol
$Cp^*_2TiN(Me)Ph$	295	0.27	0.96		2765	6.6
$Cp^*_2TiN(Me)Ph$	77	0.28	0.96		4870	12.6
Cp^*_2TiMe	295	0.33	0.94		2410	5.6
Cp^*_2TiEt	77	0.33	0.94	8460	8695	23.6
Cp^*_2TiEt	295	0.33	0.95		2291	5.3

a) For ΔE_{xz} (calc), the 77 K data uses the g values seen in the frozen glass, and for the 293 K data, $1a_1 \rightarrow b_2$ is calcluated using g_y for the anagostic conformation.

Some interesting differences exist between the low temperature and room temperature spectra. The $1a_1 \rightarrow 2a_1$ transition for Cp^*_2TiEt decreases in energy at low temperature. This is presumably due to the σ-bond of the ethyl ligand moving off of the C_2 axis of the metallocene when the ethyl group form the β-agostic interaction. The $1a_1 \rightarrow b_1$ transition of $Cp^*_2N(Me)Ph$ increases in energy at low temperature. The b_1 orbital is the π-acceptor for the nitrogen lone-pair p_y-orbital. As the N-Me group forms an agostic bond with the titanium center, the nitrogen is pulled closer to the titanium atom, forcing b_1 higher in energy. This effect is also seen in the $1a_1 \rightarrow 2a_1$

transition because, unlike Cp^*_2TiEt, the N(Me)Ph ligand remains on, or very close to, the 2-fold axis of the metallocene. An amusing consequence of the energy shift of the $1a_1 \rightarrow b_1$ transition, along with the narrowing of the peaks at low temperature is that a solution of $Cp^*_2TiN(Me)Ph$ is dark green at room temperature but light pink at 77 K.

As noted earlier, the combined visible and EPR spectra can be used to estimate the electronic contribution to the agostic bond. Results are given in Table 3b.1. For Cp^*_2TiEt, b_2 is destabilized by 18 kcal/mol in the agostic conformation, and in $Cp^*_2TiN(Me)Ph$, b_2 is destabilized by 6 kcal/mol in the agostic conformation. In both cases, the enthalpy difference, ΔH^0, is quite a bit smaller than the destabilization of the b_2 orbitals for reasons stated earlier.

The net enthalpy, ΔH^0, of the agostic bond is much smaller than in agostic interactions in other complexes. In $(Cy_3P)_2(CO)_3W$ (Cy = cyclohexyl) one of the PCy_3 ligands has a γ-agostic interaction with the tungsten center. The strength of the agostic interaction is estimated to be 16 kcal/mol.[42] Additionally, theoretical calculations on the molecule $Ti(Et)Cl_3(dmpe)$ (dmpe = bis-dimethylphosphinoethane) show that the agostic form is 12.4 kcal/mol lower in energy than the anagostic conformation.[43] In comparing this energy to that of the Cp^*_2TiX complexes, it is important to note that the strength of the agostic interaction in a titanium(III) complex is expected to be weaker than that for an analogous titanium(IV) complex since titanium(IV) complex is more electrophilic and is expected to have a stronger agostic interaction. In addition, the Cp^*_2Ti environment is more sterically demanding than either of these two examples (the Cy_3P ligand is large, but its bulk is well away from the tungsten center).

The fact that the agostic interaction in Cp^*_2TiEt is so weak explains why no other alkyl complexes of Cp^*_2Ti form β-agostic interactions. As shown in Figure 3b.4, the substituent on the β-carbon atom has an unfavorable steric interaction with the Cp* ligand. Since the net strength of the agostic bond in Cp^*_2TiEt is only about 2 kcal/mol, it seems unlikely that any other alkyl group will have a β-agostic bond.

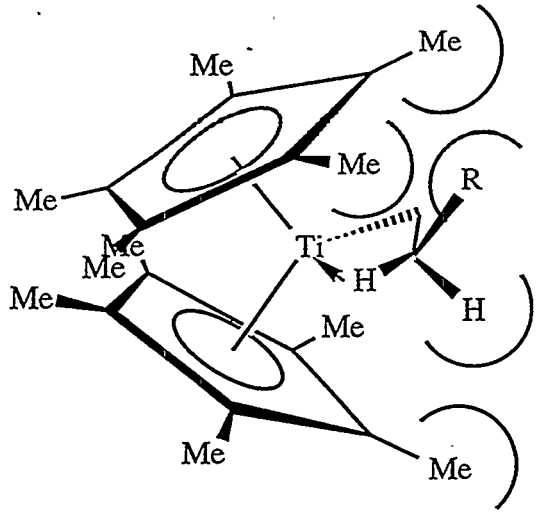

Figure 3b.4: Steric Interactions in a β-agostic alkyl complex of Cp^*_2Ti

In summary, Cp^*_2TiEt and $Cp^*_2TiN(Me)Ph$ both possess weak β-agostic interactions. The electronic contributions to the interaction were estimated using the method outlined in the preceding section. The net enthalpy and entropy of the bond were determined by variable temperature EPR spectroscopy. The agostic interactions were found to be weaker than that calculated for a Ti(IV) complexe presumably due to the weaker electrophilicity of and greater steric congestion in the Ti(III) complexes. The agostic interaction produces some interesting changes in the electronic spectra of the complexes.

3c: Reactions of a Decamethyltitanocene Anion

While investigating the EPR spectra of the Cp^*_2TiX complexes, it was thought that the spectrum of $Cp^*_2TiBH_2$ would be interesting. Since we did not wish to synthesize boryl anions, one synthetic strategy was to treat a decamethyltitanocene anion with commercially available $BrBH_2 \cdot SMe_2$.

While organometallic anions are by no means rare (*i.e.* $Co(CO)_4^-$), metallocene anions are. The scarcity of metallocene anions has been attributed to the poor π-acceptor qualities of the Cp ligand.[44] Since the π-accepting orbitals of Cp have δ symmetry (in D_{5d} metallocenes), their overlap with the transition metal d-orbitals will be poor.

Two synthetic routes are known for metallocene anions. First, they may be prepared by the reduction of the neutral metallocene. This method has been used by Jonas to prepare Cp_2V^- and Cp_2Co^-.[45,46] The anion of Cp^*_2Mn was also prepared in this way.[47] The second method is to deprotonate a metallocene hydride with a strong base. This method has been used by Green and coworkers to prepare $[Cp_2M(H)(\mu\text{-}Li)]_4$ (M = W, Mo),[44] and by Stucky and coworkers to prepare $Cp_2ReLi(PMDTA)$ (PMDTA = N, N, N', N", N"- pentamethyldiethylenetriamine).[48]

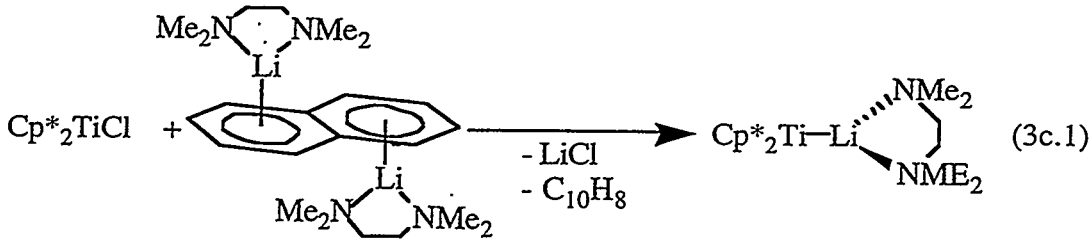

(3c.1)

Initially, the former method of synthesis was chosen since it involved fewer synthetic steps. Treatment of Cp^*_2TiCl with $[(TMEDA)Li]_2C_{18}H_8$[49,50] in ether gives $Cp^*_2TiLi(TMEDA)$ in fair yield (40-60%) as shown in eq 3c.1, but the complex can also be made by deprotonating Cp^*_2TiH with n-BuLi in the presence of TMEDA (TMEDA = N,N,N',N'-tetramethylethylenediamine). $Cp^*_2TiLi(TMEDA)$ is moderately soluble in ether and very soluble in tetrahydrofuran or toluene.

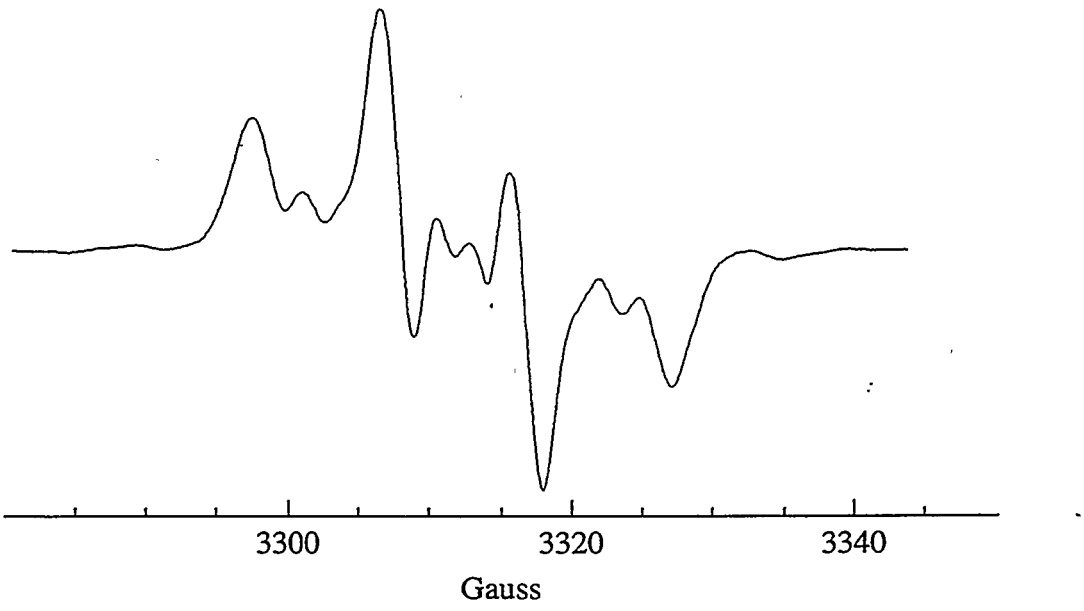

Figure 3c.1: The EPR spectrum of $Cp^*_2TiLi(TMEDA)$ in MCH at RT.

The room temperature EPR spectrum of $Cp^*_2TiLi(TMEDA)$ is shown in Figure 3c.1. The four line pattern is due to coupling to ^7Li, but the spectrum is distorted by the 3 line pattern due to coupling to ^6Li. The EPR spectrum of $Cp^*_2Ti^6Li(TMEDA)$ is shown in Figure 3c.2 for comparison. The g value for this complex is 1.989, considerably greater than the g values of the Cp^*_2TiX complexes given in Table 3a.3. The EPR spectrum shows a 26 MHz coupling to the ^7Li nucleus which is suggests

theat the $1a_1$ orbital contains about 7% lithium character.[39] The variable temperature magnetic susceptibility of $Cp^*_2TiLi(TMEDA)$ shows Curie behavior with $\mu_{eff} = 1.75$ B.M (from 5 to 300 K). In addition, the magnetic moment in solution is 1.7 B.M. (Evans' method).[51]

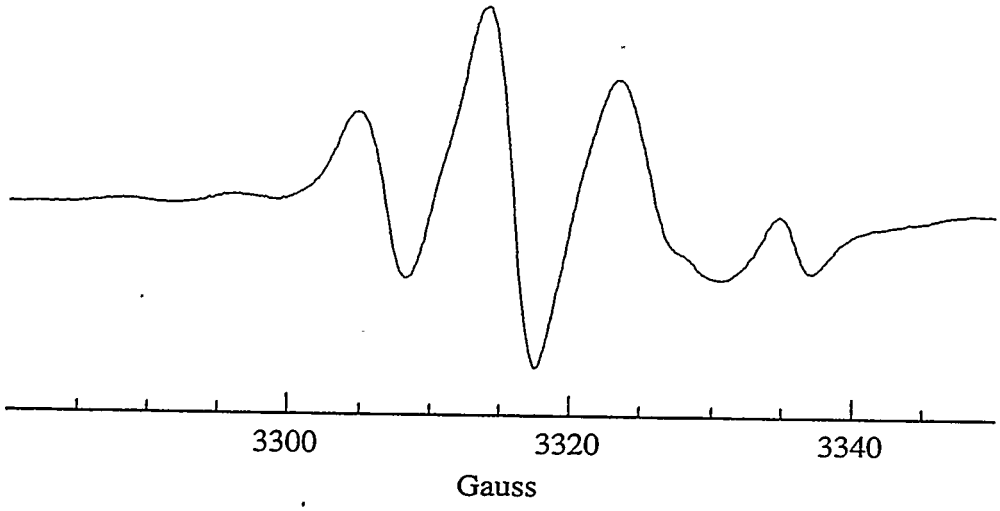

Figure 3c.2: The EPR spectrum of $Cp^*_2Ti^6Li(TMEDA)$ in MCH at RT. Peak at 3335 Gauss is due to hydrolysis.

Table 3c.1: Distances and angles in $Cp^*_2TiLi(TMEDA)$

Distances		Angles	
Ti-Li	2.94(2) Å	Cp1-Ti-Cp2	145.2°
Ti-Cp1	2.05 Å	Cp1-Ti-Li	107.9(4)°
Ti-Cp2	2.05 Å	Cp2-Ti-Li	106.7(4)°
Ti-$\langle C_{ring} \rangle$	2.36(4) Å	Ti-Li-N1	142(1)°
Li-N1	2.15(3) Å	Ti-Li-N2	136(1)°
Li-N2	2.18(2) Å	N1-Li-N2	82.1(9)°

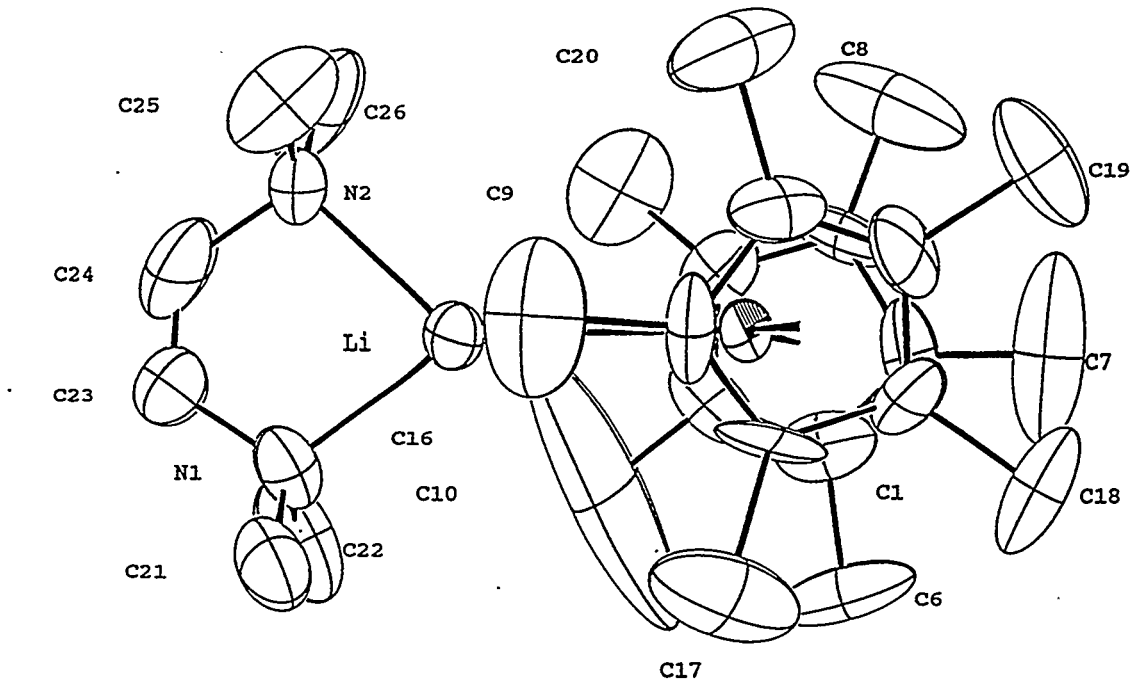

Figure 3c.3: An ORTEP drawing of $Cp^*_2TiLi(TMEDA)$ with 50% thermal ellipsoids.

The crystal structure of $Cp^*_2TiLi(TMEDA)$ is shown in Figure 3c.3. Interesting distances and angles are listed in Table 3c.1. As is obvious from Figure 3c.3, this crystal structure has some problems, namely disorder in the TMEDA ligand and in one of the Cp* ligands. The Ti-Cp* centroid distances and angles are very similar to those of the other Cp^*_2TiX complexes. The Li-N distances in the Li(TMEDA) unit are the same as in other $L_nM[Li(TMEDA)]$ complexes mainly reported by Jonas.[45] The Li-N distances in $Cp^*_2TiLi(TMEDA)$ are also the same as those in $[(Me_3Si)_3C_5H_2][Li(TMEDA)]$[52] in which Li is presumably cationic. While it is difficult to estimate the length of the Ti-Li bond, the bond length observed in $Cp^*_2TiLi(TMEDA)$ is much longer than the Li-Ni bonds in

[(norbornene)$_2$Ni;Li(TMEDA)]$_2$ and in [Ni(CDT);Li(TMEDA)]$_2$ (CDT = 1, 5, 9 - cyclododecatriene) which are 2.38 Å and 2.39 Å, respectively.[45] The difference in radii between Ni(-II) and Ti(I) is not known; however, the 0.55 Å difference between the Li-M distances in the titanium and nickel complexes is certainly larger than the difference metal radii.

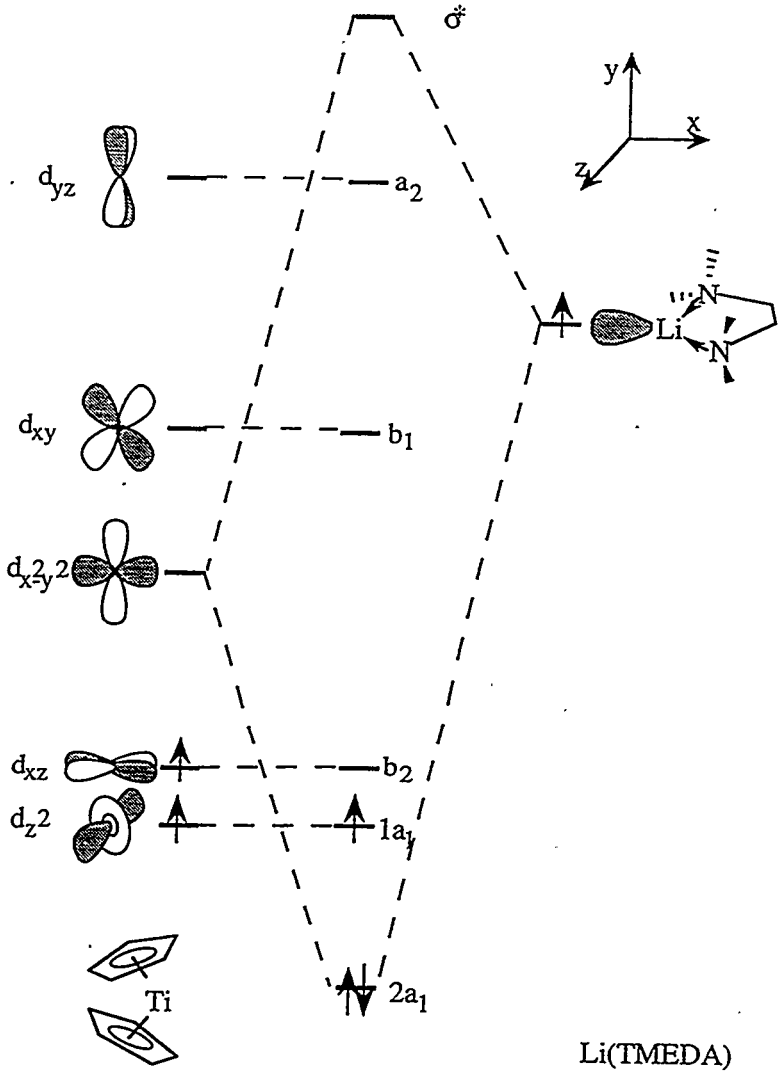

Figure 3c.4: Qualitative MO Diagram for Cp*$_2$TiLi(TMEDA)

The distances and angles of the Cp^*_2Ti unit of $Cp^*_2TiLi(TMEDA)$ suggest that it is a normal bent metallocene. A qualitative MO diagram for $Cp^*_2TiLi(TMEDA)$ is shown in Figure 3c.4. The major difference between this molecule and the trivalent titanocenes is that in $Cp^*_2TiLi(TMEDA)$, the σ-bonding orbital is localized on titanium rather than on the ligand due to the electronegativity difference between lithium and titanium. The electronegativity of lithium is 0.98 while the electronegativity of titanium is 1.54.[53] In addition, since the Cp^*_2Ti group is Ti(II) rather than Ti(0), its electronegativity will be greater than that of the metal. Presumably the $1a_1$ orbital is still the singly occupied orbital.

Since the σ-bonding orbital is localized on titanium, $Cp^*_2TiLi(TMEDA)$ is best thought of a 15 electron Ti(I) compound. The oxidation state difference explains the high g value. Since the spin-orbit coupling constant for atomic Ti(I) is only 38 cm^{-1} while that of Ti(III) is 155 cm^{-1},[31] less excited state character will be mixed into the $1a_1$ orbital leaving g closer to 2.002.[6]

In an attempt to produce $Cp^*_2Ti^-$ anion without coordinated lithium, $Cp^*_2TiLi(TMEDA)$ was treated with 4, 7, 13, 18-tetraoxa-1,10-diazabicyclo[8.5.5]eicosane (K211). The resulting brown solid has an axial EPR spectrum with $g_{\|} = 1.998$ and $g_{\perp} = 1.989$ and does not show coupling to lithium. Unfortunately, the variable temperature magnetic susceptibility gives a very low value of μ_{eff} (1.01 B. M.) which may be due to small sample size. While the EPR spectrum is axial, the g values are not consistent with a D_{5h} metallocene. If the anion possesses the ferrocene structure, then the electron configuration could be $(e_g)^2(a_{1g})^1$, $(e_g)^3(a_{1g})^0$, or $(e_g)^1(a_{1g})^2$ depending upon the ordering of the orbital energies. The EPR spectrum is not consistent with the first electron configuration since this is a S = 3/2 system, and

no fine structure is observed in the spectrum. The second electron configuration would result in $g_{||} > 2$ due to spin-orbit coupling within the triply occupied e_g level, and no EPR signal should be seen at RT for this degenerate ground state. Finally, for the third configuration, $g_{||}$ should be much less than 2 again due to spin-orbit coupling within the e_g level, and, again, no EPR signal should be seen for this degenerate ground state at room temperature. The EPR spectrum is most consistent with a d^3 configuration with the unpaired electron in a d_z2 orbital and the other two electrons paired in a $d_{x^2-y^2}$ orbital, in other words, the same electronic structure as $Cp^*_2TiLi(TMEDA)$. Without a crystal structure, not much more can be said about the electronic structure of $Cp^*_2Ti[Li(K211)]$.

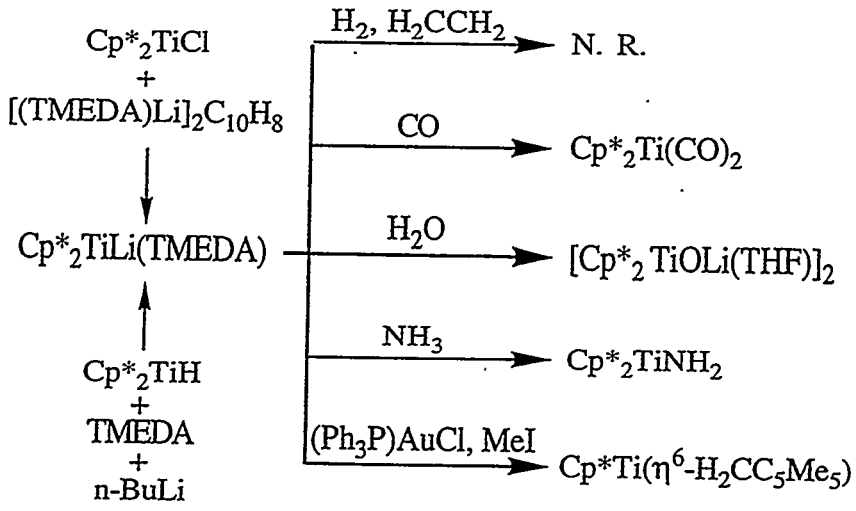

Figure 3c.5: Some reactions of $Cp^*_2TiLi(TMEDA)$

While $Cp^*_2TiLi(TMEDA)$ would appear to be an excellent starting material for making interesting molecules from its reactions with electrophiles, its reactivity was disappointing (Figure 3c.5). The compound did not react with N_2, H_2, or ethylene. It reacted with carbon monoxide to make the known $Cp^*_2Ti(CO)_2$.[3] No identifiable

product was isolated in its reactions with N_2O, $[(COD)RhCl]_2$, $[(COD)IrCl]_2$, (COD = 1,4 -cyclooctadiene), or $(Me_3P)_2RhCl$. The product of the reaction with $(Ph_3P)AuCl$ was identified as $Cp^*Ti(\eta^6\text{-}H_2CC_5Me_4)$ by is EPR spectrum. The reaction with water gave $[Cp^*_2TiOLi(THF)]_2$, and the analogous reaction with ammonia gave mainly the known amide, $Cp^*_2TiNH_2$. The reaction with MeI produced $Cp^*Ti(\eta^6\text{-}H_2CC_5Me_4)$ and Cp^*_2TiOMe, the latter is due to hydrolysis of $Cp^*_2TiLi(TMEDA)$. It is worth noting that the reaction of Cp^*_2TiI with MeLi produced Cp^*_2TiMe. In the cases where $Cp^*_2TiLi(TMEDA)$ did react, it seems mainly to have oxidized to Cp^*_2Ti instead of undergoing metathesis.

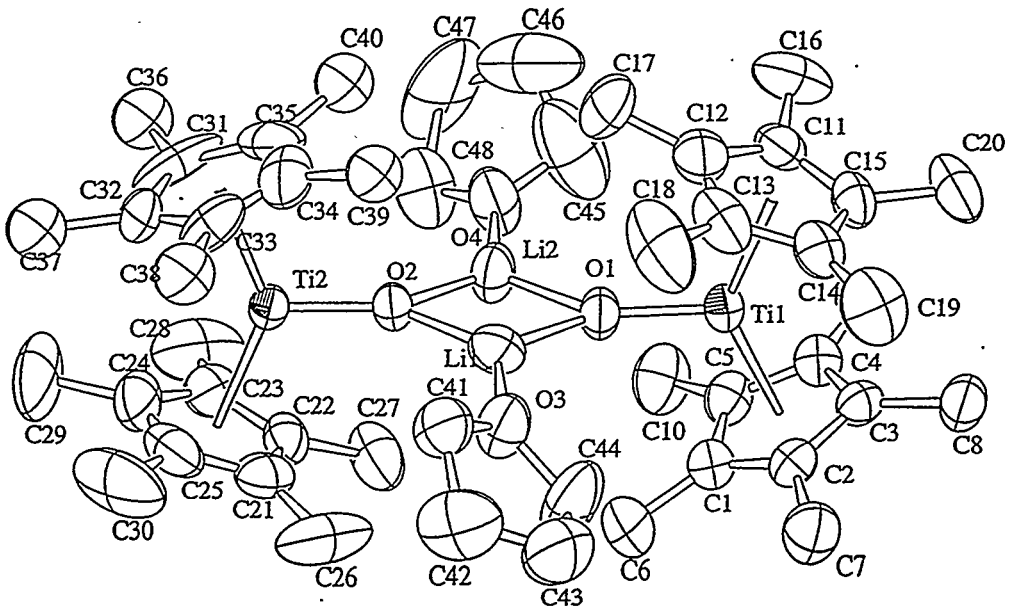

Figure 3c.6: An ORTEP diagram of $[Cp^*_2TiOLi(THF)]_2$ with 50% thermal ellipsoids

Table 3c.2: Bond distances and angles in $[Cp^*_2TiOLi(THF)]_2$

Titanium 1		Titanium 2	
Ti1-O1	1.783(4) Å	Ti2-O2	1.791(4) Å
TI1-Cp1	2.16 Å	Ti1-Cp3	2.14 Å
Ti1-Cp2	2.14 Å	Ti1-Cp4	2.14 Å
Ti1-$\langle C_{ring} \rangle$	2.47(4) Å	Ti2-$\langle C_{ring} \rangle$	2.45(4) Å
Li1-O1	1.88(1) Å	Li2-O1	1.88(1) Å
Li1-O2	1.87(1) Å	Li2-O2	1.84(1) Å
Li1-O3	1.92(1) Å	Li2-O4	1.95(1) A
Ti1-Ti2	6.111(2) Å	Li1-Li2	2.29(2) Å
Cp1-Ti1-Cp2	137.5°	Cp3-Ti2-Cp4	138.4°
Cp1-Ti1-O1	111.0°	Cp3-Ti2-O2	110.9°
Cp2-Ti1-O1	111.5°	Cp4-Ti2-O2	110.7°
Ti1-O1-Li1	141.6(5)°	Ti2-O2-Li1	142.2(4)°
Ti1-O1-Li2	143.0(4)°	Ti2-O2-Li2	141.5(5)°
O1-Li1-O2	103.7(6)°	O1-Li2-O2	105.2(7)°
O1-Li1-O3	125.6(7)°	O2-Li1-O3	130.3(6)°
O1-Li2-O4	125.4(6)°	O2-Li2-O4	129.2(7)°

The most interesting reaction of $Cp^*_2TiLi(TMEDA)$ is that with water. This reaction produces dimeric $[Cp^*_2TiOLi(THF)]_2$ along with a colorless gas, presumably hydrogen. This compound has a g_{ave} value of 1.982 consistent with strong π-bonding of the titanium center to the lithoxide. The molecular structure of the compound is shown in Figure 3c.6, and interesting distances and angles are given in Table 3c.2. In

addition to the molecule shown, a tetrahydrofuran molecule of crystallization is found in the asymmetric unit. The bonding parameters for the metallocene units are similar to the other Cp^*_2TiX complexes. The bonding parameters for the $(O_2Li_2)(THF)_2$ core are very similar to those of $[ROLi(ether)]_2$ where R = 2,6-di-*tert*-butylphenyl and ether = diethyl ether[54] or THF[55] and where R = tris-*tert*-butylmethyl and ether = THF.[56] Treatment of $Cp^*_2TiOLi(THF)$ with MeI in C_6D_6 produces Cp^*_2TiOMe as determined by EPR spectroscopy.

The apparent insertion of the oxygen atom of water into the Ti-Li bond of $Cp^*_2TiLi(TMEDA)$ is somewhat surprising. At least three routes can account for the formation of $Cp^*_2TiOLi(THF)$ (Scheme 3c.1). While route (a) seems unlikely, not much differentiates routes (b) and (c) since the Li-X (X= H or OH) bonds will be stronger than the corresponding Cp^*_2TiX bonds in both cases. Evidence supporting route (c) is provided by the reaction of $Cp^*_2TiLi(TMEDA)$ with NH_3 which produces $Cp^*_2TiNH_2$. Apparently LiH is not a strong enough base to deprotonate $Cp^*_2TiNH_2$ and make a compound analogous to $[Cp^*_2TiOLi(THF)]_2$.

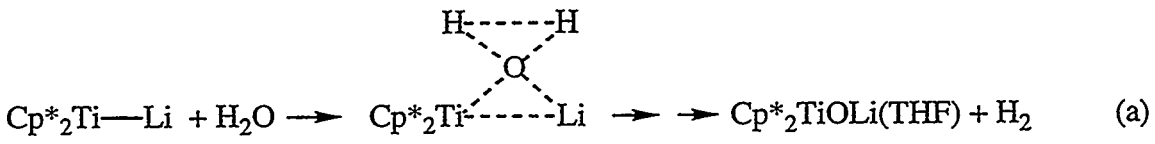

Scheme 3c.1: Potential routes to $[Cp^*_2TiOLi(THF)]_2$

In conclusion, the Ti(I) anion $Cp^*_2TiLi(TMEDA)$ has been prepared. Its structural parameters are similar to those of trivalent decamethyltitanocenes. Its reactivity mainly involves its oxidation to Cp^*_2Ti. With water it forms $[Cp^*_2TiOLi(THF)]_2$ which was structurally characterized. With ammonia it forms $Cp^*_2TiNH_2$. In general, $Cp^*_2TiLi(TMEDA)$ reacts as a strong reducing agent rather than undergoing metathesis.

References

(1) Wilkinson, G.; Birmingham, J. M. *J. Am. Chem. Soc.* **1954**, *76*, 4281-4284.

(2) Bercaw, J. E.; Brintzinger, H. H. *J. Am. Chem. Soc.* **1971**, *93*, 2046.

(3) Bercaw, J. E.; Marvich, R. H.; Bell, L. G.; Brintzinger, H. H. *J. Am. Chem. Soc.* **1972**, *94*, 1219.

(4) Pattiasina, J. W.; Heeres, H. J.; van Bolhuis, F.; Meetsma, A.; Teuben, J. H. *Organometallics* **1987**, *6*, 1004-1010.

(5) Mach, K.; Raynor, B. *J. Chem. Soc. Dalton Trans.* **1992**, 683-688.

(6) McGarvey, B. R. In *Transition Metal Chemistry, a Series of Advances*; R. L. Carlin, Ed.; Marcel Dekker, Inc.: New York, 1966; Vol. 3; pp 90-201.

(7) Köhler, F. H.; Hoffmann, P.; Prossdorf, W. *J. Am. Chem. Soc.* **1981**, *103*, 6359.

(8) Curtis, C. J.; Smart, J. C.; Robbins, J. L. *Organometallics* **1985**, *4*, 1283.

(9) Petersen, J. L.; Dahl, L. F. *J. Am. Chem. Soc.* **1975**, *97*, 6422-6433.

(10) Lauher, J. W.; Hoffmann, R. *J. Am. Chem. Soc.* **1976**, *98*, 1729-1742.

(11) Brintzinger, H. H.; Bartell, L. S. *J. Am. Chem. Soc.* **1970**, *92*, 1103.

(12) Brintzinger, H. H.; Lohr, L. L.; Wong`, K. L. T. *J. Am. Chem. Soc.* **1975**, *97*, 5146.

(13) Petersen, J. L.; Lichtenberger, D. L.; Fenske, R. F.; Dahl, L. F. *J. Am. Chem. Soc.* **1975**, *97*, 6433.

(14) Fieselmann, B. F.; Stucky, G. D. *J. Organomet. Chem.* **1977**, *139*, 43.

(15) Albright, T. A.; Burdett, J. K.; Whangbo, M. H. *Orbital Interactions in Chemistry*; Wiley: New York, 1985.

(16) Petersen, J. L.; Dahl, L. F. *J. Am. Chem. Soc.* **1975**, *97*, 6416-6422.

(17) Luinstra, G. A.; ten Cate, L. C..; Heeres, H. J.; Pattiasina, J. W.; Meetsma, A.; Teuben, J. H. *Organometallics* **1991**, *10*, 3227-3237.

(18) Druce, P. M.; Kingston, B. M.; Lappert, M. F.; Spalding, T. R.; Srivastava, R. C. *J. Chem. Soc. (A)* **1969**, 2106-2110.

(19) Schwindt, M. A.; Lejon, T.; Hegedus, L. B. *Organometallics* **1990**, *9*, 2814-2819.

(20) Herzog, A.; Liu, F.; Roesky, H. W.; Demsar, A.; Keller, K.; Noltemeyer, M.; Pauer, F. *Organometallics* **1994**, *13*, 1251 - 1256.

(21) Brady, E.; Lukens, W.; Telford, J.; Mitchell, G. *Acta. Cryst.* **1994**, *C51*, 558-560.

(22) Hillhouse, G. L.; Bulls, A. R.; Santarsiero, B. D.; Bercaw, J. E. *Organometallics* **1988**, *7*, 1309-1312.

(23) Feldman, J.; Calabrese, J. C. *J. Chem. Soc., Chem. Commun.* **1991**, 1042-1044.

(24) Dunitz, J. *X-Ray Analysis and the Structure of Organic Molecules*; Cornell: Ithaca, New York, 1979.

(25) DeKock, R.; Gray, H. *Chemical Structure and Bonding*; Benjamin: Menlo Park, California, 1990.

(26) Lever, A. B. P. *Inorganic Electronic Spectroscopy (Second Edition)*; Elsevier: New York, 1984.

(27) As noted by one of the reviewers of the manuscript

(28) Green, J. C.; Payne, M. P.; Teuben, J. H. *Organometallics* **1983**, 2, 203-210.

(29) Razuvaev, G. A.; Abakumov, G. A.; Cherkasov, V. K. *Russian Chemical Reviews* **1985**, *54*, 1235-1259.

(30) Inamoto, N.; Masuda, S. *Chem. Lett.* **1982**, 1003-1006.

(31) Moore, C. E. "Atomic Energy Levels As Derived From the Aabalyses of Optical Spectra," National Bureau of Standards, 1971.

(32) Bierwagen, E. P.; Bercaw, J. E.; Goddard III, W. A. *J. Am. Chem. Soc.* **1994**, *116*, 1481 - 1489.

(33) Wilson, R. D.; Koetzle, T. F.; Hart, D. W.; Kvick, Å.; Tipton, D. L.; Bau, R. *J. Am. Chem. Soc.* **1977**, *99*, 1775-1781.

(34) Schultz, A. J.; Stearley, K. L.; Williams, J. M.; Mink, R.; Stucky, G. D. *Inorg. Chem.* **1977**, *16*, 3303.

(35) Paciello, R. A.; Kiprof, P.; Herdtweck, E.; Herrmann, W. A. *Inorg. Chem.* **1989**, *28*, 2890-2893.

(36) Hunter, J. A.; Lindsell, W. E.; McCullough, K. J.; Parr, R. A.; Scholes, M. L. *J. Chem. Soc., Dalton Trans.* **1990**, 2145-2153.

(37) Asaro, M. A.; Cooper, S. R.; Cooper, N. J. *J. Am. Chem. Soc.* **1986**, *108*, 5187-5193.

(38) Moore, C. E. "Atomic Energy Levels As Derived From the Analyses of Optical Spectra," National Bureau of Standards, 1958.

(39) Weltner Jr., W. *Magnetic Atoms and Molecules*; Dover Publications, Inc.: New York, 1983.

(40) Brookhardt, M.; Green, M. L. H.; Wong, L.-L. In *Progress in Inorganic Chemistry*; S. J. Lippard, Ed.; John Wiley & Sons: New York, 1988; Vol. 36.

(41) Lowry, T. H.; Richardson, K. S. *Mechanism and Theory in Organic Chemistry;* Third ed.; Harper & Row: New York, 1987.

(42) Gonzales, A. A.; Zhang, K.; Nolan, S. P.; Vega, R. L. d. l.; Mukerjee, S. L.; Hoff, C. D.; Kubas, G. J. *Organometallics* **1988**, *12*, 2429-2435.

(43) Munakata, H.; Ebisawa, Y.; Takashima, Y.; Wrinn, M. C.; Sheiner, A. C.; Newsam, J. M. *Catalysis Today* **1995**, *23*, 403-408.

(44) Francis, B. R.; Green, M. L. H.; Luong-thi, T.; Moser, G. A. *J. Chem. Soc., Dalton Trans.* **1976**, 1339-1345.

(45) Jonas, K.; Krüger, C. *Angew. Chem. Int. Ed. Engl.* **1980**, *19*, 520-537.

(46) Jonas, K.; Wiskamp, V. *Z. Naturforsch.* **1983**, *38b*, 1113-1121.

(47) Robbins, J. L.; Edelstein, N. E.; Cooper, S. R.; Smart, J. C. *J. Am. Chem. Soc.* **1979**, *101*, 3853-3857.

(48) Mink, R. I.; Welter, J. J.; Young, P. R.; Stucky, G. D. *J. Am. Chem. Soc.* **1979**, *101*, 6928-6933.

(49) Brooks, J. J.; Rhine, W.; Stucky, G. D. *J. Am. Chem. Soc.* **1972**, *94*, 7346.

(50) Kahn, B. E.; Rieke, R. D. *Organometallics* **1988**, *7*, 463-469.

(51) Evans, D. F. *J. Chem. Soc.* **1959**, 2003-2005.

(52) Jutzi, P.; Schlüter, E.; Pohl, S.; Saak, W. *Chem. Ber.* **1985**, *118*, 1959-1967.

(53) DeKock, R. L.; Gray, H. B. *Chemical Structure and Bonding*; The Benjamin/Cummings Publishing Company: Menlo Park, California, 1980.

(54) Kodiok-Köhn, G.; Pickardt, J.; Schumann, H. *Acta Cryst.* **1991**, *C47*, 2649-2651.

(55) Huffman, J. C.; Greets, R. L.; Caulton, K. G. *J. Cryst. Spectrosc. Res.* **1984**, *14*, 541-547.

(56) Hvoslef, J.; Hope, H.; Murray, B. D.; Power, P. P. *J. Chem. Soc., Chem. Commun.* **1983**, 1438-1439.

Chapter Four: Experimental Details

All reactions and manipulations were carried out in an inert atmosphere using standard Schlenk and dry box techniques. Hexane, diethyl ether, and tetrahydrofuran were dried over sodium benzophenone ketyl, distilled, and degassed immediately prior to use. Toluene, methylcyclohexane, and deuterated NMR solvents dried over and distilled from potassium or sodium. Me_3SiBr and Me_3SiI were distilled under argon and stored over copper powder before using.

Infrared spectra were recorded on a Perkin-Elmer 283 spectrometer as Nujol mulls between CsI plates. ^1H NMR spectra were measured on a JEOL FX-90Q FT NMR spectrometer operating at 89.56 MHz. Chemical shifts were referenced to tetramethylsilane ($\delta = 0$) with positive values at lower field. Unless otherwise noted, all spectra were acquired at 30 °C in C_6D_6. Melting points were measured on a Thomas-Hoover melting point apparatus in sealed capillaries and are uncorrected. EPR spectra were measured powders, solutions, or frozen glasses in either methylcyclohexane or 2-methyltetrahydrofuran using a Varian E-12 spectrometer. The microwave frequency was measured using an EIP-548 microwave frequency counter and the magnetic field was measured using a Varian E-500 NMR Gaussmeter. Spectra were digitized using UNPLOTIT or UNSCANIT. Susceptibility measurements carried out on a SHE model 500 SQUID susceptometer. UV-visible spectra were recorded using a modified Cary 17 spectrophotometer at room temperature in methylcyclohexane. Electron impact mass spectra were recorded by the mass spectroscopy laboratory, and elemental analyses were performed by the analytical laboratories both at the University of California, Berkeley.

Unless otherwise noted, all calculations and numerical modeling of spectra and susceptibilities was done using the program Horizon.[1] Transition metal EPR spectra was simulated using the program ABVG. f-Element EPR spectra were fit using a locally written program (Appendix 3).

The x-ray spectroscopy measurements were done at SSRL at beam lines 4-1 and 4-3 using a Si(220) monochrometer detuned 50%. Data was recorded transmission using argon filled ionization chambers. The spectra were referenced to a 0.2 M solution of UO_2Cl_2 or UF_4 powder. Edge positions were determined by comparing the inflection point of the sample spectrum to that of the reference. Data analysis was performed using the EXAFSPAK programs written by Graham George at SSRL as follows. First, a pre-edge correction was applied to the data. A spline was chosen such that low R peaks in the Fourier transform of the EXAFS spectrum were minimized. The resulting EXAFS spectrum was fit using theoretical amplitude and phase values provided by FEFF6.[2] The coordination numbers were not allowed to vary in the analyses. The fitting results are given in Appendix 2.

Notes: a) Many of these compounds were initially made and/or characterized first by other members of the Andersen group and are included here for completeness. Where someone else has made the compounds first, their characterization is given with the syntheses that were developed in this thesis research. In addition to the footnote, their initials are given next to the complex name. The initials are as follows: A. L. S., Dr. Anthony L. Stewart; S. M. B., Dr. Sharon M. Beshouri; L. L. B., Dr. Laura L. Blosch; R. K. R., Dr. Robert K. Rosen.

b) We had difficulty getting good combustion analyses on complexes with the Cp" ligand when analogous complexes with the $Cp^{\ddagger}$ ligand would analyze correctly; this is presumably due to SiC formation resulting in low carbon content.

Chapter One

Compounds $Cp"_2UCl_2$ (**2**), $Cp"_2UBr_2$ (**4**), and $Cp"_2UI_2$ (**6**) have been reported previously.[3] Our syntheses are somewhat different so are reported here. Compounds $[Cp"_2UF]_2$ (**12**), $[Cp"_2UCl]_2$ (**14**), $[Cp"_2UBr]_2$ (**16**), $[Cp"_2UI]_2$ (**18**), and

$Cp"_2U(NMe_2)_2$ have been reported, but with little or no experimental details or characterization.[4,5]

$Cp^{‡}K$[6](A. L. S.). Potassium (4.6 g, 120 mmol) was washed with hexane, cut into little pieces and dried under vacuum in a 500 mL Schlenk flask. Tetrahydrofuran (150 mL) was added, and $Cp^{‡}H$[7,8] (20 mL, 16.6 g, 93 mmol) was added by syringe. The reaction is slow. The mixture was allowed to stir and the flask was periodically vented to the Schlenk line. After seven days, gas was no longer evolved, and the tetrahydrofuran was removed under reduced pressure. The remaining light pink solid was dried under vacuum. The flask was taken into the dry box and the remaining potassium was physically removed from the powder (18.9 g, 94%). The compound was used without further characterization. The compound is insoluble in all common solvents except for hot tetrahydrofuran in which it partially decomposes.

$Cp^{‡}_2Mg$. $Cp^{‡}H$[7,8] (18.8 mL, 15.6 g, 87.3 mmol) was added by syringe to a stirring solution of Bu_2Mg (60 mL, 0.64 M in heptane, 38.4 mmol). The solution became slightly cloudy and was heated to reflux for three days. The solution was allowed to cool and was filtered. Cooling the filtrate to -80 °C for 7 days produced colorless crystals (11.8 g, 81%). ^1H NMR (C_6D_6): δ 5.90 (m, 3H, ring protons), 1.31(s, 18H, CMe_3). The compound was used without further characterization.

$Cp^{‡}_2UCl_2$[6] (**1**) (A. L. S.). A mixture of $KCp^{‡}$ (5.25 g, 23.1 mmol) and UCl_4 (4.60 g, 11.6 mmol) was suspended in 100 mL of tetrahydrofuran. The reaction mixture immediately turned deep red and became hot. After stirring for 8 hours, the tetrahydrofuran was removed under reduced pressure. The solid residue was suspended in 150 mL of diethyl ether and filtered. The volume of the filtrate was reduced to *ca.* 20 mL and the mixture was heated to redissolve the solid. Cooling to -

20°C produced large, blood red prisms (7.5 g, 93%). MP: 165-167 °C. ^{1}H NMR: δ 97.4 (1 H, $\nu_{1/2}$ = 15 Hz, b), 0.31 (18 H, $\nu_{1/2}$ = 5 Hz, CMe_3), -40.9 (2 H, $\nu_{1/2}$ = 14 Hz, a_2). IR: 3070(w), 3060(w), 1270(w), 1258(w), 1248(w), 1200(w), 1165(w), 1162(w), 1050(w), 1020(w), 922(w), 833(w), 792(w), 775(w), 670(w), 664(w), 470(w), 355(w), 280(w) cm^{-1}. MS (M^+) *m/z* (calc., found): 662 (100, 100), 663 (30, 61), 664 (68, 66), 665 (19, 21), 666 (13, 11). Anal. Calcd for $C_{26}H_{42}Cl_2U$: C, 47.1; H, 6.33; Cl, 10.7. Found: C, 47.1; H, 6.45; Cl, 10.7.

Cp"$_2$UCl$_2$[3,9] (2) (S. M. B.). A mixture of UCl_4 (2.54 g, 6.68 mmol) and Cp"$_2$Mg[10] (2.96 g, 6.68 mmol) was suspended in 100 mL of diethyl ether. The reaction mixture slowly turned orange. After stirring for three days, the diethyl ether was removed under reduced pressure and the orange solid residue was dissolved in 150 mL of hexane. The orange solution was filtered, and the volume of the solution was reduced to *ca.* 30 mL. The solution was heated to redissolve the solid, and slow cooling to -80 °C gave golden yellow needles (3.3 g, 68%). The ^{1}H NMR spectrum agrees with that reported previously. (Note: this reaction does not work in tetrahydrofuran presumably due to the formation of Cp"$UCl_3(thf)_2$.)

Cp‡$_2$UBr$_2$ (3). Cp‡$_2$$UCl_2$ (0.50 g, 0.75 mmol) was dissolved in 50 mL of hexane, and Me_3SiBr(0.49 g, 3.0 mmol) was added using a syringe. The solution was allowed to stir for 12 hours then the volume was reduced to *ca.* 5 mL. Cooling to -80 °C produced red blocks (0.52 g, 91%). MP: 185 - 187 °C. ^{1}H NMR: δ 105.56 (1 H, $\nu_{1/2}$ = 38 Hz, b), 1.54 (18 H, $\nu_{1/2}$= 15 Hz, CMe_3), -43.85 (2 H, $\nu_{1/2}$ = 45 Hz, a_2). IR: 3110(w), 3081(w), 2721(w), 1290(w), 1249(w), 1205(m), 1195(m), 1167(s), 1058(m), 1029(w), 1024(w), 938(m), 930(w), 864(m), 844(s), 780(s), 734(w), 722(w) cm^{-1}. MS (M^+) *m/z*

(calc, found): 750(50,87), 751(15,49), 752(100,100), 753(29,72), 754(52,89), 755(14,43). Anal. Calcd for $C_{26}H_{42}Br_2U$: C, 41.5; H, 5.63. Found: C, 41.9; H: 5.69. (Note: the product often needed a second treatment with Me_3SiBr to completely metathesize all of the chlorides). The NMR spectrum of the impurity, $Cp^{‡}_2U(Br)(Cl)$, is distinct from the spectrum of both $Cp^{‡}_2UBr_2$ and $Cp^{‡}_2UCl_2$. In all cases the mixed halide complex is clearly visible in the NMR spectrum when the reaction does not proceed to completion.

$Cp"_2UBr_2$[3,9] **(4)** (S. M. B.). $Cp"_2UCl_2$ (2.00 g, 2.75 mmol) was dissolved in 50 mL of diethyl ether giving an orange-green solution. Me_3SiBr (1.1 mL, 1.3 g, 8.4 mmol) was added using a syringe. The solution slowly darkened. After stirring for 10 hours, the volatile components were removed under reduced pressure. The orange solid residue was dissolved in 50 mL of hexane giving a purple-red solution which was then filtered. The volume of the filtrate was reduced to *ca.* 25 mL and the solution was heated to dissolve the solid. Cooling to -20 °C produced bright orange needles (1.85 g, 82 %). The ^1H NMR spectrum agrees with that reported previously. (Note: the product often needed a second treatment with Me_3SiBr to completely metathesize all of the chlorides. This reaction does not work in hexane.)

$Cp^{‡}_2UI_2$ (5). $Cp^{‡}_2UCl_2$ (1.5 g, 2.3 mmol) was dissolved in 50 mL of diethyl ether and Me_3SiI (0.92 mL, 1.4 g, 6.8 mmol) was added using a syringe. The initially red solution became purple. After stirring for 3 days, the ether was removed under reduced pressure, and the dark solid residue was dissolved in 75 mL of hexane. The solution was filtered and the volume was reduced to *ca.* 45 mL. Cooling to -20 °C yielded purple-orange needles (1.52 g, 80 %). MP: 180-186 °C. ^1H NMR: δ 108.31 (1 H, $\nu_{1/2}$ = 64 Hz, b), 3.69 (18 H, $\nu_{1/2}$ = 13 Hz, CMe_3), -46.2 (2 H, $\nu_{1/2}$ = 43 Hz, a_2). IR: 3062(w), 2722(w), 1247(s), 1198(w), 1167(m), 1076(s), 1057(w), 1025(m), 847(s),

788(s) cm^{-1}. MS $(M)^+$ *m/z*(calc, found): 846(100,100), 847(30, 31). Anal. Calcd for $C_{26}H_{42}I_2U$: C, 36.9; H, 5.00. Found: C, 36.9; H, 5.14. (Note: the product often needed a second treatment with Me_3SiI to completely metathesize all of the chlorides.)

Cp''_2UI_2[3,9] **(6)** (S. M. B.). Cp''_2UCl_2 (1.5 g, 2.1 mmol) was dissolved in 50 mL of hexane and Me_3SiI (0.84 mL, 1.2 g, 6.2 mmol) was added by syringe. The initially orange solution quickly turned red. After stirring for 10 hours, the volatile components were removed under reduced pressure, and the dark red solid residue was dissolved in 75 mL of hexane. The solution was filtered and the volume of the filtrate was reduced to *ca.* 45 mL. Cooling to -20 °C gave purple-brown blocks (1.52 g, 81%). The ^1H NMR spectrum agrees with that reported previously. (Note: the product often needed a second treatment with Me_3SiBr to completely metathesize all of the chlorides.)

$Cp^{\ddagger}_2UF_2$ (7). a) $Cp^{\ddagger}_2UMe_2$ (1.23 g, 2.00 mmol) was dissolved in 30 mL of diethyl ether, and $BF_3{\bullet}OEt_2$ (0.51 mL, 0.59 g, 4.1 mmol) was added using a syringe. The solution immediately became warm and turned green. After 12 hours, the diethyl ether was removed under reduced pressure and the tube was heated to 80 °C under vacuum for 1 hour to remove $MeBF_2$. The orange solid residue was dissolved in 50 mL of hexane, and the solution was filtered. The volume of the filtrate was reduced to *ca.* 25 mL. Cooling to -20°C produced orange-yellow needles (1.00 g, 80%). MP: 173-176 °C. ^1H NMR -1.38(18 H, $\nu_{1/2}$ = 24 Hz, CMe_3), -9.61(1 H, $\nu_{1/2}$ = 30 Hz, b), -16.55 (2 H, $\nu_{1/2}$ = 36 Hz, a_2). IR: 3100(w), 2730(w), 1290(w), 1255(s), 1205(m), 1165(m), 1060(m), 1035(w), 925(m), 825(m), 820(s), 785(m), 725(w), 685(m), 665(m), 510(s), 480(s), 430(w), 355(m), 245(m) cm^{-1}. MS $(M)^+$ *m/z* 630. Anal. Calcd for $C_{26}H_{42}F_2U$: C, 49.5; H,. 6.71. Found: C, 49.5; H, 6.86.

b) $Cp^{\ddagger}_2U(OMe)_2$ (1.53 g, 2.34 mmol) was dissolved in 25 mL diethyl ether, and $BF_3 \cdot OEt_2$ (0.60 mL, 0.70 g, 4.9 mmol) was added using a syringe. The color of the solution immediately changed from green to red. After stirring for 6 hours, the ether was removed under reduced pressure, and the tube was heated to 70 °C under vacuum for 1 hour. The red solid residue was suspended in 50 mL of hexane and, and the solution was filtered. The volume of the filtrate was reduced to *ca.* 30 mL. Cooling to -20 °C gave yellow needles (1.1 g, 74 %). ^1H NMR spectrum was identical to that of $Cp^{\ddagger}_2UF_2$ produced by route (a).

$Cp^{\ddagger}_2UMe_2$[6] (A. L. S.). $Cp^{\ddagger}_2UCl_2$ (1.00g, 1.51 mmol) was dissolved in 50 mL of ether, and MeLi (4.2 mL, 0.72 M in diethyl ether, 3.0 mmol) was added by syringe. The solution immediately turned orange and cloudy. After stirring for one hour, the ether was removed under reduced pressure. The dark orange solid residue was suspended in 25 mL of hexane, and the solution was filtered giving a deep orange solution. The volume of the solution was reduced to *ca.* 2 mL. Cooling to -20 °C gave orange brown blocks (0.73 g, 78 %). MP: 120 -125 °C. ^1H NMR: δ 18.81 (1H, $\nu_{1/2}$= 12 Hz, b), -0.64 (18H, $\nu_{1/2}$ = 6 Hz, CMe_3), -35.43 (3H, $\nu_{1/2}$ = 14 Hz, U-Me), -39.02(H, $\nu_{1/2}$ = 9 Hz, a_2). IR: 1250(s), 1200(m), 1165(m), 1110(s), 1055(m), 1025(m), 935(m), 845(m), 825(s), 810(m), 765(s), 675(m), 655(m), 405(m) cm^{-1}. MS $(M\text{-}CH_3)^+$ *m/z* = 659. Anal. Calcd for $C_{28}H_{48}U$: C, 54.0, H:7.71. Found C, 53.7; H, 7.83.

$[Cp''_2UF_2]_2$ (8). $Cp''_2U(NMe_2)_2$ (0.50 g, 0.67 mmol) was dissolved in 25 mL of diethyl ether, and $BF_3 \cdot OEt_2$ (0.17 mL, 0.19 g, 1.3 mmol) was added using a syringe. The orange solution turned bright green after 5 minutes. After stirring for 12 hours, the volatile components were removed under reduced pressure, and the reaction mixture was heated to 70 °C under vacuum to remove Me_2NBF_2. The green solid residue was dissolved in 40 mL of hexane, and the solution was filtered. The volume of the

solution was reduced to *ca.* 2 mL. Cooling to -20 °C produced green blocks (0.34 g, 72 %). MP: 114-116 °C. ^{1}H NMR δ -0.76 (18 H, $\nu_{1/2}$ = 2.4 Hz, $SiMe_3$), -14.61 (2 H, $\nu_{1/2}$ = 9 Hz, a_2), -16.14 (1 H, $\nu_{1/2}$ = 13 Hz, b). IR: 3041(m), 1318(w), 1247(s), 1204(m), 1079(s), 917(s), 839(s), 793(s), 753(s), 692(m), 637(s), 619(w), 515(s), 475(s), 370(s), 355(s), 310(s), 270(m), 245(w) cm^{-1}. MS $(M)^+$ *m/z* (calc, found): 694(100,100), 695(45,68), 696(23,33), 697(7,12). Anal. Calcd for $C_{22}H_{42}F_2Si_4U$: C, 38.0; H, 6.09. Found: C, 37.5; H, 6.26.

$Cp''_2U(NMe_2)_2$.[5] Cp''_2UCl_2 (4.00 g, 5.50 mmol) and $LiNMe_2$(0.57 g, 11 mmol) were suspended in 100 mL of tetrahydrofuran. The solution immediately became warm and turned dark yellow-green. After stirring for 12 hours, the tetrahydrofuran was removed under reduced pressure. The green solid residue was suspended in 90 mL of hexane, and the solution was filtered. The volume of the filtrate was reduced to *ca.* 10 mL. Cooling to -20 °C produced orange blocks (2.82 g, 69 %). MP: 125-127 °C. ^{1}H NMR: δ 9.82(6 H, $\nu_{1/2}$ = 5 Hz, NMe_2), 0.07(18 H, $\nu_{1/2}$ = 3 Hz, $SiMe_3$), -5.70(1 H, $\nu_{1/2}$ = 6 Hz, b), -10.82(2 H, $\nu_{1/2}$ = 11 Hz, a_2). IR: 3050(w), 2767(s), 1317(w), 1245(s), 1208(m), 1141(s), 1122(w), 1079(s), 1058(m), 919(s), 833(s), 779(s), 754(s), 689(m), 636(m), 616(w) cm^{-1}. MS $(M)^+$ *m/z* (calc, found): 744(100,100), 745(50,52), 746(25,26). Anal. Calcd for $C_{26}H_{54}N_2Si_4U$: C, 41.9; H, 7.30, N, 3.76. Found: C, 41.9; H, 7.33; N, 3.29

$Cp^{\ddagger}_2U(OMe)_2$ (9). $Cp^{\ddagger}_2UCl_2$ (3.00 g, 4.52 mmol) and KOMe (0.65 g, 9.3 mmol) were suspended in 50 mL of tetrahydrofuran. After stirring at 70°C for 12 hours , the tetrahydrofuran was removed under reduced pressure yielding a viscous green oil which slowly solidified under vacuum. The green solid residue was suspended in 50 mL of hexane, and the solution was filtered. The volume of the solution was reduced to *ca.* 5 mL and additional white solid precipitated. After 12 hours the

solution was filtered and the volume was reduced to ca. 2.5 mL. Cooling to -20°C produced green blocks (2.05 g, 69%). MP: 86-88 °C. ^{1}H NMR δ 37.12 (3 H, $\nu_{1/2}$ = 5 Hz, OMe), -1.56 (18 H, $\nu_{1/2}$ = 5 Hz, CMe_3), -9.02 (1 H, $\nu_{1/2}$ = 9 Hz, b), -25.89 (2 H, $\nu_{1/2}$ = 8 Hz, a_2). IR: 3067(w), 2726(w), 1297(w), 1251(s), 1201(m), 1166(m), 1115(s), 1093(s), 1055(m), 1025(m), 975(w), 936(m), 822(s), 753(s), 723(w), 679(m), 657(m) cm^{-1}. MS $(M)^+$ *m/z* 654. Anal. Calcd for $C_{28}H_{48}O_2U$: C, 51.4; H, 7.39. Found: C, 50.3, H, 7.25.

Cp"$_2$U(OMe)$_2$ (10). Cp"$_2$UCl$_2$ (2.00 g, 2.57 mmol) and KOMe (0.40 g, 5.6 mmol) were suspended in 50 mL of tetrahydrofuran. The mixture was heated to 70°C was stirring for 12 hours. The mixture was filtered and the tetrahydrofuran was removed under reduced pressure and the solid was heated to 60 °C under vacuum for 1 hour. The dark solid residue was suspended in 50 mL of hexane and filtered. The volume of the solution was reduced to *ca.* 10 mL and a white solid precipitated. After 12 hours, the solution was filtered, and the volume of the solution was reduced to *ca.* 2 mL. Cooling to -20 °C produced dark purple blocks (1.65 g, 84 %). MP: 95-99 °C. ^{1}H NMR δ 46.32 (3 H, $\nu_{1/2}$ = 4 Hz, OMe), -1.24(18 H, $\nu_{1/2}$ = 3 Hz, $SiMe_3$), -10.75 (1 H, $\nu_{1/2}$ = 4 Hz, b), -25.09 (2 H, $\nu_{1/2}$ = 4 Hz, a_2). IR: 3043(w), 2812(m), 1316(w), 1247(s), 1212(w), 1113(s), 1086(s), 1055(m), 920(s), 835(s), 781(m), 754(s), 689(w), 634(s), 620(w) cm^{-1}. MS $(M)^+$ *m/z* 718. Anal. Calcd for $C_{24}H_{48}O_2Si_4U$: C, 40.1; H, 6.73. Found: C, 39.7; H, 6.70.

Cp"$_2$UMe$_2$[9] (S. M. B.). Cp"$_2$UCl$_2$ (2.00 g, 2.75 mmol) was dissolved in 50 mL of diethyl ether and MeLi (10.6 mL, 0.52 M in diethyl ether, 5.5 mmol) was added by syringe. The solution immediately turned red-orange and cloudy. After stirring for 10 hours, the solvent was removed under reduced pressure. The orange solid residue was suspended in 50 mL of hexane, and the solution was filtered. The volume of the

filtrate was reduced to *ca.* 3 mL. Cooling to -20 °C produced red-orange crystals (1.45 g, 77%). MP: 120-125 °C. ^{1}H NMR δ 7.7 (2 H, $\nu_{1/2}$ = 9 Hz, b), -1.0 (36 H, $\nu_{1/2}$ = 4 Hz, $SiMe_3$), -21.2 (4 H, $\nu_{1/2}$ = 10 Hz, a_2), -28.0 (6 H, $\nu_{1/2}$ = 8 Hz, U-Me). IR 1250(s), 1200(m), 1165(m), 1110(s), 1055(m), 1025(m), 935(m), 845(m), 825(s), 810(m), 765(s), 675(m), 655(m), 405(m) cm^{-1}. MS $(M\text{-}CH_3)^+$ *m/z* 659. Anal. Calcd for $C_{24}H_{48}Si_4U$: C, 54.0; H, 7.71. Found: C, 53.7; H, 7.83.

$Cp^{‡}_2U(CH_2SiMe_3)_2$. A mixture of $Cp^{‡}_2UCl_2$ (1.00 g, 1.51 mmol) and $LiCH_2SiMe_3$ (0.28 g, 3.0 mmol) was dissolved in 30 mL of hexane. After stirring for two hours, the deep red solution was filtered and the volume of the filtrate was reduced to *ca.* 4 mL. Cooling to -20 °C gave dark red blocks (0.58 g, 50 %). ^{1}H NMR δ 11.93 (1H, $\nu_{1/2}$ = 25 H, b), 2.80 (9 H, $\nu_{1/2}$ = 15 Hz, $SiMe_3$), -0.50(18 H, $\nu_{1/2}$ = 15 Hz, CMe_3), -30.89(2 H, $\nu_{1/2}$ = 30 Hz, a_2), -55.93 (2 H, $\nu_{1/2}$ = 45 Hz, CH_2). IR: 1237(s), 876(s), 844(s), 815(s), 759(s), 430(w), 357(m) cm^{-1}. MS $(M\text{-}SiMe_4)^+$ *m/z* (calc, found) 678(100, 100), 679(39,65). Anal. Calcd for $C_{34}H_{64}Si_2U$: C, 53.2; H, 8.41. Found: C, 53.0; H, 8.51.

$[Cp^{‡}_2UF]_2$ (11). $Cp^{‡}_2UF_2$ (1.68 g, 2.66 mmol) was dissolved in 50 mL hexane, and *t*-BuLi (1.5 mL, 1.85 M in hexane, 2.8 mmol) was added using a syringe. The solution immediately turned green and cloudy. After 12 hours of stirring, the hexane was removed under reduced pressure. The green solid residue was suspended in 100 mL of toluene and heated to 60 °C. The solution was filtered, and the volume of the filtrate was reduced to *ca.* 25 mL. Cooling to -20 °C produced very small dark green crystals (0.79 g). The volume of the mother liquor was reduced to *ca.* 10 mL, and cooling to -20 °C yielded another crop of green solid (0 31 g, 1.10 g total, 68 % total yield). The compound did not melt to 300 °C. ^{1}H NMR δ -11.78 ($\nu_{1/2}$ = 51 Hz, CMe_3) no other resonances observed. IR: 3067(w), 1304(w), 1291(w), 1252(s), 1234(w), 1201(m),

1163(m), 1055(m), 1021(m), 925(m), 817(m), 799(s), 743(s), 676(m), 659(m), 610(w), 435(w), 330(s) cm^{-1}. MS $(M)^+$ *m/z* (calc, found): 1223(100, 100), 1224(58, 56), 1225(17, 16). Anal. Calcd for $C_{26}H_{42}FU$: C, 51.1; H, 6.92. Found: C, 50.8; H, 6.87.

$[Cp''_2UF]_2$ (12). $[Cp''_2UF_2]_2$ (1.59 g, 2.29 mmol) was dissolved in 50 mL hexane and *t*-BuLi (1.30 mL, 1.85 M in hexane, 2.40 mmol) was added using a syringe. The solution instantly turned dark green. The hexane was removed under vacuum giving a dark green solid. The green solid residue was suspended in 50 mL hexane, and the solution was filtered. The volume of the fitrate was reduced to *ca.* 10 mL. Cooling to -20 °C produced dark green blocks (0.46 g, 30%). MP: 244-246 °C. ^1H NMR δ -10.64 ($\nu_{1/2}$ = 28 Hz, $SiMe_3$) no other resonances observed. IR: 3040(w), 1316(w), 1249(s), 1205(w), 1076(s), 1055(w), 919(s), 836(s), 773(m), 752(s), 691(m), 635(m), 621(w), 475(m), 370(m), 330(s), 200(m), 280(w), 240(w) cm^{-1}. MS $(M)^+$ *m/z* (calc, found): 1347(100, 100), 1348(90, 87), 1349(66, 60), 1350(34, 41), 1351(15, 23), 1352(5, 12). Anal. Calcd for $C_{22}H_{42}FSi_4U$: C, 39.1; H, 6.26. Found: C, 37.8; H, 6.17.

$[Cp^{\ddagger}_2UCl]_2$[6] (13) (A. L. S.). A solution of $Cp^{\ddagger}_2UCl_2$ (2.00 g, 3.01 mmol) in 100 mL of hexane was cooled to -80 °C, and *t*-BuLi (1.6 mL, 1.9 M in hexane, 3.01 mmol) was added by syringe. The mixture was allowed to warm to room temperature while stirring. After three hours, the hexane was removed under reduced pressure. The green solid residue was extracted with 2 x 30 mL of toluene, and the solution was filtered. The volume of the filtrate was reduced to *ca.* 50 mL. Cooling to -80 °C gave dark green blocks (1.2 g, 63 %). The compound did not melt to 310 °C. ^1H NMR δ 61.98(1H, $\nu_{1/2}$ = 400 Hz, b), -6.66(18H, $\nu_{1/2}$ = 36 Hz, t-Bu), -51.62 (2H, $\nu_{1/2}$ = 400 Hz, a_2). IR: 3070(w), 2820(w), 1295(w), 1250(s), 1230(w), 1205(m), 1165(m), 1055(m), 1025(m), 930(m), 815(m), 805(s), 765(m), 750(s), 720(w), 675(m), 660(m), 610(w), 425(w), 345(m) cm^{-1}. MS $(M)^+$ *m/z* (calc, found): 1255(100, 100),-

1256(58,60), 1257(81, 50), 1258(41,26). Anal. Calcd for $C_{26}H_{42}ClU$: C, 49.7; H: 6.69. Found C, 49.8; H, 6.76.

$[Cp''_2UCl]_2$[4,9] **(14)** (S. M. B.). Cp''_2UCl_2 (2.00 g, 2.75 mmol) was dissolved in 50 mL of hexane and *t*-BuLi (1.14 mL, 2.4 M in hexane, 2.8 mmol) was added by syringe. The solution quickly turned green. After stirring for 12 hours, the mixture was heated to 80 °C, and the solution was filtered. The green solid residue was washed with 50 mL of hexane which was added to the filtrate. The volume of the combined filtrate was reduced to *ca.* 40 mL, and the filtrate was heated to 80 °C to redissolve the solid. Cooling to -80°C produced green blocks (1.25 g, 66%). ^1H NMR δ 29.76 (1 H, $\nu_{1/2}$ = 190 Hz, b), -2.61(2 H, $\nu_{1/2}$ = 140 Hz, a_2), -9.01 (18 H, $\nu_{1/2}$ = 11 Hz, $SiMe_3$). IR 1310(w), 1245(s), 1200(w), 1070(s), 915(s), 830(s), 780(w), 775(w), 745(s), 685(m), 630(m), 615(m), 480(m), 365(m), 350(w), 330(3), 300(m), 280(w) cm^{-1}. MS weak peak for $(M)^+$ *m/z* (calc, found) 1382(77, 100), 1384 (100, 97); much stronger peak for Cp''_4U_2ClO. Anal. Calcd for $C_{22}H_{42}ClSi_4U$: C, 38.2; H, 6.11; Cl, 5.12. Found C, 37.9; H, 6.11; Cl, 5.28.

$[Cp^{\ddagger}_2UBr]_2$[11] **(15)** (R. K. R.). $Cp^{\ddagger}_2UBr_2$ (0.52 g, 0.69 mmol) was dissolved in 30 mL of diethyl ether, and *t*-BuLi(0.29 mL, 2.4M in hexane, 0.70 mmol) was added using a syringe. The initially red solution immediately became bright green. After 2 hours, the solvent was removed under reduced pressure, and the green solid residue was suspended in 30 mL of hexane. The mixture was filtered, and the volume of the filtrate was reduced to *ca.* 20 mL. Cooling to -80 °C gave green needles (0.25 g, 54%). The compound did not melt to 300 °C. ^1H NMR δ 76.64 (1 H, $\nu_{1/2}$ = 300 Hz, b), -5.37 (18 H, $\nu_{1/2}$ = 34 Hz, t-Bu), -62.77 (2 H, $\nu_{1/2}$ = 200 Hz, a_2). MS $(M)^+$ *m/z* (calc, found) 671(98,100), 672(29,28), 673(100,100), 674(29,26). Anal. Calcd for $C_{26}H_{42}BrU$: C, 46.4; H, 6.3; Br, 11.9. Found: C: 46.6; H, 6.4; Br, 12.0.

[Cp"$_2$UBr]$_2$[4,9] **(16)** (S. M. B.). Cp"$_2$UCl$_2$ (0.75 g, 0.92 mmol) was dissolved in 50 mL hexane and *t*-BuLi (0.38 mL, 2.4 M in hexane, 0.91 mmol) was added by syringe. The solution slowly became green and cloudy. After stirring for seven hours, the mixture was heated to 60 °C and allowed to settle. The mixture was filtered, and the volume of the filtrate was reduced to *ca.* 15 mL. Cooling to -80 °C produced little green blocks (0.45 g, 66%). The compound did not melt to 250 °C. ^{1}H NMR δ 35.49 (1 H, b), -3.17 (2 H, $\nu_{1/2}$ = 80 Hz, a_2), -7.08(18 H, $\nu_{1/2}$ = 15 Hz, SiMe$_3$). IR 3070(w), 3020(w), 1325(m), 1245(s), 1200(m), 1075(s), 915(s), 830(s), 785(m), 775(w), 750(s), 690(m), 635(s), 615(m), 475(m), 370(m), 350(w), 330(w), 300(m), 280(w), 240(w) cm^{-1}. MS $(M)^+$ *m/z* (calc, found) 1470 (38, 44), 1471 (34, 50), 1472 (100, 100), 1473 (80,94), 1474 (91, 94), 1475 (61, 60), 1476 (56, 33). Anal. Calcd for $C_{22}H_{42}BrSi_4U$: C, 35.9; H, 5.74; Br, 10.8. Found C, 35.9; H, 5.84; Br, 10.7.

[Cp‡$_2$UI]$_2$ (17). Cp‡$_2$UI$_2$ (0.65 g, 0.77 mmol) was dissolved in 60 mL of hexane giving a red solution, and *t*-BuLi (0.32 mL, 2.4 M in hexane, 0.77 mmol) was added using a syringe. After 8 hours of stirring the mixture was green and cloudy. The mixture was heated to 60 °C for 30 minutes then filtered. The volume of the filtrate was reduced to *ca.* 20 mL. Cooling to -80 °C produced green needles (0.26 g, 47 %). MP: 273-278 °C. ^{1}H NMR δ 86.9 (1 H, $\nu_{1/2}$ = 400 Hz, b), -4.32 (18 H, $\nu_{1/2}$ = 38 Hz, CMe$_3$), -68.5 (2 H, $\nu_{1/2}$ =250 Hz, a_2). IR: 3070(w), 2720(w), 1295(w), 1250(w), 1200(m), 1165(m), 1050(m), 1020(m), 925(m), 815(s), 805(s), 765(m), 750(s), 675(m), 655(m), 425(w), 345(w). MS $(M)^+$ *m/z* (calc, found) 719(100, 100), 720(30, 30), 721(4, 5). Anal. Calcd for $C_{26}H_{42}IU$: C, 43.4; H, 5.88. Found: C, 43.4; H, 5.94.

[Cp"$_2$UI]$_2$[4,9] **(18)** (S. M. B.). Cp"$_2$UI$_2$ (1.00 g, 1.10 mmol) was dissolved in 50 mL of hexane and *t*-BuLi (0.62 mL, 1.85 M in hexane, 1.1 mmol) was added by syringe. The

solution became green and cloudy. After stirring for twelve hours, 25 mL of hexane was added and the solution was heated to 60 °C. The solution was filtered, and the volume of the filtrate was reduced to *ca.* 30 mL. Cooling to -80 °C produced green blocks (0.74 g, 88%). The compound did not melt to 250 °C. ^{1}H NMR δ 41.62 (1H, $\nu_{1/2}$ = 270 Hz, b), -3.17 (2 H, $\nu_{1/2}$ = 80 Hz, a_2), -7.08 (18 H, $\nu_{1/2}$ = 15 Hz, $SiMe_3$). IR 1320(w), 1245(s), 1200(w), 1175(s), 915(s), 830(s), 790(w), 780(w), 750(m), 960(w), 645(m), 615(w), 475(m), 375(w), 350(w), 200(w) cm^{-1}. MS $(M)^+$ *m/z* (calc, found) 1566 (100,100), 1567 (90,82), 1568 (66, 57), 1569 (34, 37), 1570 (15,12). Anal. Calcd for $C_{22}H_{42}ISi_4U$: C, 33.7; H, 5.40; I, 16.2. Found: C, 33.5; H, 5.29; I, 16.2.

$Cp^{‡}_2U(Me)Cl$. $Cp^{‡}_2UCl_2$ (2.00g, 3.01 mmol) was dissolved in 50 mL of hexane. MeLi (5.80 mL, 0.52 M in ether, 3.0 mmol) was added using a syringe. The solution immediately turned a cloudy red-orange. After 8 hours, the solution was filtered, and the volume of the solvent was reduced to *ca.* 7 mL. Cooling to -20°C produced red-orange blocks (1.35 g, 70 %). MP: 128-132 °C. ^{1}H NMR δ 55.6 (2 H, $\nu_{1/2}$ = 12 Hz, b), 3.46(18 H, $\nu_{1/2}$ = 4 Hz, CMe_3), -3.82 (18 H, $\nu_{1/2}$ = 4 Hz, CMe_3'), -29.52 (3 H, $\nu_{1/2}$ = 12 Hz, U-Me), -41.78(2 H, $\nu_{1/2}$ = 10 Hz, a), -52.42(2 H, $\nu_{1/2}$ = 20 Hz, a'). IR 3091(w), 2740(w), 2720(w), 1293(w), 1248(s), 1199(m), 1166(m) 1114(m), 1056(m), 1023(m), 935(m), 927(m), 832(s), 811(w), 775(s), 659(w) cm^{-1}. MS peaks at *m/z* 607, 627, and 662 are seen corresponding to $Cp^{‡}_2UMe$, $Cp^{‡}_2UCl$, and $Cp^{‡}_2UCl_2$, respectively. Anal. Calcd for $C_{27}H_{45}ClU$: C, 50.4; H, 7.05. Found: C, 50.0; H, 6.84.

$[Cp''_2U(OH)]_2$[9]**. (19)**.(S. M. B.). A solution of degassed water (20.8 μL, 1.2 mmol) in 10 mL of tetrahydrofuran was added slowly to a solution of Cp''_3U (1.00 g, 1.2 mmol) in 25 mL of tetrahydrofuran. The dark green solution immediately became bright blue-green. After stirring for 30 min., the solvent was removed under reduced pressure, and the green solid residue was dissolved in 100 mL of hexane. The hexane solution was

filtered, and the volume of the filtrate was reduced to *ca.* 60 mL. Slow cooling to -80 °C produced dark green crystals (0.68 g, 87 %). The compound did not melt to 250 °C. ^{1}H NMR δ -9.18 ($\nu_{1/2}$ = 26 Hz, $SiMe_3$) no other resonances observed. IR: 3630(OH; 2680, OD)(m), 3070(w), 3040(w), 1315(m), 1240(s), 1205(m), 1075(s), 1055(w), 915(s) 830(s), 770(m), 750(s), 690(m), 630(s), 615(w), 575(w), 475(m), 370(m), 350(s), 300(s), 275(w), 240(w) cm^{-1}. MS $(M)^+$*m/z* (calc, found): 1347 (100, 100), 1348 (90, 91), 1349 (66, 64), 1350 (34, 33). Anal. Calcd for $C_{22}H_{43}OSi_4U$: C, 39.2; H, 6.43. Found C, 39.0; H, 6.42.

[Cp‡$_2$U(μ-OH)]$_2$ (20). [Cp‡$_2$UH]$_2$ (0.50 g, 0.42 mmol) was suspended in 30 mL of diethyl ether. Degassed water (15 μL, 0.84 mmol) was added by syringe. The solution immediately turned blue-green, and blue-green solid precipitated. After stirring for one hour, the solid was allowed to settle, and the mother liquor was removed by filtration. The resulting blue-green powder was dried under reduced pressure (0.46 g, 89 %). The compound does not melt to 300 °C. ^{1}H NMR δ -9.96 ($\nu_{1/2}$ = 500 Hz, CMe_3) no other resonances observed. IR: 3620(m) (O-H; 2675, O-D), 1251(s), 1022(w), 793(s), 739(s), 644(m), 361(m) cm^{-1}. MS $(M-2)^+$*m/z* (calc, found) 1217(100, 100), 1216(58, 57), 1215(17, 18), 1214(3, 5). Anal. Calcd for $C_{26}H_{43}OU$: C, 51.2; H, 7.11. Found: C, 51.1; H, 7.22.

[Cp‡$_2$UH]$_2$ (21). Cp‡$_2$UMe$_2$ (0.45 g, 0.72 mmol) was dissolved in 20 mL diethyl ether and transferred to a heavy-walled pressure bottle by cannula. The bottle was pressurized to 225 psi with hydrogen. After stirring for eight hours, the solution was transferred to a Schlenk tube by cannula. The ether was removed under reduced pressur, and the black solid residue was dissolved in 50 mL of warm diethyl ether. Cooling to -80°C produced small black crystals (0.21 g, 49 %). MP: 263 - 265 °C. ^{1}H NMR δ -18 ($\nu_{1/2}$ = 600 Hz, t-Bu) no other resonances observed. IR: 3070(w),

2920(w), 1290(w), 1250(s), 1230(w), 1200(m), 1150(s) (U-H; 825(shoulder), U-D), 1050(w), 1020(w), 925(m), 800(s), 740(s), 670(m), 655(m), 605(w), 555(w), 425(w), 350(w) cm^{-1}. MS: $(M)^+$ *m/z* (calc, found): 1187(100,100), 1188(58,57), 1189(17,17), 1190(3,4). Anal. Calcd for $C_{26}H_{43}U$: C, 52.6 ; H, 7.30. Found: C, 52.3; H, 7.28.

$[Cp"_2U(\mu\text{-}O)]_2$[12] **(22)** (L. L. B.). A solution of degassed water (14.9 μL, 0.83 mmol) in 10 mL of tetrahydrofuran was added dropwise to a solution of $Cp"_2UMe_2$ (0.57 g, 0.83 mmol) in 25 mL of tetrahydrofuran. The orange solution foamed and turned brown. After stirring for three hours, the solution was filtered, and the volume of the filtrate was reduced to *ca.* 2 mL. Cooling to -20 °C produced red blocks (0.17 g, 30 %). The compound does not melt to 250 °C. ^1H NMR (C_7D_8): δ 82.5 (2 H, $\nu_{1/2}$ = 97 Hz, a_2), 79.9 (1 H, $\nu_{1/2}$ = 46 Hz, b), -0.73 (18 H, $\nu_{1/2}$ = 16 Hz, $SiMe_3$), -13.2 (18 H, $\nu_{1/2}$ = 21 Hz, $SiMe_3$), -81.8 (2 H, $\nu_{1/2}$ = 41 Hz, a_2), -85.3 (1 H, $\nu_{1/2}$ = 144 Hz, b). IR: 3108(w), 3081(w), 3062(w), 1413(w), 1329(m), 1265(s), 1218(m), 1084(s), 1070(m), 926(s), 842(s), 793(s), 762(s), 701(m), 644(s), 627(w), 582 (U-O-U; 548, U-^{18}O-U)(s), 493(m), 486(m), 382(m), 322(m), 289(w), 252(w), 233(w) cm^{-1}. MS $(M)^+$*m/z* (calc, found) 1344 (100, 100), 1345 (90.6, 73.8), 1346 (66.9, 55.0), 1347 (34.6, 29.3), 1348 (15.3, 8.0), 1349 (5.6, 3.6). Anal. Calcd for $C_{22}H_{42}OSi_4U$: C, 39.3; H, 6.29. Found: C, 39.3; H, 6.15.

$[Cp^{‡}_2U(\mu\text{-}O)]_2$[12] **(23)** (L. L. B.). $Cp^{‡}_2UMe_2$ (1.69 g, 2.71 mmol) was dissolved in 40 mL of tetrahydrofuran. Degassed heavy water (49 μL, 54 mg, 2.7 mmol) was dissolved in 30 mL of tetrahydrofuran and slowly added to the $Cp^{‡}_2UMe_2$ solution by cannula. The solution became darker and gas was evolved. After stirring for twelve hours, the tetrahydrofuran was removed under reduced pressure giving an oily orange solid. The solid was suspended in 100 mL of hexane, and the solution was filtered. The remaining brown solid was dissolved in 100 mL of toluene. The toluene solution

was filtered, and the volume of the filtrate was reduced to *ca.* 25 mL. The solution was heated to 100 °C and allowed to cool slowly to room temperature. Cooling to -20 °C produced brown crystals (0.42 g, 25%). The compound did not melt to 300 °C. ^{1}H NMR (C_7D_8): δ 78.6 (2 H, $\nu_{1/2}$ = 24 Hz, A_2), 75.7 (1 H, $\nu_{1/2}$ = 19 Hz, B), 1.0 (18 H, $\nu_{1/2}$ = 6 Hz, CMe_3), -16.4 (18 H, $\nu_{1/2}$ = 7 Hz, CMe_3), -85.8 (1 H, $\nu_{1/2}$ = 20 Hz, B), -94.5 (2 H, $\nu_{1/2}$ = 20 Hz, A_2). IR: 3079(w), 1635(w), 1561(w), 1307(w), 1292(w), 1253(m), 1202(m), 1168(m), 1086(w), 1059(m), 1025(m), 923(m), 809(s), 751(s), 672(m), 659(m), 572 (U-O-U; 540, U-^{18}O-U)(s), 488(m), 428(m), 349(m), 255(m) cm^{-1}. MS $(M)^+$ *m/z* (calc, found) 1216 (100, 100), 1217 (59, 58), 1218 (18, 17), 1219 (3, 2). Anal. Calcd for $C_{26}H_{42}OU$: C, 51.3; H, 6.96. Found: C, 51.0; H, 7.03.

Chapter Two

Cp"$_3$U[9] (S. M. B.). a) U[$N(SiMe_3)_2]_3$[13] (1.00 g, 1.39 mmol) was dissolved in 50 mL of toluene, and Cp"H (1.4 mL, 1.2 g, 5.6 mmol) was added using a syringe. The solution was heated to reflux for 3 days. The toluene was removed slowly under reduced at 105 °C giving a dark oil. The flask was heated to 90 °C under dynamic vacuum. The greenish brown solid residue was dissolved in 50 mL of hexane. The solution was filtered, and the volume of the filtrate was reduced to *ca.* 3 mL. Cooling to -80 °C produced black, diamond shaped blocks (0.31 g, 25 %). MP: 232 - 235 °C. ^{1}H NMR δ 20.78 (1 H, $\nu_{1/2}$ = 17 Hz, b), -4.78 (2 H, $\nu_{1/2}$ = 18 Hz, a_2), -9.35 (18 H, $\nu_{1/2}$ = 7 Hz, $SiMe_3$). IR 3075(w), 3050(w), 1315(w), 1245(s), 1205(w), 1195(w), 1070(m), 915(s), 830(s), 770(m), 750(s), 685(m), 635(m), 610(w), 480(m), 375(m), 350(w), 325(w), 290(m), 240(w) cm^{-1}. MS $(M)^+$ *m/z* (calc, found): 865 (100, 100), 866 (67, 76), 867 (42, 48), 869 (6, 19). Anal. Calcd for $C_{33}H_{63}Si_6U$: C, 45.7; H, 7.33. Found: C, 45.5; H, 7.17.

b) $Cp"_2UCl_2$ (3.00 g, 4.12 mmol) and potassium (0.35 g, 9.1 mmol) were suspended in 60 mL of hexane and heated to 80 °C. After stirring for one day, the dark green, cloudy solution was filtered. The volume of the filtrate was reduced to *ca.* 15 mL. Cooling to -20 °C produced green blocks (0.98 g). The volume of the mother liquor was reduced to 2 mL, and cooling to -20 °C produced a second crop of green blocks (0.67 g, 1.65 g total, 69 % total). The ^1H NMR spectrum was identical to that of the product of route (a).

$Cp"_3Nd$. $Nd[N(SiMe_3)_2]_3$[14] (2.00 g, 3.20 mmol) was dissolved in 50 mL of toluene, and Cp"H (2.53 mL, 2.15 g, 10.2 mmol) was added using a syringe. The solution was heated to 110 °C. After stirring for 5 days, the color had changed from blue to green. The toluene was slowly removed under vacuum at 100 °C giving oily, green blocks. The blocks were dissolved in 50 mL of hexane, and the solution was filtered. The volume of the solution was reduced to *ca.* 25 mL. Cooling to -20 °C produced large light green, diamond shaped prisms (1.68 g, 68 %). MP: 191-196 °C. ^1H NMR δ 33.70 (1 H, $\nu_{1/2}$ = 27 Hz, b), 15.15 (2 H, $\nu_{1/2}$ = 35 Hz, a_2), -7.53 (18 H, $\nu_{1/2}$ = 5 Hz, $SiMe_3$). IR: 3050(w), 1320(w), 1245(s), 1209(w), 1201(w), 1079(s), 920(s), 833(s), 778(s), 751(s), 690(m), 641(m), 621(m) cm^{-1}. MS $(M-CH_3)^+$ *m/z* (calc, found): 754 (63, 63), 755(70, 70), 756(100, 100), 757(78, 79), 758(84, 84), 759(47, 46), 760(37, 36), 761(18, 18), 762(22, 21), 763(12, 11). Anal. Calcd for $C_{33}H_{63}Si_6Nd$: 51.3; H, 8.22. Found: C, 50.3; H, 8.29.

$Cp"_3La$. $La[N(SiMe_3)_2]_3$[14] (0.62 g, 1.0 mmol) was dissolved in 30 mL of toluene, and Cp"H (0.90 mL, 0.74 g, 3.5 mmol) was added using a syringe. The solution was heated to reflux. After three days, the toluene was removed under reduced pressure at 100 °C giving an oily white solid. The solid residue was dissolved in 50 mL of hexane, and the solution was filtered. The volume of the filtrate was reduced to *ca.*

10 mL. Cooling to -80 °C produced colorless, diamond shaped prisms (0.44 g, 57%). MP: 155-160 °C. ^{1}H NMR δ 6.86 (m, 3 H, a_2 and b), 0.33 (s, 18 H, $SiMe_3$). IR: 3074(w), 3051(m), 1319(s), 1246(s), 1210(s), 1203(m), 1078(s), 1041(m), 920(s), 832(s), 774(s), 752(s), 689(s), 640(s), 621(s) cm^{-1}. MS: $(M-H)^+$ *m/z* (calc, found): 765(100, 100), 766(87, 68), 767(54, 42), 768(27, 17). Anal. Calcd for $C_{33}H_{63}Si_6La$: C, 51.7; H, 8.28. Found: C, 51.0; H, 8.30.

Cp"$_3$U•*t*-BuNC (S. M. B.). Cp"$_3$U (0.50 g, 0.58 mmol) was dissolved in 50 mL hexane, and *t*-BuNC (0.07 mL, 0.05 g, 0.6 mmol) was added using a syringe. The color of the solution immediately changed from deep green to dark purple. After stirring for one hour, the solvent was removed under reduced pressure. The purple solid residue was dissolved in 100 mL of hexane, and the solution was filtered. The volume of the filtrate was reduced to *ca.* 40 mL, and the solution was heated to redissolve the solid. Cooling to -20 °C produced purple blocks (0.20 g, 36 %). MP: 230-232 °C. ^{1}H NMR δ 0.44 (2H, $\nu_{1/2}$ =15 Hz, a_2), -2.55 (18 H, $\nu_{1/2}$ = 12 Hz, $SiMe_3$), 8.85 (1H, $\nu_{1/2}$ = 10 Hz, b), -11.25 (3 H, $\nu_{1/2}$ = 22 Hz, t-Bu). IR: 3060(w), 2140(s), 1315(w), 1245(s), 1070(s), 925(s), 830(s), 815(w), 775(w), 750(m), 680(w), 630(m), 610(w), 480(w), 365(w), 290(w) cm^{-1}. MS. not done, see below. Anal. Calcd for $C_{36}H_{72}NSi_6U$: C, 48.10; H, 7.64; N, 1.48. Found: C, 46.8; H, 7.63; N, 1.38.

Cp"$_3$Nd•*t*-BuNC. Cp"$_3$Nd (0.50 g, 0.65 mmol) was dissolved in 30 mL hexane, and *t*-BuNC(0.08 mL, 0.06 g, 0.7 mmol) was added using a syringe. The initially bright green solution immediately turned pale blue. After 1 minute, a blue solid precipitated. The volatile components were removed under reduced pressure. The light blue solid residue was dissolved in 50 mL of hexane, and the solution was filtered. The volume of the filtrate was reduced to *ca.* 30 mL, and the solution was heated to dissolve the solid. Cooling to -20 °C produced light blue blocks (0.47 g, 85 %). MP: 222-223 °C:

^{1}H NMR δ 9.73 (1 H, $\nu_{1/2}$ = 150 Hz, b), 8.89(2 H, $\nu_{1/2}$ = 100 Hz, a_2), -1.93 (18 H, $\nu_{1/2}$ = 18 Hz, $SiMe_3$), -7.21 (3 H, $\nu_{1/2}$ = 35 Hz, t-Bu). IR: 3059(m), 2178(s), 1318(w), 1247(s), 1207(m), 1077(s), 923(m), 835(s), 779(m), 754(s), 687(m), 638(m), 622(m) cm^{-1}. MS only Cp"$_3$Nd observed. Anal. Calcd for $C_{38}H_{72}NNdSi_6$: C, 53.3; H, 8.48; N, 1.64. Found: C, 52.5; H, 8.78; N, 1.57.

Cp"$_3$La•*t*-BuNC. Cp"$_3$La (0.50 g, 0.65 mmol) was dissolved in 50 mL of hexane, and *t*-BuNC (0.08 mL, 0.06 g, 0.7 mmol) was added using a syringe. After 15 minutes, white solid precipitated from the colorless solution. After stirring for one hour, the hexane was removed under reduced pressure. The white solid residue was dissolved in 100 mL of hexane, and the solution was filtered. The volume of the filtrate was reduced to *ca.* 50 mL, and heated to redissolve all of the product. Cooling to -80 °C produced colorless blocks (0.34 g, 61 %). MP: 222-223 °C. ^{1}H NMR δ 6.83 (1 H, s, b), 6.63(2 H, s, a_2), 1.07 (3 H, s, t-Bu), 0.45 (18 H, s, $SiMe_3$). IR: 3056(m), 2178(s), 1317(m), 1247(s), 1206(m), 1076(s), 1061(w), 922(s), 830(s), 774(s), 754(s), 687(m), 638(s), 622(m) cm^{-1}. Anal. Calcd for $C_{38}H_{72}LaNSi_6$: C, 53.7; H, 8.53; N, 1.65. Found: C, 52.6; H, 8.64; N, 1.69.

Cp"$_3$U•$C_6H_{11}CN$. Cp"$_3$U (0.50 g, 0.58 mmol) was dissolved in 30 mL of hexane, and cyclohexyl isocyanide (0.08 mL, 0.07 g, 0.6 mmol) was added using a syringe. The color of the solution immediately changed from dark green to dark purple. After stirring for one hour, the hexane was removed under reduced pressure. The resulting dark purple solid residue was dried under vacuum for 3 hours then dissolved in 70 mL of hexane, and the solution was filtered. The volume of the filtrate was reduced to *ca.* 40 mL. Cooling to -20 °C produced purple blocks (0.36 g, 64 %). MP: 190-191 °C. ^{1}H NMR δ 0.87 (2 H, $\nu_{1/2}$ = 18 Hz, δ), -2.64 (56H, $\nu_{1/2}$ =10 Hz, $SiMe_3$), -4.75 (3H,

$\nu_{1/2}$ =31 Hz, b), -5.71 (2H, $\nu_{1/2}$ =30 Hz, γ), -6.21 (2H, $\nu_{1/2}$ =27 Hz, γ), -7.76 (6H, $\nu_{1/2}$ =70 Hz, a_2), -9.44 (2H, $\nu_{1/2}$ =27 Hz, β), -10.16 (2 H, $\nu_{1/2}$ = 20 Hz, β), -53.32 (1H, $\nu_{1/2}$ = 36 Hz, α) assignment of the cyclohexyl resonances was based upon the integrated areas and chemical shifts of the resonances. IR: 3062(m), 2153(s), 1318(m), 1243(s), 1207(m), 1076(s), 1055(w), 922(s), 834(s), 779(s), 749(s), 687(m), 638(s), 618(m) cm^{-1}. Anal. Calcd for $C_{40}H_{74}NSi_6U$: C, 49.2; H, 7.65; N, 1.44. Found: C, 48.7; N, 7.87; N, 1.35.

$Cp"_3Nd•C_6H_{11}CN$. $Cp"_3Nd$ (0.50 g, 0.65 mmol) was dissolved in 30 mL of hexane, and cyclohexyl isocyanide (0.09 mL, 0.08 g, 0.7 mmol) was added using a syringe. The initially green solution immediately turned pale blue. After stirring for one hour, the solvent was removed under reduced pressure, and the blue solid residue was dissolved in 100 mL of hexane. The solution was filtered, and the volume of the filtrate was reduced to *ca* 50 mL. Cooling to -20 °C produced light blue blocks (0.50 g, 88 %). MP: 186-189 °C. ^1H NMR(C_6D_6): 9.93 (3H, $\nu_{1/2}$ = 66 Hz, a_2), 8.64 (6 H, $\nu_{1/2}$ = 100 Hz, b), -1.81 (56 H, $\nu_{1/2}$ = 11 Hz,$SiMe_3$ and γ), -3.78 (4 H, $\nu_{1/2}$ = 70 Hz, δ), -7.24 (2 H, $\nu_{1/2}$ = 28 Hz, β), -8.26(2 H, $\nu_{1/2}$ = 35 Hz, β), -13.94(1 H, $\nu_{1/2}$ = 45 Hz, α) assignment of the cyclohexyl resonances was based upon integrated areas and chemical shifts of the resonances. IR: 3107(w), 3085(w), 3061(m), 2723(w), 2183(s), 1319(m), 1248(s), 1211(m), 1077(s), 1057(m), 1039(w), 1018(w), 963(w), 924(s), 894(w), 835(s), 780(s), 750(s), 686(m), 640(s), 621(s) cm^{-1}. Anal. Calcd for $C_{40}H_{74}NNdSi_6$: C, 54.5; H, 8.46; N, 1.59. Found: C, 52.7; H, 8.59; N, 1.51.

Cp_3Zr. a) A slurry of KC_8[15] (0.42 g, 3.1 mmol) in 10 mL of toluene was slowly added by cannula to Cp_4Zr[16] (1.00g, 2.84 mmol) dissolved in 200 mL of toluene. After stirring for ten hours, the reaction mixture was filtered giving a deep brown solution.

The volume of the filtrate was reduced to *ca.* 175 mL, and the solution was heated to 80 °C to redissolve the solid. Cooling to -20 °C yielded thin, brown, hexagonal plates (0.46g, 56%). The compound did not melt to 300 °C. IR: 3130(m), 1023(s), 1012(s), 912(s), 845(s), 819(s), 790(s) 730 (m, sh), 285(s), 250(s) cm^{-1}. MS $(M)^+$ *m/z* (found, calc) 285 (100,100), 286 (85,39), 287 (80,38), 288 (28,6), 289 (75,34). Anal. Calcd for $C_{15}H_{15}Zr$: C, 62.9; H, 5.28. Found: C, 63.1; H, 5.32.

b) A mixture of naphthalene (0.37 g, 2.8 mmol) and a large excess of sodium slices was suspended in 50 mL of tetrahydrofuran. After stirring for 12 hours, the green $NaC_{10}H_8$ solution was added by cannula to Cp_4Zr[16] (1.00g, 2.84 mmol) dissolved in 100 mL of tetrahydrofuran. The reaction mixture became red-brown. After stirring for 12 hours, the tetrahydrofuran was removed under reduced pressure and the solid residue was heated to 80 °C under dynamic vacuum for 4 hours to remove $C_{10}H_8$. The brown solid residue was suspended in 200 mL of toluene, and the solution was filtered. Cooling to -20 °C gave brown plates (0.40 g, 49%), but they were contaminated with 12 % Cp_3ZrH[17] as judged by the following method.

Reaction of Cp_3Zr with CCl_4. In an NMR tube, a benzene solution of Cp_3Zr was treated with an excess of dry, deoxygenated CCl_4 using a syringe. The color of the solution immediately changed from green-brown to yellow-orange. The ^1H NMR spectrum of the reaction mixture showed it to be Cp_3ZrCl.[18] In this way, the purity of the Cp_3Zr was estimated by comparing the integrated areas of the Cp peaks relative to benzene before and after the addition of CCl_4. (Note: the chemical shift of the protons of Cp_3ZrCl was reported as $\delta = 6.05$ in $CDCl_3$.[18] We find the resonance of Cp_3ZrCl, prepared as described in ref. 18 , at 5.67 in C_6D_6).

Reaction of Cp_3Ti with CCl_4. In an NMR tube, a benzene solution of Cp_3Ti[19-21] was treated with an excess of dry, deoxygenated CCl_4 added using a syringe. The color

immediately changed from dark green to dark red. The ^1H NMR spectrum of the reaction mixture showed it to be Cp_2TiCl_2 by comparison to an authentic sample Cp_2TiCl_2.

Reaction of Cp_4Zr with *t*-BuLi. Cp_4Zr[16] (0.50 g, 1.4 mmol) was dissolved in 125 mL of hot toluene then cooled to room temperature. *t*-BuLi (0.64 mL, 2.24 M in hexane) was added by syringe. The solution became viscous, and a colorless precipitate appeared. After 1 hour, the mixture was filtered giving a pale yellow solution from which white needles formed on standing. The solution was cooled to -80 °C to complete the crystallization (0.29 g, 71 %). The ^1H NMR spectrum of Cp_3ZrH was not previously reported: δ 5.28 (d, J = 0.5 Hz, 15H), 2.83 (s, 1H). The IR spectrum was identical to that previously reported.[17]

$Cp_3ZrCN \cdot 1/3C_7H_8$. Cp_3Zr (0.30 g, 1.0 mmol) was dissolved in 100 mL of warm toluene. *t*-BuNC (0.10 g, 1.2 mmol) was added using a syringe. The solution instantly became dark then lightened to red and finally to orange-red. The solution was filtered although no precipitate was evident, and the volume of the filtrate was reduced to *ca.* 25 mL. The solution was cooled to -20 °C. After two weeks, the slightly cloudy solution was filtered and cooled to -80 °C yielding small orange-red crystals (0.04 g, 12 %). MP: 220 °C (dec.). ^1H NMR δ 5.39(15H, C_5H_5), 2.10(1H, $H_3CC_6H_5$). IR: 3100(m), 3080(w), 2130(w), 1260(w), 1020(m), 1010(m), 840(m), 825(s), 810(s), 800(s), 730(w), 605(w), 375(w), 290(m), 235(m) cm $^{-1}$. MS $(M)^+$ *m/z* (found, calc.): 311(100,100), 312 (43,38), 313 (38,37), 315 (34,32). Anal. Calcd for $C_{55}H_{53}N_3Zr_3$: C, 64.2; H, 5.19; N, 4.08. Found: C, 63.7; H, 5.37; N, 3.81.

Reaction of Cp_3Ti with *t*-BuNC. Cp_3Ti[19-21] (0.50 g, 2.1 mmol) was dissolved in 80 mL of toluene, and *t*-BuNC (0.25 mL, 2.3 mmol) was added by syringe. The green

solution immediately became deep purple. After standing for 4 hours the solution was filtered. Cooling to -80 °C gave a purple powder (0.20 g, 48%). The IR spectrum, color, and solubility matched that reported for $[Cp_2TiCN]_4$.[22,23] MS $(M)^+$ *m/z* (found, calc) 814(36,40), 815(55,53), 816(100,100), 817(68,71), 818(42,47), 819(16,21).

Reactions of Cp_3Zr with water.

a) With one equivalent. Cp_3Zr (1.8 mg, 6.4 μmol) was dissolved in 0.25 mL of C_6D_6. Dry, degassed water (0.1 μmol, 6 μmol) was added using a syringe. The initially green-brown solution became cloudy, and a white precipitate formed. The only species present in solution were $[Cp_2ZrO]_3$ ($\delta = 6.21$ ppm)[24], and C_5H_6 ($\delta = 6.40$(m), 2.68(m)).

b) With 0.5 equivalents. Cp_3Zr (0.26 g, 0.91 mmol) was dissolved in 40 mL of tetrahydrofuran and cooled to -78 °C. Degassed water (8.2 μL, 0.45 mmol) was dissolved in 30 mL tetrahydrofuran and slowly added to the solution of Cp_3Zr. The solution was allowed to warm to room temperature and became pale and cloudy as the temperature increased. After stirring for 12 hours, the tetrahydrofuran was removed under reduced pressure, and 100 mL of toluene was added. The mixture was heated to 90 °C then allowed to cool to room temperature and settle giving a clear solution and a white precipitate which was removed by filtration. The white solid was almost insoluble in benzene and its IR and ^1H NMR spectra matched those reported for $[Cp_2ZrO]_3$.[24] Cooling the filtrate to -80 °C caused the precipitation of a white solid which was found to be a mixture of Cp_3ZrH[17] and $[Cp_2ZrO]_3$[24] by IR and ^1H NMR spectroscopy.

Attempted reactions of Cp_3Zr with ligands. Cp_3Zr was dissolved in toluene. Ligands were added as toluene solution ($OP(OCH_2)_3CEt$), neat (pyridine), or as a gas in a thick-walled pressure bottle (CO, and C_2H_4). After stirring for 12 hr, no color

change was noted. The solutions were filtered, and the volume of the mother liquor was reduced. Cooling to -20 °C produced the characteristic thin, brown, hexagonal crystals of Cp_3Zr. The spectra were identical to that of Cp_3Zr.

$(Cp_2Ti)_2(\mu\text{-}O)$. Cp_3Ti[19-21] (0.50 g, 2.1 mmol) was dissolved in 50 mL of THF and cooled to -78 °C. A solution of water (0.018 g, 1.0 mmol) dissolved in 40 mL of tetrahydrofuran was slowly added by cannula to the Cp_3Ti solution. The deep green solution became red. The mixture was allowed to warm to room temperature. After stirring for ten hours, the tetrahydrofuran was removed under reduced pressure, and the solid residue was dissolved in 60 mL of toluene. The solution was filtered, and the volume of the filtrate was reduced to *ca.* 15 mL. Cooling to -20 °C produced shiny green plates (0.25 g, 75 %). MP: 230-234 °C. IR: 1125(m), 1010(s), 890(m), 845(m), 780(s), 610(m), 410(s), 240(m). MS *m/z* (calc, found) 369(2, 2), 370(21, 23), 371(24, 27), 372(100, 100), 373 (37, 39), 374(20, 21), 375(5, 5). Anal. Calcd for $C_{20}H_{20}OTi_2$: C, 64.5; H, 5.42. Found: C, 64.9; H, 5.81.

$Cp_4Ti_2{}^{18}O$. The isotopomer was prepared as described above except that 80 % $^{18}OH_2$ was used. IR: 1125(m), 1010(s), 890(m), 790(s), 775(s), 760(s), 725(s), 610(m), 405(s), 240(w). MS(calc, found): 370(6, 10), 371(8, 12), 372(44, 60), 373(32, 39), 374(100, 100), 375(36, 36), 376(19, 19), 377(4, 4).

Unit Cell Determination of Cp_4Ti_2O. A crystal measuring $0.1 \times 0.2 \times 0.4$ mm was sealed in a 0.2 mm quartz capillary tube in an argon filled dry box and mounted on an automated Picker FACS-1 diffractometer. An automated search followed by indexing yielded the following unit cell:

$a = 7.95(4)$ Å $\alpha = 89.3(4)$ °

b = 10.96(4) Åβ = 89.5(5) °

c = 19.8(1) Å γ = 88.3(3) °

These values are in agreement with the reported values in the orthorhombic space group Pbcn [25]

a = 7.946(1) Å

b = 11.102(2) Å

c = 19.780(3) Å.

Chapter Three

Cp^*_2TiCl, Cp^*_2TiBr, Cp^*_2TiI;[26] Cp^*_2TiMe, Cp^*_2TiEt, $Cp^*_2Ti(n\text{-}Pr)$, $Cp^*_2TiCH_2C(Me)_3$, Cp^*_2TiH, $Cp^*_2TiCH_2C_6H_5$;[27] $Cp^*_2TiN(Me)(Ph)$;[28] $Cp^*_2TiMe_2$;[29] Cp^*_2TiH;[30] and KC_8[15] were prepared by literature methods. Cp^*_2TiBr and Cp^*_2TiI were synthesized by Dr. Phil Matsunaga.[30] $(Ph_3P)AuCl$ was prepared by Dr. Richard Andersen. $Cp^*_2TiNH_2$ was initially made and characterized by Dr. Milton Rudolf Smith. Lithium amides and alkoxides were prepared by treating the amine or alcohol with *n*-BuLi in hexane.

$Cp^*_2TiNH_2$.[31] Cp^*_2TiMe[27] (0.93 g, 2.7 mmol) was dissolved in 40 mL of diethyl ether and cooled to -78 °C. Excess NH_3, dried over sodium, was condensed into the solution. The solution was allowed to warm to room temperature, and the initially green solution became dark purple-brown. After stirring for 4 hours, the volatile components were removed under reduced pressure. The dark solid residue was dissolved in 30 mL of hexane, and the solution was filtered. Cooling to -20 °C gave dark purple crystals (0.55 g, 59%). MP: 193-196 °C. IR 3437(m), 2721(m), 1535(s),

1491(s), 1023(s), 802(w), 634(s), 626(m), 616(s), 598(s), 486(s), 431(s), 395(m) cm^{-1}. Anal. Calcd for $C_{20}H_{32}NTi$: C, 71.8; H, 9.65; N, 4.20. Found: C, 71.7; H, 9.74; N, 4.14.

$Cp^*_2TiN(Me)H$. A mixture of Cp^*_2TiCl[26] (0.71 g, 2.0 mmol) and LiN(Me)H (0.09 g, 2.4 mmol) was suspended in 30 mL of diethyl ether. After stirring for twelve hours, the solvent was removed under reduced pressure, and the solid was suspended in 50 mL of hexane forming a lilac colored solution. The solution was filtered, and the volume of the filtrate was reduced to *ca.* 5 mL. Cooling to -20 °C gave green crystals (0.32 g, 46%). MP: = 202-205 °C. IR 3360(w), 2765(m), 2725(w), 1405(m), 1160(w), 1083(s), 1037(m), 1010(m), 790(w), 711(w), 617(w), 535(m), 494(s), 419(s), 378(m) cm^{-1}. MS $(M)^+$ *m/z* (calc, found) 347(12, 44), 348(100, 100), 349(31, 32), 350(12, 11). Anal. Calcd for $C_{21}H_{34}NTi$: C, 72.4; H, 9.84; N, 4.02. Found: C, 73.0; H, 9.89; N, 4.04.

$Cp^*_2TiF_2$. $Cp^*_2TiMe_2$[29] (1.15 g, 3.30 mmol) was dissolved in 70 mL of diethyl ether, and $BF_3 \cdot OEt_2$ (0.96 g, 6.8 mmol) was added slowly using a syringe. The yellow solution became orange. After stirring for twelve hours, the solvent was removed under reduced pressure, and the residue was heated to 90 °C under dynamic vacuum for 4 hours to remove $MeBF_2$. The yellow solid residue was dissolved in 100 mL of hexane, and the solution was filtered. The volume of the filtrate was reduced to *ca.* 20 mL. Cooling to -80 °C gave orange needles (1.1 g, 93 %). MP: = 207-208 °C. ^1H NMR δ 1.82(s). IR 2720(w), 1165(w), 1065(w), 1020(m), 810(w), 725(w), 635(w), 610(m), 580(s), 565(s), 545(m), 440(s), 390(m) cm^{-1}. MS $(M)^+$ *m/z* (calc, found) 354(10, 11), 355(12, 12), 356(100, 100), 357(30, 29), 358(11, 11), 359(2, 2). Anal. Calcd for $C_{20}H_{30}F_2Ti$: C, 67.4; H, 8.48. Found: C, 67.4; H, 8.59.

Cp^*_2TiF. A slurry of KC_8 (0.21 g, 2.0 mmol) in 20 mL of tetrahydrofuran was added by cannula to a solution of $Cp^*_2TiF_2$ (0.67 g, 1.9 mmol) dissolved in 10 mL of tetrahydrofuran. The solution immediately turned dark green. After stirring for three hours, the solvent was removed under reduced pressure. The solid residue was suspended in 100 mL of hexane. The dark green suspension was filtered, and the volume of the filtrate was reduced to *ca.* 10 mL. Cooling to -20 °C gave dark green crystals (0.40 g, 63 %). MP: 201-203 °C. IR 2720(w), 1165(w), 1065(w), 1025(m), 805(w), 725(w), 635(w), 610(w), 570(s), 450(s), 415(w), 395(w) cm^{-1}. MS $(M)^+$ *m/z* (calc, found) 335(11, 16), 336(12, 18), 337(100, 100), 338(30, 31), 339(11, 12). Anal. Calcd for $C_{20}H_{30}TiF$: C, 71.1; H, 8.96. Found: C, 70.9; H, 8.94.

$Cp^*_2TiOCH_3$. A mixture of Cp^*_2TiCl[26] (0.50g, 1.4 mmol) and $LiOCH_3$ (0.06 g, 1.6 mmol) was suspended in 40 mL of tetrahydrofuran. The solution was warmed to 70 °C for 3 hours during which time the solution turned red-orange. The suspension was allowed to cool to room temperature. After stirring for twelve hours, the solvent was removed under reduced pressure, and the solid residue was suspended in 50 mL of hexane. The red-purple suspension was filtered, and the volume of the filtrate was reduced to *ca.* 1 mL. Cooling to -20°C produced brown plates (0.33 g, 67 %). MP: 135-150 °C. IR 2790(s), 2720(w), 1270(w), 1150(s), 1075(m), 1025(m), 800(w), 760(m), 725(w), 660(w), 620(w), 550(m), 500(m), 420(m) cm^{-1}. MS $(M)^+$ *m/z* (calc, found) 347(11, 4), 348(12, 5), 349(100, 100), 350(31, 12), 351(12, 5). Anal. Calcd for $C_{21}H_{33}OTi$: C, 72.2; H, 9.52. Found: C, 71.7; H, 9.65.

$Cp^*_2TiOC_6H_5$. A mixture of Cp^*_2TiCl[26] (0.50 g, 1.4 mmol) and $LiOC_6H_5$ (0.16 g, 1.6 mmol) was dissolved in 30 mL tetrahydrofuran. The solution immediately became purple-red. After stirring for ten hours, the solvent was removed under reduced pressure, and the residue was suspended in 50 mL of hexane. The purple suspension

was filtered, and the volume of the filtrate was reduced to *ca.* 10 mL. Cooling to -20 °C gave big purple-brown crystals (0.48 g, 83 %). MP: 202-207 °C. IR: 2720(w), 2610(w), 1615(w), 1585(s), 1565(m), 1485(s), 1310(s), 1160(s), 1065(w), 1020(w), 995(m), 880(s), 750(s), 695(m), 630(w), 620(m), 605(w), 520(w), 430(m), 405(w), 360(m) cm^{-1}. MS $(M)^+$ *m/z* (calc, found) 409(10, 20), 410(13, 22), 411(100, 100), 412(36, 48), 413(13, 17), 414(3, 4). Anal. Calcd for $C_{26}H_{35}OTi$: C, 75.9; H, 8.57. Found: C, 76.3; H, 8.59.

$Cp^*_2TiN(Et)Ph$. A mixture of Cp^*_2TiCl[26] (0.50 g, 1.4 mmol) and LiN(Et)Ph (0.20 g, 1.6) mmol was suspended in 40 mL of diethyl ether. After stirring for 3 hours, the solvent was removed under reduced pressure. The black solid residue was suspended in 30 mL of hexane, and the mixture was filtered. The volume of the filtrate was reduced to *ca.* 3 mL. Cooling to -20 °C gave small black crystals (0.36 g, 58%). MP: 174 - 181 °C. IR 2720(w), 1370(s), 1355(w), 1340(w), 1305(s), 1280(s), 1185(m), 1135(w), 1090(m), 1020(s), 980(s), 850(m), 775(s), 745(s), 695(s), 635(m), 535(m), 485(w), 450(s), 420(m)m 405(s), 370(m), 345(s) cm^{-1}. MS $(M)^+$ *m/x* (calc, found) 437(13, 45), 438(100, 100), 439(39, 37), 440(14, 13), 441(2, 3). Anal. Calcd for $C_{28}H_{40}NTi$: C, 76.7; H, 9.19; H, 3.19. Found C, 76.0; H, 9.28; N, 3.36.

$Cp^*_2TiN(Me)Ph$.[28] IR(not previously reported) 3075(w), 3055(w), 2720(w), 2620(w), 2570(w), 1585(s), 1555(m), 1390(s), 1190(m), 1165(m), 1050(w), 1030(m), 990(s), 855(w), 825(s), 755(s), 705(m), 630(w), 545(w), 470(w), 420(m), 350(m) cm^{-1}.

$Cp^*_2TiLi(TMEDA)$. a) A mixture of Cp^*_2TiCl[26] (1.00 g, 2.83 mmol) and $[(TMEDA)Li]_2C_{10}H_8$[32,33] (1.08 g, 2.88 mmol) was cooled to -78 °C and powdered using the stirbar. The mixture was suspended in 100 mL of cold diethyl ether, and the solution was allowed to warm to room temperature while stirring. After stirring for

one hour at room temperature, the solution was green with a green precipitate. The diethyl ether was removed under reduced pressure. The dark green solid residue was heated to 95 °C under vacuum for 2 hours to remove $C_{10}H_8$. The dark solid residue was suspended in 200 mL of diethyl ether, the solution was heated to reflux and allowed to cool and settle. The dark red solution was filtered, and the volume of the filtrate was reduced to *ca.* 40 mL. Cooling to -20°C produced dark green blade shaped crystals (0.48 g, 38 %). The compound did not melt to 300 °C. IR 2715(w), 1365(w), 1290(m), 1250(s), 1185(w), 1160(m), 1130(s), 1100(m), 1040(m), 1020(s), 950(s), 890(w), 840(w), 795(s), 725(m), 630(w), 505(w), 470(w), 445(m), 410(s), 255(w) cm^{-1}. MS no parent ion, but peaks at *m/z* 316 and 116 corresponding to $Cp^*_2Ti^+$ and $TMEDA^+$ respectively. Anal. Calcd for $C_{26}H_{46}LiN_2Ti$: C, 70.7; H, 10.5; N, 6.34. Found: C, 70.7; H, 10.6; N, 6.07.

b) Cp^*_2TiH[30] (0.28 g, 0.88 mmol) was dissolved in 50 mL of hexane and cooled to -78°C. A mixture of TMEDA (0.15 mL, 0.11 g, 0.96 mmol) and *n*-BuLi (0.49 mL, 1.97 M in hexane, 0.96 mmol) was cooled to -78 °C, dissolved in 30 mL of hexane, and added to the solution of Cp^*_2TiH. The red solution immediately turned emerald green and was allowed to warm to room temperature. After stirring for one hour, the volatile components were removed under reduced pressure, and the green solid residue was suspended in 100 mL of diethyl ether. The solution was heated to reflux briefly and then allowed to settle. The green solution was filtered, and the volume of the filtrate was reduced to *ca.* 40 mL. Cooling to -20 °C produced dark green blades (0.25 g, 69%). The EPR spectrum and appearance of the compound is identical to that of compound prepared by route (a).

Evans' Method[34] Determination of μ_{eff} for $Cp^*_2TiLI(TMEDA)$.

$Cp^*_2TiLi(TMEDA)$ (22.9 mg, 5.19×10^{-5} mol) was dissolved in C_6D_6 plus 1 μL of cyclohexane in a volumetric flask to make 1 mL of solution. The solution was placed

in disposable pipettes with the tips sealed, and the pipettes were capped with rubber bulbs. The pipettes were cooled with liquid nitrogen and flame sealed forming small tubes of the $Cp^*_2TiLi(TMEDA)$ solution. A tube which contained this solution was wrapped at the top with Teflon tape and placed in an NMR tube containing 0.2 mL of a 1 mL solution of C_6D_6 containing 1 μL of cyclohexane. The frequency difference of the cyclohexane peaks was 8.2 Hz at 30 °C. $\chi_{gram} = (3\Delta\nu)/(2\pi\nu m) = 1.9 \times 10^{-6}$ cgs units where $\Delta\nu$ is the difference in frequency of the protons, ν is the spectrometer frequency, m is the mass of substance dissolved in 1 mL of solvent, and χ_0 is the susceptibility of the solvent. (Note: this formula is only good for an electromagnet NMR spectrometer not for a solenoidal superconducting NMR spectrometer.) $\chi_{corr} = MW\chi_{gram} + \chi_{dia} = 1.2 \times 10^{-3}$ cgs units where MW is the molecular weight of the substance and χ_{dia} is diamagnetic correction for the underlying diamangetism of the substance. $\mu_{eff} = (8\chi_{mol}T)^{1/2} = 1.7$ B. M. where T is the temperature in Kelvin (303).

$Cp^*_2TiLi(K211)$. A mixture of $Cp^*_2TiLi(TMEDA)$ (0.28 g, 0.63 mmol) and 4,7,13,18-tetraoxa-7,16-diazabicyclo[8.5.5]eicosane (K211) (0.18 g, 0.63 mmol) was dissolved in 40 mL of tetrahydrofuran, and the mixture was heated to reflux. After two hours, the solution had become dark red, and the volatile components were removed under reduced pressure giving a dark red oil. The oil was treated with 100 mL of diethyl ether giving a red solution and a red-brown precipitate. The solution was filtered leaving a red-brown powder (0.13 g, 33 %). MP: 270-274 °C. IR 2700(w), 1295(s), 1280(s), 1250(m), 1240(w), 1175(w), 1135(s), 1105(s), 1085(s), 1065(s), 1010(s), 940(m), 910(m), 855(w), 825(w), 810(m), 755(w), 740(m), 715(w), 550(s), 350(s) cm^{-1}. MS no parent ion, but peaks with *m/z* 136, and 288 corresponding to Cp* and K211. Anal. Calcd for $C_{34}H_{58}LiN_2O_4Ti$: C, 66.5; H, 9.53; N, 4.56. Found: C, 66.5; H, 9.61; N, 4.73.

[$Cp^*_2TiOLi(THF)]_2$•THF. $Cp^*_2TiLi(TMEDA)$ (0.50 g, 1.1 mmol) was dissolved in 30 mL of tetrahydrofuran, and cooled to -78 °C. A solution of degassed water (20.4 μL, 1.13 mmol) in 30 mL of tetrahydrofuran was added to the $Cp^*_2TiLi(TMEDA)$ solution by cannula. The solution turned a lighter green color and evolved gas over the course of three hours. After stirring for twelve hours, green solid had precipitated. An additional 100 mL of tetrahydrofuran was added to the mixture which was the heated to 80 °C and allowed to cool to room temperature. The solution was filtered. The volume of the filtrate was reduced to *ca.* 90 mL, and the soluiton was heated to 80 °C to redissolve the solid. Cooling to -20 °C produced large green prisms (0.27 g, 53 %). The compound does not melt to 250 °C. IR 2720(w), 160(w), 1020(m), 800(w), 705(s), 625(m), 610(m), 410(s), 370(w), 305(w) cm^{-1}. MS only a peak for Cp^*_2TiOH observed *m/z* 335; it is not known whether the complex was not volatile or was hydrolyzed. Anal. Calcd for $C_{52}H_{84}Li_2O_5Ti$: C, 69.5; N, 9.42. Found: C, 69.6; H, 9.53. Adding MeI to the EPR sample produces Cp^*_2TiOMe (g = 1.977).

Attempted reactions of $Cp^*_2TiLi(TMEDA)$ with hydrogen or ethylene. $Cp^*_2TiLi(TMEDA)$ (0.25 g, 0.57 mmol) was dissolved in 30 mL of toluene and transferred to a heavy-walled pressure bottle by cannula. The solution was pressurized to 100 psi with the gas. After stirring for 12 hours, the pressure was released, and the solution was transferred to a Schlenk tube by cannula. The ethylene reaction mixture contained a small amount of fluffy white solid (presumably polyethylene). The solution was filtered, and the volume of the filtrate was reduced to *ca.* 10 mL. Cooling to -20 °C gave dark green crystals: $Cp^*_2TiLi(TMEDA)$ by EPR.

$Cp^*_2TiLi(TMEDA)$ + CO. $Cp^*_2TiLi(TMEDA)$ (0.25 g, 0.57 mmol) was dissolved in 30 mL of toluene, and the solution was transferred to a heavy-walled pressure bottle by cannula. The green solution was pressurized to 125 psi with carbon monoxide. The

solution immediately became red and cloudy. After stirring for twelve hours, the solution was transferred to a Schlenk tube using a cannula and filtered. The volume of the filtrate was reduced to *ca.* 0.25 mL. Cooling to -20 °C produced red needles (0.12 g, 62%). The ^1H NMR spectrum (δ = 1.65 ppm), and the CO stretching frequencies (1920, 1840 cm^{-1}) agree with those previously reported for $Cp^*_2Ti(CO)_2$.[35]

$Cp^*_2TiLi(TMEDA) + NH_3$. $Cp^*_2TiLi(TMEDA)$ (0.35 g, 0.79 mmol) was dissolved in 50 mL of tetrahydrofuran and the Schlenk tube was cooled to 77 K with liquid nitrogen and was evacuated. Ammonia (181.8 mL, 78 torr, 0.83 mmol), dried over sodium, was condensed onto the frozen $Cp^*_2TiLi(TMEDA)$ solution. The mixture was warmed to -78 °C, and the Schlenk tube was filled with argon. The mixture was allowed to warm to room temperature while stirring. The solution became green and a pale solid precipitated. After 4 hours, the tetrahydrofuran was removed under reduced pressure, and the green solid was suspended in 125 mL of tetrahydrofuran. The solution was filtered, and the volume of the filtrate was reduced to *ca.* 5 mL. Cooling to -20 °C produced green crystals (0.04 g) of unreacted $Cp^*_2TiLi(TMEDA)$ as identified by EPR spectroscopy. The volume of the mother liquor was reduced to *ca.* 0.5 mL. Cooling to -20 °C produced a green solid (0.12 g, 45 %) which was found to be $Cp^*_2TiNH_2$ by EPR and IR spectroscopy. The product was contaminated some unreacted $Cp^*_2TiLi(TMEDA)$.

$Cp^*_2TiLi(TMEDA)$ + MeI. $Cp^*_2TiLi(TMEDA)$ (0.25 g, 0.57 mmol) was dissolved in 40 mL of tetrahydrofuran and cooled to -78 °C. MeI (35 µL, 0.080 g, 0.56 mmol) dissolved in 20 mL of tetrahydrofuran was added to the $Cp^*_2TiLi(TMEDA)$ solution using a cannula. The solution was allowed to warm to room temperature. The solution slowly turned purple over several hours. After stirring for twelve hours, the THF was

removed under reduced pressure. The dark solid residue was suspended in 20 mL of hexane, and the mixture was filtered giving a purple solution. The volume of the filtrate was reduced to *ca.* 1 mL. Cooling to -20 °C gave purple crystals whose IR and EPR spectra agree with those of $Cp^*Ti(\eta^6\text{-}H_2CC_5Me_4)$[35,36] (prepared by the decomposition of Cp^*_2TiEt).

$Cp^*_2TiLi(TMEDA)$ + $(Ph_3P)AuCl$. $(Ph_3P)AuCl$ (0.28 g, 0.57 mmol) was dissolved in 50 mL of toluene. $Cp^*_2TiLi(TMEDA)$ (0.25 g, 0.57 mmol) was dissolved in 50 mL of toluene and added by cannula to the $(Ph_3P)AuCl$ solution. The solution instantly turned purple. After stirring for twelve hours, the toluene was removed under reduced pressure The purple solid was suspended in 60 mL of hexane, and the solution was filtered. The volume of the filtrate was reduced to *ca.* 2 mL. Cooling to -20° produced purple needles (0.18 g) which were a mixture of $Cp^*Ti(\eta^6\text{-}H_2CC_5Me_4)$ and PPh_3 as determined by ^1H NMR, IR, and EPR spectroscopy.

References

(1) Guenther, D.; Jaffe, A. *Horizon;* 1.3.0 ed.; Blue Star Software, Inc.: Honolulu, 1992.

(2) Rehr, J. J.; Zabinsky, S. I.; Albers, R. D. *Phys. Rev. Lett.* **1992**, *69*, 3397.

(3) Blake, P. C.; Lappert, M. F.; Taylor, R. G. In 1990; Vol. 27; pp 172.

(4) Blake, P. C.; Lappert, M. F.; Taylor, R. G.; Atwood, J. L.; Hunter, W. E.; Zhang, H. *J. Chem. Soc., Chem. Commun.* **1986**, 1394-1395.

(5) Blake, P. C.; Lappert, M. F.; Taylor, R. G.; Atwood, J. L.; Zhang, H. *Inorg. Chim. Acta* **1987**, *129*, 12-20.

(6) Stewart, A. L.; Unpublished results

(7) Venier, C. G.; Casserly, E. W. *J. Am. Chem. Soc.* **1990**, *112*, 2808-2809.

(8) Riemschneider, R. *Z. Naturforsch. B* **1963**, *18*, 641-645.

(9) Beshouri, S. M., Unpublished results

(10) Duff, A. W.; Hitchcock, P. B.; Lappert, M. F.; Taylor, R. G.; Segal, J. A. *J. Organomet. Chem.* **1985**, *293*, 271-283.

(11) Rosen, R. K., Unpublished results

(12) Blosch, L. L., Unpublished results

(13) Andersen, R. A. *Inorg. Chem.* **1979**, *18*, 1507-1509.

(14) Bradley, D. C.; Ghotra, J. S.; Hart, F. A. *J. Chem. Soc., Dalton Trans.* **1973**, 1021-1023.

(15) Schwindt, M. A.; Lejon, T.; Hegedus, L. B. *Organometallics* **1990**, *9*, 2814-2819.

(16) Rogers, R. D.; Bynum, R. V.; Atwood, J. L. *J. Am. Chem. Soc.* **1978**, *100*, 5238-5239.

(17) Lokshin, B. V.; Klemenkova, Z. S.; Ezernitskaya, M. G.; Strunkina, L. I.; Brainina, E. M. *J Organomet Chem* **1982**, *235*, 69 - 75.

(18) Etievant, P.; Gautheron, B.; Tainturier, G. *Bull. Soc. Chim. Fra.* **1978**, *5-6*, 292-298.

(19) Canty, A. J.; Coutts, R. S. P.; Wailes, P. C. *Aust. J. Chem.* **1968**, *21*, 807 - 810.

(20) Siegert, F. W.; de Lifde Meijer, H. J. *J. Organomet. Chem.* **1968**, *15*, 131-137.

(21) Fischer, E. O.; Löchner, A. *Z. Naturforsch.* **1960**, *15b*, 266.

(22) Coutts, R.; Wailes, P. C. *Inorg. Nucl. Chem. Lett.* **1967**, *3*, 1-5.

(23) Schinnerling, P.; Thewalt, U. *J. Organomet. Chem.* **1992**, *431*, 41 - 45.

(24) Fachinetti, G.; Floriani, C.; Chiesi-Villa, A.; Guastini, G. *J. Am. Chem. Soc.* **1979**, *101*, 1767-1775.

(25) Honold, B.; Thewalt, U.; Herberhold, M.; Alt, H. G.; Kool, L. B.; Rausch, M. D. *J. Organomet. Chem.* **1986**, *314*, 105 - 111.

(26) Pattiasina, J. W.; Heeres, H. J.;van Bolhuis, F.; Meetsma, A.; Teuben, J. H. *Organometallics* **1987**, *6*, 1004-1010.

(27) Luinstra, G. A.; ten Cate, L. C.; Heeres, H. J.; Pattiasina, J. W.; Meetsma, A.; Teuben, J. H. *Organometallics* **1991**, *10*, 3227-3237.

(28) Feldman, J.; Calabrese, J. C. *J. Chem. Soc., Chem. Commun.* **1991**, 1042-1044.

(29) Bercaw, J. E.; Marvich, R. H.; Bell, L. G.; Brintzinger, H. H. *J. Am. Chem. Soc.* **1972**, *94*, 1219.

(30) Matsunaga, P. T. Ph. D. Thesis, University of California, Berkeley, 1991.

(31) Smith III, M. R., Unpublished results

(32) Brooks, J. J.; Rhine, W.; Stucky, G. D. *J. Am. Chem. Soc.* **1972**, *94*, 7346.

(33) Kahn, B. E.; Rieke, R. D. *Organometallics* **1988**, *7*, 463-469.

(34) Evans, D. F. *J. Chem. Soc.* **1959**, 2003-2005.

(35) Bercaw, J. E.; Marvich, R. H.; Bell, L. G.; Brintzinger, H. H. *J. Am. Chem. Soc.* **1972**, *94*, 1219.

(36) Luinstra, G. A.; Teuben, J. H. *J. Am. Chem. Soc.* **1992**, *114*, 3361 - 3367.

Appendix One: Crystallography Details

$Cp"_2UCl_2$:

Orange needles of the compound were grown by cooling a saturated hexane solution to -30 °C. The crystals were dried under reduced pressure and loaded into quartz capillaries in an inert atmosphere box. A crystal measuring 0.08 × 0.20 × 0.60 mm was transferred to an automated Picker FACS-1 diffractometer. The crystal was centered in the beam. Automatic peak search and indexing procedures indicated that the crystal possessed a body centered monoclinic cell and yielded the cell parameters. The cell parameters and data collection parameters are given in the following table.

The 5882 raw intensity data were converted to structure factor amplitudes and their esds by correction for scan speed, background, and Lorentz-polarization effects.[1] Inspection of the intensity standards showed no great change in intensity. An intensity correction varying from 1.073 to 0.982 was applied to the data. The systematic absences (h,0,l), h odd; and (h,0,l), l odd were then rejected and the data were averaged (R_{int}= 0.030) yielding 2818 unique data of which 2179 had $F_o > 3\sigma(F_o)$. Azimuthal scan data showed fairly flat absorption curves. No absorption correction was applied. The systematic absences indicated that the space group was I2/a or I2/c. I2/a was chosen.

The cell volume indicates that 4 molecules are present in the unit cell. The uranium atom had to be on a special position. Since the molecule could have C_2 symmetry, the first special position was chosen. The uranium atom position, and the position of the chlorine and silicon atoms were obtained by solving the Patterson map. Successive Fourier searches yielded the rest of the heavy atom positions. The heavy atom structure was refined by standard least squares and Fourier techniques. The heavy atoms were refined anisotropically. The hydrogen atoms were located in a difference Fourier, and the hydrogen positions were then calculated based upon idealized bonding

geometry and assigned thermal parameters equal to 5 $Å^2$ for the cyclopentadienyl hydrogen atoms and 10 $Å^2$ for the trimethylsilyl hydrogen atoms. After one least squares cycle, the hydrogen atoms were refined isotropically. A final difference Fourier map showed no additional atoms in the asymmetric unit. Examination of intermolecular close contacts (<3.5Å) showed that the molecule was a monomer.

The final residuals for 216 variables refined against the 2179 unique data with $F_o > 3\sigma(F_o)$ were R = 2.3%, R_w = 2.8%, and GOF = 0.83. The R value for all data (including unobserved reflections) was 4.2%. The quantity minimized by the least squares refinements was $w(|F_o| - |F_c|)^2$, where w is the weight given to a particular reflection. The p-factor, used to reduce the weight of intense reflections, was set to 0.05.[2] The analytical forms of the scattering factor tables for neutral atoms were used and all non-hydrogen scattering factors were corrected for both the real and imaginary components of anomalous dispersion.[3] The largest positive and negative peaks in the final difference Fourier map have electron densities of 0.51 and -0.49.

Crystal Data for Cp''_2UCl_2

Space group:	I2/a
a, Å	22.28(1)
b, Å	7.069(4)
c, Å	20.558(8)
α, deg.	90
β, deg.	102.03(3)
γ, deg.	90
V, $Å^3$	3166.87
Z	4.2
fw	680.98
d (calc.) g/cm^3	1.428
μ (calc.) 1/cm	50.154
radiation	MoKα(λ= 0.71073 Å)
monochrometer	highly oriented graphite
scan range, type	$4° \leq 2\theta \leq 50°$, θ-2θ
scan speed, deg/min	2-8, variable
scan width, deg	$\Delta\theta = 1.50 + 0.693\tan\theta$
reflections collected	5822; ±h,+k,±l
unique reflections	2818
reflections $F_o^2 > 3\sigma(F_o^2)$	2179
R, %	2.3
R_w, %	2.8
R_{all}, %	4.2
GOF	0.83
Largest Δ/σ in final least squares cycle	0

Intensity standards: (6, 0, 0); (0, 0, 4); (0, 4, 0) measured every 250 reflections. The intensity changed little over the experiment.

Orientation Standards: 2 reflections were checked after every 5000 measurements. Crystal orientation was redetermined if any of the reflections were offset from their predicted positions by more than 0.1°. Reorientation was done once over the course of the data collection. The cell constants and errors are listed as their final values.

Table of atomic positions in Cp''_2UCl_2

Atom	X	Y	Z
U	0.250000	0.097323	0.000000
Cl	0.277106	0.342592	-0.081748
Si(1)	0.387992	-0.111586	-0.085529
Si(2)	0.377276	0.164344	0.178346
C1	0.357575	-0.074381	-0.007968
C2	0.373425	0.073437	0.038452
C3	0.351488	0.037286	0.097436
C4	0.320495	-0.138458	0.085921
C5	0.324743	-0.207319	0.022900
C6	0.432283	0.101320	-0.098857
C7	0.325929	-0.156457	-0.158867
C8	0.437840	-0.325629	-0.070626
C9	0.321484	0.134668	0.232532
C10	0.451289	0.054148	0.219290
C11	0.390977	0.414211	0.162460
H2	0.395205	0.183948	0.031966
H4	0.301677	-0.203462	0.118432
H5	0.309721	-0.359645	0.004764
H6a	0.465987	0.086551	-0.063727
H6b	0.403883	0.209836	-0.111599
H6c	0.442856	0.113729	-0.142585
H7a	0.298070	-0.055607	-0.170906
H7b	0.299102	-0.260937	-0.150712
H7c	0.341871	-0.137727	-0.199202
H8a	0.417394	-0.424854	-0.056704
H8b	0.471971	-0.277463	-0.045018
H8c	0.451917	-0.370835	-0.108933
H9a	0.311887	-0.004724	0.236230
H9b	0.284839	0.203914	0.216045
H9c	0.337970	0.179510	0.277307
H10a	0.480379	0.073303	0.188912
H10b	0.444103	-0.069603	0.223022
H10c	0.461248	0.102586	0.261963
H11a	0.356010	0.480676	0.136815
H11b	0.414780	0.459199	0.129478
H11c	0.401906	0.481641	0.200678

Table of atomic thermal parameters for $Cp"_2UCl_2$ in $Å^2$

Atom	B(1,1) or B_{iso}	B(2,2)	B(3,3)	B(1,2)	B(1,3)	B(2,3)
U	3.6806	2.5558	3.0634	0	0.4894	0
Cl	5.9028	4.6549	4.7924	-1.0662	0.7692	1.1319
Si(1)	5.5603	5.0902	4.8106	0.5903	1.9842	-1.0207
Si(2)	4.6382	5.1213	3.4920	1.1593	-0.0415	-0.4366
C1	4.7250	3.5916	4.1190	0.6285	0.8755	-0.5895
C2	3.8635	3.4654	4.0435	0.3470	0.7098	-0.0812
C3	4.2294	3.8670	3.6015	0.7987	0.6578	0.0521
C4	5.1326	3.4201	4.0269	0.9282	1.1135	0.6952
C5	5.1676	2.9346	4.4837	0.3154	1.1955	-0.0430
C6	8.3623	7.6944	7.2601	-1.3034	3.9413	-0.0751
C7	8.0107	9.0931	4.29	-0.1099	1.4795	-0.6849
C8	8.5993	7.1854	9.5457	2.9871	2.8975	-1.3265
C9	7.3904	10.5791	3.7147	0.7251	1.2403	-0.87
C10	6.5927	10.1483	5.6106	3.2586	-1.3490	-1.3993
C11	8.9502	6.58	6.9673	-1.1198	-1.0687	-0.4931
H2	2.8274					
H4	3.4973					
H5	6.9707					
H6a	10.5038					
H6b	14.1334					
H6c	8.5997					
H7a	8.6364					
H7b	9.2501					
H7c	12.4116					
H8a	15.1592					
H8b	14.2434					
H8c	11.0379					
H9a	11.8120					
H9b	9.9658					
H9c	8.6533					
H10a	10.3623					
H10b	6.9437					
H10c	10.0977					
H11a	10.0796					
H11b	11.1673					
H11c	10.2021					

The form of the anisotropic temperature factor is:

$$\exp[-0.25\{h^2a^2B(1,1) + k^2b^2B(2,2) + l^2c^2B(3,3) + 2hkabB(1,2) + 2hlacB(1,3) + 2klbcB(2,3)\}]$$

where a,b, and c are reciprocal lattice constants.

$[Cp''_2UF_2]_2$

Dark green crystals of the compound were grown by heating a hexane solution to about 80 °C then cooling slowly to room temperature. A suitable, roughly cubic crystal measuring 0.28 mm × 0.30 mm × 0.30 mm was mounted on the end of a 0.2 mm thin walled glass capillary. The crystal was transferred to an Enraf-Nonius CAD-4 diffractometer and cooled to -111 °C under a cold stream previously calibrated by a thermocouple placed in the sample position. The crystal was centered in the beam. Automatic peak search and indexing procedures indicated that the crystal was possessed a primitive monoclinic cell and yielded the unit cell parameters. The cell parameters and data collection parameters are given in the following table.

The data was collected in two blocks (+h,±k,+l) and (+h,+k,-l). The 5868 raw intensity data were converted to structure factor amplitudes and their esds by correction for scan speed, background, and Lorentz-polarization effects.[1] Inspection of the intensity standards showed no decrease in intensity over the duration of data collection for the first block of data and a 5% decrease in intensity for the second block of data. The second block was then corrected for a decay of 5%. The 157 systematic absences (0,k,0), k odd, and (h,0,l), h+l odd and the 1499 redundant data (+h,-k,+l) and the 195 duplicated (h,k,0) data were then rejected yielding 4007 unique data. No empirical absorption correction could be applied because a large piece of ice had grown on the glass capillary, and when the goniomenter head was raised to 90° in χ, the capillary snapped off. Inspection of the collected data showed systematic absences for (0,k,0), k odd and (h,0,l), h+l odd indicating that the space group was $P2_1/n$.

The molecule was initially believed to be a monomer with Z=4. The uranium atom positions were obtained by solving the Patterson map. Refinement on the uranium positions followed by a difference Fourier search yielded the other heavy atom positions. The heavy atom structure was refined by standard least squares and Fourier techniques.

The heavy atoms were refined isotropically, and the hydrogen atom positions were calculated. A numerical absorption correction (DIFABS) was applied, and the heavy atom positions were refined anisotropically with the hydrogen atoms in calculated positions. The hydrogen positions were calculated based upon idealized bonding geometry and assigned thermal parameters equal to 1.3 $Å^2$ larger than the carbon atom to which they were connected. The hydrogen positions were included in the structure factor calculations but not refined by least squares. A final difference Fourier map showed no additional atoms in the asymmetric unit. Examination of intermolecular close contacts(<3.5Å) showed that the molecule was actually a dimer with two bridging fluoride ligands.

The final residuals for 263 variables refined against the 4007 unique data with $F_o > 3\sigma(F_o)$ were R = 3.35%, R_w = 3.58%, and GOF = 1.97. The R value for all data (including unobserved reflections) was 5.42%. The quantity minimized by the least squares refinements was $w(|F_o| - |F_c|)^2$, where w is the weight given to a particular reflection. The p-factor, used to reduce the weight of intense reflections, was set to 0.03 initially, but later changed to 0.02.[2] The analytical form of the scattering factor tables for neutral atoms were used and all non-hydrogen scattering factors were corrected for both the real and imaginary components of anomalous dispersion.[3]

Inspection of the residuals ordered in the ranges of $\sin(\theta/\lambda)$, $|F_o|$, and parity and values of the individual indexes showed no trends. Fourteen reflections had anomalously high values of $w\Delta^2$, and were weighted to zero toward the end of the refinement. The largest positive and negative peaks in the final difference Fourier map have electron densities of 0.93 and -0.30, respectively, and are associated with the uranium atom.

Crystal Data for $[Cp"_2UF_2]_2$

Space group:	$P2_1/n$
a, Å	11.519(3)
b, Å	21.892(7)
c, Å	12.846(3)
α, deg.	90
β, deg.	116.07(2)
γ, deg.	90
V, Å^3	2910
Z	2
fw	1389.90
d (calc.) g/cm^3	1.586
μ (calc.) 1/cm	54.708
radiation	MoKα(λ= 0.71073 Å)
monochrometer	highly oriented graphite
scan range, type	$3° \leq 2\theta \leq 45°$, θ-2θ
scan speed, deg/min	3
scan width, deg	$\Delta\theta = 0.90 + 0.35\tan\theta$
reflections collected	5868; +h, ±k, +l; +h,+k,-l
unique reflections	4007
reflections $F_o^2 > 3\sigma(F_o^2)$	3109
R, %	3.35
R_w, %	3.38
R_{all}, %	5.42
GOF	1.97
Largest Δ/σ in final least squares cycle	0

Intensity standards: (1,4,2); (2,6,4); (3,1,-6) measured every hour of x-ray exposure time. The first block of data showed no decay. The second block of data showed a 5% linear decay over the collection period and was corrected for.

Orientation Standards: 3 reflections were checked after every 200 measurements. Crystal orientation was redetermined if any of the reflections were offset from their predicted positions by more than 0.1°. Reorientation was required seventeen times over the course of the data collection due to the growth of ice on the capillary. The cell constants and errors are listed as their final values.

Table of atomic positions in $[Cp''_2UF_2]_2$

Atoms	X	Y	Z	B_{eq} (A^2)
U	0.00474(1)	0.02395(1)	0.15006(1)	1.392(6)
SI1	-0.1723(2)	0.1699(1)	0.2210(2)	2.05(6)
SI2	-0.2855(2)	-0.0869(1)	0.1972(2)	2.36(6)
SI3	0.1612(2)	-0.1562(1)	0.2569(2)	2.06(6)
SI4	0.3626(2)	0.0940(1)	0.3432(2)	1.97(6)
F1	0.0584(4)	0.1151(2)	0.1759(4)	2.1(1)
F2	-0.0320(5)	-0.0511(2)	0.0143(4)	2.4(1)
C1	-0.1786(7)	0.0362(4)	0.2321(6)	1.7(2)
C2	-0.1919(7)	0.0896(4)	0.1674(7)	1.8(2)
C3	-0.2388(8)	0.0688(4)	0.0484(6)	2.2(2)
C4	-0.2587(8)	0.0056(4)	0.0447(6)	2.0(2)
C5	-0.2217(7)	-0.0161(4)	0.1595(6)	1.9(2)
C6	0.2478(7)	-0.0281(4)	0.2651(6)	1.8(2)
C7	0.1653(7)	-0.0718(4)	0.2806(6)	1.5(2)
C8	0.1201(7)	-0.0413(4)	0.3537(6)	1.7(2)
C9	0.1708(7)	0.0184(4)	0.3750(7)	1.8(2)
C10	0.2527(7)	0.0272(4)	0.3233(6)	1.8(2)
C11	-0.3257(8)	0.1909(5)	0.2274(8)	3.3(2)
C12	-0.1455(9)	0.2227(4)	0.1215(8)	3.3(3)
C13	-0.0390(9)	0.1739(5)	0.3707(8)	3.9(3)
C14	-0.1645(9)	-0.1250(5)	0.3305(7)	3.1(2)
C15	-0.352(1)	-0.1409(5)	0.0756(8)	4.3(3)
C16	-0.4207(9)	-0.0594(6)	0.2275(9)	5.6(3)
C17	0.3071(9)	-0.1768(4)	0.2369(8)	3.2(3)
C18	0.0146(9)	-0.1836(4)	0.1303(8)	3.4(3)
C19	0.1759(9)	-0.1948(4)	0.3912(8)	3.1(3)
C20	0.533(1)	0.0691(5)	0.432(1)	4.8(3)
C21	0.352(1)	0.1227(5)	0.2054(8)	4.1(3)
C22	0.324(1)	0.1544(5)	0.4248(9)	4.9(3)
H1	-0.14497(1)	0.03509(1)	0.31412(1)	2.3*
H3	-0.25363(1)	0.09398(1)	-0.01643(1)	2.8*
H4	-0.29151(1)	-0.01890(1)	-0.02334(1)	2.6*
H6	0.29415(1)	-0.03524(1)	0.22073(1)	2.3*
H8	0.06488(1)	-0.05848(1)	0.38328(1)	2.2*
H9	0.15158(1)	0.04841(1)	0.41862(1)	2.4*
H11A	-0.31994(1)	0.23174(1)	0.25444(1)	4.3*
H11B	-0.39561(1)	0.18772(1)	0.15223(1)	4.3*
H11C	-0.33984(1)	0.16410(1)	0.27883(1)	4.3*
H12A	-0.13590(1)	0.26310(1)	0.15091(1)	4.3*
H12B	-0.06949(1)	0.21102(1)	0.11507(1)	4.3*
H12C	-0.21746(1)	0.22097(1)	0.04726(1)	4.3*
H13A	-0.02922(1)	0.21480(1)	0.39775(1)	5.1*
H13B	-0.05898(1)	0.14835(1)	0.42042(1)	5.1*
H13C	0.03923(1)	0.16046(1)	0.37025(1)	5.1*

Table of atomic positions in $[Cp''_2UF_2]_2$ (continued)

Atoms	X	Y	Z	B_{eq} (A^2)
H14A	-0.20169(1)	-0.16062(1)	0.34567(1)	4.0*
H14B	-0.09099(1)	-0.13613(1)	0.31936(1)	4.0*
H14C	-0.13914(1)	-0.09776(1)	0.39422(1)	4.0*
H15A	-0.38305(1)	-0.17612(1)	0.09827(1)	5.5*
H15B	-0.42057(1)	-0.12202(1)	0.01159(1)	5.5*
H15C	-0.28581(1)	-0.15243(1)	0.05402(1)	5.5*
H16A	-0.45871(1)	-0.09311(1)	0.24757(1)	7.2*
H16B	-0.38829(1)	-0.03114(1)	0.28992(1)	7.2*
H16C	-0.48384(1)	-0.03995(1)	0.16042(1)	7.2*
H17A	0.30763(1)	-0.21953(1)	0.22465(1)	4.1*
H17B	0.30541(1)	-0.15559(1)	0.17172(1)	4.1*
H17C	0.38261(1)	-0.16564(1)	0.30425(1)	4.1*
H18A	0.01926(1)	-0.22663(1)	0.12372(1)	4.4*
H18B	-0.05996(1)	-0.17347(1)	0.14051(1)	4.4*
H18C	0.00937(1)	-0.16466(1)	0.06182(1)	4.4*
H19A	0.17405(1)	-0.23781(1)	0.38083(1)	4.1*
H19B	0.25528(1)	-0.18343(1)	0.45426(1)	4.1*
H19C	0.10605(1)	-0.18286(1)	0.40707(1)	4.1*
H20A	0.58965(1)	0.10259(1)	0.44306(1)	6.3*
H20B	0.54252(1)	0.05512(1)	0.50573(1)	6.3*
H20C	0.55379(1)	0.03694(1)	0.39381(1)	6.3*
H21A	0.40955(1)	0.15632(1)	0.21981(1)	5.4*
H21B	0.37612(1)	0.09113(1)	0.16766(1)	5.4*
H21C	0.26648(1)	0.13542(1)	0.15742(1)	5.4*
H22A	0.37904(1)	0.18859(1)	0.43554(1)	6.4*
H22B	0.23652(1)	0.16667(1)	0.38236(1)	6.4*
H22C	0.33692(1)	0.13896(1)	0.49817(1)	6.4*
CP1	-0.21795(1)	0.03679(1)	0.13042(1)	0.3*
CP2	0.19134(1)	-0.01911(1)	0.31956(1)	0.3*

Starred atoms were included with isotropic thermal parameters. The thermal parameter given for anisotropically refined atoms is the isotropic equivalent thermal parameter defined as:

$$(4/3)[a^2B(1,1) + b^2B(2,2) + c^2B(3,3) + ab(\cos\gamma)B(1,2) + ac(\cos\beta)B(1,3) + bc(\cos\alpha)B(2,3)]$$

where a,b,c are real cell parameters, and B(i,j) are anisotropic betas.

Table of anisotropic thermal parameters for $[Cp"_2UF_2]_2$

Atom	B(1,1)	B(2,2)	B(3,3)	B(1,2)	B(1,3)	B(2,3)
U	1.417(9)	1.39(1)	1.379(9)	-0.06(2)	0.621(7)	-0.06(1)
SI1	2.01(9)	1.9(1)	2.35(9)	0.28(9)	1.04(6)	0.02(9)
SI2	1.90(9)	2.7(1)	2.43(9)	-0.62(9)	0.88(7)	0.19(9)
SI3	2.35(9)	1.6(1)	2.33(9)	-0.14(9)	1.12(7)	-0.01(9)
SI4	1.93(9)	1.7(1)	2.21(9)	-0.39(9)	0.83(7)	-0.24(8)
F1	2.8(2)	1.3(2)	2.5(2)	0.1(2)	1.5(1)	0.1(2)
F2	3.4(2)	2.1(2)	1.9(2)	-0.6(2)	1.2(1)	-0.1(2)
C1	1.5(3)	2.5(4)	1.1(3)	0.1(3)	0.4(2)	0.0(3)
C2	1.2(3)	1.8(4)	2.6(3)	0.2(3)	1.2(2)	0.3(3)
C3	1.8(3)	3.1(4)	1.4(3)	0.3(4)	0.5(2)	0.5(3)
C4	1.4(3)	2.8(4)	1.3(3)	-0.5(3)	0.1(2)	-0.9(3)
C5	1.5(3)	1.8(4)	2.2(3)	-0.2(3)	0.7(2)	0.9(3)
C6	1.7(3)	2.1(4)	1.4(3)	0.5(3)	0.6(2)	-0.4(3)
C7	1.8(3)	1.7(4)	0.7(3)	-0.3(3)	0.3(2)	0.3(3)
C8	1.5(3)	1.6(4)	2.0(3)	-0.1(3)	0.9(2)	0.1(3)
C9	1.7(3)	1.2(3)	2.4(3)	0.2(3)	0.7(2)	-0.1(3)
C10	0.9(3)	2.2(4)	1.4(3)	0.3(4)	-0.2(2)	0.1(3)
C11	3.4(4)	2.9(5)	4.8(4)	-0.0(4)	2.8(3)	-0.4(4)
C12	3.7(4)	1.9(4)	5.1(4)	0.1(4)	2.6(3)	0.4(4)
C13	3.5(4)	4.0(5)	3.5(4)	1.1(4)	0.9(3)	-1.0(4)
C14	3.0(4)	3.2(5)	3.2(4)	-1.0(4)	1.5(3)	0.3(4)
C15	5.0(5)	4.4(5)	2.6(4)	-2.6(4)	0.9(3)	0.0(4)
C16	2.8(4)	8.0(8)	6.3(5)	-0.9(5)	2.3(3)	1.4(6)
C17	3.5(4)	2.5(4)	3.7(4)	0.3(4)	1.7(3)	-0.3(4)
C18	3.5(4)	1.8(4)	4.6(5)	-0.6(4)	1.6(3)	-1.0(4)
C19	3.6(4)	2.3(4)	3.1(4)	-0.5(4)	1.2(3)	0.3(4)
C20	2.2(4)	3.7(5)	6.4(6)	-0.5(5)	-0.2(4)	0.4(5)
C21	4.2(4)	5.2(6)	2.5(4)	-2.5(4)	1.1(3)	0.2(4)
C22	5.3(4)	4.3(6)	6.9(5)	-2.4(4)	4.4(3)	-2.3(5)

The form of the anisotropic temperature factor is:

$$\exp[-0.25\{h^2\acute{a}^2B(1,1) + k^2b^2B(2,2) + l^2c^2B(3,3) + 2hkabB(1,2) + 2hlacB(1,3) + 2klbcB(2,3)\}]$$

where a,b, and c are reciprocal lattice constants.

$Cp^{\ddagger}_2UF_2$

Light orange crystals of the compound were grown by cooling a hexane solution to -20 °C. The supernatant was removed using a cannula, and degassed Paratone N, a high molecular weight, aliphatic hydrocarbon oil was poured into the Schlenk tube. The Paratone N containing the crystals was then scooped out into a Petri dish and more Paratone N was added. A suitable, square crystal measuring 0.28 mm × 0.28 mm × 0.08 mm was mounted on the end of a 0.2 mm thin walled glass capillary. The crystal was transferred to an Enraf-Nonius CAD-4 diffractometer and cooled to -88 °C under a cold stream previously calibrated by a thermocouple placed in the sample position. The crystal was centered in the beam. Automatic peak search and indexing procedures indicated that the crystal was possessed a primitive monoclinic cell and yielded the unit cell parameters. The cell parameters and data collection parameters are given in the following table.

Inspection of the raw data indicated that the space group contained and n-glide plane, so the centric space group P2/n was chosen. The 1930 raw intensity data were converted to structure factor amplitudes and their esds by correction for scan speed, background, and Lorentz-polarization effects.[1] Inspection of the intensity standards showed no decrease in intensity over the duration of data collection. Inspection of the azimuthal scan data showed a variation of $I_{min}/I_{max} = 0.52$ for the averaged curve. An empirical absorption correction was applied to the intensity data based upon the average curve. Removal of the 181 systematic absences (h,0,l), h+l odd and the 68 redundant data (+h, +k,-l) left 1684 unique data.

The uranium atom positions were obtained by solving the Patterson map. The uranium atom was on a special position (0.25, 0.13, 0.25) with 2 fold rotational symmetry. Refinement on the uranium positions followed by a difference Fourier search yielded the other heavy atom positions. The heavy atom structure was refined by

standard least squares and Fourier techniques. The heavy atoms were refined with isotropic and then anisotropic thermal parameters. The hydrogen positions were calculated based upon idealized bonding geometry and assigned thermal parameters equal to 1.15 $Å^2$ larger than the carbon atom to which they were connected. The hydrogen positions were included in the structure factor calculations but not refined by least squares. Towards the end of the refinement, examination of the extinction test listing indicated that secondary extinction was occurring. The secondary extinction coefficient was initially set to 1.7×10^{-7} and was refined to a final value of 2.67×10^{-7}. A final difference Fourier map showed no additional atoms in the asymmetric unit. No close (< 3.5 Å) intermolecular contacts were found.

The final residuals for 133 variables refined against the 1415 unique data with $F_o > 3\sigma(F_o)$ were R = 1.78%, R_w = 2.20%, and GOF = 1.19. The R value for all data (including unobserved reflections) was 2.02%. The quantity minimized by the least squares refinements was $w(|F_o| - |F_c|)^2$, where w is the weight given to a particular reflection. The p-factor, used to reduce the weight of intense reflections, was set to 0.03.[2] The analytical form of the scattering factor tables for neutral atoms were used and all non-hydrogen scattering factors were corrected for both the real and imaginary components of anomalous dispersion.[3]

Inspection of the residuals ordered in the ranges of $\sin(\theta/\lambda)$, $|F_o|$, and parity and values of the individual indexes showed no trends other than the previously mentioned secondary extinction. No reflections had anomalously high values of $w\Delta^2$. The largest positive and negative peaks in the final difference Fourier map have electron densities of 1.02 and -0.54, respectively, and are associated with the uranium atom.

Crystal Data for $Cp^{\ddagger}_2UF_2$

Space group:	P2/n
a, Å	14.155(4)
b, Å	6.302(1)
c, Å	14.250(5)
α, deg.	90
β, deg.	92.46(3)
γ, deg.	90
V, $Å^3$	1270
Z	2
fw	630.65
d (calc.) g/cm^3	1.65
μ (calc.) 1/cm	60.83
radiation	MoKα(λ= 0.71073 Å)
monochrometer	highly oriented graphite
scan range, type	$3° \leq 2\theta \leq 45°$, θ-2θ
scan speed, deg/min	5.3
scan width, deg	$\Delta\theta = 0.60 + 0.35\tan\theta$
reflections collected	1930; +h, +k, ±l
unique reflections	1684
reflections $F_o^2 > 3\sigma(F_o^2)$	1415
R, %	1.8
R_w, %	2.2
R_{all}, %	2.0
GOF	1.18
Largest Δ/σ in final least squares cycle	0

Intensity standards: (-5, -1, -6); (8, 1, 1); (1, -1, -8); measured every hour of x-ray exposure time. The data showed no decay.

Orientation Standards: 3 reflections were checked after every 200 measurements. Crystal orientation was redetermined if any of the reflections were offset from their predicted positions by more than 0.1°. Reorientation was required five times over the course of the data collection. The cell constants and errors are listed as their final values.

Table of Positional Parameters and Their Estimated Standard Deviations

Atom	x	y	z	B(A2)
U	Ø.25Ø	Ø.137Ø1(4)	Ø.25Ø	1.9Ø7(5)
F	Ø.3Ø45(2)	-Ø.Ø856(5)	Ø.3462(2)	3.71(6)
C1	Ø.Ø851(3)	Ø.1535(7)	Ø.3454(3)	2.2(1)
C2	Ø.1481(3)	Ø.2898(8)	Ø.3964(3)	2.23(9)
C3	Ø.165Ø(3)	Ø.4617(7)	Ø.3363(3)	2.Ø6(9)
C4	Ø.1114(3)	Ø.4336(8)	Ø.2513(3)	2.32(9)
C5	Ø.Ø595(3)	Ø.2441(8)	Ø.2566(3)	2.Ø2(9)
C6	Ø.179Ø(3)	Ø.2688(9)	Ø.4991(3)	2.6(1)
C7	Ø.1Ø21(4)	Ø.369(1)	Ø.5573(4)	5.2(2)
C8	Ø.19Ø4(5)	Ø.Ø4Ø(1)	Ø.5294(3)	4.8(1)
C9	Ø.2698(4)	Ø.3896(9)	Ø.52Ø6(4)	5.Ø(1)
C1Ø	-Ø.Ø2Ø7(3)	Ø.172Ø(7)	Ø.1899(3)	2.5(1)
C11	-Ø.ØØ7Ø(4)	Ø.244(1)	Ø.Ø9ØØ(3)	3.9(1)
C12	-Ø.Ø318(4)	-Ø.Ø72(1)	Ø.1912(4)	4.4(1)
C13	-Ø.1111(3)	Ø.272(1)	Ø.2244(4)	3.8(1)

The thermal parameter given for anisotropically refined atoms is the isotropic equivalent thermal parameter defined as:
(4/3) * [a2*B(1,1) + b2*B(2,2) + c2*B(3,3) + ab(cos gamma)*B(1,2) + ac(cos beta)*B(1,3) + bc(cos alpha)*B(2,3)]
where a,b,c are real cell parameters, and B(i,j) are anisotropic betas.

Table of Anisotropic Thermal Parameters - B's

Name	B(1,1)	B(2,2)	B(3,3)	B(1,2)	B(1,3)	B(2,3)	Beqv
U	1.864(8)	1.38(1)	2.454(8)	Ø	-Ø.232(7)	Ø	1.9Ø7(5)
F	3.1(1)	3.2(1)	4.8(1)	Ø.7(1)	Ø.1(1)	1.7(1)	3.71(6)
C1	2.4(2)	1.6(3)	2.7(2)	-Ø.Ø(2)	-Ø.1(1)	Ø.2(2)	2.2(1)
C2	2.2(2)	1.9(2)	2.6(2)	Ø.3(2)	-Ø.5(1)	-Ø.2(2)	2.23(9)
C3	2.1(2)	Ø.7(2)	3.3(2)	-Ø.Ø(2)	-Ø.4(1)	-Ø.2(2)	2.Ø6(9)
C4	2.3(2)	2.2(2)	2.4(2)	Ø.8(2)	-Ø.3(1)	Ø.6(2)	2.32(9)
C5	1.8(1)	1.7(2)	2.6(2)	Ø.2(2)	-Ø.4(1)	-Ø.1(2)	2.Ø2(9)
C6	3.1(2)	2.6(3)	2.Ø(2)	Ø.2(2)	-Ø.5(2)	-Ø.Ø(2)	2.6(1)
C7	5.4(3)	7.9(4)	2.5(2)	2.1(3)	Ø.1(2)	-Ø.Ø(2)	5.2(2)
C8	7.6(3)	4.2(3)	2.5(2)	Ø.6(3)	-1.5(2)	Ø.5(2)	4.8(1)
C9	5.Ø(2)	5.9(4)	3.9(2)	-1.Ø(3)	-2.Ø(2)	Ø.2(2)	5.Ø(1)
C1Ø	2.1(2)	2.6(3)	2.7(2)	Ø.3(2)	-Ø.6(1)	-Ø.1(2)	2.5(1)
C11	3.7(2)	5.1(3)	2.7(2)	-Ø.4(2)	-Ø.8(2)	-Ø.5(2)	3.9(1)
C12	3.4(2)	4.Ø(3)	5.5(3)	-Ø.7(2)	-1.9(2)	-Ø.4(3)	4.4(1)
C13	2.3(2)	5.1(3)	3.8(2)	-Ø.Ø(2)	-Ø.7(2)	-Ø.8(2)	3.8(1)

The form of the anisotropic temperature factor is:
exp[-Ø.25(h2a2B(1,1) + k2b2B(2,2) + l2c2B(3,3) + 2hkabB(1,2) + 2hlacB(1,3) + 2klbcB(2,3))] where a,b, and c are reciprocal lattice constants.

$[Cp''_2UF]_2$

Dark blue-green crystals of the compound were grown by cooling a hexane solution to -20 °C. The crystals were placed in Petri dish of Paratone N in a glove box. A suitable, square crystal measuring 0.27 mm × 0.27 mm × 0.14 mm was mounted on the end of a 0.2 mm thin walled glass capillary. The crystal was transferred to an Enraf-Nonius CAD-4 diffractometer and cooled to -111 °C under a cold stream previously calibrated by a thermocouple placed in the sample position. The crystal was centered in the beam. Automatic peak search and indexing procedures indicated that the crystal possessed a primitive triclinic cell and yielded the unit cell parameters. The cell parameters and data collection parameters are given in the following table.

The 8121 raw intensity data were converted to structure factor amplitudes and their esds by correction for scan speed, background, and Lorentz-polarization effects.[1] Inspection of the intensity standards showed no decrease in intensity over the duration of data collection. Inspection of the azimuthal scan data showed a variation of I_{min}/I_{max} = 0.85 for the averaged curve. An empirical absorption correction was applied to the intensity data based upon the average curve. Removal redundant data (0, -k,-l) left 7655 unique data.

The uranium atom positions were obtained by solving the Patterson map. The solution indicated that the molecule was in space group $P\bar{1}$ with Z = 2 and that the asymmetric unit contained two crystallographically independent molecules with inversion symmetry. Refinement on the uranium positions followed by a difference Fourier search yielded the other heavy atom positions. The heavy atom structure was refined by standard least squares and Fourier techniques. The heavy atoms were refined with isotropic and then anisotropic thermal parameters. The hydrogen positions were calculated based upon idealized bonding geometry and assigned thermal parameters equal to 1.15 $Å^2$ larger than the carbon atom to which they were connected. The hydrogen

positions were included in the structure factor calculations but not refined by least squares. Towards the end of the refinement, examination of the extinction test listing indicated that secondary extinction was occurring. The secondary extinction coefficient was initially set to 3.4×10^{-8} and was refined. A final difference Fourier map showed no additional atoms in the asymmetric unit. No close (< 3.5 Å) intermolecular contacts were found.

The final residuals for 133 variables refined against the 6339 unique data with $F_o > 3\sigma(F_o)$ were R = 2.23%, R_w = 2.58%, and GOF = 1.12. The R value for all data (including unobserved reflections) was 4.34%. The quantity minimized by the least squares refinements was $w(|F_o| - |F_c|)^2$, where w is the weight given to a particular reflection. The p-factor, used to reduce the weight of intense reflections, was set to 0.03 initially and later changed to 0.02.[2] The analytical form of the scattering factor tables for neutral atoms were used and all non-hydrogen scattering factors were corrected for both the real and imaginary components of anomalous dispersion.[3] Inspection of the residuals ordered in the ranges of $\sin(\theta/\lambda)$, $|F_o|$, and parity and values of the individual indexes showed no trends other than the previously mentioned secondary extinction. No reflections had anomalously high values of $w\Delta^2$. The largest positive and negative peaks in the final difference Fourier map have electron densities of 0.76 and -0.53, respectively, and are associated with the uranium atom.

Crystal Data for $[Cp''_2UF]_2$

Space group:	$P\bar{1}$
a, Å	11.363(4)
b, Å	14.963(3)
c, Å	17.845(4)
α, deg.	89.81(2)
β, deg.	76.86(2)
γ, deg.	84.32(2)
V, Å^3	2939.7
Z	2
fw	1351.90
d (calc.) g/cm^3	1.53
μ (calc.) 1/cm	54.09
radiation	MoKα(λ= 0.71073 Å)
monochrometer	highly oriented graphite
scan range, type	$3° \leq 2\theta \leq 45°$, θ-2θ
scan speed, deg/min	3.4
scan width, deg	$\Delta\theta$= 0.60 + 0.35tanθ
reflections collected	8121; +h, ±k, ±l
unique reflections	7655
reflections $F_o^2 > 3\sigma(F_o^2)$	6339
R, %	2.2
R_w, %	2.4
R_{all}, %	4.3
GOF	1.12
Largest Δ/σ in final least squares cycle	0.05

Intensity standards: (1, 4, 2); (2, 6, 4); (3, 1, -6); measured every hour of x-ray exposure time. The data showed no decay.

Orientation Standards: 3 reflections were checked after every 200 measurements. Crystal orientation was redetermined if any of the reflections were offset from their predicted positions by more than 0.1°. Reorientation was required nine times over the course of the data collection. The cell constants and errors are listed as their final values.

Table of Positional Parameters and Their Estimated Standard Deviations

Atom	x	y	z	B(A2)
U1	Ø.48495(2)	Ø.11474(1)	Ø.Ø5126(1)	1.369(4)
U2	Ø.48362(2)	Ø.38654(1)	Ø.55Ø55(1)	1.377(4)
SI11	Ø.7933(1)	Ø.2535(1)	Ø.ØØ367(9)	1.86(3)
SI12	Ø.2945(1)	Ø.3313(1)	-Ø.Ø3425(9)	1.96(3)
SI13	Ø.1471(1)	Ø.Ø968(1)	Ø.19278(9)	1.86(3)
SI14	Ø.65Ø1(1)	Ø.Ø225(1)	Ø.22471(9)	1.84(3)
SI21	Ø.7977(2)	Ø.2Ø94(1)	Ø.5182(1)	2.31(4)
SI22	Ø.3146(2)	Ø.1885(1)	Ø.46Ø71(9)	2.31(4)
SI23	Ø.1341(1)	Ø.4457(1)	Ø.67837(9)	2.15(4)
SI24	Ø.6181(1)	Ø.4652(1)	Ø.73529(9)	1.82(3)
F1	Ø.3875(3)	Ø.Ø157(2)	-Ø.ØØ86(2)	1.92(7)
F2	Ø.39Ø8(3)	Ø.4993(2)	Ø.4865(2)	1.93(7)
C1Ø1	Ø.53ØØ(5)	Ø.2886(4)	Ø.Ø1Ø6(3)	1.6(1)
C1Ø2	Ø.6424(5)	Ø.2372(4)	-Ø.Ø17Ø(3)	1.8(1)
C1Ø3	Ø.6254(5)	Ø.1833(4)	-Ø.Ø777(3)	1.8(1)
C1Ø4	Ø.5Ø59(5)	Ø.2ØØ9(4)	-Ø.Ø875(3)	1.8(1)
C1Ø5	Ø.4434(5)	Ø.2672(4)	-Ø.Ø323(3)	1.6(1)
C1Ø6	Ø.4Ø45(5)	Ø.Ø429(3)	Ø.1947(3)	1.4(1)
C1Ø7	Ø.311Ø(5)	Ø.1101(4)	Ø.1884(3)	1.6(1)
C1Ø8	Ø.36Ø7(5)	Ø.1932(4)	Ø.19Ø2(3)	1.9(1)
C1Ø9	Ø.4814(5)	Ø.1761(4)	Ø.1973(3)	1.5(1)
C11Ø	Ø.51Ø6(5)	Ø.Ø815(4)	Ø.1999(3)	1.6(1)
C111	Ø.7835(5)	Ø.2665(4)	Ø.1Ø92(3)	2.7(1)
C112	Ø.9Ø26(5)	Ø.156Ø(4)	-Ø.Ø389(4)	2.9(1)
C113	Ø.8485(5)	Ø.3582(4)	-Ø.Ø431(3)	2.5(1)
C114	Ø.2Ø32(6)	Ø.3596(4)	Ø.Ø639(4)	3.1(2)
C115	Ø.2127(5)	Ø.2629(5)	-Ø.Ø883(4)	3.3(2)
C116	Ø.3233(6)	Ø.4379(4)	-Ø.Ø869(4)	3.3(2)

Table of Positional Parameters and Their Estimated Standard Deviations (cont.)

Atom	x	y	z	B(A2)
C117	Ø.1Ø87(6)	-Ø.ØØ91(4)	Ø.2431(4)	3.4(2)
C118	Ø.Ø512(5)	Ø.1937(4)	Ø.2474(4)	3.Ø(1)
C119	Ø.1156(5)	Ø.Ø936(5)	Ø.Ø951(3)	3.Ø(1)
C12Ø	Ø.7772(6)	-Ø.ØØ19(4)	Ø.139Ø(3)	2.9(1)
C121	Ø.6Ø91(6)	-Ø.Ø844(4)	Ø.271Ø(3)	3.Ø(1)
C122	Ø.7Ø2Ø(5)	Ø.Ø939(4)	Ø.2936(3)	2.7(1)
C2Ø1	Ø.54Ø4(5)	Ø.2Ø55(3)	Ø.5137(3)	1.6(1)
C2Ø2	Ø.6522(5)	Ø.2426(4)	Ø.4896(3)	2.Ø(1)
C2Ø3	Ø.6379(5)	Ø.2976(4)	Ø.4262(3)	1.9(1)
C2Ø4	Ø.5223(5)	Ø.2931(4)	Ø.4129(3)	1.9(1)
C2Ø5	Ø.4569(5)	Ø.2354(4)	Ø.468Ø(3)	1.7(1)
C2Ø6	Ø.3839(5)	Ø.4713(4)	Ø.69Ø5(3)	1.5(1)
C2Ø7	Ø.296Ø(5)	Ø.4138(4)	Ø.6813(3)	1.7(1)
C2Ø8	Ø.35Ø7(5)	Ø.3245(4)	Ø.6871(3)	1.8(1)
C2Ø9	Ø.4669(5)	Ø.3284(4)	Ø.6996(3)	1.6(1)
C21Ø	Ø.4918(5)	Ø.4198(3)	Ø.7Ø2Ø(3)	1.5(1)
C211	Ø.772Ø(6)	Ø.19Ø7(5)	Ø.6233(4)	3.5(2)
C212	Ø.9ØØ4(6)	Ø.2993(5)	Ø.4893(4)	3.7(2)
C213	Ø.872Ø(6)	Ø.1Ø39(4)	Ø.4658(4)	3.3(2)
C214	Ø.3534(6)	Ø.Ø757(5)	Ø.4118(4)	4.1(2)
C215	Ø.2355(6)	Ø.264Ø(5)	Ø.4ØØ2(4)	3.9(2)
C216	Ø.2141(5)	Ø.174Ø(5)	Ø.5575(3)	3.1(1)
C217	Ø.1133(6)	Ø.4523(5)	Ø.5778(4)	3.2(2)
C218	Ø.Ø416(6)	Ø.3591(5)	Ø.73Ø5(4)	3.5(2)
C219	Ø.Ø849(6)	Ø.5571(5)	Ø.728Ø(4)	4.3(2)
C22Ø	Ø.7524(6)	Ø.48Ø3(5)	Ø.6551(4)	3.2(2)
C221	Ø.5585(6)	Ø.577Ø(4)	Ø.7825(3)	2.9(1)
C222	Ø.6682(5)	Ø.3869(4)	Ø.8Ø63(3)	3.Ø(1)

The thermal parameter given for anisotropically refined atoms is the isotropic equivalent thermal parameter defined as:
(4/3) * [a2*B(1,1) + b2*B(2,2) + c2*B(3,3) + ab(cos gamma)*B(1,2) + ac(cos beta)*B(1,3) + bc(cos alpha)*B(2,3)]
where a,b,c are real cell parameters, and B(i,j) are anisotropic betas.

Table of Anisotropic Thermal Parameters - B's

Name	B(1,1)	B(2,2)	B(3,3)	B(1,2)	B(1,3)	B(2,3)	Beqv
U1	1.682(8)	1.245(8)	1.164(8)	-Ø.118(7)	-Ø.3Ø3(6)	-Ø.ØØ42(7)	1.369(4)
U2	1.679(8)	1.2Ø5(8)	1.22Ø(8)	-Ø.1Ø5(7)	-Ø.291(6)	Ø.155(7)	1.377(4)
SI11	1.55(6)	2.18(7)	1.92(6)	-Ø.2Ø(5)	-Ø.53(5)	Ø.1Ø(6)	1.86(3)
SI12	1.67(6)	2.21(7)	1.9Ø(6)	Ø.12(6)	-Ø.34(5)	Ø.38(6)	1.96(3)
SI13	1.54(6)	2.11(7)	1.86(6)	-Ø.23(5)	-Ø.21(5)	Ø.Ø7(6)	1.86(3)
SI14	1.98(6)	1.83(6)	1.86(6)	Ø.Ø7(5)	-Ø.88(5)	-Ø.Ø3(5)	1.84(3)
SI21	2.Ø8(7)	2.12(7)	2.7Ø(7)	Ø.25(6)	-Ø.66(5)	Ø.Ø2(6)	2.31(4)
SI22	2.13(7)	2.89(7)	1.91(6)	-Ø.6Ø(6)	-Ø.29(5)	-Ø.52(6)	2.31(4)
SI23	1.4Ø(6)	2.61(7)	2.3Ø(7)	Ø.Ø5(6)	-Ø.23(5)	Ø.11(6)	2.15(4)
SI24	1.96(6)	1.99(7)	1.68(6)	-Ø.43(5)	-Ø.65(5)	Ø.22(5)	1.82(3)
F1	1.7(1)	2.Ø(1)	2.1(1)	Ø.1(1)	-Ø.6(1)	-Ø.2(1)	1.92(7)
F2	1.7(1)	2.Ø(1)	2.1(1)	-Ø.2(1)	-Ø.6(1)	Ø.4(1)	1.93(7)
C1Ø1	1.8(2)	1.5(2)	1.5(2)	-Ø.4(2)	-Ø.1(2)	Ø.Ø(2)	1.6(1)
C1Ø2	2.Ø(2)	1.8(2)	1.4(2)	Ø.Ø(2)	-Ø.5(2)	Ø.2(2)	1.8(1)
C1Ø3	1.7(2)	1.6(2)	1.6(2)	Ø.4(2)	Ø.3(2)	Ø.Ø(2)	1.8(1)
C1Ø4	2.Ø(2)	1.9(2)	1.5(2)	-Ø.Ø(2)	-Ø.3(2)	-Ø.1(2)	1.8(1)
C1Ø5	1.4(2)	1.3(2)	2.Ø(2)	-Ø.Ø(2)	-Ø.3(2)	Ø.3(2)	1.6(1)
C1Ø6	1.8(2)	1.5(2)	1.1(2)	-Ø.4(2)	-Ø.3(2)	Ø.5(2)	1.4(1)
C1Ø7	2.2(2)	1.5(2)	1.Ø(2)	-Ø.1(2)	-Ø.1(2)	-Ø.1(2)	1.6(1)
C1Ø8	1.8(2)	2.Ø(2)	1.6(2)	Ø.2(2)	-Ø.2(2)	Ø.Ø(2)	1.9(1)
C1Ø9	1.6(2)	1.8(2)	1.1(2)	-Ø.3(2)	-Ø.2(2)	-Ø.1(2)	1.5(1)
C11Ø	1.6(2)	1.8(2)	1.2(2)	-Ø.2(2)	-Ø.1(2)	Ø.2(2)	1.6(1)
C111	2.4(2)	3.9(3)	2.1(2)	-Ø.8(2)	-Ø.6(2)	-Ø.1(2)	2.7(1)
C112	1.9(2)	3.5(3)	3.3(3)	-Ø.Ø(2)	-Ø.6(2)	Ø.2(2)	2.9(1)
C113	2.4(2)	2.6(3)	2.6(2)	-Ø.8(2)	-Ø.8(2)	Ø.4(2)	2.5(1)
C114	2.7(3)	3.5(3)	2.7(3)	Ø.9(2)	-Ø.3(2)	Ø.5(2)	3.1(2)
C115	2.3(3)	3.8(3)	4.1(3)	-Ø.Ø(2)	-1.5(2)	Ø.3(3)	3.3(2)
C116	3.1(3)	3.Ø(3)	3.1(3)	Ø.6(3)	Ø.3(2)	Ø.8(2)	3.3(2)

Table of Anisotropic Thermal Parameters - B's (Continued)

Name	B(1,1)	B(2,2)	B(3,3)	B(1,2)	B(1,3)	B(2,3)	Beqv
C117	2.8(3)	3.6(3)	3.7(3)	-1.0(2)	-0.5(2)	0.9(3)	3.4(2)
C118	2.0(2)	3.5(3)	3.3(3)	0.0(2)	-0.6(2)	-0.8(2)	3.0(1)
C119	2.0(2)	4.7(3)	2.6(3)	-0.7(2)	-1.1(2)	0.0(2)	3.0(1)
C120	2.7(3)	3.7(3)	2.3(2)	0.5(2)	-0.9(2)	-0.4(2)	2.9(1)
C121	3.8(3)	2.4(3)	2.7(3)	0.4(2)	-1.3(2)	-0.1(2)	3.0(1)
C122	2.1(2)	3.2(3)	3.1(3)	-0.2(2)	-1.2(2)	-0.3(2)	2.7(1)
C201	1.9(2)	0.9(2)	1.8(2)	-0.3(2)	-0.2(2)	0.1(2)	1.6(1)
C202	2.3(2)	1.7(2)	1.7(2)	0.3(2)	-0.4(2)	0.1(2)	2.0(1)
C203	2.4(2)	1.5(2)	1.5(2)	-0.0(2)	0.1(2)	-0.2(2)	1.9(1)
C204	2.1(2)	1.8(2)	1.8(2)	-0.0(2)	-0.8(2)	0.2(2)	1.9(1)
C205	2.1(2)	1.5(2)	1.4(2)	-0.3(2)	-0.3(2)	-0.0(2)	1.7(1)
C206	1.9(2)	1.6(2)	1.0(2)	0.0(2)	-0.1(2)	-0.2(2)	1.5(1)
C207	1.6(2)	1.5(2)	2.1(2)	-0.1(2)	-0.2(2)	0.1(2)	1.7(1)
C208	2.1(2)	1.7(2)	1.7(2)	-0.5(2)	-0.5(2)	0.1(2)	1.8(1)
C209	2.1(2)	1.5(2)	1.1(2)	-0.0(2)	-0.4(2)	0.8(2)	1.6(1)
C210	1.7(2)	1.3(2)	1.4(2)	0.4(2)	-0.5(2)	0.2(2)	1.5(1)
C211	3.1(3)	4.7(4)	2.7(3)	0.5(3)	-1.2(2)	0.5(3)	3.5(2)
C212	2.5(3)	3.9(3)	4.7(3)	-0.9(2)	-0.7(2)	-0.6(3)	3.7(2)
C213	3.0(3)	2.7(3)	4.2(3)	0.8(2)	-1.4(2)	-0.5(3)	3.3(2)
C214	3.8(3)	3.9(3)	4.2(3)	-1.7(2)	0.3(3)	-1.7(3)	4.1(2)
C215	3.0(3)	7.0(4)	2.0(3)	-1.1(3)	-1.1(2)	0.3(3)	3.9(2)
C216	2.5(3)	4.6(3)	2.2(3)	-1.3(2)	-0.4(2)	-0.2(2)	3.1(1)
C217	2.4(3)	4.4(3)	3.0(3)	-0.8(2)	-0.7(2)	0.4(3)	3.2(2)
C218	2.1(3)	5.1(4)	3.1(3)	-0.1(3)	-0.0(2)	1.0(3)	3.5(2)
C219	2.7(3)	4.3(4)	5.3(4)	1.5(3)	-0.4(3)	-1.6(3)	4.3(2)
C220	2.7(3)	4.8(3)	2.5(3)	-1.2(2)	-0.9(2)	0.8(3)	3.2(2)
C221	3.9(3)	2.5(3)	2.8(3)	-0.5(2)	-1.5(2)	-0.3(2)	2.9(1)
C222	2.5(2)	4.0(3)	2.8(2)	-0.3(2)	-1.6(2)	0.5(2)	3.0(1)

The form of the anisotropic temperature factor is:
exp[-0.25(h2a2B(1,1) + k2b2B(2,2) + l2c2B(3,3) + 2hkabB(1,2) + 2hlacB(1,3) + 2klbcB(2,3))] where a,b, and c are reciprocal lattice constants.

$[Cp^{\ddagger}_2UO]_2$

Brown crystals of the compound were grown by cooling a toluene solution from 100 °C to room temperature. The crystals were placed in Petri dish of Paratone N in a glove box. A suitable block shaped crystal measuring 0.20 mm × 0.16 mm × 0.16 mm was mounted on the end of a 0.2 mm thin walled glass capillary. The crystal was transferred to an Siemens SMART diffractometer and cooled to -95 °C under a cold stream previously calibrated by a thermocouple placed in the sample position. The crystal was centered in the beam. Automatic peak search and indexing procedures indicated that the crystal possessed a primitive triclinic cell and yielded the unit cell parameters. The cell parameters and data collection parameters are given in the following table. Based upon a statistical analysis of intensity distribution and the successful solution and refinement of the crystal structure, the space group was found to be $P\bar{1}$.

An arbitrary hemisphere of data was collected using the default parameters for the diffractometer. The data were collected as 30 s images with an area detector. Two images were averaged to give the net image data. The image data were converted to intensity data using the program SAINT. The 5485 raw intensity data were converted to structure factor amplitudes and their esds by correction for scan speed, background, and Lorentz-polarization effects.[1] Inspection of the intensity standards showed no decrease in intensity over the duration of data collection. An empirical absorption correction using an ellipsoidal model for the crystal was applied to the intensity data based upon the intensities of all intense equivalent reflections ($T_{max} = 0.823$, $T_{min} = 0.621$). Averaging equivalent reflections gave 3906 unique data ($R_{int} = 0.071$).

The uranium atom positions were obtained by direct methods. Refinement on the uranium positions followed by a difference Fourier search yielded the other heavy atom positions. The heavy atom structure was refined by standard least squares and Fourier techniques. The heavy atoms were refined with anisotropic thermal parameters except

for C24-C29 which form a disordered *t*-butyl group. The disorder was modeled using two sets of methyl carbon atoms rotated by *ca.* 60° with respect to each other. The occupancy of the disordered carbon atoms was allowed to vary but remained near 0.5. The hydrogen positions were calculated based upon idealized bonding geometry and assigned thermal parameters equal to 1.15 $Å^2$ larger than the carbon atom to which they were connected. The hydrogen positions were included in the structure factor calculations but not refined by least squares. Towards the end of the refinement, examination of the extinction test listing indicated that secondary extinction was occurring. The secondary extinction coefficient was refined to 1.05×10^{-6}. A final difference Fourier map showed no additional atoms in the asymmetric unit. No close (< 3.5 Å) intermolecular contacts were found.

The final residuals for 252 variables refined against the 2543 unique data with $I > 3\sigma(I)$ were $R = 5.2\%$, $R_w = 7.3\%$, and GOF = 3.12. The quantity minimized by the least squares refinements was $w(|F_o| - |F_c|)^2$, where w is the weight given to a particular reflection. The p-factor, used to reduce the weight of intense reflections, was set to 0.03.[2] The analytical form of the scattering factor tables for neutral atoms were used and all non-hydrogen scattering factors were corrected for both the real and imaginary components of anomalous dispersion.[3]

Inspection of the residuals ordered in the ranges of $\sin(\theta/\lambda)$, $|F_o|$, and parity and values of the individual indexes showed no trends other than the previously mentioned secondary extinction. No reflections had anomalously high values of $w\Delta^2$. The largest positive and negative peaks in the final difference Fourier map have electron densities of 1.81 and -2.15, respectively.

Crystal Data for $[Cp^{\ddagger}_2UO]_2$

Space group:	$P\bar{1}$
a, Å	10.6985(8)
b, Å	11.2046(8)
c, Å	12.2575(9)
α, deg.	64.522(1)
β, deg.	73.698(1)
γ, deg.	89.962(1)
V,Å^3	1261.9(1)
Z	1
fw	1217.24
d (calc.) g/cm^3	1.602
μ (calc.) 1/cm	64.46
radiation	MoKα(λ= 0.71073 Å)
monochrometer	highly oriented graphite
resolution, % coverage	0.86 Å, 93%; 0.83 Å, 85%
scan time, per image	30 s
scan type	ω, 0.3°
reflections integrated	5485
unique reflections	3906 (R_{int} = 0.071)
reflections $I > 3\sigma(I)$	2543
R, %	5.2
R_w, %	7.3
GOF	3.12
Largest Δ/σ in final least squares cycle	0.0

Table of atomic positions in $[Cp^{\ddagger}_2UO]_2$

Atom	X	Y	Z	$B_{eq}(Å^2)$
U(1)	1.00070(3)	0.50227(3)	0.36076(3)	3.47(4)
O(1)	1.12070(67)	0.48375(66)	0.47703(65)	3.6(5)
C(1)	1.1713(10)	0.7257(11)	0.1531(11)	3.9(8)
C(2)	1.1113(11)	0.6596(11)	0.1007(12)	4(1)
C(3)	0.9785(12)	0.6764(11)	0.1266(12)	4.4(9)
C(4)	0.9514(10)	0.7547(11)	0.19453(96)	3.6(7)
C(5)	1.07129(94)	0.77957(92)	0.2148(10)	3.5(7)
C(6)	1.0541(10)	0.2775(11)	0.3165(11)	3.9(8)
C(7)	1.0009(11)	0.2344(11)	0.4506(11)	4.2(9)
C(8)	0.8708(12)	0.2507(11)	0.4781(11)	4.5(8)
C(9)	0.8338(11)	0.3030(10)	0.3659(11)	4.0(8)
C(10)	0.9514(12)	0.3206(12)	0.2637(12)	5(1)
C(11)	0.6931(12)	0.3088(12)	0.3609(12)	5(1)
C(12)	0.6883(13)	0.3998(16)	0.2249(15)	6(1)
C(13)	0.6101(17)	0.3561(24)	0.4545(18)	9(2)
C(14)	0.6349(19)	0.1669(18)	0.3979(26)	11(2)
C(15)	1.1853(14)	0.2474(12)	0.2481(13)	5(1)
C(16)	1.2454(12)	0.3563(13)	0.1113(13)	5(1)
C(17)	1.2865(16)	0.2333(16)	0.3161(18)	6(1)
C(18)	1.1599(15)	0.1162(14)	0.2426(18)	7(1)
C(19)	1.32097(95)	0.75000(99)	0.1280(11)	3.7(8)
C(20)	1.3540(11)	0.8709(12)	0.1471(12)	5(1)
C(21)	1.3934(14)	0.7770(16)	-0.0063(14)	6(1)
C(22)	1.3685(13)	0.6301(14)	0.2173(16)	6(1)
C(23)	0.8270(10)	0.8213(11)	0.2190(11)	4.0(8)
C(24)	0.8737(32)	0.9794(31)	0.1213(35)	7.0(7)
C(25)	0.7820(34)	0.8122(34)	0.3507(34)	7.1(8)
C(26)	0.7085(37)	0.7591(37)	0.2065(39)	7.9(8)
C(27)	0.8666(31)	0.9573(31)	0.2109(34)	5.7(7)
C(28)	0.7277(37)	0.7319(37)	0.3411(37)	6.8(8)
C(29)	0.7648(27)	0.8410(28)	0.1121(29)	4.9(6)
H(1)	1.156	0.611	0.056	5.0
H(2)	0.915	0.644	0.099	5.0
H(3)	1.083	0.827	0.262	4.1
H(4)	1.053	0.204	0.507	5.0
H(5)	0.811	0.231	0.561	5.2
H(6)	0.954	0.349	0.180	5.6
H(7)	0.717	0.491	0.202	7.0
H(8)	0.742	0.374	0.166	7.0
H(9)	0.599	0.393	0.224	7.0
H(10)	0.641	0.442	0.431	11.1
H(11)	0.521	0.350	0.450	11.1
H(12)	0.610	0.295	0.536	11.1
H(13)	0.547	0.162	0.398	13.7

Table of atomic positions in $[Cp^{\ddagger}_2UO]_2$ (continued)

Atom	X	Y	Z	$B_{eq}(Å^2)$
H(14)	0.686	0.132	0.345	13.7
H(15)	0.635	0.108	0.485	13.7
H(16)	1.323	0.336	0.065	6.0
H(17)	1.183	0.371	0.064	6.0
H(18)	1.268	0.443	0.108	6.0
H(19)	1.257	0.163	0.399	7.9
H(20)	1.366	0.214	0.269	7.9
H(21)	1.306	0.315	0.318	7.9
H(22)	1.127	0.042	0.331	8.4
H(23)	1.092	0.120	0.206	8.4
H(24)	1.235	0.094	0.200	8.4
H(25)	1.445	0.887	0.133	5.6
H(26)	1.327	0.948	0.090	5.6
H(27)	1.308	0.855	0.233	5.6
H(28)	1.486	0.795	-0.024	6.7
H(29)	1.376	0.703	-0.021	6.7
H(30)	1.367	0.854	-0.065	6.7
H(31)	1.322	0.609	0.304	6.9
H(32)	1.349	0.553	0.205	6.9
H(33)	1.459	0.645	0.202	6.9
C((p1))	1.057	0.719	0.158	0.4
C((p2))	0.942	0.277	3/8	0.4

The thermal parameter given for anisotropically refined atoms is the isotropic equivalent thermal parameter defined as:

$$(4/3)[a^2B(1,1) + b^2B(2,2) + c^2B(3,3) + ab(\cos\gamma)B(1,2) + ac(\cos\beta)B(1,3) + bc(\cos\alpha)B(2,3)]$$

where a,b,c are real cell parameters, and B(i,j) are anisotropic betas.

Table of atomic thermal parameters for $[Cp^{\ddagger}_2UO]_2$

Atom	U(1,1)	U(2,2)	U(3,3)	U(1,2)	U(1,3)	U(2,3)
U(1)	0.04986(28)	0.04223(28)	0.04184(29)	0.00702(15)	-0.01661(17)	-0.01909(19)
O(1)	0.0506(38)	0.0494(38)	0.0352(36)	0.0089(28)	-0.0151(29)	-0.0164(29)
C(1)	0.0450(54)	0.0549(60)	0.0479(62)	0.0055(43)	-0.0190(45)	-0.0198(49)
C(2)	0.0497(58)	0.0569(64)	0.0692(76)	0.0140(47)	-0.0233(52)	-0.0357(57)
C(3)	0.0645(67)	0.0479(57)	0.0593(71)	0.0057(47)	-0.0374(56)	-0.0181(52)
C(4)	0.0450(52)	0.0573(59)	0.0355(52)	0.0029(42)	-0.0135(41)	-0.0200(45)
C(5)	0.0400(49)	0.0325(46)	0.0552(63)	0.0034(36)	-0.0115(42)	-0.0170(43)
C(6)	0.0494(55)	0.0545(60)	0.0558(66)	0.0098(44)	-0.0250(48)	-0.0301(52)
C(7)	0.0536(60)	0.0590(64)	0.0541(68)	0.0139(47)	-0.0255(50)	-0.0278(54)
C(8)	0.0722(75)	0.0446(57)	0.0391(57)	-0.0094(49)	-0.0089(50)	-0.0114(46)
C(9)	0.0544(59)	0.0452(55)	0.0554(67)	0.0109(43)	-0.0239(49)	-0.0228(49)
C(10)	0.0622(68)	0.0547(65)	0.0632(76)	0.0088(51)	-0.0262(56)	-0.0279(57)
C(11)	0.0537(63)	0.0605(70)	0.0619(75)	-0.0056(50)	-0.0257(54)	-0.0150(57)
C(12)	0.0513(67)	0.101(11)	0.083(10)	-0.0014(66)	-0.0270(66)	-0.0352(82)
C(13)	0.0711(95)	0.177(20)	0.074(11)	0.032(11)	-0.0123(81)	-0.062(12)
C(14)	0.093(12)	0.071(11)	0.198(25)	-0.0305(94)	-0.071(14)	0.007(12)
C(15)	0.0786(82)	0.0510(66)	0.0592(78)	0.0071(55)	-0.0114(61)	-0.0220(57)
C(16)	0.0541(62)	0.0721(76)	0.0743(87)	0.0322(54)	-0.0179(57)	-0.0396(66)
C(17)	0.0818(93)	0.0762(90)	0.106(13)	0.0301(73)	-0.0516(89)	-0.0451(89)
C(18)	0.0858(94)	0.0625(84)	0.110(13)	0.0060(68)	0.0022(86)	-0.0575(88)
C(19)	0.0399(50)	0.0416(53)	0.0559(65)	0.0049(39)	-0.0094(43)	-0.0218(46)
C(20)	0.0429(54)	0.0592(66)	0.0687(78)	0.0027(45)	-0.0150(50)	-0.0261(57)
C(21)	0.0676(76)	0.0876(95)	0.0671(87)	0.0136(65)	-0.0173(63)	-0.0427(75)
C(22)	0.0558(68)	0.0616(77)	0.093(11)	0.0111(55)	-0.0269(67)	-0.0195(70)
C(23)	0.0440(52)	0.0568(62)	0.0531(65)	0.0139(43)	-0.0252(45)	-0.0188(50)

The form of the anisotropic temperature factor is:

$$\exp[-2\pi^2\{h^2a^2U(1,1) + k^2b^2U(2,2) + l^2c^2U(3,3) + 2hkabU(1,2) + 2hlacU(1,3) + 2klbcU(2,3)\}]$$

where a,b, and c are reciprocal lattice constants.

$Cp"_2UMe_2$

Orange crystals of the compound were grown by cooling a saturated ether solution to -30 °C. The crystals were then placed in a small Petri dish and covered with Paratone N, a high molecular weight hydrocarbon oil. The dish was removed from the box, and the crystals were examined with a microscope in the atmosphere. A block shaped single crystal measuring 0.45 × 0.40 × 0.40 mm was mounted on the end of a 0.4 mm diameter quartz capillary. The crystal was transferred to an Enraf-Nonius CAD-4 diffractometer and cooled to -98 °C under a cold stream of nitrogen gas previously calibrated by a thermocouple placed in the sample position. The crystal was centered in the beam. Automatic peak search and indexing procedures indicated that the crystal possessed a primitive orthorhombic cell and yielded the cell parameters. The cell parameters and data collection parameters are given in the following table.

The 2366 raw intensity data were converted to structure factor amplitudes and their esds by correction for scan speed, background, and Lorentz-polarization effects.[1] Inspection of the intensity standards showed no loss of intensity during the data collection. The 23 systematic absences (h,0,0, h odd; (0,k,0), k odd; and (0,0,l), l odd were then rejected yielding 2343 unique data of which 2075 possessed $F_o > 3\sigma(F_o)$. Azimuthal scan data showed a difference of $I_{min}/I_{max} = 0.69$ for the average curve. An empirical absorption correction was applied based upon the average curve. The systematic absences indicated that the space group was $P2_12_12_1$.

The cell volume indicated that 4 molecules were present in the unit cell. The uranium atom position was obtained by solving the Patterson map. Successive Fourier searches yielded the rest of the heavy atom positions. The heavy atom structure was refined by standard least squares and Fourier techniques. The heavy atoms were refined anisotropically. Hydrogen atoms were placed at calculated positions with thermal parameters 1.3 $Å^2$ times the thermal parameters of the carbon atoms to which they were

bound. At the end of the refinement, the enantiomer was changed, and the structure refined. The refinement was very slightly worse, so the enantiomer was changed back to the original one, and the structure was rerefined. A final difference Fourier map showed no additional atoms in the asymmetric unit. Examination of intermolecular close contacts(<3.5Å) showed that the molecule was a monomer.

The final residuals for 263 variables refined against the 2075 unique data with $F_o > 3\sigma(F_o)$ were R = 4.22%, R_w = 5.38%, and GOF = 1.39. The R value for all data (including unobserved reflections) was 5.01%. The quantity minimized by the least squares refinements was $w(|F_o| - |F_c|)^2$, where w is the weight given to a particular reflection. The p-factor, used to reduce the weight of intense reflections, was set to 0.03 initially, but later changed to 0.06.[2] The analytical form of the scattering factor tables for neutral atoms were used and all non-hydrogen scattering factors were corrected for both the real and imaginary components of anomalous dispersion.[3]

Inspection of the residuals ordered in the ranges of $\sin(\theta/\lambda)$, $|F_o|$, and parity and values of the individual indexes showed that secondary extinction was occurring. A secondary extinction coefficient was included in the refinement; it's final value was 1.2×10^{-8}. One reflection had anomalously high values of $w\Delta^2$, and was weighted to zero toward the end of the refinement. The largest positive and negative peaks in the final difference Fourier map have electron densities of 2.44 and -0.29, respectively, and are associated with the uranium atom.

Crystal Data for Cp''_2UMe_2

Space group:	$P2_12_12_1$
a, Å	10.806(2)
b, Å	16.185(8)
c, Å	18.034(6)
α, deg.	90
β, deg.	90
γ, deg.	90
V, Å^3	3154(2)
Z	4
fw	687.02
d (calc.) g/cm^3	1.448
μ (calc.) 1/cm	50.438
radiation	MoKα(λ= 0.71073 Å)
monochrometer	highly oriented graphite
scan range, type	$3° \leq 2\theta \leq 45°$, θ-2θ
scan speed, deg/min	4
scan width, deg	$\Delta\theta = 0.90 + 0.35\tan\theta$
reflections collected	2366; +h,+k,+l
unique reflections	2343
reflections $F_o^2 > 3\sigma(F_o^2)$	2075
R, %	4.22
R_w, %	5.38
R_{all}, %	5.01
GOF	1.39
Largest Δ/σ in final least squares cycle	0

Intensity standards: (-6,1,-2); (5,-5,3); (-2,-1,-10) measured every hour of X-ray exposure time. No loss of in intensity occurred.

Orientation Standards: 3 reflections were checked after every 200 measurements. Crystal orientation was redetermined if any of the reflections were offset from their predicted positions by more than 0.1°. Reorientation was required once over the course of the data collection. The cell constants and errors are listed as their final values.

Table of atomic positions in Cp''_2UMe_2

Atoms	X	Y	Z	B_{eq} (A^2)
U	0.14723(1)	0.26012(1)	0.25763(1)	1.821(9)
SI1	-0.2221(4)	0.2191(3)	0.2963(3)	2.7(1)
SI2	0.2412(4)	0.0691(3)	0.3953(2)	2.15(9)
SI3	0.3465(5)	0.4220(3)	0.3825(2)	2.70(9)
SI4	0.3564(5)	0.3182(3)	0.0742(2)	2.54(9)
C1	0.111(2)	0.162(1)	0.1586(9)	3.8(4)
C2	0.026(2)	0.381(1)	0.224(1)	3.8(4)
C3	0.019(1)	0.136(1)	0.3278(8)	2.0(3)
C4	-0.060(1)	0.210(1)	0.3312(8)	2.3(3)
C5	-0.000(1)	0.266(1)	0.3794(8)	2.6(3)
C6	0.114(1)	0.233(1)	0.4041(8)	2.2(3)
C7	0.125(1)	0.149(1)	0.3731(8)	2.5(3)
C8	0.325(1)	0.3754(8)	0.2281(8)	1.8(3)
C9	0.346(1)	0.3498(8)	0.3012(7)	1.5(3)
C10	0.388(1)	0.267(1)	0.2937(8)	2.6(3)
C11	0.387(1)	0.2472(9)	0.2248(7)	2.4(3)
C12	0.350(1)	0.3096(8)	0.1786(7)	1.4(3)
C13	-0.313(2)	0.134(1)	0.337(1)	4.8(5)
C14	-0.230(2)	0.212(2)	0.193(1)	6.2(6)
C15	-0.286(2)	0.319(1)	0.328(1)	5.1(5)
C16	0.161(2)	-0.017(1)	0.441(1)	3.7(4)
C17	0.312(2)	0.030(1)	0.308(1)	3.8(4)
C18	0.363(2)	0.112(1)	0.4591(9)	3.4(4)
C19	0.451(2)	0.510(1)	0.3588(9)	3.4(4)
C20	0.401(2)	0.368(1)	0.4665(9)	4.1(4)
C21	0.189(2)	0.464(1)	0.399(1)	5.1(5)
C22	0.484(2)	0.388(1)	0.0514(9)	4.8(5)
C23	0.387(2)	0.214(1)	0.034(1)	6.0(6)
C24	0.213(2)	0.364(2)	0.036(1)	6.0(6)
H1C	0.13727(1)	0.18497(1)	0.11279(1)	5.0*
H1A	0.15610(1)	0.11258(1)	0.16810(1)	5.0*
H1B	0.02506(1)	0.14939(1)	0.15597(1)	5.0*
H2C	-0.05880(1)	0.36573(1)	0.22111(1)	5.0*
H2A	0.03611(1)	0.42207(1)	0.26129(1)	5.0*
H2B	0.05340(1)	0.40130(1)	0.17794(1)	5.0*
H3	0.00291(1)	0.08725(1)	0.29991(1)	2.5*
H5	-0.03272(1)	0.31874(1)	0.39323(1)	3.4*
H6	0.17312(1)	0.26027(1)	0.43478(1)	2.8*
H8	0.29833(1)	0.42899(1)	0.21382(1)	2.4*
H10	0.41221(1)	0.23248(1)	0.33338(1)	3.4*
H11	0.41081(1)	0.19395(1)	0.20747(1)	3.1*
H13C	-0.31125(1)	0.13789(1)	0.38915(1)	6.2*
H13A	-0.39601(1)	0.13732(1)	0.31970(1)	6.2*
H13B	-0.27821(1)	0.08252(1)	0.32174(1)	6.2*
H14C	-0.19805(1)	0.16048(1)	0.17686(1)	8.0*
H14A	-0.31357(1)	0.21745(1)	0.17700(1)	8.0*
H14B	-0.18217(1)	0.25562(1)	0.17142(1)	8.0*

Table of atomic positions in Cp''_2UMe_2 (continued)

Atoms	X	Y	Z	B_{eq} (A^2)
H15C	-0.23747(1)	0.36288(1)	0.30848(1)	6.6*
H15A	-0.36900(1)	0.32443(1)	0.31006(1)	6.6*
H15B	-0.28600(1)	0.32098(1)	0.38020(1)	6.6*
H16C	0.09970(1)	-0.03885(1)	0.40905(1)	4.8*
H16A	0.21908(1)	-0.05905(1)	0.45328(1)	4.8*
H16B	0.12278(1)	0.00238(1)	0.48549(1)	4.8*
H17C	0.35044(1)	0.07381(1)	0.28217(1)	5.0*
H17A	0.37137(1)	-0.01158(1)	0.31929(1)	5.0*
H17B	0.24883(1)	0.00625(1)	0.27740(1)	5.0*
H18C	0.32502(1)	0.13020(1)	0.50380(1)	4.5*
H18A	0.42189(1)	0.07029(1)	0.46996(1)	4.5*
H18B	0.40294(1)	0.15740(1)	0.43578(1)	4.5*
H19B	0.42149(1)	0.53691(1)	0.31571(1)	4.5*
H19A	0.45370(1)	0.54769(1)	0.39899(1)	4.5*
H19C	0.53235(1)	0.48918(1)	0.34972(1)	4.5*
H20C	0.48294(1)	0.34826(1)	0.45861(1)	5.4*
H20A	0.40081(1)	0.40523(1)	0.50727(1)	5.4*
H20B	0.34797(1)	0.32270(1)	0.47694(1)	5.4*
H21C	0.13327(1)	0.41979(1)	0.40916(1)	6.6*
H21A	0.19069(1)	0.50040(1)	0.44063(1)	6.6*
H21B	0.16163(1)	0.49335(1)	0.35661(1)	6.6*
H22C	0.55915(1)	0.36557(1)	0.07008(1)	6.2*
H22A	0.48970(1)	0.39340(1)	-0.00096(1)	6.2*
H22B	0.46933(1)	0.44033(1)	0.07307(1)	6.2*
H23C	0.32263(1)	0.17751(1)	0.04733(1)	7.8*
H23A	0.39026(1)	0.21872(1)	-0.01895(1)	7.8*
H23B	0.46388(1)	0.19410(1)	0.05153(1)	7.8*
H24C	0.20177(1)	0.41735(1)	0.05650(1)	7.7*
H24A	0.21929(1)	0.36705(1)	-0.01600(1)	7.7*
H24B	0.14469(1)	0.32969(1)	0.04943(1)	7.7*
Cp1	0.03960(1)	0.19885(1)	0.36312(1)	4.0*
Cp2	0.35936(1)	0.30989(1)	0.24527(1)	4.0*

Starred atoms were included with isotropic thermal parameters. The thermal parameter given for anisotropically refined atoms is the isotropic equivalent thermal parameter defined as:

$$(4/3)[a^2B(1,1) + b^2B(2,2) + c^2B(3,3) + ab(\cos\gamma)B(1,2) + ac(\cos\beta)B(1,3) + bc(\cos\alpha)B(2,3)]$$

where a,b,c are real cell parameters, and B(i,j) are anisotropic betas.

Table of anisotropic thermal parameters for $Cp"_2UMe_2$

Atom	B(1,1)	B(2,2)	B(3,3)	B(1,2)	B(1,3)	B(2,3)
U	1.47(2)	2.40(2)	1.59(2)	-0.18(2)	-0.05(2)	0.23(2)
SI1	1.4(2)	3.1(2)	3.7(2)	-0.1(2)	-0.2(2)	0.4(2)
SI2	1.9(2)	2.5(2)	2.1(2)	0.2(2)	-0.1(2)	0.0(2)
SI3	2.8(2)	3.3(2)	2.1(2)	-0.5(2)	-0.2(2)	-0.7(2)
SI4	2.8(2)	3.2(2)	1.6(2)	-0.7(2)	0.2(2)	-0.2(2)
C1	3.7(9)	5(1)	2.5(7)	-1.3(8)	0.2(7)	-2.0(7)
C2	2.4(8)	4.6(9)	4.4(9)	1.3(7)	-0.7(7)	0.5(8)
C3	1.5(6)	2.8(7)	1.6(6)	0.3(6)	0.1(5)	0.4(6)
C4	1.5(6)	2.7(7)	2.7(7)	-0.1(6)	0.7(6)	0.8(6)
C5	1.7(6)	3.3(8)	2.7(6)	0.1(7)	1.1(5)	-0.6(7)
C6	1.4(6)	2.7(7)	2.4(6)	0.3(6)	-0.4(5)	-1.2(6)
C7	1.9(7)	3.8(7)	1.8(6)	-0.3(6)	0.4(6)	1.9(5)
C8	2.0(7)	1.3(5)	2.1(6)	0.3(5)	-0.1(6)	-0.1(5)
C9	1.3(5)	1.3(5)	2.0(5)	-0.1(6)	0.8(6)	-1.2(5)
C10	0.4(5)	3.9(8)	3.4(6)	0.4(5)	0.8(5)	2.6(6)
C11	2.4(6)	2.5(7)	2.2(5)	-0.7(5)	-1.2(5)	1.9(5)
C12	0.6(5)	1.2(5)	2.5(6)	-0.7(6)	0.8(6)	-0.8(5)
C13	2.5(9)	5(1)	7(1)	-0.8(8)	-1.4(8)	0(1)
C14	3.3(9)	11(2)	4.2(9)	-1(1)	-1.3(8)	1(1)
C15	1.3(7)	6(1)	8(1)	0.5(8)	-1.4(9)	1(1)
C16	2.0(7)	3.9(8)	5.2(9)	-1.5(7)	-1.1(7)	1.1(7)
C17	5(1)	3.7(8)	2.9(8)	0.3(8)	0.6(8)	0.9(7)
C18	3.6(8)	3.4(8)	3.3(7)	1.0(8)	-1.4(8)	0.1(7)
C19	4.3(8)	3.9(9)	2.2(7)	-0.9(8)	-0.8(7)	-0.2(7)
C20	6(1)	5.2(9)	1.4(6)	-3.3(8)	-1.2(7)	-0.3(7)
C21	3.3(9)	4.4(9)	8(1)	-0.3(8)	1.7(9)	-2.9(9)
C22	5(1)	7(1)	2.0(7)	-2.6(9)	1.1(8)	0.5(8)
C23	10(2)	4(1)	3.0(8)	-1(1)	1(1)	-0.1(8)
C24	2.4(9)	12(2)	3.5(9)	-1(1)	-0.8(8)	3(1)

The form of the anisotropic temperature factor is:

$$\exp[-0.25\{h^2a^2B(1,1) + k^2b^2B(2,2) + l^2c^2B(3,3) + 2hkabB(1,2) + 2hlacB(1,3) + 2klbcB(2,3)\}]$$

where a,b, and c are reciprocal lattice constants.

Cp_3Zr:

Brown, hexagonal prismatic crystals of the compound were grown by slow cooling of an ether solution to -80°C. In a dry box under N_2, the crystals were dumped into a small Petri dish and covered with degassed Paratone N, a viscous, high molecular weight oil. A hexagonal prism measuring 0.20 mm across by 0.40 mm long was mounted on a 0.2 mm thin walled capillary. The crystal was transferred to an Enraf-Nonius CAD-4 automated diffractometer and cooled to -108 °C under a cold stream previously calibrated by a thermocouple placed in the sample position. The crystal was centered in the beam. Automatic peak search and indexing procedures indicated that the crystal possessed a trigonal cell and yielded the unit cell parameters. The cell parameters and data collection parameters are given in the following table.

The data collected was the (±h,+k,+l) quadrant. The 851 raw intensity data were converted to structure factor amplitudes and their esds by correction for scan speed, background, and Lorentz-polarization effects.[1] Inspection of the intensity standards showed very severe decay at the middle of the data collection (presumably due to crystal movement). The last half of the data was discarded; it was redundant. No decay correction was applied to the remaining 532 data Systematic absences for (0,0,l), l odd was observed, and these 5 data were discarded. Azimuthal scan data showed a difference of I_{min}/I_{max}=0.78 for the averaged curve. An empirical absorption correction was applied based upon the averaged curve. Finally, redundant data were averaged (R_{int} =0.037) yielding 266 unique data and 245 data with $F_o>3\sigma$.

The cell volume 570 cm^3 indicated that Z=2 by comparison to the volume of the Cp_3Ti structure. In addition, EPR experiments suggested axial symmetry. These data along with systematic absences suggested a space group of $P6_3$ or $P6_3/m$ with the molecule possessing either 3 or $\bar{3}$ symmetry, respectively. The solution of the Patterson map placed the zirconium at (0.67, 0.33, 0.25). Initially solution was attempted in $P6_3$:

The carbon positions were obtained by a difference Fourier search after refining on the zirconium position. With the carbon atoms refined isotropically and the zirconium refined anisotropically, the R value was 5.1%. However, when anisotropic refinement was attempted on the carbon atoms, the thermal parameters were highly correlated, and the carbon atoms became non-positive definite. Refinement was then attempted in $P6_3/m$ since the molecule seemed to possess $\bar{3}$ symmetry anyway. With the carbon atoms refined isotropically, and the zirconium atom refined anisotropically, the R value was 5.2%. In addition, the carbon atoms could be refined anisotropically. When the heavy atom refinement had converged, a difference Fourier showed the position of the 3 hydrogen atoms. The hydrogen atoms were included in the refinement and refined isotropically. Toward the end of the refinement, an examination of the extinction test listing suggested that secondary extinction was occurring, so a secondary extinction coefficient was included and refined to 1.67×10^{-6}.

The final residuals for 39 variables refined against the 245 data with $F_o > 3\sigma(F_o)$ were R=2.97%, R_w=3.25%, and GOF=1.179. The R value for all data (including unobserved reflections) was 3.2%. The quantity minimized by the least squares refinements was $w(|F_o|-|F_c|)^2$, where w is the weight given to a particular reflection. The p-factor, used to reduce the weight of intense reflections, was set to 0.03 initially, but later change to 0.04.[2] The analytical form of the scattering factor tables for neutral atoms were used to all non-hydrogen scattering factors were corrected for both the real and the imaginary components of anomalous dispersion.[3]

Inspection of the residuals ordered in the ranges of $\sin(\theta/\lambda)$, $|F_o|$, and parity and value of the individual indexes showed no trend other than the one previously mentioned in connection with secondary extinction. Three reflections had anomalously high values of $w\Delta^2$, and were weighted to zero toward the end of the refinement. The largest positive and negative peaks in the final difference Fourier map have electron densities of 0.58 and -0.65, respectively, and are associated with the zirconium atom.

Table of crystal data for Cp_3Zr

Space group:	$P6_3/m$
a (Å)	8.003(1)
b (Å)	8.003(1)
c (Å)	10.276(2)
α (deg)	90
β (deg)	90
γ (deg)	120
V ($Å^3$)	570.0
Z	2
d(calc.) g/cm^3	1.668
μ(calc) 1/cm	9.148
radiation	MoKα
monochrometer	highly oriented graphite
scan range, type	$3° \leq 2\theta \leq 45°$, θ-2θ
scan speed (deg/min)	2.8
scan width, deg.	$\Delta\theta = 0.90 + 0.35\tan(\theta)$
reflections collected	851($\pm$h,+k,+l), 532 used
unique reflections	266 (R_{int} = 0.037)
reflections $F_o^2 > 3\sigma(F_o^2)$	245
R, %	2.97
R_w, %	3.25
R_{all}, %	3.20
GOF	1.179
Largest Δ/σ in final least squares cycle	0

Intensity standards: (4, 0, 1); (0, 3, 4); (-1, 1, -5) measured every hour of X-ray exposure time. No loss of in intensity occurred.

Orientation Standards: 3 reflections were checked after every 200 measurements. Crystal orientation was redetermined if any of the reflections were offset from their predicted positions by more than 0.1°. Reorientation was required once over the course of the data collection. The cell constants and errors are listed as their final values.

Table of atomic positions in Cp_3Zr

Atoms	X	Y	Z	B_{eq} (A^2)
Zr	-1/3	1/3	1/4	1.33(1)
C1	0.0168(3)	0.5827(3)	0.3170(3)	1.44(5)
C2	-0.1032(4)	0.6551(3)	0.3607(3)	1.66(6)
C3	-0.1683(5)	0.7062(5)	1/4	1.47(8)
H3	-0.245(4)	0.749(5)	1/4	1.0(8)*
H1	0.088(4)	0.538(3)	0.366(3)	2.1(6)*
H2	-0.125(4)	0.670(3)	0.452(2)	2.4(6)*
Cp	-0.068	0.636	1/4	0.4

Starred atoms were included with isotropic thermal parameters. The thermal parameter given for anisotropically refined atoms is the isotropic equivalent thermal parameter defined as:

$$(4/3)[a^2B(1,1) + b^2B(2,2) + c^2B(3,3) + ab(\cos\gamma)B(1,2) + ac(\cos\beta)B(1,3) + bc(\cos\alpha)B(2,3)]$$

where a,b,c are real cell parameters, and B(i,j) are anisotropic betas.

Table of anisotropic thermal parameters for Cp_3Zr

Atom	B(1,1)	B(2,2)	B(3,3)	B(1,2)	B(1,3)	B(2,3)
Zr	0.82(2)	B(1,1)	2.36(3)	B(1,1)	0	0
C1	0.84(7)	1.13(7)	2.1(1)	0.33(5)	-0.37(8)	-0.15(9)
C2	1.55(8)	1.45(8)	1.5(1)	0.39(6)	0.0(1)	-0.50(9)
C3	1.0(1)	0.8(1)	2.6(2)	0.44(7)	0	0

The form of the anisotropic temperature factor is:

$$\exp[-0.25\{h^2a^2B(1,1) + k^2b^2B(2,2) + l^2c^2B(3,3) + 2hkabB(1,2) + 2hlacB(1,3) + 2klbcB(2,3)\}]$$

where a,b, and c are reciprocal lattice constants.

$Cp^*_2TiN(Me)H$

Rose colored crystals of the title compound were grown by cooling a saturated hexane solution to -30 °C. In a dry box, the crystals were placed in a small Petri dish and covered with Paratone N, a high molecular weight hydrocarbon oil. The crystals were examined with a microscope. A blade shaped single crystal was selected, and a roughly pyramidal chunk measuring $0.37 \times 0.40 \times 0.40$ mm was cut off of the tip. The crystal was mounted on the end of a 0.3 mm diameter glass capillary. The crystal was transferred to an Enraf-Nonius CAD-4 diffractometer and cooled to -130 °C under a cold stream of nitrogen gas previously calibrated by a thermocouple placed in the sample position. The crystal was centered in the beam. Automatic peak search and indexing procedures indicated that the crystal possessed a primitive orthorhombic cell and yielded the cell parameters. The cell parameters and data collection parameters are given in the following table.

The 1514 raw intensity data were converted to structure factor amplitudes and their esds by correction for scan speed, background, and Lorentz-polarization effects.[1] Inspection of the intensity standards showed a smooth, slightly curved decay of 14% over the data collection. The data was corrected for a linear decay of 14%. The 20 systematic absences (h,0,0), h odd; (0,k,0), k odd; and (0,0,l), l odd were then rejected yielding 1494 unique data of which 1323 had $F_o > 3\sigma(F_o)$. Azimuthal scan data showed a difference of $I_{min}/I_{max} = 0.85$ for the averaged curve. An empirical absorption correction was applied based upon the averaged curve. The systematic absences indicated that the space group was $P2_12_12_1$.

The cell volume indicated that 4 molecules were present in the unit cell. The titanium atom position was obtained by solving the Patterson map. Refinement on the titanium position lead to the titanium becoming non-positive definite. However, a difference Fourier search yielded most of the other heavy atom positions. The heavy-

atom structure was refined by standard least squares and Fourier techniques. The heavy atoms were refined anisotropically, and a difference Fourier search located almost all of the hydrogen atoms. The amide hydrogen was included in the refinement with an isotropic thermal parameter and behaved normally. The other hydrogen positions were then calculated based upon idealized bonding geometry and assigned thermal parameters equal to 1.3 $Å^2$ larger than the carbon atom to which they were connected. The non-amide hydrogen positions were included in the structure factor calculations but not refined by least squares. At the end of the refinement, the enantiomer was changed, and the structure refined. The refinement was very slightly worse, so the enantiomer was changed back to the original one. A final difference Fourier map showed no additional atoms in the asymmetric unit. Examination of intermolecular close contacts (<3.5Å) showed that the molecule was a monomer.

The final residuals for 212 variables refined against the 1315 unique data with $F_o > 3\sigma(F_o)$ were R = 4.83%, R_w = 6.22%, and GOF = 2.04. The R value for all data (including unobserved reflections) was 5.58%. The quantity minimized by the least squares refinements was $w(|F_o| - |F_c|)^2$, where w is the weight given to a particular reflection. The p-factor, used to reduce the weight of intense reflections, was set to 0.03 initially, but later changed to 0.05.[2] The analytical form of the scattering factor tables for neutral atoms were used and all non-hydrogen scattering factors were corrected for both the real and imaginary components of anomalous dispersion.[3]

Inspection of the residuals ordered in the ranges of $\sin(\theta/\lambda)$, $|F_o|$, and parity and values of the individual indexes showed no trends. Eight reflections had anomalously high values of $w\Delta^2$, and were weighted to zero toward the end of the refinement. The largest positive and negative peaks in the final difference Fourier map have electron densities of 0.43 and -0.58, respectively, and are associated with the titanium atom.

Table of crystal data for $Cp^*_2TiN(Me)H$

Space group:	$P2_12_12_1$
a, Å	8.718(2)
b, Å	14.133(4)
c, Å	15.999(3)
α, deg.	90
β, deg.	90
γ, deg.	90
V, $Å^3$	1971.26
Z	4
fw	348.41
d (calc.) g/cm^3	1.174
μ (calc.) 1/cm	4.287
radiation	MoKα(λ= 0.71073 Å)
monochrometer	highly oriented graphite
scan range, type	$3° \leq 2\theta \leq 45°$, θ-2θ
scan speed, deg/min	3.4
scan width, deg	$\Delta\theta = 0.85 + 0.35\tan\theta$
reflections collected	1514; +h,+k,+l
unique reflections	1494
reflections $F_o^2 > 3\sigma(F_o^2)$	1315
R, %	4.83
R_w, %	6.22
R_{all}, %	5.58
GOF	2.036
Largest Δ/σ in final least squares cycle	0

Intensity standards: (-1,7,-5); (2,-8,1); (-5,-1,-3) measured every hour of X-ray exposure time. A 14% decay in intensity over the collection period was corrected for linearly.

Orientation Standards: 3 reflections were checked after every 200 measurements. Crystal orientation was redetermined if any of the reflections were offset from their predicted positions by more than 0.1°. Reorientation was not required over the course of the data collection. The cell constants and errors are listed as their final values.

Table of atomic positions in $Cp^*_2TiN(Me)H$

Atoms	X	Y	Z	B_{eq} (A^2)
Ti	0.8659(1)	0.95497(6)	0.96779(1)	1.50(2)
N	0.8735(7)	0.8168(3)	0.9675(3)	3.3(1)
C1	0.9347(7)	0.9375(4)	1.1148(3)	2.0(1)
C2	0.7703(6)	0.9471(4)	1.1096(3)	1.9(1)
C3	0.7353(6)	1.0364(4)	1.0778(3)	1.9(1)
C4	0.8766(7)	1.0855(4)	1.0648(3)	1.9(1)
C5	0.9975(6)	1.0236(4)	1.0831(3)	2.2(1)
C6	0.9722(6)	1.0514(4)	0.8573(3)	1.9(1)
C7	0.8162(7)	1.0764(4)	0.8637(4)	2.5(1)
C8	0.7282(7)	0.9963(5)	0.8441(4)	3.1(1)
C9	0.8282(8)	0.9230(4)	0.8204(3)	2.8(1)
C10	0.9814(6)	0.9574(4)	0.8313(3)	1.8(1)
C11	1.0276(9)	0.8605(5)	1.1506(4)	3.8(2)
C12	0.6510(8)	0.8789(4)	1.1430(4)	3.2(1)
C13	0.5755(7)	1.0756(5)	1.0716(4)	2.9(1)
C14	0.8939(8)	1.1909(4)	1.0536(4)	3.4(1)
C15	1.1634(7)	1.0484(6)	1.0858(4)	4.0(2)
C16	1.1093(9)	1.1170(5)	0.8626(4)	4.4(2)
C17	0.753(1)	1.1751(6)	0.8721(5)	5.7(2)
C18	0.5579(8)	0.9886(7)	0.8375(4)	6.9(2)
C19	0.789(1)	0.8291(6)	0.7827(4)	6.7(2)
C20	1.130(1)	0.9053(5)	0.8117(4)	4.5(2)
C21	0.856(1)	0.7325(4)	1.0179(3)	4.3(2)
H1	0.901(6)	0.799(3)	0.925(3)	3(1)*
H11A	1.13339(1)	0.87509(1)	1.14439(1)	4.9*
H11B	1.00535(1)	0.80307(1)	1.12233(1)	4.9*
H11C	1.00407(1)	0.85383(1)	1.20830(1)	4.9*
H12A	0.69996(1)	0.82262(1)	1.16134(1)	4.1*
H12B	0.57976(1)	0.86413(1)	1.09995(1)	4.1*
H12C	0.59834(1)	0.90731(1)	1.18852(1)	4.1*
H13A	0.50348(1)	1.02701(1)	1.08347(1)	3.8*
H13B	0.55860(1)	1.09902(1)	1.01674(1)	3.8*
H13C	0.56353(1)	1.12561(1)	1.11077(1)	3.8*
H14A	0.79667(1)	1.21797(1)	1.04161(1)	4.4*
H14B	0.96233(1)	1.20318(1)	1.00870(1)	4.4*
H14C	0.93364(1)	1.21782(1)	1.10351(1)	4.4*
H15A	1.17844(1)	1.10885(1)	1.06127(1)	5.2*
H15B	1.22052(1)	1.00239(1)	1.05574(1)	5.2*
H15C	1.19710(1)	1.04968(1)	1.14230(1)	5.2*
H16A	1.20095(1)	1.08131(1)	0.85624(1)	5.7*
H16B	1.10991(1)	1.14772(1)	0.91540(1)	5.7*
H16C	1.10311(1)	1.16299(1)	0.81945(1)	5.7*
H17A	0.83331(1)	1.21763(1)	0.88564(1)	7.4*
H17B	0.67766(1)	1.17627(1)	0.91521(1)	7.4*
H17C	0.70681(1)	1.19370(1)	0.82080(1)	7.4*

Table of atomic positions in $Cp^*_2TiN(Me)H$ (continued)

Atoms	X	Y	Z	B_{eq} (A^2)
H18A	0.51202(1)	1.04562(1)	0.85664(1)	9.0*
H18B	0.52307(1)	0.93722(1)	0.87068(1)	9.0*
H18C	0.53006(1)	0.97815(1)	0.78079(1)	9.0*
H19A	0.68029(1)	0.82166(1)	0.78188(1)	8.7*
H19B	0.83319(1)	0.78001(1)	0.81516(1)	8.7*
H19C	0.82712(1)	0.82617(1)	0.72725(1)	8.7*
H20A	1.10751(1)	0.84222(1)	0.79526(1)	5.8*
H20B	1.19359(1)	0.90442(1)	0.85994(1)	5.8*
H20C	1.18218(1)	0.93677(1)	0.76749(1)	5.8*
H21A	0.87350(1)	0.67813(1)	0.98431(1)	5.6*
H21B	0.75454(1)	0.73019(1)	1.03985(1)	5.6*
H21C	0.92745(1)	0.73373(1)	1.06257(1)	5.6*
Cp1	0.86288(1)	1.00602(1)	1.09000(1)	4.0*
Cp2	0.86523(1)	1.00092(1)	0.84338(1)	4.0*

Starred atoms were included with isotropic thermal parameters. The thermal parameter given for anisotropically refined atoms is the isotropic equivalent thermal parameter defined as:

$$(4/3)\,[a^2B(1,1) + b^2B(2,2) + c^2B(3,3) + ab(\cos\gamma)B(1,2) + ac(\cos\beta)B(1,3) + bc(\cos\alpha)B(2,3)]$$

where a,b,c are real cell parameters, and B(i,j) are anisotropic betas.

Table of anisotropic thermal parameters for $Cp^*_2TiN(Me)H$

Atom	B(1,1)	B(2,2)	B(3,3)	B(1,2)	B(1,3)	B(2,3)
Ti	1.80(3)	1.63(3)	1.07(3)	0.09(4)	0.03(4)	0.19(3)
N	6.6(3)	1.9(2)	1.5(2)	0.6(2)	0.3(3)	-0.2(2)
C1	3.1(2)	1.8(2)	1.1(2)	0.1(2)	0.0(2)	-0.6(2)
C2	2.0(2)	2.6(2)	1.0(2)	-0.5(2)	0.4(2)	0.4(2)
C3	1.6(2)	2.5(2)	1.6(2)	0.6(2)	0.4(2)	0.3(2)
C4	1.9(2)	2.3(2)	1.5(2)	-0.7(2)	0.3(2)	-0.5(2)
C5	1.6(2)	3.4(3)	1.6(2)	0.4(2)	-0.2(2)	-0.1(2)
C6	2.1(2)	2.6(2)	1.0(2)	-1.0(2)	0.5(2)	0.4(2)
C7	2.6(3)	2.8(2)	2.1(2)	1.3(2)	0.7(2)	1.1(2)
C8	1.4(2)	5.7(3)	2.0(2)	-0.1(3)	0.1(2)	1.2(3)
C9	5.4(4)	2.5(2)	0.6(2)	-1.3(3)	-0.6(2)	0.3(2)
C10	2.2(2)	2.0(2)	1.2(2)	0.1(2)	0.3(2)	0.1(2)
C11	3.9(3)	5.5(3)	1.9(2)	1.8(3)	-1.0(3)	-0.4(3)
C12	3.9(3)	3.2(3)	2.4(2)	-0.8(3)	0.7(3)	0.4(2)
C13	2.3(3)	4.2(3)	2.3(2)	0.6(2)	0.8(2)	0.0(2)
C14	4.3(3)	2.7(3)	3.1(3)	-0.3(3)	1.1(3)	-0.3(2)
C15	2.5(3)	6.5(4)	3.0(3)	-1.1(4)	-0.3(2)	-0.0(3)
C16	5.3(4)	4.8(3)	3.0(3)	-2.8(3)	0.8(3)	-0.3(3)
C17	8.6(5)	5.3(3)	3.1(3)	3.8(4)	1.8(4)	1.5(3)
C18	2.1(3)	14.2(6)	4.4(3)	-1.2(4)	-1.2(3)	5.5(4)
C19	11.9(6)	6.6(4)	1.5(3)	-6.5(4)	-1.7(3)	0.6(3)
C20	5.6(4)	5.1(3)	2.7(3)	2.5(4)	2.0(3)	1.1(3)
C21	8.3(5)	2.6(3)	2.0(3)	-0.2(4)	0.8(4)	0.1(2)

The form of the anisotropic temperature factor is:

$$\exp[-0.25\{h^2a^2B(1,1) + k^2b^2B(2,2) + l^2c^2B(3,3) + 2hkabB(1,2) + 2hlacB(1,3) + 2klbcB(2,3)\}]$$

where a,b, and c are reciprocal lattice constants.

Cp^*_2TiF

Dark green crystals of the compound were grown by cooling a saturated hexane solution to -30 °C. The crystals were taken into an inert atmosphere box. They were placed in a small Petri dish and covered with Paratone N, a high molecular weight hydrocarbon oil. The dish was removed from the box, and the crystals were examined with a microscope. A large, blocky single crystal was selected and a block shaped piece measuring $0.30 \times 0.40 \times 0.45$ mm was cut from one corner. The crystal was mounted on the end of a 0.4 mm diameter quartz capillary. The crystal was transferred to an Enraf-Nonius CAD-4 diffractometer and cooled to -115 °C under a cold stream of nitrogen gas previously calibrated by a thermocouple placed in the sample position. The crystal was centered in the beam. Automatic peak search and indexing procedures indicated that the crystal possessed a primitive monoclinic cell and yielded the cell parameters. The cell parameters and data collection parameters are given in the following table.

The 5178 raw intensity data were converted to structure factor amplitudes and their esds by correction for scan speed, background, and Lorentz-polarization effects.[1] Inspection of the intensity standards showed a sudden intensity loss of 12% between hours 6 and 7. The data collected after hour 7 was corrected for a 12% loss in intensity. The 226 systematic absences (h,0,l), l odd; (0,k,0), k odd; the 191 redundant data (0,k,l), l<0; and the 225 data collected between hours 6 and 7 were then rejected yielding 4536 unique data of which 3188 possessed $F_o > 3\sigma(F_o)$. Azimuthal scan data showed a difference of $I_{min}/I_{max} = 0.81$ for the averaged curve; however, the absorption curves were asymmetric. No empirical absorption correction was applied. The systematic absences indicated that the space group was $P2_1/c$.

The cell volume indicated that 8 molecules were present in the unit cell. The titanium atom positions for the two independent molecules were obtained by solving the

Patterson map. The remaining heavy atom positions were obtained by successive Fourier searches and cycles of refinement. The heavy atom structure was refined by standard least squares techniques. The heavy atoms were refined isotropically, and the hydrogen positions were then calculated based upon idealized bonding geometry and assigned thermal parameters equal to 1.3 $Å^2$ larger than the carbon atom to which they were connected. A Gaussian absorption correction, DIFABS, was applied. The heavy atoms were then refined anisotropically. The fluorine atom positions in both molecules are disordered. A final difference Fourier map showed no additional atoms in the asymmetric unit. Examination of intermolecular close contacts (<3.5 Å) showed that the molecules were monomers.

The final residuals for 397 variables refined against the 3188 unique data with $F_o > 3\sigma(F_o)$ were R = 6.90%, R_w = 9.11%, and GOF = 2.054. The R value for all data (including unobserved reflections) was 9.91%. The quantity minimized by the least squares refinements was $w(|F_o| - |F_c|)^2$, where w is the weight given to a particular reflection. The p-factor, used to reduce the weight of intense reflections, was set to 0.03 initially, but later changed to 0.07.[2] The analytical form of the scattering factor tables for neutral atoms were used and all non-hydrogen scattering factors were corrected for both the real and imaginary components of anomalous dispersion.[3]

Inspection of the residuals ordered in the ranges of $\sin(\theta/\lambda)$, $|F_o|$, and parity and values of the individual indexes showed no trends. Five reflections had anomalously high values of $w\Delta^2$, and were weighted to zero toward the end of the refinement. The largest positive and negative peaks in the final difference Fourier map have electron densities of 0.66 and -0.17, respectively, and are associated with the one titanium atoms.

Table of crystal data for Cp^*_2TiF

Space group:	$P2_1/c$
a, Å	16.033(2)
b, Å	15.113(2)
c, Å	16.027(2)
α, deg.	90
β, deg.	109.70(1)
γ, deg.	90
V, $Å^3$	3656(2)
Z	8
fw	337.36
d (calc.) g/cm^3	1.226
μ (calc.) 1/cm	4.663
radiation	MoKα(λ= 0.71073 Å)
monochrometer	highly oriented graphite
scan range, type	$3° \leq 2\theta \leq 45°$, θ-2θ
scan speed, deg/min	3.4
scan width, deg	$\Delta\theta = 0.80 + 0.35\tan\theta$
reflections collected	5178(+h,+k,±l)
unique reflections	4536
reflections $F_o^2 > 3\sigma(F_o^2)$	3188
R, %	6.90
R_w, %	9.11
R_{all}, %	9.91
GOF	2.054
Largest Δ/σ in final least squares cycle	0

Intensity standards: (8, 3, 2); (-1, -9, 2); (4, -8, -4) measured every hour of X-ray exposure time. A 12% loss of intensity occurred between hours 6 and 7 was corrected for by removing the data collected between hours 6 and 7 and correcting the following data for a 12% loss of intensity..

Orientation Standards: 3 reflections were checked after every 200 measurements. Crystal orientation was redetermined if any of the reflections were offset from their predicted positions by more than 0.1°. Reorientation was required twice over the course of the data collection. The cell constants and errors are listed as their final values.

Table of atomic positions in Cp^*_2TiF

Atoms	X	Y	Z	B_{eq} (A^2)
Ti1	0.10425(8)	0.25047(7)	0.24046(7)	1.83(2)
Ti2	0.40535(8)	0.81165(7)	0.20336(7)	1.69(2)
F1	0.1289(4)	0.2516(3)	0.1360(3)	7.3(1)
F2	0.4224(5)	0.9319(3)	0.2034(3)	8.1(2)
C101	0.1460(4)	0.1002(4)	0.2437(4)	1.9(1)
C102	0.0569(4)	0.1039(4)	0.1903(4)	1.7(1)
C103	0.0073(4)	0.1328(4)	0.2444(4)	1.6(1)
C104	0.0647(4)	0.1420(4)	0.3310(4)	1.9(1)
C105	0.1527(4)	0.1235(4)	0.3322(4)	1.9(1)
C106	0.0348(4)	0.3902(4)	0.2179(4)	2.2(1)
C107	0.0399(4)	0.3630(4)	0.3054(4)	2.2(1)
C108	0.1293(4)	0.3560(4)	0.3595(4)	1.9(1)
C109	0.1813(4)	0.3810(4)	0.3054(4)	1.8(1)
C110	0.1244(4)	0.4039(4)	0.2220(4)	2.0(1)
C111	0.2218(5)	0.0730(5)	0.2144(5)	3.3(2)
C112	0.0182(5)	0.0847(4)	0.0933(4)	2.6(2)
C113	-0.0931(4)	0.1354(5)	0.2119(4)	2.6(2)
C114	0.0387(5)	0.1507(5)	0.4117(4)	2.6(1)
C115	0.2342(5)	0.1163(5)	0.4120(5)	3.4(2)
C116	-0.0469(5)	0.4070(5)	0.1428(5)	3.2(2)
C117	-0.0404(5)	0.3563(5)	0.3328(5)	3.1(2)
C118	0.1647(5)	0.3424(4)	0.4562(4)	2.8(2)
C119	0.2813(4)	0.3865(5)	0.3407(4)	2.7(2)
C120	0.1520(5)	0.4380(5)	0.1469(4)	3.0(2)
C201	0.4357(4)	0.7415(4)	0.0836(4)	1.6(1)
C202	0.3620(4)	0.6959(4)	0.0934(4)	1.6(1)
C203	0.2910(4)	0.7580(4)	0.0774(4)	1.6(1)
C204	0.3190(4)	0.8396(4)	0.0529(4)	1.9(1)
C205	0.4088(4)	0.8294(4)	0.0572(4)	1.8(1)
C206	0.4439(4)	0.8461(4)	0.3552(4)	1.7(1)
C207	0.3705(4)	0.7910(4)	0.3344(4)	1.6(1)
C208	0.3937(4)	0.7063(4)	0.3114(4)	1.7(1)
C209	0.4854(4)	0.7102(4)	0.3188(4)	2.1(1)
C210	0.5145(4)	0.7977(4)	0.3439(4)	1.9(1)
C211	0.5234(4)	0.7022(4)	0.0897(4)	2.2(1)
C212	0.3559(4)	0.5984(4)	0.1039(4)	2.6(1)
C213	0.1983(4)	0.7358(5)	0.0729(4)	2.8(2)
C214	0.2653(5)	0.9217(5)	0.0284(4)	2.8(2)
C215	0.4642(5)	0.8992(4)	0.0369(4)	2.6(1)
C216	0.4493(5)	0.9403(5)	0.3869(4)	2.8(2)
C217	0.2815(5)	0.8139(5)	0.3426(4)	3.0(2)
C218	0.3376(5)	0.6252(5)	0.3006(4)	3.0(2)
C219	0.5429(5)	0.6353(5)	0.3124(5)	3.8(2)
C220	0.6066(5)	0.8326(6)	0.3592(5)	3.8(2)

Table of atomic positions in Cp^*_2TiF (continued)

Atoms	X	Y	Z	B_{eq} (A^2)
H1	0.27551(1)	0.07611(1)	0.26322(1)	4.3*
H2	0.21272(1)	0.01409(1)	0.19253(1)	4.3*
H3	0.22505(1)	0.11162(1)	0.16882(1)	4.3*
H4	0.06388(1)	0.06656(1)	0.07171(1)	3.4*
H5	-0.02455(1)	0.03884(1)	0.08371(1)	3.4*
H6	-0.00943(1)	0.13653(1)	0.06275(1)	3.4*
H7	-0.11520(1)	0.12728(1)	0.14949(1)	3.4*
H8	-0.11472(1)	0.08943(1)	0.23963(1)	3.4*
H9	-0.11238(1)	0.19096(1)	0.22632(1)	3.4*
H10	-0.02288(1)	0.16296(1)	0.39454(1)	3.4*
H11	0.05128(1)	0.09693(1)	0.44436(1)	3.4*
H12	0.07120(1)	0.19757(1)	0.44757(1)	3.4*
H13	0.22147(1)	0.13591(1)	0.46273(1)	4.4*
H14	0.25320(1)	0.05644(1)	0.41996(1)	4.4*
H15	0.27966(1)	0.15206(1)	0.40404(1)	4.4*
H16	-0.03206(1)	0.42420(1)	0.09246(1)	4.1*
H17	-0.08171(1)	0.35470(1)	0.12947(1)	4.1*
H18	-0.07960(1)	0.45305(1)	0.15783(1)	4.1*
H19	-0.09218(1)	0.36362(1)	0.28232(1)	4.0*
H20	-0.04168(1)	0.29984(1)	0.35843(1)	4.0*
H21	-0.03838(1)	0.40112(1)	0.37497(1)	4.0*
H22	0.11783(1)	0.32633(1)	0.47688(1)	3.6*
H23	0.20777(1)	0.29662(1)	0.46968(1)	3.6*
H24	0.19134(1)	0.39566(1)	0.48431(1)	3.6*
H25	0.30242(1)	0.36626(1)	0.40031(1)	3.5*
H26	0.30503(1)	0.35057(1)	0.30557(1)	3.5*
H27	0.29912(1)	0.44613(1)	0.33847(1)	3.5*
H28	0.21481(1)	0.44137(1)	0.16551(1)	3.9*
H29	0.13116(1)	0.39896(1)	0.09777(1)	3.9*
H30	0.12752(1)	0.49518(1)	0.13008(1)	3.9*
H31	0.56082(1)	0.74718(1)	0.08060(1)	2.9*
H32	0.55019(1)	0.67668(1)	0.14665(1)	2.9*
H33	0.51474(1)	0.65777(1)	0.04560(1)	2.9*
H34	0.41238(1)	0.57232(1)	0.11388(1)	3.3*
H35	0.33701(1)	0.58639(1)	0.15291(1)	3.3*
H36	0.31444(1)	0.57421(1)	0.05157(1)	3.3*
H37	0.19670(1)	0.67687(1)	0.09312(1)	3.7*
H38	0.18015(1)	0.77547(1)	0.10947(1)	3.7*
H39	0.15946(1)	0.74085(1)	0.01348(1)	3.7*
H40	0.20764(1)	0.91113(1)	0.03055(1)	3.6*
H41	0.29291(1)	0.96752(1)	0.06890(1)	3.6*
H42	0.26100(1)	0.93906(1)	-0.02987(1)	3.6*
H43	0.43068(1)	0.95220(1)	0.02079(1)	3.3*
H44	0.51488(1)	0.90977(1)	0.08766(1)	3.3*
H45	0.48244(1)	0.88042(1)	-0.01086(1)	3.3*
H46	0.50704(1)	0.96278(1)	0.39621(1)	3.7*
H47	0.40702(1)	0.97518(1)	0.34351(1)	3.7*

Table of atomic positions in Cp^*_2TiF (continued)

Atoms	X	Y	Z	B_{eq} (A^2)
H48	0.43710(1)	0.94235(1)	0.44088(1)	3.7*
H49	0.28123(1)	0.87443(1)	0.35862(1)	3.9*
H50	0.23598(1)	0.80393(1)	0.28738(1)	3.9*
H51	0.27149(1)	0.77784(1)	0.38679(1)	3.9*
H52	0.27940(1)	0.64165(1)	0.29748(1)	3.9*
H53	0.33517(1)	0.59541(1)	0.24766(1)	3.9*
H54	0.36248(1)	0.58703(1)	0.34985(1)	3.9*
H55	0.50786(1)	0.58348(1)	0.29423(1)	4.9*
H56	0.57071(1)	0.64904(1)	0.27022(1)	4.9*
H57	0.58678(1)	0.62541(1)	0.36861(1)	4.9*
H58	0.64194(1)	0.78728(1)	0.34709(1)	4.9*
H59	0.60357(1)	0.88149(1)	0.32103(1)	4.9*
H60	0.63219(1)	0.85104(1)	0.41910(1)	4.9*
Cp1	0.08554(1)	0.12050(1)	0.26833(1)	0.4*
Cp2	0.10195(1)	0.37881(1)	0.28205(1)	0.4*
Cp3	0.36329(1)	0.77286(1)	0.07290(1)	0.4*
Cp4	0.44160(1)	0.77025(1)	0.33272(1)	0.4*

Starred atoms were included with isotropic thermal parameters. The thermal parameter given for anisotropically refined atoms is the isotropic equivalent thermal parameter defined as:

$$(4/3)[a^2B(1,1) + b^2B(2,2) + c^2B(3,3) + ab(\cos\gamma)B(1,2) + ac(\cos\beta)B(1,3) + bc(\cos\alpha)B(2,3)]$$

where a,b,c are real cell parameters, and B(i,j) are anisotropic betas.

Table of anisotropic thermal parameters for Cp^*_2TiF

Atom	B(1,1)	B(2,2)	B(3,3)	B(1,2)	B(1,3)	B(2,3)
Ti1	1.99(4)	1.56(4)	2.22(4)	-0.34(4)	1.07(3)	-0.29(3)
Ti2	1.86(5)	1.49(4)	1.55(4)	-0.25(4)	0.36(3)	-0.08(3)
F1	16.7(3)	2.5(2)	6.4(2)	-1.0(2)	8.7(1)	-0.7(1)
F2	18.0(5)	2.6(2)	2.3(2)	-2.8(3)	1.6(2)	-0.3(1)
C101	1.5(3)	1.6(2)	2.4(2)	0.6(2)	0.5(2)	0.3(2)
C102	1.6(2)	1.3(2)	2.0(2)	-0.2(2)	0.5(2)	-0.2(2)
C103	1.1(2)	1.0(2)	2.7(2)	-0.0(2)	0.5(2)	0.1(2)
C104	1.8(3)	1.6(2)	2.2(2)	0.1(2)	0.7(2)	0.1(2)
C105	1.3(3)	1.9(2)	2.1(2)	0.1(2)	0.0(2)	0.4(2)
C106	1.3(3)	2.1(2)	2.6(3)	-0.1(2)	0.1(2)	-0.6(2)
C107	1.4(2)	2.2(2)	3.6(3)	-0.6(2)	1.4(2)	-0.6(2)
C108	1.4(2)	2.0(2)	2.5(2)	-0.3(2)	0.7(2)	-0.8(2)
C109	1.0(2)	2.0(2)	2.3(2)	-0.7(2)	0.3(2)	-0.4(2)
C110	2.1(3)	1.3(2)	2.8(2)	-0.6(2)	1.1(2)	-0.5(2)
C111	2.7(3)	3.4(3)	4.4(3)	0.6(3)	1.9(2)	-0.4(3)
C112	2.7(3)	2.2(3)	2.7(3)	-0.4(3)	0.7(2)	-0.3(2)
C113	1.4(3)	3.0(3)	3.2(3)	-0.3(3)	0.5(2)	-0.1(2)
C114	2.6(3)	3.2(3)	2.1(2)	-0.7(3)	1.0(2)	0.0(2)
C115	2.4(3)	3.9(3)	3.1(3)	-0.0(3)	-0.2(3)	-0.3(3)
C116	2.7(3)	2.4(3)	3.9(3)	-0.1(3)	0.5(3)	0.1(2)
C117	2.0(3)	2.9(3)	4.6(3)	0.2(3)	1.6(2)	-0.8(2)
C118	3.0(3)	2.4(3)	3.2(3)	-1.1(3)	1.3(2)	-1.1(2)
C119	1.7(3)	3.1(3)	3.3(3)	-0.7(3)	1.0(2)	-0.4(2)
C120	3.2(3)	2.7(3)	3.2(3)	-0.4(3)	1.4(2)	0.2(2)
C201	1.3(2)	1.8(2)	1.7(2)	0.0(2)	0.6(2)	-0.3(2)
C202	1.4(2)	1.9(2)	1.7(2)	-0.4(2)	0.5(2)	-0.4(2)
C203	0.7(2)	2.6(2)	1.3(2)	-0.3(2)	0.0(2)	-0.8(2)
C204	1.7(3)	2.5(3)	1.3(2)	0.2(2)	0.1(2)	-0.1(2)
C205	1.2(2)	2.7(3)	1.5(2)	-0.3(2)	0.6(2)	-0.7(2)
C206	1.7(3)	2.1(2)	0.9(2)	-0.6(2)	0.1(2)	0.1(2)
C207	1.1(2)	2.2(2)	1.6(2)	-0.2(2)	0.6(2)	0.1(2)
C208	1.7(3)	2.0(2)	1.2(2)	-0.2(2)	0.2(2)	0.5(2)
C209	2.0(3)	2.6(3)	1.7(2)	0.7(2)	0.6(2)	0.7(2)
C210	1.2(2)	2.3(2)	1.9(2)	-0.4(2)	0.1(2)	0.0(2)
C211	1.9(3)	2.2(2)	3.0(2)	0.1(2)	1.3(2)	-0.1(2)
C212	2.3(3)	2.5(3)	3.2(3)	-0.6(2)	1.4(2)	-1.3(2)
C213	1.2(3)	4.2(3)	3.0(3)	-0.2(3)	0.5(2)	-0.3(3)
C214	2.4(3)	2.8(3)	2.9(3)	0.0(3)	0.7(2)	-0.1(2)
C215	2.3(3)	3.1(3)	2.5(2)	-0.8(2)	1.1(2)	0.1(2)
C216	3.0(3)	3.1(3)	2.3(2)	-1.0(3)	0.8(2)	-0.7(2)
C217	2.2(3)	4.0(3)	3.1(3)	0.3(3)	1.2(2)	0.4(3)
C218	3.6(3)	3.3(3)	2.6(2)	-1.3(3)	1.6(2)	-0.1(2)
C219	3.8(3)	3.6(3)	4.2(3)	2.2(3)	1.7(2)	1.2(3)
C220	1.2(3)	5.9(4)	3.9(3)	-0.8(3)	0.4(2)	0.1(3)

The form of the anisotropic temperature factor is:

$\exp[-0.25\{h^2a^2B(1,1) + k^2b^2B(2,2) + l^2c^2B(3,3) + 2hkabB(1,2) + 2hlacB(1,3) + 2klbcB(2,3)\}]$ where a,b, and c are reciprocal lattice constants.

Cp^*_2TiH

Red crystals of the compound were grown by cooling a hexane solution of the compound to -20 °C. The crystals were placed in Petri dish of Paratone N in a glove bag. A suitable irregularly shaped crystal measuring 0.26 mm × 0.20 mm × 0.20 mm was mounted on the end of a 0.2 mm thin walled quartz capillary. The crystal was transferred to an Siemens SMART diffractometer and cooled to -137 °C under a cold stream previously calibrated by a thermocouple placed in the sample position. The crystal was centered in the beam. Automatic peak search and indexing procedures indicated that the crystal possessed a C centered monoclinic cell and yielded the unit cell parameters. The cell parameters and data collection parameters are given in the following table. Based upon a statistical analysis of intensity distribution and the successful solution and refinement of the crystal structure, the space group was found to be C2/c.

An arbitrary hemisphere of data was collected using the default parameters for the diffractometer. The data were collected as 30 s images with an area detector. Two images were averaged to give the net image data. The image data were converted to intensity data using the program SAINT. The 16761 raw intensity data were converted to structure factor amplitudes and their esds by correction for scan speed, background, and Lorentz-polarization effects.[1] Inspection of the intensity standards showed no decrease in intensity over the duration of data collection. Due to the small value of μ, no absorption correction was used. Averaging equivalent reflections gave 6740 unique data (R_{int} = 0.043).

The titanium atom positions were obtained by direct methods. Refinement on the titanium positions followed by a difference Fourier search yielded the other heavy atom positions. The heavy atom structure was refined by standard least squares and Fourier techniques. The heavy atoms were refined with anisotropic thermal parameters. The Cp* hydrogen positions were refined on with all thermal parameters equal to 4.98 $Å^2$.

The hydrides were refined with isotropic thermal parameters. Towards the end of the refinement, examination of the extinction test listing indicated that secondary extinction was occurring. The secondary extinction coefficient was refined to 5.37×10^{-8}. A final difference Fourier map showed no additional atoms in the asymmetric unit. No close (< 3.5 Å) intermolecular contacts were found.

The final residuals for 568 variables refined against the 4528 unique data with $I > 3\sigma(I)$ were $R = 4.8\%$, $R_w = 5.7\%$, and GOF = 2.01. The quantity minimized by the least squares refinements was $w(|F_o| - |F_c|)^2$, where w is the weight given to a particular reflection. The p-factor, used to reduce the weight of intense reflections, was set to 0.03.[2] The analytical form of the scattering factor tables for neutral atoms were used and all non-hydrogen scattering factors were corrected for both the real and imaginary components of anomalous dispersion.[3]

Inspection of the residuals ordered in the ranges of $\sin(\theta/\lambda)$, $|F_o|$, and parity and values of the individual indexes showed no trends other than the previously mentioned secondary extinction. No reflections had anomalously high values of $w\Delta^2$. The largest positive and negative peaks in the final difference Fourier map have electron densities of 0.30 and-0.33, respectively.

Table of crystal data for Cp^*_2TiH

Space group:	C2/c
a, Å	44.9509(7)
b, Å	8.4846(2)
c, Å	22.7333(4)
α, deg.	90
β, deg.	119.905(1)
γ, deg.	90
V, $Å^3$	7515.8(3)
Z	16
fw	319.36
d (calc.) g/cm^3	1.129
μ (calc.) 1/cm	4.49
radiation	MoKα(λ= 0.71073 Å)
monochrometer	highly oriented graphite
resolution, % coverage	0.85 Å, 97%; 0.83 Å, 90%
scan time, per image	30 s
scan type	ω, 0.3°
reflections integrated	16761
unique reflections	6740 (R_{int} = 0.043)
reflections I> 3σ(I)	4528
R, %	4.8
R_w, %	5.7
GOF	2.01
Largest Δ/σ in final least squares cycle	0.0

Table of atomic positions in Cp^*_2TiH

Atoms	X	Y	Z	B_{eq} (A^2)
TI1	0.82089(2)	0.04127(7)	0.19858(3)	2.54(3)
TI2	0.43729(2)	0.11325(7)	0.04429(3)	2.55(2)
C1	0.87134(9)	0.0065(4)	0.1929(2)	2.5(1)
C2	0.8461(1)	0.0684(4)	0.1296(2)	2.8(1)
C3	0.81964(9)	-0.0440(4)	0.0976(2)	2.6(1)
C4	0.82818(8)	-0.1760(4)	0.1415(2)	2.3(1)
C5	0.86007(8)	-0.1440(4)	0.2007(2)	2.4(1)
C6	0.9049(1)	0.0840(6)	0.2406(2)	4.0(2)
C7	0.8474(1)	0.2254(5)	0.1001(3)	4.5(2)
C8	0.7894(1)	-0.0320(6)	0.0267(2)	4.1(2)
C9	0.8098(1)	-0.3321(5)	0.1247(2)	3.3(2)
C10	0.8793(1)	-0.2556(5)	0.2590(2)	3.9(2)
C11	0.80152(8)	0.0373(4)	0.2778(2)	2.2(1)
C12	0.78360(8)	-0.0847(4)	0.2304(2)	2.3(1)
C13	0.76288(8)	-0.0132(4)	0.1659(2)	2.5(1)
C14	0.76811(8)	0.1514(4)	0.1739(2)	2.8(1)
C15	0.79213(8)	0.1829(4)	0.2431(2)	2.3(1)
C16	0.8027(1)	0.3435(4)	0.2748(2)	3.6(2)
C17	0.8250(1)	0.0156(5)	0.3531(2)	3.4(2)
C18	0.7850(1)	-0.2562(4)	0.2481(2)	3.3(2)
C19	0.7362(1)	-0.0941(6)	0.1033(2)	4.0(2)
C20	0.7502(1)	0.2750(6)	0.1200(2)	4.8(2)
C21	0.39881(8)	0.1573(4)	-0.0723(2)	2.5(1)
C22	0.38016(8)	0.0796(4)	-0.0451(2)	2.5(1)
C23	0.37931(8)	0.1815(4)	0.0033(2)	2.4(1)
C24	0.39701(8)	0.3222(4)	0.0058(2)	2.4(1)
C25	0.40929(8)	0.3064(4)	-0.0406(2)	2.4(1)
C26	0.4044(1)	0.0935(5)	-0.1278(2)	3.4(2)
C27	0.3640(1)	-0.0812(5)	-0.0647(2)	3.6(2)
C28	0.3595(1)	0.1529(5)	0.0398(2)	3.4(2)
C29	0.3961(1)	0.4716(5)	0.0403(2)	3.4(2)
C30	0.4270(1)	0.4335(5)	-0.0585(2)	3.8(2)
C31	0.48957(8)	0.0010(4)	0.1242(2)	2.5(1)
C32	0.46805(9)	0.0023(4)	0.1535(2)	2.6(1)
C33	0.46183(8)	0.1607(4)	0.1629(2)	2.8(1)
C34	0.47919(9)	0.2577(4)	0.1392(2)	3.0(1)
C35	0.49617(8)	0.1589(4)	0.1141(2)	2.8(1)
C36	0.5052(1)	-0.1443(5)	0.1116(2)	3.9(2)
C37	0.4548(1)	-0.1397(6)	0.1729(2)	4.4(2)
C38	0.4423(1)	0.2107(6)	0.1982(2)	4.3(2)
C39	0.4829(1)	0.4334(5)	0.1463(3)	4.9(2)
C40	0.5193(1)	0.2145(6)	0.0884(2)	4.5(2)
H1a	0.847(1)	0.193(5)	0.242(2)	9(1)
H2a	0.441(1)	-0.079(5)	0.012(2)	8(1)
H3	0.921(1)	0.073(5)	0.227(2)	5.0
H4	0.903(1)	0.202(5)	0.240(2)	5.0
H5	0.916(1)	0.037(5)	0.288(2)	5.0

Table of atomic positions in Cp^*_2TiH (continued)

Atoms	X	Y	Z	B_{eq} (A^2)
H6	0.859(1)	0.306(5)	0.133(2)	5.0
H7	0.863(1)	0.232(5)	0.084(2)	5.0
H8	0.826(1)	0.258(5)	0.066(2)	5.0
H9	0.778(1)	0.065(5)	0.018(2)	5.0
H10	0.797(1)	-0.037(5)	-0.004(2)	5.0
H11	0.770(1)	-0.114(5)	0.014(2)	5.0
H12	0.787(1)	-0.323(5)	0.093(2)	5.0
H13	0.818(1)	-0.402(5)	0.104(2)	5.0
H14	0.811(1)	-0.391(4)	0.162(2)	5.0
H15	0.895(1)	-0.320(5)	0.252(2)	5.0
H16	0.893(1)	-0.201(5)	0.306(2)	5.0
H17	0.865(1)	-0.323(5)	0.265(2)	5.0
H18	0.783(1)	0.394(4)	0.278(2)	5.0
H19	0.808(1)	0.418(5)	0.246(2)	5.0
H20	0.824(1)	0.347(5)	0.321(2)	5.0
H21	0.842(1)	0.111(5)	0.374(2)	5.0
H22	0.812(1)	0.020(5)	0.377(2)	5.0
H23	0.839(1)	-0.079(5)	0.360(2)	5.0
H24	0.810(1)	-0.301(4)	0.270(2)	5.0
H25	0.775(1)	-0.272(4)	0.278(2)	5.0
H26	0.773(1)	-0.312(5)	0.212(2)	5.0
H27	0.743(1)	-0.202(5)	0.105(2)	5.0
H28	0.715(1)	-0.092(5)	0.100(2)	5.0
H29	0.732(1)	-0.057(5)	0.059(2)	5.0
H30	0.741(1)	0.233(5)	0.073(2)	5.0
H31	0.731(1)	0.318(5)	0.121(2)	5.0
H32	0.763(1)	0.351(5)	0.118(2)	5.0
H33	0.386(1)	0.113(5)	-0.171(2)	5.0
H34	0.425(1)	0.150(4)	-0.125(2)	5.0
H35	0.411(1)	-0.024(5)	-0.123(2)	5.0
H36	0.376(1)	-0.142(5)	-0.083(2)	5.0
H37	0.341(1)	-0.076(5)	-0.099(2)	5.0
H38	0.364(1)	-0.131(4)	-0.027(2)	5.0
H39	0.360(1)	0.039(5)	0.051(2)	5.0
H40	0.336(1)	0.181(5)	0.014(2)	5.0
H41	0.370(1)	0.207(5)	0.082(2)	5.0
H42	0.399(1)	0.452(5)	0.083(2)	5.0
H43	0.373(1)	0.529(5)	0.012(2)	5.0
H44	0.411(1)	0.544(5)	0.043(2)	5.0
H45	0.442(1)	0.498(5)	-0.021(2)	5.0
H46	0.410(1)	0.494(5)	-0.097(2)	5.0
H47	0.445(1)	0.394(5)	-0.065(2)	5.0
H48	0.511(1)	-0.125(4)	0.073(2)	5.0
H49	0.528(1)	-0.163(4)	0.153(2)	5.0
H50	0.491(1)	-0.232(5)	0.104(2)	5.0
H51	0.452(1)	-0.221(5)	0.145(2)	5.0
H52	0.468(1)	-0.178(5)	0.218(2)	5.0

Table of atomic positions in Cp^*_2TiH (continued)

Atoms	X	Y	Z	B_{eq} (A^2)
H53	0.435(1)	-0.115(5)	0.167(2)	5.0
H54	0.422(1)	0.149(5)	0.183(2)	5.0
H55	0.458(1)	0.216(5)	0.246(2)	5.0
H56	0.436(1)	0.321(5)	0.188(2)	5.0
H57	0.466(1)	0.487(5)	0.158(2)	5.0
H58	0.505(1)	0.467(5)	0.180(2)	5.0
H59	0.481(1)	0.484(5)	0.108(2)	5.0
H60	0.513(1)	0.312(5)	0.064(2)	5.0
H61	0.542(1)	0.235(5)	0.124(2)	5.0
H62	0.519(1)	0.137(5)	0.056(2)	5.0
C(p1)	0.85	-0.06	0.15	0.4
C(p2)	0.78	0.05	0.22	0.4
C(p3)	0.39	0.21-0.03	0.4	
C(p4)	0.48	0.12	0.14	0.4

Starred atoms were included with isotropic thermal parameters. The thermal parameter given for anisotropically refined atoms is the isotropic equivalent thermal parameter defined as:

$$(4/3)[a^2B(1,1) + b^2B(2,2) + c^2B(3,3) + ab(\cos\gamma)B(1,2) + ac(\cos\beta)B(1,3) + bc(\cos\alpha)B(2,3)]$$

where a,b,c are real cell parameters, and B(i,j) are anisotropic betas.

Table of anisotropic thermal parameters for Cp^*_2TiH

Atom	U(1,1)	U(2,2)	U(3,3)	U(1,2)	U(1,3)	U(2,3)
TI1	0.0301(4)	0.0343(4)	0.0371(4)	-0.0041(3)	0.0205(3)	-0.0094(3)
TI2	0.0286(3)	0.0314(4)	0.0285(3)	0.0056(3)	0.0079(3)	-0.0055(3)
C1	0.033(2)	0.034(2)	0.038(2)	-0.001(2)	0.025(2)	-0.006(2)
C2	0.047(2)	0.029(2)	0.040(2)	0.004(2)	0.030(2)	0.001(2)
C3	0.037(2)	0.036(2)	0.028(2)	0.007(2)	0.018(2)	-0.001(2)
C4	0.035(2)	0.027(2)	0.031(2)	0.001(2)	0.022(2)	-0.002(1)
C5	0.036(2)	0.032(2)	0.031(2)	0.006(2)	0.022(2)	0.003(1)
C6	0.038(2)	0.063(3)	0.061(3)	-0.009(2)	0.033(2)	-0.015(2)
C7	0.087(4)	0.031(2)	0.077(3)	0.004(2)	0.058(3)	0.011(2)
C8	0.056(3)	0.061(3)	0.032(2)	0.015(2)	0.018(2)	0.004(2)
C9	0.051(2)	0.038(2)	0.044(2)	-0.007(2)	0.030(2)	-0.008(2)
C10	0.047(3)	0.059(3)	0.044(2)	0.015(2)	0.025(2)	0.013(2)
C11	0.026(2)	0.029(2)	0.026(2)	-0.001(1)	0.012(2)	0.000(1)
C12	0.025(2)	0.029(2)	0.033(2)	-0.001(1)	0.016(2)	-0.002(1)
C13	0.027(2)	0.040(2)	0.031(2)	-0.001(2)	0.017(2)	-0.003(2)
C14	0.032(2)	0.039(2)	0.038(2)	0.009(2)	0.019(2)	0.010(2)
C15	0.030(2)	0.028(2)	0.036(2)	0.001(1)	0.021(2)	-0.002(2)
C16	0.057(3)	0.028(2)	0.070(3)	-0.002(2)	0.044(2)	-0.007(2)
C17	0.045(2)	0.050(3)	0.031(2)	-0.009(2)	0.016(2)	-0.000(2)
C18	0.048(2)	0.028(2)	0.058(3)	-0.004(2)	0.032(2)	0.001(2)
C19	0.034(2)	0.077(3)	0.038(2)	-0.009(2)	0.017(2)	-0.015(2)
C20	0.054(3)	0.065(3)	0.059(3)	0.019(2)	0.026(3)	0.032(3)
C21	0.028(2)	0.039(2)	0.025(2)	0.006(2)	0.011(2)	0.000(2)
C22	0.027(2)	0.035(2)	0.026(2)	0.002(2)	0.008(2)	-0.000(2)
C23	0.026(2)	0.039(2)	0.024(2)	0.003(2)	0.010(1)	-0.000(2)
C24	0.028(2)	0.029(2)	0.030(2)	0.004(2)	0.012(2)	-0.003(1)
C25	0.025(2)	0.032(2)	0.029(2)	0.002(1)	0.011(2)	0.002(2)
C26	0.040(2)	0.056(3)	0.035(2)	0.002(2)	0.020(2)	-0.010(2)
C27	0.045(2)	0.039(2)	0.044(2)	-0.009(2)	0.017(2)	-0.006(2)
C28	0.037(2)	0.061(3)	0.035(2)	-0.001(2)	0.021(2)	-0.002(2)
C29	0.048(2)	0.034(2)	0.040(2)	0.010(2)	0.016(2)	-0.003(2)
C30	0.043(2)	0.055(3)	0.047(3)	-0.008(2)	0.022(2)	0.006(2)
C31	0.026(2)	0.030(2)	0.032(2)	0.005(1)	0.009(2)	-0.001(1)
C32	0.027(2)	0.033(2)	0.031(2)	-0.002(1)	0.009(2)	0.001(2)
C33	0.029(2)	0.044(2)	0.024(2)	0.003(2)	0.006(2)	-0.006(2)
C34	0.042(2)	0.026(2)	0.029(2)	0.003(2)	0.004(2)	0.001(2)
C35	0.029(2)	0.040(2)	0.029(2)	-0.002(2)	0.009(2)	0.003(2)
C36	0.042(2)	0.047(3)	0.058(3)	0.011(2)	0.023(2)	0.001(2)
C37	0.051(3)	0.059(3)	0.054(3)	-0.007(2)	0.024(2)	0.013(2)
C38	0.044(2)	0.079(3)	0.034(2)	0.015(2)	0.014(2)	-0.016(2)
C39	0.063(3)	0.032(3)	0.056(3)	-0.004(2)	0.004(3)	-0.008(2)
C40	0.043(2)	0.071(3)	0.053(3)	-0.013(2)	0.021(2)	0.012(2)

The form of the anisotropic temperature factor is:

$$\exp[-2\pi^2\{h^2a^2U(1,1) + k^2b^2U(2,2) + l^2c^2U(3,3) + 2hkabU(1,2) + 2hlacU(1,3) + 2klbcU(2,3)\}]$$

where a,b, and c are reciprocal lattice constants.

$Cp^*_2TiLi(TMEDA)$

Dark purple-black crystals of the compound were grown by cooling a saturated ether solution to -30 °C. In a dry box, the crystals were placed in a small Petri dish and covered with Paratone N, a high molecular weight hydrocarbon oil. The crystals were examined with a microscope. A blade shaped single crystal was selected, and a wedge shaped piece measuring $0.45 \times 0.40 \times 0.40$ mm was cut out of the middle. The crystal was mounted on the end of a 0.4 mm diameter quartz capillary. The crystal was transferred to an Enraf-Nonius CAD-4 diffractometer and cooled to -89 °C under a cold stream of nitrogen gas previously calibrated by a thermocouple placed in the sample position. The crystal was centered in the beam. Automatic peak search and indexing procedures indicated that the crystal possessed a primitive orthorhombic cell and yielded the cell parameters. The cell parameters and data collection parameters are given in the following table.

The 2038 raw intensity data were converted to structure factor amplitudes and their esds by correction for scan speed, background, and Lorentz-polarization effects.[1] Inspection of the intensity standards showed a large dip of 25% between hours one and four. A non-linear decay correction was applied. The 219 systematic absences (h,0,l), h odd; (0,k,l), k+l odd were then rejected yielding 1819 unique data of which 1306 possessed $F_o > 3\sigma(F_o)$. Azimuthal scan data showed a difference of $I_{min}/I_{max} = 0.68$ for the averaged curve; however, the different reflections had different absorption curves. No empirical absorption correction was applied. The systematic absences indicated that the space group was $Pna2_1$ or Pnma. Since the molecule would have to sit on special position possessing mirror symmetry in Pnma which seemed unlikely, $Pna2_1$ was chosen.

The cell volume indicated that 4 molecules were present in the unit cell. The titanium atom position was obtained by solving the Patterson map. Successive Fourier

searches yielded the rest of the heavy atom positions. The heavy atom structure was refined by standard least squares and Fourier techniques. The heavy atoms were refined isotropically, and the hydrogen positions were calculated based upon idealized bonding geometry and assigned thermal parameters equal to 1.5 $Å^2$ larger than the carbon atom to which they were connected. A numerical absorption correction, DIFABS, was applied. The heavy atoms except for the lithium atom were t refined anisotropically. One of the methyl carbon atoms of the Cp* ring has a very large thermal parameter, and both the TMEDA and one of the Cp* groups appear either to be disordered. The disorder was not modeled. At the end of the refinement, the enantiomer was changed, and the structure refined. The refinement was very slightly worse, so the enantiomer was changed back to the original one. A final difference Fourier map showed no additional atoms in the asymmetric unit. Examination of intermolecular close contacts (<3.5Å) showed that the molecule was a monomer.

The final residuals for 265 variables refined against the 1306 unique data with $F_o > 3\sigma(F_o)$ were R = 7.73%, R_w = 9.59%, and GOF = 2.166. The R value for all data (including unobserved reflections) was 11.28%. The quantity minimized by the least squares refinements was $w(|F_o| - |F_c|)^2$, where w is the weight given to a particular reflection. The p-factor, used to reduce the weight of intense reflections, was set to 0.03 initially, but later changed to 0.07.[2] The analytical form of the scattering factor tables for neutral atoms were used and all non-hydrogen scattering factors were corrected for both the real and imaginary components of anomalous dispersion.[3]

Inspection of the residuals ordered in the ranges of $\sin(\theta/\lambda)$, $|F_o|$, and parity and values of the individual indexes showed no trends. Eleven reflections had anomalously high values of $w\Delta^2$, and were weighted to zero toward the end of the refinement. The largest positive and negative peaks in the final difference Fourier map have electron densities of 0.51 and -0.49, respectively, and are associated with the one of the Cp* rings.

Table of crystal data for $Cp^*_2TiLi(TMEDA)$

Space group:	$Pna2_1$
a, Å	17.911(2)
b, Å	8.563(2)
c, Å	17.460(3)
α, deg.	90
β, deg.	90
γ, deg.	90
V, $Å^3$	2678(1)
Z	4
fw	441.51
d (calc.) g/cm^3	1.095
μ (calc.) 1/cm	3.277
radiation	MoKα(λ= 0.71073 Å)
monochrometer	highly oriented graphite
scan range, type	$3° \leq 2\theta \leq 45°$, θ-2θ
scan speed, deg/min	3.4
scan width, deg	$\Delta\theta = 0.80 + 0.35\tan\theta$
reflections collected	2038(+h,+k,+l)
unique reflections	1819
reflections $F_o^2 > 3\sigma(F_o^2)$	1306
R, %	7.73
R_w, %	9.59
R_{all}, %	11.28
GOF	2.166
Largest Δ/σ in final least squares cycle	0

Intensity standards: (4,1,7); (2,8,6); (1,5,9) measured every hour of X-ray exposure time. A 25% dip in intensity occurred between hours one and four was corrected for non-linearly.

Orientation Standards: 3 reflections were checked after every 200 measurements. Crystal orientation was redetermined if any of the reflections were offset from their predicted positions by more than 0.1°. Reorientation was required twice over the course of the data collection. The cell constants and errors are listed as their final values.

Table of atomic positions in $Cp^*_2TiLi(TMEDA)$

Atoms	X	Y	Z	B_{eq} (A^2)
Ti	0.19069(9)	0.0606(2)	0.000	2.72(3)
N1	0.0290(6)	0.363(1)	0.1633(7)	5.2(3)
N2	0.0315(7)	0.050(1)	0.2177(7)	6.2(3)
C1	0.3016(6)	0.202(1)	0.001(1)	5.7(3)
C2	0.3253(6)	0.059(2)	-0.0219(7)	4.9(3)
C3	0.3073(7)	-0.047(1)	0.0390(9)	5.4(3)
C4	0.2796(6)	0.043(2)	0.1009(8)	4.6(3)
C5	0.2756(6)	0.195(2)	0.0756(9)	5.5(3)
C6	0.3049(9)	0.365(2)	-0.043(1)	9.4(5)
C7	0.370(1)	0.008(4)	-0.087(1)	14.6(9)
C8	0.330(1)	-0.216(2)	0.050(2)	12.4(8)
C9	0.264(1)	-0.014(3)	0.183(1)	9.8(6)
C10	0.249(3)	0.345(5)	0.114(3)	45(2)
C11	0.0735(6)	0.035(2)	-0.0548(6)	4.2(3)
C12	0.1114(7)	0.135(1)	-0.1002(8)	4.9(3)
C13	0.1709(7)	0.048(2)	-0.1359(7)	4.3(3)
C14	0.1656(9)	-0.099(2)	-0.1095(8)	5.3(3)
C15	0.1084(8)	-0.109(1)	-0.0612(8)	4.7(3)
C16	0.0016(8)	0.062(3)	-0.011(1)	9.4(5)
C17	0.091(1)	0.306(2)	-0.115(1)	9.9(5)
C18	0.224(1)	0.112(3)	-0.2004(9)	9.0(5)
C19	0.219(1)	-0.234(2)	-0.141(1)	9.8(5)
C20	0.080(1)	-0.265(2)	-0.0223(9)	8.5(5)
C21	-0.0168(8)	0.443(2)	0.109(1)	6.2(4)
C22	0.0821(9)	0.478(2)	0.191(1)	9.0(5)
C23	-0.019(1)	0.307(2)	0.224(1)	12.5(6)
C24	-0.005(1)	0.184(3)	0.258(1)	12.8(6)
C25	-0.023(1)	-0.061(2)	0.191(1)	8.9(5)
C26	0.081(1)	-0.031(3)	0.270(1)	9.5(5)
Li	0.0882(9)	0.162(2)	0.122(1)	3.0(4)*
H1	0.35324(1)	0.40899(1)	-0.03730(1)	14.1*
H2	0.29457(1)	0.34842(1)	-0.09553(1)	14.1*
H3	0.26879(1)	0.43388(1)	-0.02178(1)	14.1*
H4	0.42141(1)	0.02459(1)	-0.07611(1)	21.9*
H5	0.36144(1)	-0.09962(1)	-0.09607(1)	21.9*
H6	0.35640(1)	0.06654(1)	-0.13109(1)	21.9*
H7	0.38047(1)	-0.22110(1)	0.06590(1)	18.6*
H8	0.29892(1)	-0.26270(1)	0.08782(1)	18.6*
H9	0.32419(1)	-0.27081(1)	0.00292(1)	18.6*
H10	0.30865(1)	-0.00986(1)	0.21246(1)	14.7*
H11	0.22729(1)	0.05102(1)	0.20633(1)	14.7*
H12	0.24615(1)	-0.11856(1)	0.18178(1)	14.7*
H13	0.28857(1)	0.38828(1)	0.14334(1)	67.6*
H14	0.23352(1)	0.41732(1)	0.07624(1)	67.6*
H15	0.20810(1)	0.32173(1)	0.14707(1)	67.6*
H16	-0.03986(1)	0.04588(1)	-0.04378(1)	14.1*

Table of atomic positions in $Cp^*_2TiLi(TMEDA)$ (continued)

Atoms	X	Y	Z	B_{eq} (A^2)
H17	-0.00101(1)	-0.00832(1)	0.03105(1)	14.1*
H18	0.00061(1)	0.16654(1)	0.00788(1)	14.1*
H19	0.05873(1)	0.31192(1)	-0.15825(1)	14.9*
H20	0.06729(1)	0.34829(1)	-0.07165(1)	14.9*
H21	0.13556(1)	0.36322(1)	-0.12585(1)	14.9*
H22	0.20198(1)	0.09125(1)	-0.24902(1)	13.5*
H23	0.22987(1)	0.22133(1)	-0.19419(1)	13.5*
H24	0.27074(1)	0.06170(1)	-0.19696(1)	13.5*
H25	0.19726(1)	-0.28072(1)	-0.18544(1)	14.7*
H26	0.26638(1)	-0.19100(1)	-0.15492(1)	14.7*
H27	0.22610(1)	-0.31156(1)	-0.10303(1)	14.7*
H28	0.04690(1)	-0.31781(1)	-0.05621(1)	12.8*
H29	0.12138(1)	-0.33064(1)	-0.01129(1)	12.8*
H30	0.05438(1)	-0.24100(1)	0.02389(1)	12.8*
H31	0.01349(1)	0.48112(1)	0.06807(1)	9.3*
H32	-0.05316(1)	0.37340(1)	0.08876(1)	9.3*
H33	-0.04112(1)	0.52847(1)	0.13300(1)	9.3*
H34	0.11274(1)	0.51213(1)	0.15012(1)	13.5*
H35	0.05580(1)	0.56469(1)	0.21191(1)	13.5*
H36	0.11237(1)	0.43250(1)	0.22992(1)	13.5*
H37	-0.06743(1)	0.29557(1)	0.20237(1)	18.8*
H38	-0.02018(1)	0.38681(1)	0.26190(1)	18.8*
H39	0.02658(1)	0.21045(1)	0.29945(1)	19.2*
H40	-0.05124(1)	0.14578(1)	0.27675(1)	19.2*
H41	0.00149(1)	-0.14480(1)	0.16609(1)	13.4*
H42	-0.05036(1)	-0.10015(1)	0.23382(1)	13.4*
H43	-0.05630(1)	-0.01123(1)	0.15665(1)	13.4*
H44	0.10368(1)	-0.11614(1)	0.24427(1)	14.3*
H45	0.11789(1)	0.03868(1)	0.28805(1)	14.3*
H46	0.05250(1)	-0.06944(1)	0.31219(1)	14.3*
Cp1	0.29787(1)	0.09058(1)	0.03898(1)	0.4*
Cp2	0.12595(1)	0.00219(1)	-0.09232(1)	0.4*

Starred atoms were included with isotropic thermal parameters. The thermal parameter given for anisotropically refined atoms is the isotropic equivalent thermal parameter defined as:

$$(4/3)[a^2B(1,1) + b^2B(2,2) + c^2B(3,3) + ab(\cos\gamma)B(1,2) + ac(\cos\beta)B(1,3) + bc(\cos\alpha)B(2,3)]$$

where a,b,c are real cell parameters, and B(i,j) are anisotropic betas.

Table of anisotropic thermal parameters for $Cp^*_2TiLi(TMEDA)$

Atom	B(1,1)	B(2,2)	B(3,3)	B(1,2)	B(1,3)	B(2,3)
Ti	2.83(6)	2.41(6)	2.93(6)	0.04(7)	0.48(9)	-0.2(1)
N1	4.5(5)	5.1(5)	6.0(6)	1.6(5)	0.6(5)	-0.6(5)
N2	7.3(6)	4.9(6)	6.5(6)	0.4(5)	4.1(5)	-0.4(6)
C1	3.1(4)	6.2(6)	7.8(6)	-1.4(5)	-2.5(6)	2(1)
C2	2.4(4)	7.7(7)	4.6(7)	1.2(6)	-0.8(4)	-2.9(6)
C3	3.9(5)	2.6(5)	9.8(9)	1.6(5)	-2.9(6)	0.0(6)
C4	2.5(4)	7.0(8)	4.4(6)	-0.4(6)	-1.4(5)	1.4(7)
C5	2.6(4)	5.7(7)	8.1(8)	1.4(5)	-2.6(5)	-2.6(7)
C6	8.0(9)	8.2(8)	12(1)	-4.3(7)	-3.4(8)	6.5(7)
C7	5.7(9)	32(3)	6.2(9)	2(1)	0.2(8)	-6(1)
C8	8.7(9)	4.6(9)	24(2)	1.4(8)	-5(1)	-1(1)
C9	7.2(9)	15(1)	7(1)	-1(1)	-2.4(9)	1(1)
C10	37(4)	58(3)	41(4)	28(3)	-7(3)	**(2)
C11	2.8(4)	7.7(7)	2.1(5)	1.5(5)	0.3(4)	-0.7(6)
C12	7.2(7)	1.6(4)	5.9(6)	1.3(5)	-3.6(6)	1.2(5)
C13	3.6(5)	6.1(7)	3.2(5)	-0.1(5)	0.3(4)	1.6(6)
C14	8.2(8)	5.3(7)	2.5(5)	1.8(6)	-0.5(6)	-1.9(5)
C15	7.0(7)	3.4(5)	3.7(6)	-1.8(5)	-1.9(5)	-0.1(5)
C16	4.2(6)	16(1)	8(1)	-0.1(9)	-1.3(8)	-2(1)
C17	14(1)	6.3(9)	9(1)	2.1(9)	-7.0(8)	-0.3(8)
C18	8.5(9)	14(1)	4.0(7)	-2(1)	2.6(7)	1.6(9)
C19	12(1)	8.6(9)	9(1)	2(1)	-1(1)	-6.3(7)
C20	13(1)	7.0(7)	5(1)	-4.6(8)	-1.0(8)	1.7(7)
C21	4.7(6)	5.9(7)	8.1(9)	0.8(6)	1.0(7)	-1.5(8)
C22	5.9(8)	11(1)	10(1)	3.0(8)	-1.8(9)	-4(1)
C23	19(1)	8(1)	11(1)	5(1)	10.8(8)	4.7(9)
C24	19(1)	9(1)	10.5(9)	-0(1)	11.1(8)	1(1)
C25	8.1(9)	11(1)	8(1)	-2.8(9)	0.5(9)	2(1)
C26	7.8(9)	15(1)	5.9(9)	-1(1)	1.7(8)	4(1)

The form of the anisotropic temperature factor is:

$$\exp[-0.25\{h^2a^2B(1,1) + k^2b^2B(2,2) + l^2c^2B(3,3) + 2hkabB(1,2) + 2hlacB(1,3) + 2klbcB(2,3)\}]$$

where a,b, and c are reciprocal lattice constants.

$[Cp^*_2TiOLi(THF)]_2 \cdot THF$

Green crystals of the compound were grown by cooling a tetrahydrofuran solution of the compound to -20 °C. The crystals were placed in Petri dish of Paratone N in a glove bag. A suitable irregularly shaped crystal measuring 0.30 mm × 0.35 mm × 0.40 mm was mounted on the end of a 0.3 mm thin walled quartz capillary. The crystal was transferred to an Siemens SMART diffractometer and cooled to -100 °C under a cold stream previously calibrated by a thermocouple placed in the sample position. The crystal was centered in the beam. Automatic peak search and indexing procedures indicated that the crystal was possessed a primitive orthorhombic cell and yielded the unit cell parameters. The cell parameters and data collection parameters are given in the following table. Based upon a statistical analysis of intensity distribution and the successful solution and refinement of the crystal structure, the space group was found to be $Pca2_1$.

An arbitrary hemisphere of data was collected using the default parameters for the diffractometer. The data were collected as 30 s images with an area detector. Two images were averaged to give the net image data. The image data were converted to intensity data using the program SAINT. The 22754 raw intensity data were converted to structure factor amplitudes and their esds by correction for scan speed, background, and Lorentz-polarization effects.[1] An empirical absorption correction using an ellipsoidal model for the crystal was applied to the intensity data based upon the intensities of all intense equivalent reflections ($T_{max} = 0.969$, $T_{min} = 0.863$). Inspection of the intensity standards showed no decrease in intensity over the duration of data collection. Averaging equivalent reflections gave 4862 unique data ($R_{int} = 0.059$).

The structure was solved by direct methods by direct methods. The molecule was found to be a dimer with a tetrahydrofuran molecule of crystallization. The heavy atom structure was refined by standard least squares and Fourier techniques. Most of the

heavy atoms were refined with anisotropic thermal parameters. One of the Cp* ligands was found to be severely disordered. The disorder was modeled using two sets of Cp* methyl carbon atoms whose net occupancy (for related atoms) was one. The hydrogen atoms were placed in calculated positions and included in structure factor calculations but were not refined. A final difference Fourier map showed no additional atoms in the asymmetric unit. No close (< 3.5 Å) intermolecular contacts were found.

The final residuals for 545 variables refined against the 3730 unique data with $I > 3\sigma(I)$ were R = 5.9%, R_w = 7.1%, and GOF = 2.48. The quantity minimized by the least squares refinements was $w(|F_o| - |F_c|)^2$, where w is the weight given to a particular reflection. The p-factor, used to reduce the weight of intense reflections, was set to 0.03, but was later increased to 0.04.[2] The analytical form of the scattering factor tables for neutral atoms were used and all non-hydrogen scattering factors were corrected for both the real and imaginary components of anomalous dispersion.[3]

Inspection of the residuals ordered in the ranges of $\sin(\theta/\lambda)$, $|F_o|$, and parity and values of the individual indexes showed no trends other than the previously mentioned secondary extinction. No reflections had anomalously high values of $w\Delta^2$. The largest positive and negative peaks in the final difference Fourier map have electron densities of 0.31 and -0.38, respectively.

Table of crystal data for $[Cp^*_2TiOLi(THF)]_2 \cdot THF$

Space group:	$Pca2_1$
a, Å	18.6055(3)
b, Å	17.1084(3)
c, Å	16.1954(2)
α, deg.	90
β, deg.	90
γ, deg.	90
V, $Å^3$	5155.2(1)
Z	4
fw	898.92
d (calc.) g/cm^3	1.158
μ (calc.) 1/cm	3.52
radiation	MoKα(λ= 0.71073 Å)
monochrometer	highly oriented graphite
scan resolution, % coverage	0.83 Å, 93% coverage
scan time, per image	30 s
scan type	ω, 0.3°
reflections integrated	22754
unique reflections	4862 (R_{int} = 0.059)
reflections $I > 3\sigma(I)$	3730
R, %	5.9
R_w, %	7.1
GOF	2.48
Largest Δ/σ in final least squares cycle	0.0

Table of atomic positions in $[Cp^*_2TiOLi(THF)]_2$ THF

Atoms	X	Y	Z	B_{eq} (A^2)
TI1	-0.38480(5)	0.38965(6)	0.62 (fixed)	3.41(4)
TI2	-0.60003(5)	0.12325(6)	0.7658(1)	3.38(4)
O1	-0.4463(2)	0.3205(2)	0.6603(3)	4.2(2)
O2	-0.5407(2)	0.1956(2)	0.7243(3)	3.9(2)
O3	-0.5843(3)	0.2724(3)	0.5342(4)	5.9(3)
O4	-0.4031(3)	0.2520(4)	0.8512(4)	6.5(3)
O5	0.4529(9)	0.2498(6)	0.2788(6)	19(1)
C1	-0.4723(3)	0.4866(4)	0.6699(5)	4.3(3)
C2	-0.4414(3)	0.5168(4)	0.5949(4)	4.2(3)
C3	-0.3692(3)	0.5351(3)	0.6106(5)	3.7(3)
C4	-0.3522(3)	0.5112(4)	0.6916(4)	4.0(3)
C5	-0.4148(4)	0.4827(4)	0.7278(4)	4.3(3)
C6	-0.5483(4)	0.4676(5)	0.6845(5)	5.7(4)
C7	-0.4840(4)	0.5404(4)	0.5194(5)	5.5(4)
C8	-0.3246(4)	0.5868(4)	0.5547(5)	5.0(4)
C9	-0.2827(4)	0.5231(4)	0.7365(5)	5.2(4)
C10	-0.4238(5)	0.4560(5)	0.8164(5)	6.4(5)
C11	-0.2654(3)	0.3314(4)	0.5980(5)	4.6(3)
C12	-0.3171(4)	0.2734(5)	0.5783(6)	6.1(4)
C13	-0.3552(4)	0.3000(5)	0.5077(6)	6.0(4)
C14	-0.3249(4)	0.3748(4)	0.4828(4)	4.6(3)
C15	-0.2679(3)	0.3908(4)	0.5390(5)	4.4(3)
C16	-0.2073(4)	0.3235(6)	0.6642(7)	8.0(5)
C17	-0.3299(5)	0.1956(5)	0.622(1)	9.4(6)
C18	-0.4108(6)	0.2549(7)	0.4618(8)	10.2(7)
C19	-0.3429(5)	0.4169(6)	0.4042(5)	7.7(5)
C20	-0.2096(4)	0.4514(5)	0.5271(6)	6.4(4)
C21	-0.6986(4)	0.2153(4)	0.7674(5)	5.1(3)
C22	-0.6542(4)	0.2343(4)	0.8351(5)	4.3(3)
C23	-0.6568(4)	0.1742(4)	0.8909(4)	4.8(3)
C24	-0.7076(5)	0.1172(5)	0.8602(7)	6.9(5)
C25	-0.7302(4)	0.1431(5)	0.7825(7)	6.5(5)
C26	-0.7150(6)	0.2652(6)	0.6927(6)	9.3(6)
C27	-0.6136(4)	0.3111(5)	0.8439(7)	7.0(5)
C28	-0.6260(7)	0.1721(8)	0.9751(6)	9.7(7)
C29	-0.7386(9)	0.0513(6)	0.912(1)	15(1)
C30	-0.7875(5)	0.1043(7)	0.730(1)	12.2(9)
C31	-0.5585(8)	-0.0063(5)	0.8116(5)	8.0(6)
C32	-0.6178(4)	-0.0223(4)	0.7578(7)	5.8(4)
C33	-0.5980(5)	0.0065(4)	0.6805(5)	5.7(4)
C34	-0.5310(6)	0.0329(4)	0.6838(7)	6.6(5)
C35	-0.5046(4)	0.0284(4)	0.7571(9)	6.6(5)
C36	-0.5356(7)	-0.0249(8)	0.8992(9)	6.6(3)
C37	-0.6758(7)	-0.0760(8)	0.7923(9)	6.2(3)
C38	-0.6545(6)	-0.0107(7)	0.610(1)	6.5(3)
C39	-0.4965(6)	0.0635(7)	0.5997(7)	5.4(3)

Table of atomic positions in $[Cp^*_2TiOLi(THF)]_2$ THF (continued)

Atoms	X	Y	Z	B_{eq} (A^2)
C40	-0.4278(6)	0.0538(7)	0.7781(8)	6.0(3)
C41	-0.6255(4)	0.2155(5)	0.4887(6)	6.1(4)
C42	-0.6791(6)	0.2635(7)	0.4418(7)	8.8(6)
C43	-0.6440(5)	0.3410(6)	0.4295(7)	7.4(5)
C44	-0.5979(6)	0.3490(6)	0.4974(7)	9.3(7)
C45	-0.3316(7)	0.277(1)	0.8556(8)	12(1)
C46	-0.2958(7)	0.216(1)	0.899(1)	13(1)
C47	-0.347(1)	0.190(1)	0.960(1)	15(1)
C48	-0.4187(5)	0.2241(6)	0.9294(6)	7.3(5)
C49	0.495(1)	0.279(1)	0.147(1)	14(1)
C50	0.468(1)	0.3067(7)	0.221(1)	16(1)
C51	0.5068(8)	0.1898(8)	0.168(1)	13(1)
C52	0.4937(8)	0.1877(8)	0.255(1)	12(1)
C53	-0.449(2)	0.056(2)	0.662(2)	7.0(7)
C54	-0.451(2)	0.030(2)	0.853(2)	6.4(6)
C55	-0.606(1)	-0.054(2)	0.895(2)	5.9(6)
C57	-0.603(2)	0.007(2)	0.582(2)	6.1(6)
C58	-0.694(1)	-0.065(2)	0.734(2)	6.3(6)
LI1	-0.5266(6)	0.2593(7)	0.6316(9)	5.2(6)
LI2	-0.4627(6)	0.2560(7)	0.7523(8)	5.1(5)
H1	-0.57	0.49	0.73	7.3
H2	-0.58	0.47	0.63	7.3
H3	-0.55	0.42	0.70	7.3
H4	-0.49	0.59	0.52	6.7
H5	-0.46	0.52	0.47	6.7
H6	-0.54	0.52	0.52	6.7
H7	-0.27	0.59	0.57	6.0
H8	-0.32	0.57	0.50	6.0
H9	-0.35	0.63	0.55	6.0
H10	-0.26	0.48	0.76	6.4
H11	-0.24	0.54	0.70	6.4
H12	-0.29	0.55	0.78	6.4
H13	-0.46	0.48	0.84	7.8
H14	-0.44	0.41	0.81	7.8
H15	-0.37	0.46	0.84	7.8
H16	-0.23	0.31	0.72	10.3
H17	-0.17	0.29	0.65	10.3
H18	-0.18	0.37	0.67	10.3
H19	-0.38	0.19	0.64	10.6
H20	-0.32	0.16	0.58	10.6
H21	-0.30	0.19	0.67	10.6
H22	-0.45	0.24	0.50	12.2
H23	-0.43	0.28	0.42	12.2
H24	-0.39	0.21	0.44	12.2
H25	-0.36	0.46	0.42	9.6
H26	-0.30	0.42	0.37	9.6

Table of atomic positions in $[Cp^*_2TiOLi(THF)]_2$ THF

Atoms	X	Y	Z	B_{eq} (A^2)
H27	-0.38	0.39	0.38	9.6
H28	-0.18	0.45	0.58	7.7
H29	-0.18	0.44	0.48	7.7
H30	-0.24	0.50	0.52	7.7
H31	-0.67	0.28	0.67	11.2
H32	-0.75	0.24	0.65	11.2
H33	-0.74	0.31	0.71	11.2
H34	-0.58	0.31	0.89	8.6
H35	-0.58	0.32	0.80	8.6
H36	-0.65	0.35	0.84	8.6
H37	-0.67	0.17	1.01	13.0
H38	-0.60	0.13	0.98	13.0
H39	-0.60	0.21	0.98	13.0
H40	-0.77	0.07	0.95	18.8
H41	-0.77	0.02	0.87	18.8
H42	-0.70	0.02	0.93	18.8
H43	-0.84	0.10	0.76	15.5
H44	-0.80	0.12	0.68	15.5
H45	-0.77	0.05	0.72	15.5
H61	-0.59	0.19	0.45	7.7
H62	-0.65	0.18	0.52	7.7
H63	-0.69	0.24	0.39	10.1
H64	-0.73	0.27	0.47	10.1
H65	-0.61	0.34	0.38	8.9
H66	-0.68	0.38	0.43	8.9
H67	-0.63	0.38	0.54	10.7
H68	-0.55	0.37	0.49	10.7
H69	-0.31	0.30	0.81	12.4
H70	-0.33	0.32	0.89	12.4
H71	-0.29	0.18	0.85	14.4
H72	-0.25	0.23	0.91	14.4
H73	-0.34	0.14	0.95	15.8
H74	-0.32	0.21	1.01	15.8
H75	-0.43	0.26	0.97	9.0
H76	-0.46	0.19	0.93	9.0
H77	0.46	0.29	0.11	16.5
H78	0.54	0.31	0.13	16.5
H79	0.43	0.34	0.21	18.4
H80	0.52	0.34	0.24	18.4
H81	0.47	0.16	0.14	15.8
H82	0.56	0.18	0.15	15.8
H83	0.54	0.19	0.28	16.1
H84	0.47	0.15	0.27	16.1
H85	-0.58	-0.01	0.94	7.6
H86	-0.54	-0.08	0.91	7.6
H87	-0.48	0.01	0.90	8.0

Table of atomic positions in $[Cp^*_2TiOLi(THF)]_2$ THF

Atoms	X	Y	Z	B_{eq} (A^2)
H88	-0.73	-0.05	0.78	8.0
H89	-0.68	-0.12	0.74	8.0
H90	-0.66	-0.09	0.85	7.8
H91	-0.70	-0.03	0.63	7.8
H92	-0.64	0.04	0.56	7.5
H93	-0.61	-0.04	0.56	7.5
H94	-0.45	0.03	0.58	6.4
H95	-0.54	0.07	0.56	6.4
H96	-0.47	0.11	0.61	6.4
H97	-0.40	0.02	0.80	6.7
H98	-0.40	0.07	0.73	6.7
H99	-0.43	0.09	0.82	6.7
H100	-0.41	0.05	0.72	8.2
H101	-0.42	0.03	0.62	8.2
H102	-0.44	0.11	0.65	8.2
H103	-0.40	0.00	0.85	8.0
H104	-0.44	0.08	0.87	8.0
H105	-0.61	-0.02	0.94	6.7
H106	-0.65	-0.07	0.88	6.7
H107	-0.57	-0.09	0.91	6.7
H108	-0.55	0.02	0.56	7.5
H109	-0.71	-0.06	0.68	8.0
C(p1)	-0.41	0.51	0.66	0.4
C(P2)	-0.31	0.33	0.54	0.4
C(P3)	-0.69	0.18	0.83	0.4
C(P4)	-0.56	0.01	0.74	0.4

Starred atoms were included with isotropic thermal parameters. The thermal parameter given for anisotropically refined atoms is the isotropic equivalent thermal parameter defined as:

$$(4/3)[a^2B(1,1) + b^2B(2,2) + c^2B(3,3) + ab(\cos\gamma)B(1,2) + ac(\cos\beta)B(1,3) + bc(\cos\alpha)B(2,3)]$$

where a,b,c are real cell parameters, and B(i,j) are anisotropic betas.

Table of anisotropic thermal parameters for $[Cp^*_2TiOLi(THF)]_2$ THF

Atom	U(1,1)	U(2,2)	U(3,3)	U(1,2)	U(1,3)	U(2,3)
TI1	0.0417(5)	0.0447(5)	0.0432(6)	-0.0082(4)	0.0009(5)	0.0019(5)
TI2	0.0440(5)	0.0367(5)	0.0475(6)	-0.0034(4)	0.0048(5)	0.0026(5)
O1	0.049(2)	0.051(3)	0.058(3)	-0.013(2)	0.001(2)	0.012(2)
O2	0.046(2)	0.043(2)	0.060(3)	-0.006(2)	0.012(2)	0.004(2)
O3	0.076(3)	0.070(3)	0.077(4)	-0.020(3)	-0.028(3)	0.016(3)
O4	0.057(3)	0.121(5)	0.067(4)	-0.021(3)	-0.012(3)	0.036(3)
O5	0.45(2)	0.154(9)	0.131(9)	0.16(1)	0.08(1)	0.043(7)
C1	0.050(4)	0.052(4)	0.061(4)	-0.002(3)	0.003(3)	0.003(3)
C2	0.057(4)	0.049(4)	0.054(4)	0.002(3)	-0.001(3)	0.012(3)
C3	0.049(3)	0.045(3)	0.048(4)	0.002(2)	-0.004(3)	0.007(3)
C4	0.056(4)	0.050(4)	0.044(4)	-0.005(3)	0.004(3)	-0.006(3)
C5	0.067(4)	0.051(4)	0.044(4)	-0.002(3)	0.007(3)	-0.000(3)
C6	0.058(4)	0.077(5)	0.082(6)	-0.002(4)	0.016(4)	0.004(4)
C7	0.067(4)	0.071(5)	0.070(5)	-0.003(4)	-0.018(4)	0.012(4)
C8	0.072(5)	0.049(4)	0.071(5)	-0.007(3)	0.013(4)	0.008(4)
C9	0.067(4)	0.073(5)	0.057(5)	-0.003(4)	-0.007(4)	-0.011(4)
C10	0.107(6)	0.089(6)	0.047(4)	-0.012(5)	0.014(4)	0.005(4)
C11	0.040(3)	0.061(4)	0.076(5)	0.001(3)	0.007(3)	-0.005(4)
C12	0.072(5)	0.057(4)	0.103(7)	0.006(4)	0.028(5)	-0.012(4)
C13	0.064(4)	0.086(6)	0.077(6)	-0.016(4)	0.016(4)	-0.041(5)
C14	0.059(4)	0.068(5)	0.049(4)	-0.008(3)	0.012(3)	-0.012(3)
C15	0.051(4)	0.050(4)	0.066(5)	-0.015(3)	0.014(3)	-0.014(3)
C16	0.061(5)	0.136(9)	0.106(7)	0.034(5)	-0.007(5)	-0.001(7)
C17	0.121(7)	0.040(4)	0.20(1)	-0.001(5)	0.044(9)	0.013(6)
C18	0.109(7)	0.13(1)	0.15(1)	-0.062(7)	0.032(7)	-0.087(8)
C19	0.111(7)	0.132(8)	0.049(5)	-0.012(6)	0.014(5)	-0.004(5)
C20	0.055(4)	0.088(6)	0.100(7)	-0.024(4)	0.025(4)	-0.026(5)
C21	0.060(4)	0.065(4)	0.070(5)	0.019(3)	0.008(4)	-0.006(4)
C22	0.051(4)	0.050(4)	0.063(5)	-0.004(3)	0.016(3)	-0.007(3)
C23	0.072(4)	0.066(5)	0.044(4)	0.010(4)	0.017(3)	0.002(4)
C24	0.088(6)	0.065(5)	0.111(8)	0.005(5)	0.054(6)	0.014(5)
C25	0.043(4)	0.069(5)	0.135(9)	-0.002(3)	0.013(5)	-0.034(6)
C26	0.15(1)	0.129(8)	0.074(6)	0.097(8)	-0.002(6)	0.007(6)
C27	0.075(5)	0.063(5)	0.129(8)	-0.021(4)	0.038(5)	-0.044(5)
C28	0.15(1)	0.16(1)	0.058(6)	0.070(8)	0.022(6)	-0.004(6)
C29	0.21(1)	0.081(7)	0.29(2)	0.009(8)	0.21(1)	0.03(1)
C30	0.063(6)	0.15(1)	0.25(2)	-0.005(6)	-0.046(8)	-0.08(1)
C31	0.21(1)	0.057(5)	0.039(4)	0.069(7)	-0.019(6)	0.004(4)
C32	0.068(4)	0.035(3)	0.119(8)	-0.008(3)	0.017(6)	0.007(5)
C33	0.117(7)	0.037(4)	0.063(5)	0.001(4)	-0.034(5)	-0.006(4)
C34	0.102(7)	0.046(4)	0.102(8)	0.002(5)	0.043(6)	-0.014(5)
C35	0.056(4)	0.047(4)	0.15(1)	0.016(3)	-0.022(6)	-0.021(6)
C41	0.074(5)	0.065(5)	0.094(6)	-0.008(4)	-0.018(5)	-0.002(5)
C42	0.102(7)	0.112(8)	0.12(1)	0.007(6)	-0.059(7)	-0.027(7)
C43	0.104(7)	0.089(7)	0.088(7)	0.024(6)	0.000(6)	0.011(5)
C44	0.15(1)	0.089(7)	0.119(9)	-0.034(7)	-0.054(8)	0.054(7)

Table of anisotropic thermal parameters for $Cp^*_2TiLi(TMEDA)$ (continued)

Atom	U(1,1)	U(2,2)	U(3,3)	U(1,2)	U(1,3)	U(2,3)
C45	0.101(8)	0.28(2)	0.084(8)	-0.05(1)	-0.003(7)	0.03(1)
C46	0.13(1)	0.13(1)	0.22(2)	0.048(9)	-0.07(1)	-0.06(1)
C47	0.22(2)	0.16(1)	0.19(2)	-0.06(1)	-0.14(1)	0.12(1)
C48	0.100(6)	0.118(8)	0.059(5)	-0.029(6)	0.009(5)	-0.013(5)
C49	0.21(2)	0.16(1)	0.17(2)	0.05(1)	-0.01(1)	0.05(1)
C50	0.41(3)	0.080(7)	0.13(1)	0.09(1)	0.09(2)	0.028(8)
C51	0.20(1)	0.14(1)	0.14(1)	0.10(1)	-0.03(1)	-0.04(1)
C52	0.19(1)	0.14(1)	0.13(1)	0.08(1)	0.02(1)	-0.00(1)
LI1	0.049(6)	0.071(7)	0.077(9)	0.003(5)	-0.011(6)	0.003(7)
LI2	0.065(6)	0.066(7)	0.060(8)	-0.018(6)	-0.005(6)	0.022(6)

The form of the anisotropic temperature factor is:

$$\exp[-2\pi^2\{h^2a^2U(1,1) + k^2b^2U(2,2) + l^2c^2U(3,3) + 2hkabU(1,2) + 2hlacU(1,3) + 2klbcU(2,3)\}]$$

where a,b, and c are reciprocal lattice constants.

References

(1) The data reduction formulas are:

$$F_o^2 = \frac{\omega}{Lp}(C\text{-}2B) \qquad \sigma_o(F_o^2) = \frac{\omega}{Lp}(C + 4B)^{1/2}$$

$$F_o = (F_o^2)^{1/2} \qquad \omega_o(F) = [F_o^2 + \sigma_o(F_o^2)]^{1/2} - F_o$$

where C is the total count of the scan, B is the sum of the two background counts, ω is the scan speed used in deg/min, and

$$\frac{1}{Lp} = \frac{\sin 2\theta \ (1 + \cos^2 2\theta_m)}{1 + \cos^2 2\theta_m - \sin^2 2\theta}$$

is the correction for Lorentz and polarization effects for a reflection with scattering angle 2θ and radiation monochromatized with a 50% perfect single crystal monochrometer with scattering angle $2\theta_m$.

(2) $$R = \frac{\Sigma||F_o| - |F_c||}{\Sigma|F_o|} \qquad wR = \left[\frac{\Sigma(|F_o| - |F_c|)^2}{\Sigma wF_o^2}\right]^{1/2}$$

$$GOF = \left[\frac{\Sigma(|F_o| - |F_c|)^2}{(n_o - n_v)}\right]^{1/2}$$

where n_o is the number of observations and n_v is the number of variable parameters, and the weights were given by

$$w = \frac{1}{\sigma^2(F_o)} \qquad \sigma(F_o^2) = [\sigma_o^2(F_o^2) + (pF^2)^2]^{1/2}$$

where $\sigma^2(F_o)$ is calculated as above from $\sigma(F_o^2)$ and where p is the factor use to lower the weight of intense reflections.

(3) Cromer, D. T.; Waber, J. T. In *Interantional Tables for X-Ray Crystallography*; Kynoch Press: Birmingham, England, 1974; Vol. IV.

Appendix Two: EXAFS Fitting Results

$[Cp''_2UF]_2$

Kmin= 4.05 Kmax=13.88 Deltak=0.000 190 Pts 5 Comp'ts 11 Variables
15 Iter'ns 35. F eval's Elfin=.10E-05 Dmp=.10E+02 F=0.117E+02 Za=92.0
1 Scale Factor = 0.900
2 Data Delta E0 = 0.00 eV
3 Wave 1 Sigma-D = 0.00 Angstroms
4 0.00
5 0.00

Component # 1 ..... Zba= 1.00 Zbp= 1.00 Nat=5 Npt=5 Integral= 44.208% [1]
6 Atom # = 2.000000
* 7 Distance = 2.352938 (0.004604) Angstroms
* 8 Sigma**2 = 0.005586 (0.000263) a**2
* 9 Delta E0 = -4.391780 (1.079602) eV
10 Delta E1 = 0.000000 eV

Component # 2 ..... Zba= 3.00 Zbp= 3.00 Nat=5 Npt=5 Integral= 15.355% [4]
11 Atom # = 10.000000
* 12 Distance = 2.861686 (0.008271) Angstroms
* 13 Sigma**2 = 0.014311 (0.000594) a**2
/ 14 Delta E0 = -4.391780 eV
15 Delta E1 = 0.000000 eV

Component # 3 ..... Zba=13.00 Zbp=13.00 Nat=5 Npt=5 Integral= 23.333% [2]
16 Atom # = 20.000000
* 17 Distance = 3.417702 (0.006547) Angstroms
* 18 Sigma**2 = 0.000100 (0.000492) a**2
/ 19 Delta E0 = -4.391780 eV
20 Delta E1 = 0.000000 eV

Component # 4 ..... Zba=24.00 Zbp=24.00 Nat=5 Npt=5 Integral= 15.644% [3]
21 Atom # = 1.000000
* 22 Distance = 3.933826 (0.009337) Angstroms
* 23 Sigma**2 = 0.007692 (0.000746) a**2
/ 24 Delta E0 = -4.391780 eV
25 Delta E1 = 0.000000 eV

Component # 5 ..... Zba=35.00 Zbp=35.00 Nat=5 Npt=5 Integral= 1.460% [5]
26 Atom # = 4.000000
* 27 Distance = 4.174458 (0.029129) Angstroms
* 28 Sigma**2 = 0.024439 (0.005168) a**2
/ 29 Delta E0 = -4.391780 eV
30 Delta E1 = 0.000000 eV

- Correlation Matrix -

Comp't	1	1	1	2	2	3	3	4	4	5	5
	R	Sig^2	Eo	R	Sig^2	R	Sig^2	R	Sig^2	R	Sig^2
Par.#	7	8	9	12	13	17	18	22	23	27	28
7	1.000	-0.581	0.937	0.852	-0.320	0.710	-0.443	0.687	0.334	0.472	-0.581
8		1.000	-0.594	-0.547	-0.286	-0.431	0.271	-0.454	-0.264	-0.318	0.384
9			1.000	0.938	-0.348	0.759	-0.476	0.736	0.353	0.502	-0.626
12				1.000	-0.349	0.760	-0.554	0.692	0.374	0.494	-0.615
13					1.000	0.475	0.377	-0.336	0.126	0.209	0.210
17						1.000	-0.381	0.516	0.442	0.421	-0.506
18							1.000	-0.509	-0.335	-0.157	0.315
22								1.000	0.087	-0.282	0.034
23									1.000	-0.276	-0.574
27										1.000	-0.437
28											1.000

Additional Statistical Information :
Normalised error (chi-squared) : 0.616166E-01 F/(No.pts)
Reduced error (chi-squared) : 0.654031E-01 F/(No.pts-No.Vars)
Weighted F-factor : 0.303117 (30.31%)
Expected Weighted F-factor : 1.18525
Expected resolution in distance, R : 0.159874 Angstroms

$[Cp''_2UCl]_2$

Kmin= 1.02 Kmax=13.00 Deltak=0.000 255 Pts 4 Comp'ts 8 Variables
22 Iter'ns 47. F eval's Elfin=.10E-05 Dmp=.10E+00 F=0.136E+02 Za=92.0
1 Scale Factor = 0.900
2 Data Delta E0 = 0.00 eV
3 Wave 1 Sigma-D = 0.00 Angstroms
4 0.00
5 0.00

Component # 1 ..... Zba= 1.00 Zbp= 1.00 Nat=5 Npt=5 Integral= 71.187% [1]
6 Atom # = 10.000000
* 7 Distance = 2.719114 (0.002147) Angstroms
* 8 Sigma**2 = 0.005881 (0.000134) a**2
* 9 Delta E0 = -18.583122 (0.381324) eV
10 Delta E1 = 0.000000 eV

Component # 2 ..... Zba=13.00 Zbp=13.00 Nat=5 Npt=5 Integral= 17.825% [2]
11 Atom # = 20.000000
* 12 Distance = 3.415987 (0.005967) Angstroms
13 Sigma**2 = 0.000000 A**2
/ 14 Delta E0 = -18.583122 eV
15 Delta E1 = 0.000000 eV

Component # 3 ..... Zba=33.00 Zbp=33.00 Nat=5 Npt=5 Integral= 4.837% [4]
16 Atom # = 4.000000
* 17 Distance = 4.205726 (0.012458) Angstroms

```
*  18 Sigma**2 =   0.014723 (  0.001654) a**2
/  19 Delta E0 = -18.583122 eV
   20 Delta E1 =   0.000000 eV

Component #  4  ..... Zba=58.00 Zbp=58.00 Nat=5 Npt=5 Integral=   6.152% [  3]
   21  Atom # =   1.000000
*  22 Distance =   4.328993 (  0.015377) Angstroms
*  23 Sigma**2 =   0.009659 (  0.001576) a**2
/  24 Delta E0 = -18.583122 eV
   25 Delta E1 =   0.000000 eV

 - Correlation Matrix -
 Comp't   1    1    1    2    3    3    4    4
        R Sig^2  Eo    R    R Sig^2   R Sig^2
 Par.#    7    8    9   12   17   18   22   23
  7      1.000-0.432 0.909 0.330 0.497-0.228 0.280 0.161
  8          1.000-0.485-0.490-0.270 0.137-0.159-0.135
  9              1.000 0.604 0.547-0.221 0.342 0.047
 12                  1.000 0.334 0.139 0.308-0.308
 17                      1.000-0.261-0.448 0.289
 18                          1.000-0.288-0.549
 22                              1.000-0.192
 23                                  1.000

 Additional Statistical Information :
    Normalised error (chi-squared) : 0.532353E-01  F/(No.pts)
      Reduced error (chi-squared) : 0.549595E-01  F/(No.pts-No.Vars)
            Weighted F-factor : 0.238973    ( 23.90% )
       Expected Weighted F-factor :  1.01936
 Expected resolution in distance, R : 0.131101     Angstroms
```

$[Cp^{\ddagger}_2OH]_2$

```
Kmin= 1.01 Kmax=12.90 Deltak=0.000 264 Pts   7 Comp'ts  15 Variables
  133 Iter'ns  270. F eval's Elfin=.10E-05 Dmp=.10E+00 F=0.311E+02 Za=92.0
  1  Scale Factor  =  0.900
  2  Data Delta E0 =  0.00 eV
  3 Wave 1 Sigma-D =  0.00 Angstroms
  4   0.00
  5   0.00

 Component #  1  ..... Zba= 1.00 Zbp= 1.00 Nat=5 Npt=5 Integral=  17.704% [  2]
    6  Atom # =  2.000000
*   7 Distance =  2.375473 (  0.005774) Angstroms
*   8 Sigma**2 =  0.005119 (  0.000445) a**2
*   9 Delta E0 = -7.170007 (  1.140692) eV
   10 Delta E1 =  0.000000 eV

 Component #  2  ..... Zba= 2.00 Zbp= 2.00 Nat=5 Npt=5 Integral=  14.789% [  4]
```

```
  11  Atom # =  10.000000
*  12 Distance =  2.864089 (  0.007882) Angstroms
*  13 Sigma**2 =  0.010220 (  0.000499) a**2
/  14 Delta E0 = -7.170007 eV
   15 Delta E1 =  0.000000 eV

Component #  3  ..... Zba= 7.00 Zbp= 7.00 Nat=5 Npt=5 Integral=  5.154% [  6]
  16  Atom # =  20.000000
*  17 Distance =  3.375099 (  0.013685) Angstroms
*  18 Sigma**2 =  0.002970 (  0.001700) a**2
/  19 Delta E0 = -7.170007 eV
   20 Delta E1 =  0.000000 eV

Component #  4  ..... Zba=12.00 Zbp=12.00 Nat=5 Npt=5 Integral= 28.698% [  1]
  21  Atom # =  1.000000
*  22 Distance =  3.886069 (  0.032246) Angstroms
*  23 Sigma**2 =  0.001312 (  0.001448) a**2
/  24 Delta E0 = -7.170007 eV
   25 Delta E1 =  0.000000 eV

Component #  5  ..... Zba=19.00 Zbp=19.00 Nat=5 Npt=5 Integral= 16.533% [  3]
  26  Atom # =  4.000000
*  27 Distance =  3.843581 (  0.020332) Angstroms
*  28 Sigma**2 =  0.001035 (  0.001428) a**2
/  29 Delta E0 = -7.170007 eV
   30 Delta E1 =  0.000000 eV

Component #  6  ..... Zba=22.00 Zbp=22.00 Nat=5 Npt=5 Integral= 13.012% [  5]
  31  Atom # =  4.000000
*  32 Distance =  4.060682 (  0.039618) Angstroms
*  33 Sigma**2 =  0.001381 (  0.004849) a**2
/  34 Delta E0 = -7.170007 eV
   35 Delta E1 =  0.000000 eV

Component #  7  ..... Zba=29.00 Zbp=29.00 Nat=5 Npt=5 Integral=  4.110% [  7]
  36  Atom # =  4.000000
*  37 Distance =  4.437043 (  0.040019) Angstroms
*  38 Sigma**2 =  0.005398 (  0.002656) a**2
/  39 Delta E0 = -7.170007 eV
   40 Delta E1 =  0.000000 eV
```

- Correlation Matrix -

```
 Comp't    1    1    1    2    2    3    3    4    4    5    5    6    6    7    7
         R Sig^2  Eo    R Sig^2   R Sig^2   R Sig^2   R Sig^2   R Sig^2   R Sig^2
 Par.#     7    8    9   12   13   17   18   22   23   27   28   32   33   37   38
  7      1.000-0.584 0.890 0.795-0.333 0.131 0.256 0.263-0.274 0.444-0.429 0.102-0.299 0.318-
0.497
  8           1.000-0.619-0.586 0.034-0.254-0.294-0.286 0.320-0.373 0.353-0.240 0.149-0.301 0.452
  9                1.000 0.928-0.404 0.304-0.128 0.406-0.241 0.536-0.371 0.248-0.166 0.436-0.539
 12                     1.000-0.364 0.588-0.419 0.432-0.196 0.545-0.227 0.309 0.112 0.448-0.478
 13                          1.000 0.505 0.501 0.184 0.252-0.193 0.365 0.144 0.286 0.146 0.286
 17                               1.000-0.393 0.148 0.467-0.296 0.444-0.285 0.320 0.161 0.369
 18                                    1.000-0.553-0.370-0.494-0.608-0.468-0.538-0.524-0.388
 22                                         1.000 0.199 0.843 0.825 0.866 0.932 0.929-0.338
 23                                              1.000-0.745 0.686-0.755 0.683 0.471 0.749
 27                                                   1.000 0.507 0.949 0.538 0.751-0.618
 28                                                        1.000 0.620 0.886 0.783 0.637
 32                                                             1.000 0.626 0.717-0.545
 33                                                                  1.000 0.888 0.414
 37                                                                       1.000-0.228
 38                                                                            1.000
```

Additional Statistical Information :
Normalised error (chi-squared) : 0.117865 F/(No.pts)
Reduced error (chi-squared) : 0.124965 F/(No.pts-No.Vars)
Weighted F-factor : 0.445669 (44.57%)
Expected Weighted F-factor : 1.26072
Expected resolution in distance, R : 0.132194 Angstroms

$[Cp^{\ddagger}_2UF]_2$

```
Kmin= 1.03 Kmax=13.88 Deltak=0.000 244 Pts  4 Comp'ts  9 Variables
 146 Iter'ns  295. F eval's Elfin=.10E-05 Dmp=.10E+00 F=0.261E+02 Za=92.0
  1 Scale Factor =  0.900
  2 Data Delta E0 =  0.00 eV
  3 Wave 1 Sigma-D =  0.00 Angstroms
  4   0.00
  5   0.00

 Component #  1  ..... Zba= 1.00 Zbp= 1.00 Nat=5 Npt=5 Integral=  25.798% [  2]
    6  Atom # =  2.000000
*   7 Distance =  2.264410 (  0.006162) Angstroms
*   8 Sigma**2 =  0.005717 (  0.000620) a**2
*   9 Delta E0 = -11.018958 (  0.733909) eV
   10 Delta E1 =  0.000000 eV

 Component #  2  ..... Zba= 2.00 Zbp= 2.00 Nat=5 Npt=5 Integral=  20.986% [  3]
   11  Atom # =  4.000000
*  12 Distance =  2.427923 (  0.007522) Angstroms
*  13 Sigma**2 =  0.006740 (  0.000738) a**2
```

/ 14 Delta E0 = -11.018958 eV
15 Delta E1 = 0.000000 eV

Component # 3 ..... Zba=12.00 Zbp=12.00 Nat=5 Npt=5 Integral= 34.272% [1]
16 Atom # = 1.000000
* 17 Distance = 3.890924 (0.005039) Angstroms
* 18 Sigma**2 = 0.002743 (0.000344) a**2
/ 19 Delta E0 = -11.018958 eV
20 Delta E1 = 0.000000 eV

Component # 4 ..... Zba=13.00 Zbp=13.00 Nat=5 Npt=5 Integral= 18.944% [4]
21 Atom # = 4.000000
* 22 Distance = 3.859828 (0.007945) Angstroms
* 23 Sigma**2 = 0.001948 (0.000654) a**2
/ 24 Delta E0 = -11.018958 eV
25 Delta E1 = 0.000000 eV

- Correlation Matrix -

Comp't	1	1	1	2	2	3	3	4	4
	R	Sig^2	Eo	R	Sig^2	R	Sig^2	R	Sig^2
Par.#	7	8	9	12	13	17	18	22	23
7	1.000	0.284	0.844	0.612	0.741	0.754	-0.246	0.705	-0.106
8		1.000	-0.545	-0.863	0.815	-0.431	0.409	-0.362	0.258
9			1.000	0.846	0.119	0.863	-0.368	0.802	-0.113
12				1.000	-0.606	0.711	-0.432	0.646	-0.232
13					1.000	0.258	0.249	0.263	0.069
17						1.000	-0.361	0.904	-0.165
18							1.000	-0.306	0.881
22								1.000	-0.152
23									1.000

Additional Statistical Information :
Normalised error (chi-squared) : 0.106911 F/(No.pts)
Reduced error (chi-squared) : 0.111005 F/(No.pts-No.Vars)
Weighted F-factor : 0.381388 (38.14%)
Expected Weighted F-factor : 1.14471
Expected resolution in distance, R : 0.122308 Angstroms

$[Cp^{\ddagger}_2UCl]_2$

Kmin= 1.02 Kmax=11.96 Deltak=0.000 246 Pts 5 Comp'ts 11 Variables
21 Iter'ns 47. F eval's Elfin=.10E-05 Dmp=.10E+01 F=0.170E+02 Za=92.0
1 Scale Factor = 0.900
2 Data Delta E0 = 0.00 eV
3 Wave 1 Sigma-D = 0.00 Angstroms
4 0.00
5 0.00

Component # 1 ..... Zba= 1.00 Zbp= 1.00 Nat=5 Npt=5 Integral= 67.726% [1]

```
   6  Atom # =  10.000000
*  7 Distance =  2.759265 (  0.002784) Angstroms
*  8 Sigma**2 =  0.006163 (  0.000193) a**2
*  9 Delta E0 = -11.752733 (  0.415115) eV
  10 Delta E1 =  0.000000 eV

Component #  2 ..... Zba= 7.00 Zbp= 7.00 Nat=5 Npt=5 Integral=  14.295% [  2]
  11  Atom # =  20.000000
*  12 Distance =  3.419267 (  0.007967) Angstroms
*  13 Sigma**2 =  0.000687 (  0.000952) a**2
/  14 Delta E0 = -11.752733 eV
  15 Delta E1 =  0.000000 eV

Component #  3 ..... Zba=12.00 Zbp=12.00 Nat=5 Npt=5 Integral=  5.632% [  4]
  16  Atom # =  4.000000
*  17 Distance =  3.860266 (  0.025354) Angstroms
*  18 Sigma**2 =  0.009622 (  0.003781) a**2
/  19 Delta E0 = -11.752733 eV
  20 Delta E1 =  0.000000 eV

Component #  4 ..... Zba=21.00 Zbp=21.00 Nat=5 Npt=5 Integral=  1.265% [  5]
  21  Atom # =  4.000000
*  22 Distance =  4.018923 (  0.058860) Angstroms
*  23 Sigma**2 =  0.018990 (  0.014670) a**2
/  24 Delta E0 = -11.752733 eV
  25 Delta E1 =  0.000000 eV

Component #  5 ..... Zba=33.00 Zbp=33.00 Nat=5 Npt=5 Integral=  11.084% [  3]
  26  Atom # =  1.000000
*  27 Distance =  4.572283 (  0.010500) Angstroms
*  28 Sigma**2 =  0.005533 (  0.001021) a**2
/  29 Delta E0 = -11.752733 eV
  30 Delta E1 =  0.000000 eV

- Correlation Matrix -
Comp't   1    1    1    2    2    3    3    4    4    5    5
       R  Sig^2  Eo    R  Sig^2   R  Sig^2   R  Sig^2   R  Sig^2
Par.#    7    8    9   12   13   17   18   22   23   27   28
 7      1.000-0.437 0.909 0.205-0.459-0.249 0.259-0.352-0.167 0.448 0.166
 8           1.000-0.435 0.494-0.550-0.169-0.241 0.205-0.209-0.227 0.172
 9                1.000 0.510-0.247-0.263 0.155-0.326-0.247 0.475 0.177
 12                    1.000-0.199-0.422-0.454 0.180-0.468 0.112 0.375
 13                         1.000 0.191-0.534 0.458-0.387-0.346 0.108
 17                              1.000 0.575 0.552 0.817-0.248-0.370
 18                                   1.000-0.701 0.871 0.333-0.477
 22                                        1.000-0.420-0.294 0.281
 23                                             1.000 0.160-0.435
 27                                                  1.000-0.234
 28                                                       1.000

Additional Statistical Information :
   Normalised error (chi-squared) : 0.689272E-01  F/(No.pts)
     Reduced error (chi-squared) : 0.721536E-01  F/(No.pts-No.Vars)
```

Weighted F-factor : 0.270993 (27.10%)
Expected Weighted F-factor : 1.00886
Expected resolution in distance, R : 0.143638 Angstroms

$[Cp^{\ddagger}_2UBr]_2$

Kmin= 3.02 Kmax=13.97 Deltak=0.000 211 Pts 6 Comp'ts 12 Variables
23 Iter'ns 50. F eval's Elfin=.10E-05 Dmp=.10E+00 F=0.178E+02 Za=92.0
1 Scale Factor = 0.900
2 Data Delta E0 = 0.00 eV
3 Wave 1 Sigma-D = 0.00 Angstroms
4 0.00
5 0.00

Component # 1 ..... Zba= 2.00 Zbp= 2.00 Nat=5 Npt=5 Integral= 19.701% [2]
6 Atom # = 10.000000
* 7 Distance = 2.827648 (0.004022) Angstroms
* 8 Sigma**2 = 0.011130 (0.000773) a**2
9 Delta E0 = -10.000000 eV
10 Delta E1 = 0.000000 eV

Component # 2 ..... Zba= 6.00 Zbp= 6.00 Nat=5 Npt=5 Integral= 33.078% [1]
11 Atom # = 2.000000
* 12 Distance = 2.992989 (0.004561) Angstroms
* 13 Sigma**2 = 0.009868 (0.000346) a**2
/ 14 Delta E0 = -10.000000 eV
15 Delta E1 = 0.000000 eV

Component # 3 ..... Zba= 7.00 Zbp= 7.00 Nat=5 Npt=5 Integral= 17.324% [4]
16 Atom # = 20.000000
* 17 Distance = 3.410595 (0.007773) Angstroms
* 18 Sigma**2 = 0.000531 (0.000633) a**2
/ 19 Delta E0 = -10.000000 eV
20 Delta E1 = 0.000000 eV

Component # 4 ..... Zba=12.00 Zbp=12.00 Nat=5 Npt=5 Integral= 17.872% [3]
21 Atom # = 4.000000
* 22 Distance = 3.834175 (0.008396) Angstroms
* 23 Sigma**2 = 0.003444 (0.000669) a**2
/ 24 Delta E0 = -10.000000 eV
25 Delta E1 = 0.000000 eV

Component # 5 ..... Zba=19.00 Zbp=19.00 Nat=5 Npt=5 Integral= 5.380% [6]
26 Atom # = 4.000000
* 27 Distance = 4.035983 (0.020835) Angstroms
* 28 Sigma**2 = 0.007887 (0.002187) a**2
/ 29 Delta E0 = -10.000000 eV
30 Delta E1 = 0.000000 eV

```
Component #  6  ..... Zba=35.00 Zbp=35.00 Nat=5 Npt=5 Integral=   6.645% [  5]
  31   Atom # =   1.000000
*  32 Distance =   4.655141 (  0.015096) Angstroms
*  33 Sigma**2 =   0.008045 (  0.001443) a**2
/  34 Delta E0 = -10.000000 eV
   35 Delta E1 =   0.000000 eV

 - Correlation Matrix -
 Comp't   1    1    2    2    3    3    4    4    5    5    6    6
        R Sig^2   R Sig^2   R Sig^2   R Sig^2   R Sig^2   R Sig^2
 Par.#    7    8   12   13   17   18   22   23   27   28   32   33
  7      1.000 0.500 0.566-0.771 0.420-0.637 0.427 0.338 0.384-0.258 0.140-0.246
  8          1.000 0.900-0.511 0.794-0.463-0.084 0.528 0.334 0.319 0.244-0.053
 12               1.000-0.548 0.718-0.515-0.110 0.497 0.318 0.306 0.226-0.079
 13                    1.000-0.318 0.503-0.383-0.366-0.372 0.221-0.153 0.237
 17                         1.000-0.388-0.215 0.577 0.306 0.419 0.274-0.005
 18                              1.000-0.562-0.290-0.506 0.359-0.070 0.348
 22                                   1.000 0.277 0.762-0.749-0.271-0.254
 23                                        1.000 0.654 0.466 0.182-0.338
 27                                             1.000-0.499-0.168-0.340
 28                                                  1.000 0.306-0.166
 32                                                       1.000-0.199
 33                                                            1.000

 Additional Statistical Information :
    Normalised error (chi-squared) : 0.845516E-01  F/(No.pts)
      Reduced error (chi-squared) : 0.896502E-01  F/(No.pts-No.Vars)
            Weighted F-factor : 0.428583     ( 42.86% )
       Expected Weighted F-factor :  1.43139
 Expected resolution in distance, R : 0.143509     Angstroms
```

$[Cp''_2UF_2]_2$

```
Kmin= 3.02 Kmax=13.99 Deltak=0.000 210 Pts   4 Comp'ts   9 Variables
   7 Iter'ns   21. F eval's Elfin=.10E-05 Dmp=.10E+04 F=0.262E+02 Za=92.0
  1  Scale Factor  =  0.900
  2  Data Delta E0 =  0.00 eV
  3 Wave 1 Sigma-D =  0.00 Angstroms
  4   0.00
  5   0.00

 Component #  1  ..... Zba= 1.00 Zbp= 1.00 Nat=5 Npt=5 Integral=  51.312% [  1]
    6   Atom # =   3.000000
*   7 Distance =   2.316043 (  0.004917) Angstroms
*   8 Sigma**2 =   0.006040 (  0.000267) a**2
*   9 Delta E0 =  -7.471438 (  1.215785) eV
   10 Delta E1 =   0.000000 eV

 Component #  2  ..... Zba= 4.00 Zbp= 4.00 Nat=5 Npt=5 Integral=   0.603% [  4]
   11   Atom # =  10.000000
```

```
*  12 Distance =   2.602986 (  0.027171) Angstroms
*  13 Sigma**2 =   0.051521 (  0.009146) a**2
/  14 Delta E0 =  -7.471438 eV
   15 Delta E1 =   0.000000 eV

Component #  3  ..... Zba=37.00 Zbp=37.00 Nat=5 Npt=5 Integral=  33.215% [  2]
   16  Atom # =   1.000000
*  17 Distance =   3.741144 (  0.008484) Angstroms
*  18 Sigma**2 =   0.004826 (  0.000550) a**2
/  19 Delta E0 =  -7.471438 eV
   20 Delta E1 =   0.000000 eV

Component #  4  ..... Zba=42.00 Zbp=42.00 Nat=5 Npt=5 Integral=  14.870% [  3]
   21  Atom # =   2.000000
*  22 Distance =   4.122193 (  0.014013) Angstroms
*  23 Sigma**2 =   0.005491 (  0.001291) a**2
/  24 Delta E0 =  -7.471438 eV
   25 Delta E1 =   0.000000 eV

 - Correlation Matrix -
 Comp't    1     1     1     2     2     3     3     4     4
         R  Sig^2  Eo     R  Sig^2    R  Sig^2    R  Sig^2
 Par.#     7     8     9    12    13    17    18    22    23
  7      1.000-0.547 0.941 0.263-0.715 0.718-0.365 0.566-0.411
  8            1.000-0.567-0.339 0.594-0.468 0.337-0.377 0.327
  9                  1.000-0.204-0.830 0.757-0.395 0.592-0.442
 12                        1.000 0.125-0.069-0.071 0.082-0.093
 13                              1.000-0.623 0.352-0.474 0.377
 17                                    1.000-0.392 0.883-0.573
 18                                          1.000 0.208 0.844
 22                                                1.000-0.406
 23                                                      1.000

 Additional Statistical Information :
    Normalised error (chi-squared) : 0.124743      F/(No.pts)
      Reduced error (chi-squared) : 0.130328      F/(No.pts-No.Vars)
            Weighted F-factor : 0.397556     ( 39.76% )
       Expected Weighted F-factor :  1.10123
 Expected resolution in distance, R : 0.143228     Angstroms
```

Cp''_2UBr_2

```
Kmin= 1.00 Kmax=13.87 Deltak=0.000 244 Pts   5 Comp'ts  11 Variables
  27 Iter'ns   58. F eval's Elfin=.10E-05 Dmp=.10E+00 F=0.282E+02 Za=92.0
  1  Scale Factor  =  0.900
  2  Data Delta E0 =  0.00 eV
  3 Wave 1 Sigma-D =  0.00 Angstroms
  4   0.00
  5   0.00
```

Component # 1 ..... Zba= 1.00 Zbp= 1.00 Nat=5 Npt=5 Integral= 9.415% [2]
6 Atom # = 10.000000
* 7 Distance = 2.707915 (0.006743) Angstroms
* 8 Sigma**2 = 0.012094 (0.000809) a**2
* 9 Delta E0 = -10.902983 (0.602856) eV
10 Delta E1 = 0.000000 eV

Component # 2 ..... Zba= 6.00 Zbp= 6.00 Nat=5 Npt=5 Integral= 71.325% [1]
11 Atom # = 2.000000
* 12 Distance = 2.741603 (0.002162) Angstroms
* 13 Sigma**2 = 0.004637 (0.000114) a**2
/ 14 Delta E0 = -10.902983 eV
15 Delta E1 = 0.000000 eV

Component # 3 ..... Zba= 7.00 Zbp= 7.00 Nat=5 Npt=5 Integral= 9.024% [3]
16 Atom # = 20.000000
* 17 Distance = 3.408585 (0.007988) Angstroms
* 18 Sigma**2 = 0.000155 (0.000696) a**2
/ 19 Delta E0 = -10.902983 eV
20 Delta E1 = 0.000000 eV

Component # 4 ..... Zba=21.00 Zbp=21.00 Nat=5 Npt=5 Integral= 6.879% [4]
21 Atom # = 4.000000
* 22 Distance = 4.174691 (0.008384) Angstroms
* 23 Sigma**2 = 0.008219 (0.000808) a**2
/ 24 Delta E0 = -10.902983 eV
25 Delta E1 = 0.000000 eV

Component # 5 ..... Zba=45.00 Zbp=45.00 Nat=5 Npt=5 Integral= 3.356% [5]
26 Atom # = 6.000000
* 27 Distance = 4.722832 (0.016602) Angstroms
* 28 Sigma**2 = 0.006526 (0.001703) a**2
/ 29 Delta E0 = -10.902983 eV
30 Delta E1 = 0.000000 eV

- Correlation Matrix -

Comp't	1	1	1	2	2	3	3	4	4	5	5
	R	Sig^2	Eo	R	Sig^2	R	Sig^2	R	Sig^2	R	Sig^2
Par.#	7	8	9	12	13	17	18	22	23	27	28
7	1.000	0.441	0.877	0.901	0.537	0.247	-0.566	0.647	-0.286	0.466	0.069
8		1.000	0.630	0.252	0.796	0.660	-0.463	0.475	-0.125	0.318	0.091
9			1.000	0.916	0.517	0.510	-0.483	0.731	-0.286	0.526	0.073
12				1.000	0.325	0.304	-0.567	0.676	-0.284	0.494	0.098
13					1.000	0.674	-0.504	0.394	0.086	0.236	0.138
17						1.000	-0.338	0.396	0.231	0.262	0.185
18							1.000	-0.431	0.236	-0.315	-0.073
22								1.000	-0.288	0.348	-0.252
23									1.000	0.252	0.039
27										1.000	-0.163
28											1.000

Additional Statistical Information :
Normalised error (chi-squared) : 0.115726 F/(No.pts)

Reduced error (chi-squared) : 0.121190 F/(No.pts-No.Vars)
Weighted F-factor : 0.258610 (25.86%)
Expected Weighted F-factor : 0.742871
Expected resolution in distance, R : 0.122055 Angstroms

$[CP^{\ddagger}_2UO]_2$

Kmin= 4.04 Kmax=13.95 Deltak=0.000 204 Pts 5 Comp'ts 11 Variables
6 Iter'ns 17. F eval's Elfin=.10E-05 Dmp=.10E+01 F=0.100E+02 Za=92.0
1 Scale Factor = 0.900
2 Data Delta E0 = 0.00 eV
3 Wave 1 Sigma-D = 0.00 Angstroms
4 0.00
5 0.00

Component # 1 ..... Zba= 1.00 Zbp= 1.00 Nat=5 Npt=5 Integral= 10.703% [3]
6 Atom # = 1.000000
* 7 Distance = 2.159456 (0.009876) Angstroms
* 8 Sigma**2 = 0.007995 (0.001084) a**2
* 9 Delta E0 = -9.575643 (0.807822) eV
10 Delta E1 = 0.000000 eV

Component # 2 ..... Zba= 1.00 Zbp= 1.00 Nat=5 Npt=5 Integral= 8.618% [4]
11 Atom # = 1.000000
* 12 Distance = 2.328800 (0.011737) Angstroms
* 13 Sigma**2 = 0.008027 (0.001389) a**2
/ 14 Delta E0 = -9.575643 eV
15 Delta E1 = 0.000000 eV

Component # 3 ..... Zba= 3.00 Zbp= 3.00 Nat=5 Npt=5 Integral= 11.213% [2]
16 Atom # = 10.000000
* 17 Distance = 2.823552 (0.006487) Angstroms
* 18 Sigma**2 = 0.014493 (0.000517) a**2
/ 19 Delta E0 = -9.575643 eV
20 Delta E1 = 0.000000 eV

Component # 4 ..... Zba=12.00 Zbp=12.00 Nat=5 Npt=5 Integral= 62.926% [1]
21 Atom # = 1.000000
* 22 Distance = 3.398515 (0.002928) Angstroms
* 23 Sigma**2 = 0.002931 (0.000122) a**2
/ 24 Delta E0 = -9.575643 eV
25 Delta E1 = 0.000000 eV

Component # 5 ..... Zba=14.00 Zbp=14.00 Nat=5 Npt=5 Integral= 6.540% [5]
26 Atom # = 4.000000
* 27 Distance = 4.247950 (0.013110) Angstroms
* 28 Sigma**2 = 0.006379 (0.001188) a**2
/ 29 Delta E0 = -9.575643 eV
30 Delta E1 = 0.000000 eV

- Correlation Matrix -

Comp't	1	1	1	2	2	3	3	4	4	5	5
	R	Sig^2	Eo	R	Sig^2	R	Sig^2	R	Sig^2	R	Sig^2
Par.#	7	8	9	12	13	17	18	22	23	27	28
7	1.000	-0.337	0.757	0.882	0.031	0.568	0.175	0.710	-0.452	0.540	-0.182
8		1.000	-0.332	-0.566	0.867	-0.306	-0.344	-0.230	-0.129	-0.299	0.081
9			1.000	0.690	-0.490	0.903	-0.275	0.931	-0.526	0.726	-0.307
12				1.000	-0.456	0.447	0.277	0.635	-0.382	0.491	-0.166
13					1.000	-0.496	-0.409	-0.416	-0.111	-0.402	0.161
17						1.000	-0.333	0.844	-0.491	0.673	-0.274
18							1.000	-0.184	0.180	-0.209	0.167
22								1.000	-0.517	0.636	-0.149
23									1.000	-0.467	-0.300
27										1.000	-0.288
28											1.000

Additional Statistical Information :
Normalised error (chi-squared) : 0.491272E-01 F/(No.pts)
Reduced error (chi-squared) : 0.519272E-01 F/(No.pts-No.Vars)
Weighted F-factor : 0.309571 (30.96%)
Expected Weighted F-factor : 1.35851
Expected resolution in distance, R : 0.158400 Angstroms

$Cp^{\ddagger}_2UF_2$

Kmin= 1.01 Kmax=10.99 Deltak=0.000 188 Pts 4 Comp'ts 8 Variables
1 Iter'ns 8. F eval's Elfin=.10E-05 Dmp=.10E+02 F=0.110E+02 Za=92.0
1 Scale Factor = 0.900
2 Data Delta E0 = 0.00 eV
3 Wave 1 Sigma-D = 0.00 Angstroms
4 0.00
5 0.00

Component # 1 ..... Zba= 2.00 Zbp= 2.00 Nat=5 Npt=5 Integral= 52.088% [1]
6 Atom # = 10.000000
* 7 Distance = 2.335441 (0.003025) Angstroms
* 8 Sigma**2 = 0.011294 (0.000222) a**2
* 9 Delta E0 = -14.021249 (0.458035) eV
10 Delta E1 = 0.000000 eV

Component # 2 ..... Zba=12.00 Zbp=12.00 Nat=5 Npt=5 Integral= 24.483% [2]
11 Atom # = 4.000000
* 12 Distance = 3.874517 (0.007931) Angstroms
13 Sigma**2 = 0.001000 A**2
/ 14 Delta E0 = -14.021249 eV
15 Delta E1 = 0.000000 eV

Component # 3 ..... Zba=22.00 Zbp=22.00 Nat=5 Npt=5 Integral= 16.704% [3]

```
  16  Atom # =  8.000000
*  17 Distance =  4.103917 ( 0.007973) Angstroms
*  18 Sigma**2 =  0.006303 ( 0.001162) a**2
/  19 Delta E0 = -14.021249 eV
   20 Delta E1 =  0.000000 eV

Component #  4  ..... Zba=46.00 Zbp=46.00 Nat=5 Npt=5 Integral=  6.725% [  4]
   21  Atom # =  4.000000
*  22 Distance =  5.289042 ( 0.016917) Angstroms
*  23 Sigma**2 =  0.002725 ( 0.001743) a**2
/  24 Delta E0 = -14.021249 eV
   25 Delta E1 =  0.000000 eV

 - Correlation Matrix -
 Comp't   1    1    1    2    3    3    4    4
        R  Sig^2  Eo    R    R  Sig^2   R  Sig^2
 Par.#    7    8    9   12   17   18   22   23
  7      1.000-0.357 0.927 0.463 0.527 0.131 0.440-0.166
  8          1.000-0.317-0.311-0.289 0.169-0.189 0.188
  9              1.000 0.504 0.575 0.103 0.469-0.184
 12                  1.000 0.801-0.868-0.352 0.229
 17                      1.000-0.689-0.357 0.271
 18                          1.000 0.374-0.390
 22                              1.000-0.223
 23                                  1.000

 Additional Statistical Information :
    Normalised error (chi-squared) : 0.584291E-01  F/(No.pts)
      Reduced error (chi-squared) : 0.610260E-01  F/(No.pts-No.Vars)
            Weighted F-factor : 0.244344     ( 24.43% )
       Expected Weighted F-factor : 0.989111
 Expected resolution in distance, R : 0.157498     Angstroms
```

$Cp^{\ddagger}_2UBr_2$

```
Kmin= 1.01 Kmax=12.96 Deltak=0.000 225 Pts  4 Comp'ts  9 Variables
  13 Iter'ns  31. F eval's Elfin=.10E-05 Dmp=.10E+01 F=0.295E+02 Za=92.0
  1  Scale Factor  =  0.900
  2  Data Delta E0 =  0.00 eV
  3 Wave 1 Sigma-D =  0.00 Angstroms
  4   0.00
  5   0.00

Component #  1  ..... Zba= 1.00 Zbp= 1.00 Nat=5 Npt=5 Integral=  7.163% [  3]
   6  Atom # =  10.000000
*  7 Distance =  2.709496 ( 0.008358) Angstroms
*  8 Sigma**2 =  0.015475 ( 0.001115) a**2
*  9 Delta E0 =  -9.740412 ( 0.705912) eV
  10 Delta E1 =  0.000000 eV
```

```
Component #  2  ..... Zba= 3.00 Zbp= 3.00 Nat=5 Npt=5 Integral=  69.079% [  1]
  11  Atom # =  2.000000
*  12 Distance =  2.744217 (  0.002488) Angstroms
*  13 Sigma**2 =  0.005233 (  0.000119) a**2
/  14 Delta E0 = -9.740412 eV
   15 Delta E1 =  0.000000 eV

Component #  3  ..... Zba=12.00 Zbp=12.00 Nat=5 Npt=5 Integral=  17.209% [  2]
  16  Atom # =  4.000000
*  17 Distance =  3.817166 (  0.006588) Angstroms
*  18 Sigma**2 =  0.000894 (  0.000570) a**2
/  19 Delta E0 = -9.740412 eV
   20 Delta E1 =  0.000000 eV

Component #  4  ..... Zba=28.00 Zbp=28.00 Nat=5 Npt=5 Integral=   6.550% [  4]
  21  Atom # =  8.000000
*  22 Distance =  3.981467 (  0.012965) Angstroms
*  23 Sigma**2 =  0.008036 (  0.001558) a**2
/  24 Delta E0 = -9.740412 eV
   25 Delta E1 =  0.000000 eV

 - Correlation Matrix -
Comp't   1    1    1    2    2    3    3    4    4
       R  Sig^2  Eo    R  Sig^2   R  Sig^2   R  Sig^2
Par.#    7    8    9   12   13   17   18   22   23
 7     1.000 0.545 0.871 0.880 0.539 0.587-0.490 0.442-0.496
 8           1.000 0.708 0.453 0.700 0.593-0.376 0.479-0.417
 9                 1.000 0.926 0.468 0.691-0.476 0.546-0.515
12                       1.000 0.307 0.582-0.497 0.450-0.508
13                             1.000 0.473-0.456 0.372-0.408
17                                   1.000-0.429 0.844-0.577
18                                         1.000-0.022 0.843
22                                               1.000-0.414
23                                                     1.000

Additional Statistical Information :
   Normalised error (chi-squared) : 0.131001     F/(No.pts)
     Reduced error (chi-squared) : 0.136460     F/(No.pts-No.Vars)
           Weighted F-factor : 0.286982     ( 28.70% )
      Expected Weighted F-factor : 0.776878
Expected resolution in distance, R : 0.131429     Angstroms
```

$Cp^{\ddagger}_2UI_2$

```
Kmin= 1.02 Kmax=13.98 Deltak=0.000 258 Pts   4 Comp'ts   9 Variables
  17 Iter'ns   39. F.eval's Elfin=.10E-05 Dmp=.10E+01 F=0.203E+02 Za=92.0
  1  Scale Factor  =  0.900
  2  Data Delta E0 =  0.00 eV
```

```
  3 Wave 1 Sigma-D =  0.00 Angstroms
  4   0.00
  5   0.00

Component #  1  ..... Zba= 1.00 Zbp= 1.00 Nat=5 Npt=5 Integral=  13.001% [  3]
    6  Atom # =  10.000000
*   7 Distance =  2.728017 (  0.003396) Angstroms
*   8 Sigma**2 =  0.010411 (  0.000337) a**2
*   9 Delta E0 = -8.445836 (  0.354190) eV
   10 Delta E1 =  0.000000 eV

Component #  2  ..... Zba= 6.00 Zbp= 6.00 Nat=5 Npt=5 Integral=  66.860% [  1]
   11  Atom # =  2.000000
*  12 Distance =  2.975433 (  0.001443) Angstroms
*  13 Sigma**2 =  0.005061 (  0.000074) a**2
/  14 Delta E0 = -8.445836 eV
   15 Delta E1 =  0.000000 eV

Component #  3  ..... Zba=12.00 Zbp=12.00 Nat=5 Npt=5 Integral=  13.130% [  2]
   16  Atom # =  4.000000
*  17 Distance =  3.816530 (  0.006801) Angstroms
*  18 Sigma**2 =  0.002087 (  0.000564) a**2
/  19 Delta E0 = -8.445836 eV
   20 Delta E1 =  0.000000 eV

Component #  4  ..... Zba=21.00 Zbp=21.00 Nat=5 Npt=5 Integral=   7.009% [  4]
   21  Atom # =  4.000000
*  22 Distance =  3.978187 (  0.011427) Angstroms
*  23 Sigma**2 =  0.004119 (  0.001080) a**2
/  24 Delta E0 = -8.445836 eV
   25 Delta E1 =  0.000000 eV

- Correlation Matrix -
Comp't    1    1    1    2    2    3    3    4    4
        R  Sig^2  Eo    R  Sig^2   R  Sig^2   R  Sig^2
Par.#     7    8    9   12   13   17   18   22   23
 7      1.000 0.156 0.842 0.796-0.575 0.458-0.415 0.307-0.392
 8          1.000 0.277 0.511 0.319 0.380-0.041 0.322-0.182
 9              1.000 0.897-0.508 0.517-0.391 0.376-0.381
12                  1.000-0.467 0.572-0.416 0.430-0.412
13                      1.000 0.144 0.494 0.262 0.420
17                          1.000-0.241 0.861-0.634
18                              1.000 0.509 0.829
22                                  1.000-0.340
23                                      1.000

Additional Statistical Information :
   Normalised error (chi-squared) : 0.785403E-01  F/(No.pts)
     Reduced error (chi-squared) : 0.813791E-01  F/(No.pts-No.Vars)
           Weighted F-factor : 0.239849     ( 23.98% )
      Expected Weighted F-factor : 0.840777
Expected resolution in distance, R : 0.121182     Angstroms
```

Appendix Three: EPR Fitting Program

The EPR fitting program is largely derived from the program ABVG.[1] The calculation short cuts, the Simpson integration, the numerical derivative scheme, and the subroutine for inverting matrices are from this program.[1] The lineshape used here is that previously used by Soulie[2] which is based upon that suggested by Pilbrow.[3] The lineshape is based on a Gaussian curve rather than a Lorentzian curve. The Gaussian shape was chosen since the lines in these samples will be inhomogeneously broadened due to dipole-dipole interactions in the solid.[3] This program does not fit frozen solution spectra well since the lineshape in this case is likely Lorentzian.

The fitting strategy is Levenberg-Marquardt as outlined in "Numerical Recipes".[4] The derivatives of the absorption spectrum with respect to the fitting parameters are calculated analytically. The derivatives of the spectrum and of the derivatives with respect to magnetic field are calculated numerically.[1] It should be noted that the range of the field over which the derivative is calculated, mu, can greatly affect the appearance of the spectrum.[1] The formula used to determine mu was found empirically to work well.

Finally, this program is very slow and does not work well if the initial values for g and for the linewidth are far from the actual values. In addition, since the program allows different linewidths for the different g components, very good fits can sometimes be obtained which have very different values of the linewidth for different components. Such fits are probably incorrect.

```
program SPUD
c
c    This program is designed to run in a batch mode (or nohup). It
c      reads a file called "FITFILE" first. FITFILE contains the
c      following, in order:
c    Line 1: the name of the fit parameter file
c    Line 2: the name of the spectrum (must be x,y form)
c    Line 3: the name of the output files. These will be generated
c      with the suffix .001 .002 ... each time the fit improves.
c    Line 4: the name of the plot files. These will be generated
```

```
c      with the suffix .001 .002 ... each time the fit improves.
c     Line 5: the maximum number of fitting cycles
c
c     The program reads in the spectrum and adjusts the number of
c      fitting points accordingly.
c
c
c     The input has the following form:
c     First line contains the three g values format 3F9.6
c     The second line contains the freqency in GHz
c      and the three line widths also in GHz format 4F10.8
c     The third line contains the initial bounds on the field.
c      The program determines the upper bound from the spectrum,
c      but will not determine the lower bound.  Format 2F7.1.
c     The third line contains the number of steps in phi and
c      in cos(theta) for the numberical integration. Format 2I9.
c     The fourth line contains the initial value of the parameter
c      lambda for the Levenberg-Marquardt fitting.  Usually 1e-3.
c      Format E15.6.
c     The final line contains text for labelling the fitting run.
c      Format A100.


      dimension G(3),G2(3,3),WATE(100),G1(500,500),BETA(6)
     1,PROB(500,500),ALL(2),SIV(500,500),S(2000),SV(3),SVO(3),
     1SPEC(2000),Y(2000),GO(3),SIG(2000),E(3),DA(6),EE(500,
     1500,3),ALPHA(6,6),AL(6,6),DFDY(2000,6),DFDYDB
     1(2000,6),BACTOR(500,500,3),COVAR(6,6),DET(2)
      character*20 INPUT,OUTPUT,PLOT,NAME
      character*100 TEXT
       open (unit=9,file='FITFILE',status='old')
      read(9,*) INPUT
      read(9,*) NAME
      read(9,*) OUTPUT
      read(9,*) PLOT
      read(9,*) ICYCLE
      close(9)
       open (unit=11,file=OUTPUT,status='new')
       open (unit=10,file=INPUT,status='old',err=9999)
      go to 10
100   format(3F9.6)
200   format(4F10.8)
300   format(2F7.1)
350   format(2I9)
400   format(F6.0)
500   format(E15.6)
600   format(A100)
10    read(10,100) G(1),G(2),G(3)
      read(10,200) FREQ,SV(1),SV(2),SV(3)
      read(10,300) BLOW,BHIGH
      read(10,350) NTHETA,NPHI
      read(10,400) POINTS
      read(10,500) WHY
```

```
      read(10,600) TEXT
      POINTY=POINTS
      close(10)
      write(11,*) 'This simulation is ',TEXT
      write(11,*) 'The plot is called ',PLOT
      write(11,*) 'The g-values are ',g(1),g(2),g(3)
      write(11,*) 'The linewith (GHz) is ',sv
      write(11,*) 'The spectrometer frequency is ',FREQ
      write(11,*) 'The spectrum is from ',blow,' to ',bhigh,' Gauss.'
      write(11,*) 'The number of steps in theta and phi are ',ntheta
     1,nphi
      write(11,*) 'There are ',points,' points in the simulation.'
      write(11,*) 'The initial value of lambda is ',WHY
      write(11,*) 'The maximum number of cycles is ',ICYCLE
      close(11)
      PI=3.1415926535
      do 11, I=1,3
      SVO(I)=SV(I)
      GO(I)=G(I)
11    continue
      CON=714.47752
      IFLAG=0.
      BSTEP=(BHIGH-BLOW)/(POINTS-1.)
      IPLOT=0
      NPLOT=ifix(INDEX(PLOT,' ')-1)
      CHIOLD=1.E10
      TRG2=0.
c
c     read in the spectrum
c
      call SETUP(NAME,Y,SIG,POINTS,BLOW,BHIGH,BSTEP,ALLY,BIGY)
c
c     Start of the main fitting loop
c
      do 9997 ICICLE=1,ICYCLE
      SIGV=(SV(1)+SV(2)+SV(3))/3.
c
c     Set up g squared matrix
c
1001  do 30 I=1,3
      do 30 J=1,3
      G2(I,J)=0.
      IF (I.EQ.J) G2(I,J)=G(I)*G(I)
      TRG2=TRG2+G2(I,J)
30    continue
c
c     Set up integration over crystallite orientations
c
      if (NTHETA.eq.0) NTHETA=IFIX(SQRT(50.*POINTS))
      if (NTHETA.gt.1000) NTHETA=1000
      if (NPHI.eq.0) NPHI=NTHETA
      IPLOT=IPLOT+1
      CSTEP=1./float(NTHETA)
```

```
      PSTEP=PI/float(NPHI)/2.
      B=BLOW-BSTEP
      CTHE=-CSTEP
c
c     Set up weights for Simpson Integration
c     and set up variables that are field independent
c
      do 40 I=1,NTHETA
      CTHE=CTHE+CSTEP
      PHI=-PSTEP
      WTHETA=4.
      if(mod(I,2).eq.1) WTHETA=2.
      if(I.eq.1.or.I.EQ.NTHETA) WTHETA=1.
      do 40 J=1,NPHI
      PHI=PHI+PSTEP
      WPHI=4.
      if(mod(J,2).eq.1) WPHI=2.
       if(J.eq.1.or.J.eq.NPHI) WPHI=1.
      WTOT=WTHETA*WPHI
      STHE=sqrt(1.-CTHE*CTHE)
c
c     All calculation shortcuts from the program ABVG
c
      E(1)=STHE*cos(PHI)
      E(2)=STHE*sin(PHI)
      E(3)=CTHE
      DG1=E(1)*G(1)
      DG2=E(2)*G(2)
      DG3=E(3)*G(3)
      GSQR=DG1*DG1+DG2*DG2+DG3*DG3
      G1(I,J)=sqrt(GSQR)
      EG4E=DG1*DG1*G2(1,1)+DG2*DG2*G2(2,2)+DG3*DG3*G2(3,3)
      SIV(I,J)=sqrt(E(1)**2.*SV(1)**2.+E(2)**2.
     1*SV(2)**2.+E(3)**2.*SV(3)**2.)
      PROB(I,J)=WTOT*(TRG2-EG4E/GSQR)
      do 35 K=1,3
      EE(I,J,K)=E(K)*E(K)
      SM=(2.*G(K)*G(K)*GSQR)-EG4E
      BACTOR(I,J,K)=2.*(1-EE(I,J,K)*SM/(GSQR*GSQR))
35    continue
40    continue
c
c     Loop over the magnetic field of the spectrum
c     Calculate the absorption spectrum and the derivatives
c
      do 41 K=1,ifix(POINTS)
      B=B+BSTEP
      S(K)=0.
      SPEC(K)=0.
      do 44,IND=1,6
      DFDY(K,IND)=0.
      DFDYDB(K,IND)=0.
44    continue
```

```
      do 42 I=1,NTHETA
      do 42 J=1,NPHI
      V=G1(I,J)*B/CON
      SPUD=(FREQ-V)/SIV(I,J)
      GAUSS=exp(-0.5*SPUD*SPUD)/SIV(I,J)
      S(K)=S(K)+PROB(I,J)*GAUSS
      do 42 L=1,3
      SM=GAUSS*(SPUD*SPUD-1.)/(SIV(I,J)*SIV(I,J))
      DFDY(K,L)=DFDY(K,L)+(PROB(I,J)*SV(L)*EE(I,J,L)*SM)
      SM=B*EE(I,J,L)*PROB(I,J)*SPUD/(G1(I,J)*SIV(I,J)*CON)
      DFDY(K,L+3)=DFDY(K,L+3)+G(L)*GAUSS*(SM+BACTOR(I,J,L))
42    continue
41    continue
c
c     Determine the width of the magnetic field over which
c     to calculate the derivative
c     Note: this is somewhat arbitrary here
c
      GAV=(G(1)+G(2)+G(3))/3.
      do 49, I=1,3
      if (SV(I).LT.SIGV) then SIGV = SV(I)
49    continue
      SB=714.47752*SIGV/GAV
      MU=ifix(SB/BSTEP/5.)+1
      do 50 I=1,MU
      WATE(I)=float(I*I*2.)
50    continue
      WATE(MU)=WATE(MU)/2.
      N2=POINTS-MU
      SM=0.
      SM2=0.
      YK=0.
      BIGS=0.
c
c     Calculate the derivative of the spectrum
c     and of the derivative of the derivatives w/respect to
c     the magnetic field
c
      do 80 I=1,ifix(POINTS)
      if(I.le.MU.or.I.ge.N2) go to 80
      do 70 J=1,MU
      SPEC(I)=SPEC(I)+(S(I+J)-S(I-J))*WATE(J)
      do 70 K=1,6
      DFDYDB(I,K)=DFDYDB(I,K)+(DFDY(I+J,K)-DFDY(I-J,K))
     1*WATE(J)
70    continue
      SM2=SM2+SPEC(I)*SPEC(I)
      YK=YK+Y(I)*SPEC(I)
      IF (abs(SPEC(I)).gt.abs(BIGS)) BIGS=spec(I)
80    continue
c
c     Determine the scaling factor for the spectrum
c
```

```
      FACTOR=BIGY/BIGS
      A1=YK/SM2
      B=BLOW-BSTEP
      do 17 I=1,ifix(POINTS)
      B=B+BSTEP
      SPEC(I)=SPEC(I)*A1
 17   continue
      CHI2=0.
      do 85 J=1,6
      BETA(J)=0.
      DA(J)=0.
      do 85 K=1,6
      ALPHA(J,K)=0.
 85   continue
c
c     calculate how to change the spectrum in the next cycle
c
      do 91 I=1,ifix(POINTS)
       ANUM=Y(I)-SPEC(I)
       CHI2=CHI2+ANUM*ANUM
       do 90 J=1,6
        BETA(J)=BETA(J)+A1*ANUM*DFDYDB(I,J)
        do 90 K=1,6
         ALPHA(J,K)=ALPHA(J,K)+A1*A1*DFDYDB(I,J)
     1*DFDYDB(I,K)
 90   continue
 91   continue
 101   do 111 I=1,6
       do 112 J=1,6
        AL(I,J)=ALPHA(I,J)
 112    continue
       AL(I,I)=ALPHA(I,I)*(1.+WHY)
 111  continue
 151  format(6E16.4)
c
c     invert the modified 2nd derivative matrix
c
      DET(1) = 1.0
      DET(2) = 0.0
      call gaussj(AL,6,0.00001)
      do 113 I=1,6
      do 113 J=1,6
     DA(I)=DA(I)+AL(I,J)*BETA(J)
 113  continue
     RATIO=(CHIOLD-CHI2)/CHI2
c
c     see if the fit got better or worse
c
      if (CHI2.le.CHIOLD) then
       IBEST=ICICLE
       WHY=WHY/10.
       CHIOLD=CHI2
       do 114 I=1,3
```

```
      SVO(I)=SV(I)
      GO(I)=G(I)
114   continue
     do 115 I=1,6
     do 115 J=1,6
     COVAR(I,J)=ALPHA(I,J)
115   continue
    call UPDATE(CHI2,ALPHA,BETA,ICICLE,G,SV,WHY,AL,GO,SVO,OUTPUT)
    call OUTPLOT(PLOT,SPEC,POINTS,ICICLE,NPLOT,BLOW,BSTEP)
     if (RATIO.lt.1.E-3) then
      if (IFLAG.eq.1) go to 9998
      IFLAG=1
     end if
    else
     WHY=WHY*10.
    endif
c
c   determine the new g and sigma values
c
    do 116 I=1,3
    G(I)=abs(GO(I)+DA(I+3))
    SV(I)=abs(SVO(I)+DA(I))
    if (G(I).lt.0..or.SV(I).lt.0.) go to 9998
116  continue
    if (WHY.ge.1.E10) go to 9998
9997 continue
9998 butt=etime(all)
    WHY=0.001
c
c   when finished append the best fitting parameters
c   to the parameter file
c
     open(unit=10,file=INPUT,access='append',status='old')
    write(10,100) GO(1),GO(2),GO(3)
    write(10,200) FREQ,SVO(1),SVO(2),SVO(3)
    write(10,300) BLOW,BHIGH
    write(10,350) NTHETA,NPHI
    write(10,400) POINTY
    write(10,500) WHY
    write(10,600) TEXT
    close(10)
     open(unit=11,file=OUTPUT,access='append',status='old')
    UEFF=0.5*sqrt(GO(1)**2+GO(2)**2+GO(3)**2)
     write(11,*) 'The runtime was ',butt/60,' minutes.'
    write(11,*)
    write(11,*) 'The best fit was #',IBEST
    write(11,*) 'Best values of G:        ',(GO(I),I=1,3)
    write(11,*) 'Best values of sigma:    ',(SVO(I),I=1,3)
    write(11,*) 'Corresponding chi-squared:',CHIOLD
    write(11,*) 'Effective magnetic moment:',UEFF
    write(11,*)
9999 close(11)
    IPLOT=IPLOT+1
```

```
      call UPDATE(CHI2,ALPHA,BETA,IPLOT,G,SV,WHY,AL,GO,SVO,OUTPUT)
      call OUTPLOT(PLOT,SPEC,POINTS,IPLOT,NPLOT,BLOW,BSTEP)
      end
c
c
c
c
      subroutine SETUP(NAME,Y,SIG,POINTS,BLOW,BHIGH,BSTEP,ALLY,BIGY)
c
c     reads in the actual spectrum and determines the
c     boundaries of the magnetic field over which to fit
c
      dimension Y(10000),SIG(10000)
      open (unit=13,file=NAME,status='old')
      B=BLOW-BSTEP
      Y(1)=0.
      ALLY=0.
      BIGY=0.
      read(13,*) XOLD,YOLD
      read(13,*) XNEW,YNEW
      do 10 I=1,ifix(POINTS)
      B=B+BSTEP
      if (I.gt.1.) Y(I)=Y(I-1)
11    if (B.lt.XOLD) go to 10
      if (B.gt.XOLD.and.B.le.XNEW) then
        Y(I)=0.5*(YOLD+YNEW)
        SIG(I)=abs(YOLD-YNEW)/(Y(I)*6)
        go to 10
      end if
      if (abs(Y(I)).gt.abs(BIGY)) BIGY=Y(I)
      XOLD=XNEW
      YOLD=YNEW
      read(13,*,end=12) XNEW,YNEW
      go to 11
10    continue
12    POINTS=I-1
      do 13 I=1,ifix(POINTS)
      ALLY=ALLY+Y(I)
13    continue
      close(13)
      return
      end

      subroutine UPDATE(CHI2,ALPHA,BETA,IPLOT,G,SV
     1,WHY,AL,GO,SVO,OUTPUT)
c
c     subroutine to put fit data to a file if the fit
c     get better
c
      dimension ALPHA(6,6),BETA(6),G(3),AL(6,6)
     1,GO(3),SVO(3),all(2),ball(2),SV(3)
      character NAME*24,OUTPUT*20,LIST*10
```

```
      LIST='0123456789'
      KPLOT=INDEX(OUTPUT,' ')-1
      NAME=OUTPUT(1:KPLOT)//'.'
      ICON=100
      ICOUNT=KPLOT+1
      JPLOT=IPLOT
      do 10 I=1,3
      M=ifix(float(JPLOT)/ICON)+1
      NAME=NAME(1:ICOUNT)//LIST(M:M)
      JPLOT=MOD(JPLOT,ICON)
      ICON=ICON/10
      ICOUNT=ICOUNT+1
10    continue
      butt=etime(all)
      UEFF=0.5*sqrt(G(1)**2+G(2)**2+G(3)**2)
      smut=dtime(ball)
      open (unit=11,file=NAME,status='new')
      write(11,*) 'Results of iteration #',IPLOT
      write(11,*) 'Total elapsed time:',butt
      write(11,*) 'Time used on this iteration:',smut
      write(11,*)
      write(11,*) 'Current values of G:    ',(G(I),I=1,3)
      write(11,*) 'Best values of G:       ',(GO(I),I=1,3)
      write(11,*)
      write(11,*) 'Current values of sigma:',(SV(I),I=1,3)
      write(11,*) 'Best values of sigma:   ',(SVO(I),I=1,3)
      write(11,*)
      write(11,*) 'Current Mu effective:',UEFF
      write(11,*)
      write(11,*) 'Here"s Johnny, Beta vector'
      write(11,*) (BETA(I),I=1,6)
      write(11,*)
      write(11,*) 'Chi squared, for this iteration, is ',CHI2
      write(11,*)
      write(11,*) 'Lambda is ',WHY
      write(11,*)
      write(11,*)
      close(11)
      return
      end
c
c
      subroutine OUTPLOT(PLOT,SPEC,POINTS,IPLOT,NPLOT
     1,BLOW,BSTEP)
c
c     plots the spectrum if the fit gets better
c
      dimension SPEC(10000)
      character PLOTNAME*24,PLOT*20,LIST*10
      LIST='0123456789'
      PLOTNAME=PLOT(1:NPLOT)//'.'
      ICON=100
      ICOUNT=NPLOT+1
```

```
      JPLOT=IPLOT
      do 10 I=1,3
      M=ifix(float(JPLOT)/ICON)+1
      PLOTNAME=PLOTNAME(1:ICOUNT)//LIST(M:M)
      JPLOT=MOD(JPLOT,ICON)
      ICON=ICON/10
      ICOUNT=ICOUNT+1
10    continue
      open(unit=12,file=PLOTNAME,status='new')
      B=BLOW-BSTEP
      do 20, I=1,ifix(POINTS)
      B=B+BSTEP
      write (12,*) B,SPEC(I)
20    continue
      close(12)
      return
      end
c
c
      SUBROUTINE GAUSSJ(A,N,EPS)
C     FROM IBM 1130 - SCIENTIFIC SUBROUTINE PACKAGE
C
C     PURPOSE OF THE SUBROUTINE
C       CALCULATION OF THE INVERSE OF A MATRIX
C
C     PARAMETERS
C       A  - INPUT AND OUTPUT-MATRIX A
C       N  - ORDER OF THE MATRIX TO BE INVERTED
C       EPS - TOLERANCE FOR ACCEPTANCE OF THE SINGULARITY OF THE
C             GIVEN MATRIX, IF MATRIX SINGULAR, THEN EPS=-1 AND
C             PRINTOUT OF A MESSAGE
C
C     REMARKS
C       N MUST BE SMALLER THAN 51
C
C     NECESSARY SUBROUTINES AND FUNCTIONS
C       NONE
C
C     METHOD
C       GAUSS-JORDAN-RUTISHAUSER
C
C
C.....
      DIMENSION A(1) ,L(50), M(50)
C     DETERMINATION OF THE PIVOT ELEMENT
      IF(N-50) 1,1,99
    1 CONTINUE
C       SEARCH FOR LARGEST ELEMENT
      D=1.0
      NK=-N
      DO 80 K=1,N
      NK=NK+N
      L(K)=K
```

```
      M(K)=K
       KK=NK+K
      BIGA=A(KK)
      DO 20 J=K,N
      IZ=N*(J-1)
      DO 20 I=K,N
      IJ=IZ+I
   10 IF( ABS(BIGA)- ABS(A(IJ))) 15,20,20
   15 BIGA=A(IJ)
      L(K)=I
      M(K)=J
   20 CONTINUE
C       INTERCHANGE ROWS
      J=L(K)
      IF(J-K) 35,35,25
   25 KI=K-N
      DO 30 I=1,N
      KI=KI+N
      HOLD=-A(KI)
      JI=KI-K+J
      A(KI)=A(JI)
   30 A(JI) =HOLD
C       INTERCHANGE COLUMNS
   35 I=M(K)
      IF(I-K) 45,45,38
   38 JP=N*(I-1)
      DO 40 J=1,N
      JK=NK+J
      JI=JP+J
      HOLD=-A(JK)
      A(JK)=A(JI)
   40 A(JI) =HOLD
C       DIVIDE COLUMN BY MINUS PIVOT (VALUE OF PIVOT ELEMENT IS
C       CONTAINED IN BIGA)
   45 IF(ABS(BIGA)- EPS) 46,46,48
   46 EPS = - 1.0
      IF(N.EQ.1) X1=X-.5
      WRITE(2,47)K,BIGA
   47 FORMAT(24H0MATRIX SINGULAR*  STAGE,I6,4X,5HPIVOTE20.10)
      RETURN
   48 DO 55 I=1,N
      IF(I-K) 50,55,50
   50 IK=NK+I
      A(IK)=A(IK)/(-BIGA)
   55 CONTINUE
C       REDUCE MATRIX
      DO 65 I=1,N
      IK=NK+I
      HOLD=A(IK)
      IJ=I-N
      DO 65 J=1,N
      IJ=IJ+N
      IF(I-K) 60,65,60
```

```
   60 IF(J-K) 62,65,62
   62 KJ=IJ-I+K
      A(IJ)=HOLD*A(KJ)+A(IJ)
   65 CONTINUE
C       DIVIDE ROW BY PIVOT
      KJ=K-N
      DO 75 J=1,N
      KJ=KJ+N
      IF(J-K) 70,75,70
   70 A(KJ)=A(KJ)/BIGA
   75 CONTINUE
C       PRODUCT OF PIVOTS
      D=D*BIGA
C       REPLACE PIVOT BY RECIPROCAL
      A(KK)=1.0/BIGA
   80 CONTINUE
C       FINAL ROW AND COLUMN INTERCHANGE
      K=N
  100 K=(K-1)
      IF(K) 150,150,105
  105 I=L(K)
      IF(I-K) 120,120,108
  108 JQ=N*(K-1)
      JR=N*(I-1)
      DO 110 J=1,N
      JK=JQ+J
      HOLD=A(JK)
      JI=JR+J
      A(JK)=-A(JI)
  110 A(JI) =HOLD
  120 J=M(K)
      IF(J-K) 100,100,125
  125 KI=K-N
      DO 130 I=1,N
      KI=KI+N
      HOLD=A(KI)
      JI=KI-K+J
      A(KI)=-A(JI)
  130 A(JI) =HOLD
      GO TO 100
  150 RETURN
   99 CONTINUE
      WRITE(2,101)N
  101 FORMAT(48H0***** SUBROUTINE GJRD  N GREATER THAN 50   N =
,I10/)
      STOP
      END
```

References

(1) Daul, C.; Schlapfer, C. W.; Mohos, B.; Ammeter, J.; Gamp, E. *Comp. Phys. Commun.* **1981**, *21*, 385-395.

(2) Soulie, E. J.; Lesieur, P. C. *J. Chem. Soc., Faraday Trans. I* **1989**, *85*, 4053-4062.

(3) Pilbrow, J. R. *Transition Ion Electron Paramagnetic Resonance*; Clarendon Press: Oxford, 1990, pp 717.

(4) Press, W. H.; Teukolsky, S. A.; Vetterling, W. T.; Flannery, B. P. In *Numerical Recipes in FORTRAN The Art of Scientific Computing Second Edition*; Cambridge Unversity Press: Cambridge, 1992; pp 650-700.